BIOPHYSICAL CHARACTERIZATION OF CHEMICALLY UNFOLDED STATES OF THE MEMBRANE PROTEIN RHODOPSIN

by

Arpana Dutta

Bachelor of Science, St. Xavier's College, University of Calcutta, 2003

Master of Science, Indian Institute of Technology, Roorkee, 2005

Submitted to the Graduate Faculty of

School of Medicine in partial fulfillment

of the requirements for the degree of

Doctor of Philosophy

University of Pittsburgh

2010

UNIVERSITY OF PITTSBURGH

SCHOOL OF MEDICINE

This dissertation was presented

by

Arpana Dutta

It was defended on

November 11, 2010

and approved by

Professor Jeffrey Brodsky, Department of Biological Sciences

Professor Roger Hendrix, Department of Biological Sciences

Professor Linda Jen-Jacobson, Department of Biological Sciences

Professor Ronald Wetzel, Department of Structural Biology

Dissertation Advisor: Professor Judith Klein-Seetharaman, Department of Structural Biology

BIOPHYSICAL CHARACTERIZATION OF CHEMICALLY UNFOLDED STATES

OF THE MEMBRANE PROTEIN RHODOPSIN

Arpana Dutta, M.S.

University of Pittsburgh, 2010

Membrane proteins function as important communication channels of the cell and its environment that aid in regulating the overall homeostasis of organisms. Understanding the pathways by which these proteins adopt their three-dimensional structures can provide us with key insights into their functions. Failure of a membrane protein to fold into its native structure can lead to disruption of their functions and cause diseases. Through an understanding of the folding mechanisms of membrane proteins it may be possible to identify avenues for the treatment of such diseases. Towards these goals, this thesis describes the biophysical characterization of denatured states of rhodopsin, a model system selected to study helical membrane protein folding.

The first contribution of this thesis was to establish approaches that can be used to identify suitable conditions for studying membrane protein folding *in vitro*. This required screening different denaturing conditions to obtain maximum unfolding without causing aggregation of rhodopsin. 30% SDS and 3% SDS + 8 M urea were found to be the most suitable denaturing conditions. Next, structural features of largely unfolded states of rhodopsin under optimized denaturing conditions were systematically characterized focussing on three levels of structural resolution: global, local and site-specific. Global tertiary structure changes upon SDS denaturation were observed to correlate with SDS micellar structure changes and also hinted at formation of compact intermediate states. Local structural dynamics, probed by NMR

spectroscopy, showed that the cytoplasmic domain is more flexible than extracellular and transmembrane domains taken together in spite of an overall increase in flexibility with denaturation. Mobility studies probing site-specific changes by EPR spectroscopy, showed that specific extracellular residues retain more rigidity than cytoplasmic residues in denatured states. These results indicate that the former domain is involved in more stable interactions forming a possible folding core like structure, the location of which correlates with that described by the long-range interaction model of folding. Finally, the importance of dynamics in understanding folding mechanisms of rhodopsin led us to contribute to the development of two novel methodologies: terahertz spectroscopy to detect global motions and ^{19}F NMR using new monofluoro labels to quantify residue specific motions.

ACKNOWLEDGEMENTS

First and foremost, I would like to acknowledge my advisor, Dr. Judith Klein-Seetharaman, for believing in me and giving me the opportunity to dwell into interesting research questions under her mentorship. Judith has been a constant source of inspiration for me throughout my graduate studies. I always wished that I could work like her. I would like to thank her for giving me the freedom to think about my experiments and also for her support, optimism and encouragement in my research endeavors. One of the most wonderful things that I have learnt from Judith is how to create an appealing presentation of one's work. For this, I thank Judith's immense level of patience in doing multiple rounds of corrections for manuscripts, presentation slides, reports, posters, abstracts for conferences and countless others.

Judith has given me the opportunity to be involved in several collaborations that has led me to interact with many researchers. I would like to offer my deepest gratitude to Dr. Rieko Ishima who has helped me tremendously with carrying out ^{19}F NMR experiments and explaining the underlying concepts. Rieko has always offered her help whenever I needed it. I would like to thank Dr. Wayne Hubbell and people in his lab especially Dr. Christian Altenbach and Sheryll Mangahas for their help with EPR experiments and engaging discussions. I am thankful to Dr. Kristina Woods for introducing me to the technique of terahertz spectroscopy, which was

completely new to me. I would also like to thank Dr. Alex Doemling for synthesizing new and exciting compounds that I tested.

I have always enjoyed and learnt a lot from the discussions during thesis committee meetings. I thank my committee members Dr. Jeff Brodsky, Dr. Roger Hendrix, Dr. Linda Jen-Jacobson and Dr. Ron Wetzel for their interesting questions and helpful and exciting ideas.

I offer my thanks to labs that have been kind and helpful in sharing their instruments: Dr. Catalina Achim (stopped flow absorbance spectroscopy), Dr. Michael Trakselis (stopped flow fluorescence spectroscopy), Dr. William Furey and Dr. Guillermo Calero and Dr. Filippo Pullara (dynamic light scattering) and Dr. Roger Hendrix (refractometer). I would like to offer my appreciation for help in administrative matters to Jennifer Walker, Susanna Godwin, Dean Duncan, Janet Zambotti, Doug Bevan, Phil Greer, Amy Farell, Ian Bennet and Val Kagan. I would like to extend my thanks to Mike Delk who has always helped me set up my 'bad samples' for NMR experiments. Without him it would have been very difficult for me to even start measuring my samples.

I am thankful to my boyfriend, Kalyan for his constant love and support. I thank him for the enjoyable moments and for believing me in me when I did not. Kalyan has also been a wonderful colleague. I have enjoyed designing and discussing experiments with him, critically analyzing results, sharing exciting scientific stories and often pondering about mysteries of science in general. For my dear friends and colleagues (here and back in India): lots of thanks for being there for me. I also thank past and present members of my lab: David Man, Hussein Baradia, Harpreet Dhiman, Madhavi Ganpathiraju, Yanjun Qi, Oznur Tastan, Neelima Mulpuri, Eric Gardner, Fernanda Balem, Naveena Yanamala (extra thanks to you for helping me with NMR experiments), Subhodeep Moitra, Meghana Kshirsagar and Dr. Leelavathi Murthy.

Finally, I would like to take this opportunity to thank or to say much more than the words 'thank you' can convey to recognize the efforts of Ma and Bapi. I bow to them for everything I have learnt about hard work, discipline and humility that are helping me in shaping my life. I appreciate their support in letting me choose my career path. I love them for their unconditional affection that they have bestowed on me.

TABLE OF CONTENTS

LIST OF TABLES

LIST OF FIGURES

ABBREVIATIONS

3S8U	3% SDS + 8 M Urea
4-PDS	4,4'-dithiodipyrydine
ATR	Absorption/transmission/reflectance
BN-PAGE	Blue-native PAGE
bR	Bacteriorhodopsin
CD	Circular Dichroism
CP	Cytoplasmic
CPMG	Carr-Purcell-Meiboom-Gill
CSA	Chemical shift anisotropy
CW	Continuous wave
DEER	Double electron-electron resonance spectroscopy
DHA	Docosahexaenoic acid
DM	Dodecyl maltoside
DPFGSE	Double pulse field gradient spin echo sequence
DSS	2,2-Dimethyl-2-silapentane-5-sulfonic acid
EC	Extracellular
EPR	Electron paramagnetic resonance spectroscopy
ER	Endoplasmic reticulum
FIRST	Floppy inclusion and rigid substructure topography
GPCR	G-protein coupled receptor
GuHCl	Guanidine hydrochloride
HEK293	Human embryonic kidney
HSQC	Heteronuclear single quantum correlation
LRI	Long-range interaction
MCT-B	Midband MCT detector
MD	Molecular dynamics
MP	Membrane protein
MRE	Mean residue ellipticity
NMR	Nuclear magnetic resonance spectroscopy
PAGE	Polyacrylamide gel electrophoresis
PME	Particle Mesh Ewald
R	Dark state rhodopsin
R*	Photobleached rhodopsin
R1	(1-oxy-2,2,5,5-tetramethylpyrroline-3-methyl)-methanethiosulfonate
R_1	Longitudinal relaxation rates
$R_{1\rho}$	Spin-lock relaxation rate

R_2	Transverse relaxation rates
R_{2disp}	Constant time CPMG relaxation rate
R_h	Hydrodynamic radius
RP	Retinitis Pigmentosa
SAS	Solvent accessible surface area
SDS	Sodium dodecyl sulfate
T1	Longitudinal relaxation time
T2	Transverse relaxation time
TET	Trifluoroethylthiol
tet	Tetracycline
TetR	Tet repressor
TFA	Trifluoroacetic acid
TFE	Trifluoroethanol
THz	Terahertz
TM	Transmembrane

1.0   CHAPTER 1: INTRODUCTION

1.1   BACKGROUND OF MEMBRANE PROTEIN FOLDING

Membrane proteins (MPs) play an important role in controlling the overall homeostasis of an organism and have become important drug targets because they act as communication gates for biological signals between the cell and its environment. Like soluble proteins, in order to carry out their functions, MPs need to adopt a functional three-dimensional structure. Understanding the facets of structure and the manner in which structure is formed are important in understanding functional properties of proteins. The mechanism by which proteins adopt a structure is by folding their linear polypeptide sequence by means of a network of inter-residue interactions. The failure to adopt such a functional structure or in other words misfolding of proteins leads to many diseases that are collectively called misfolding or conformational diseases. Apart from importance in understanding function, characterization of folding pathways of proteins can also enhance understanding of misfolding diseases and ways to counter them. The mechanisms of folding of proteins belong to the most challenging questions in protein biochemistry. A lot of progress has been made in understanding soluble protein folding such as forces that drive their folding, thermodynamic-kinetic details of folding pathways leading to detection of folding intermediates and forces that stabilize native structure. However, the way MPs fold into their functional structure is much less understood as compared to soluble proteins.

This is largely due to technical difficulties in working with a system that is buried in the membrane environment (details are discussed in Section 1.1.2.2). Most of the efforts in the field of MP folding are carried out *in vitro* and are focused on optimizing conditions required for thermodynamic analyses of folding (details are explained in Sections 1.1.2.3 and 1.1.2.4). Although it is an important endeavour, due to the difficulties associated with this type of analysis, other studies have been neglected, ultimately causing the field of MP folding to lag behind. Hence, along with existing approaches other avenues are necessary to garner as much information as is practically feasible to increase our understanding of folding mechanisms of MPs. The approach that we have undertaken towards this goal is to determine structural characteristics of denatured states of MPs *in vitro*. These are unfolded states obtained by chemically inducing proteins to unfold their structure. Characterization of these states may reveal information on early intermediates in folding.

We have taken rhodopsin, a helical MP, as a model system to study folding of MPs. Rhodopsin is a dim light photoreceptor in the retina and is the most well-studied G-protein coupled receptor (GPCR). It is the first among the few GPCRs for which a crystal structure has been determined (Palczewski et al., 2000). Further, extensive biochemical and biophysical studies have been done, which provide detailed detailed structural and functional information, are available making rhodopsin a very good model system for our studies. The information available makes it convenient to identify sites for introduction of biophysical probes and analysis of their behavior in structural studies. Moreover, most of the advances in MP folding have been with bacterial MPs so far. Therefore, to understand folding of mammalian helical MPs, rhodopsin is an ideal model. Further, folding studies of rhodopsin will also aid in understanding misfolding disease mechanisms as its misfolding causes Retinitis Pigmentosa (RP), a retinal

degenerative disease. An outline of the structure and function of rhodopsin and its misfolding disease, RP, are provided in Sections 1.1.1.1. and 1.1.1.2. Very few chemical denaturation studies of rhodopsin have been reported earlier and these are discussed in Section 1.1.1.3. and 1.1.2.4. Based on previous studies on folding and stability of rhodopsin, a folding model for helical MP has been hypothesized. This is discussed in Section 1.1.2.4.

In this thesis, folding studies on rhodopsin were carried out first by optimizing denaturing conditions suitable to study largely unfolded and unaggregated states. This was necessary since a systematic approach had been lacking, hampering *in vitro* folding studies of MPs. Following this, biophysical experiments were performed to structurally characterize denatured states at different levels of resolution: global, local and site-specific. Such a characterization has provided information on the nature of interactions that may also have relevance for unfolded states of rhodopsin *in vivo*.

1.1.1 Rhodopsin as a model system

1.1.1.1 Rhodopsin: Structure and Function

Rhodopsin is present in the discs of the outer segment of rod photoreceptor cells in the retina and helps us to see under dim light conditions. It constitutes ~85% of the total protein in the rod outer segment. A chromophore, 11-*cis* retinal, that acts as an inverse agonist is covalently bound to Lys296 in the transmembrane (TM) domain of rhodopsin via a protonated Schiff base linkage stabilized by the counter-ion Glu113 (Bownds, 1967). The chromophore-protein interaction is responsible for the 500 nm peak observed in absorption spectra of rhodopsin along with the 280 nm protein peak. On light activation of rhodopsin, 11-*cis* retinal isomerizes to all-*trans* retinal. This event is followed by the formation of a number of intermediates ending with meta-II that

then decays to opsin and all-*trans* retinal. The meta-II state is the active state of rhodopsin that interacts with the G-protein, transducin, and triggers the visual cascade. Within minutes after light-activation, rhodopsin is regenerated from opsin with a new molecule of 11-*cis* retinal. Rhodopsin can now be activated again by light. For a review of the pathways that occur during visual signaling, see (Molday, 1998). Rhodopsin is an integral MP with seven TM helices, the extracellular (EC) domain extending into the intradiscal space and the C-terminus facing the cytoplasmic (CP) domain as shown in the secondary structure representation of rhodopsin in Figure 1.A. About 50% of the total protein is TM domain and ~25% is CP and intradiscal domains each. Based on its 7TM structure, it belongs to a family of membrane receptors, the GPCRs. GPCRs are cell surface receptors that respond to a variety of signals e.g. light, chemicals, hormones, etc. The 3D structure of rhodopsin with its TM helices arranged in a bundle and its EC and CP domains as loops is shown in Figure 1.B. Figure 1.C. shows the complex overall shape of rhodopsin. About 3% of all human genes are GPCRs (Bourne and Meng, 2000). Rhodopsin is the first GPCR to be crystallized leading to a detailed understanding of its structure-function relationship (Palczewski et al., 2000). Rhodopsin is a prototypic member of the GPCR family.
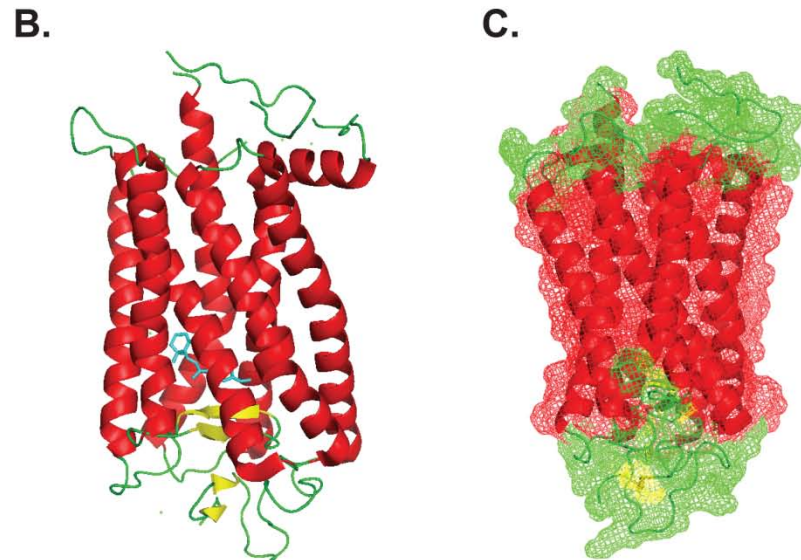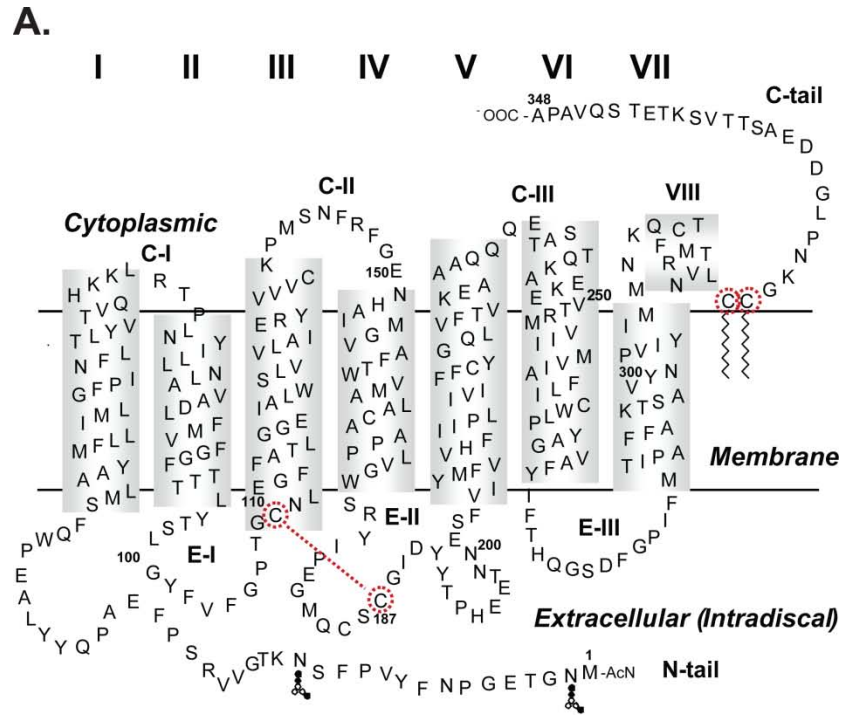
Figure 1: Secondary and tertiary structure of rhodopsin

A. Secondary structure representation of rhodopsin. Disulfide bond between cysteines at positions 110 and 187 is shown in red dotted line and palmitoylation sites at Cys322 and Cys323 are encircled in red. B. 3D structure of rhodopsin (PDB ID: 1L9H) showing TM helices in red, loops in green, β-sheet in yellow and 11-*cis* retinal in cyan. C. 3D structure of rhodopsin in mesh representation showing the shape of rhodopsin.

1.1.1.2 Rhodopsin misfolding in Retinitis Pigmentosa

Mutations in rhodopsin that cause it to misfold are implicated in the retinal degenerative disease, RP (RetNet: http://www.sph.uth.tmc.edu/Retnet/disease.htm#03.202d). RP is a disorder that causes night blindness and leads to progressive loss of vision in later life due to a gradual loss of rod and cone photoreceptor cells. About 1 in 4000 people in the world is affected by this disease (Hartong et al., 2006). In 50-60% of the cases reported so far, RP is inherited as autosomal recessive, 30-40% cases are autosomal dominant and 5-15% cases are due to X-linked inheritance. About 45 genes have been identified in which mutations cause the disorder. However, these genes account for only 60% of the cases, the rest remains unidentified. Mutations in rhodopsin, highlighted in purple in Figure 2, are responsible for 25% of autosomal dominant cases (RetNet: http://www.sph.uth.tmc.edu/Retnet/disease.htm#03.202d). According to the human gene mutation database, more than 100 rhodopsin mutations are known to cause autosomal dominant RP (Krebs et al., 2010). Most of these mutations lead to misfolding and/or instability of rhodopsin as a result of which it is retained in the endoplasmic reticulum and is incapable of binding to its chromophore 11-*cis* retinal (Sung et al., 1991; Sung et al., 1993; Kaushal and Khorana, 1994). Thus, absence of correctly folded rhodopsin in the rod outer segments is one of the major causes of death of rod cells in autosomal dominant cases (Mendes et al., 2005).

Limited understanding of the mechanisms by which gene mutations cause RP has been a major hindrance in designing effective therapies. Several lines of treatment for RP have been proposed. Increasing concentrations of 11-*cis* retinal can partly rescue folded rhodopsin (Noorwez et al., 2004) and response from RP patients towards dietary supplements of Vitamin A, the precursor of 11-*cis* retinal, has been reported (Li et al., 1998). Another avenue for RP

treatment is docosahexaenoic acid (DHA), the most abundant fatty acid present in the membranes containing rhodopsin, which has also been shown to slow down RP progression via an unknown mechanism (Berson et al., 2004b; Berson et al., 2004a). A variant of 11-*cis* retinal,
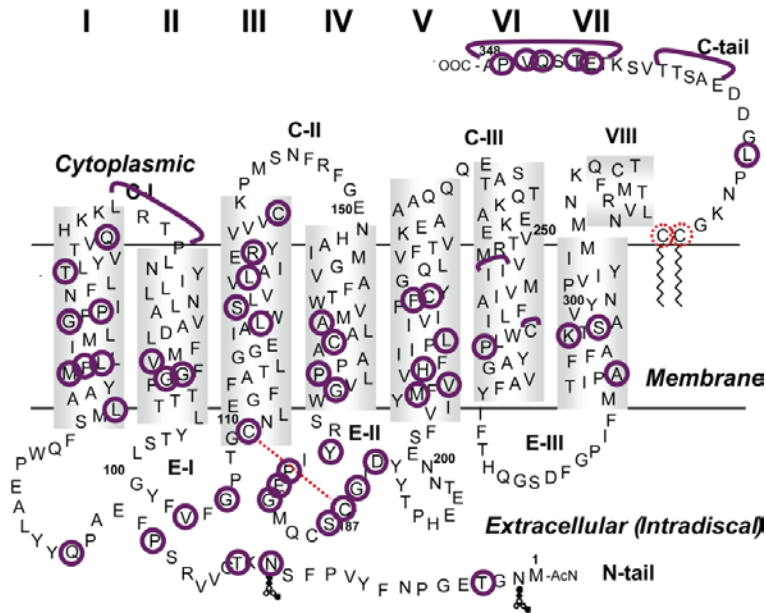
Figure 2: Retinitis Pigmentosa mutations in rhodopsin

Secondary structure representation of rhodopsin with residues responsible for RP highlighted in purple. Residues encircled in purple undergo point mutations and those marked with a purple line undergo deletions in RP. A disulfide bond between cysteines at positions 110 and 187 is shown in red dotted line and palmitoylation sites at Cys322 and Cys323 are encircled in red.

11-*cis*-7-ring retinal has been recently reported to trigger folding of the RP mutant P23H *in vivo* (Noorwez et al., 2003). Recently, retinobenzaldehydes, non-retinal like molecules, have been shown to be effective in properly trafficking P23H mutant rhodopsin in cells (Ohgane et al., 2010). These findings of pharmacological chaperones rescuing rhodopsin from its misfolded form have fueled hopes to find a treatment for RP. However, to date there is no cure for RP. An understanding of folding mechanisms of rhodopsin may help design effective strategies to combat RP by providing deeper insights into the underlying causes of misfolding.

1.1.1.3 Folding studies of rhodopsin

In order to understand the folding mechanism of rhodopsin, folding studies in the cell, *in vitro* and *in silico* have been carried out (for details see Section 1.1.2.4.). The cellular studies involved a fragment based experiment in which sets of fragments containing different numbers of TM helices separated at specific loops were cotransfected and were found to bind 11-*cis* retinal to form rhodopsin. These studies have shown that a minimum of three helices are required to form a folding domain (Ridge et al., 1995a). *In silico* studies simulating thermal denaturation of rhodopsin showed that long-range interactions between residues in the TM and EC domains form a rigid folding core at the end of thermal denaturation (Rader et al., 2004; Tastan et al., 2007). *In vitro* experiments were carried out in native rod outer segment membranes by single molecule force spectroscopic methods. These studies identified regions of rigidity during unfolding rhodopsin and found them to correlate with that observed in *in silico* experiments, i.e. in the EC ends of TM helices and EC loops (Sapra et al., 2006; Sapra et al., 2008). These studies gave rise to the long-range interaction (LRI) model of folding of helical MPs which hypothesized that long-range interactions between helices and loops are essential in early stages of folding of rhodopsin (Klein-Seetharaman, 2005). This model necessitates a detailed characterization of denatured states to characterize the possible interactions in early stages of folding of rhodopsin. Denatured states are the closest to the unfolded states in the cell, from which a protein begins to fold, that can be achieved *in vitro*. Thus, properties of denatured states and thermodynamic and kinetic characteristics of the pathway of denaturation and renaturation may reflect on the actual pathway occurring in the cell. One way to obtain denatured states is by chemically denaturing a protein. Chemical denaturation studies of rhodopsin to understand its folding are lacking in the literature. A few reports on the use of denaturants guanidine hydrochloride (GuHCl) and urea

exist but the effect of such denaturants is only described in the context of understanding conformational changes in rhodopsin upon activation and stability in native membranes (Hubbard, 1969; Shichi, 1973). These studies are not aimed at understanding the folding mechanisms of rhodopsin *per se*.

GuHCl denaturation of rhodopsin in vesicles formed from rod outer segments showed greater stability of rhodopsin in its native environment compared to that in delipidated outer segments and that without 11-*cis* retinal (Shichi, 1973). The former was observed to denature only beyond 4 M GuHCl, the mid-point of denaturaiton curve of the former was 5M GuHCl and the total decrease in mean residue ellipticity (MRE) at 222 nm, which reports on the amount of helicity, was ~50%. Delipidated and retinal free rhodopsin sample was shown to denature from 1 M GuHCl onwards with the mid-point of transition being 3.5 M GuHCl and total decrease in MRE at 222 nm was 50%. Rhodopsin in its native environment was shown to refold to a much greater extent than the latter. In another report, GuHCl denaturation of rhodopsin in 2% digitonin were carried out to identify the origins of different absorption maxima that arise due to interaction of 11-*cis* retinal with rhodopsin in native, acidic and light activated conditions (Hubbard, 1969). Changes in absorbance at 500 nm were followed after addition of different concentrations of GuHCl. No changes in secondary structure on urea and GuHCl denaturation were reported. Two different effects were seen on GuHCl denaturation based on absorbance spectra of retinal protein contacts. These are rapid reversible effect and slower irreversible effect. The former effect was seen when rhodopsin was titrated by GuHCl from 2.2 M to 6.2 M. A slight change in absorbance maxima from 499 nm to 495.5 nm was seen which could be reversed by lowering GuHCl concentration. The slower change was seen over time when rhodopsin was incubated with 6.2 M GuHCl. A peak at 445 nm was seen which corresponded to protonated

Schiff base of retinal in solution and slowly converted to 362.5 nm which corresponds to free Schiff base in solution and was reported to be stable for 75 min. At a pH of 6, where the experiments were done, Schiff base of retinal is not expected to be protonated due to its low pKa but the existence of a protonated Schiff base on denaturation which gradually loses its proton indicates that the chromophore was protonated in the native state. The observation of a Schiff base in denatured states indicate that the retinal remains attached to its binding site in rhodopsin in these states as it is not hydrolysed. Hydrolysis of Schiff base of retinal in solution was seen to occur in 15 min with free retinaldehyde (Pitt et al., 1955). This is proposed to be due to the fact that 6 M GuHCl lowers the activity of water to such an extent that hydrolysis of retinal in denatured rhodopsin does not occur (Hubbard, 1969).

The effect of urea on absorbance at 500 nm showed that even at 8 M concentration, it has no effect on rhodospin (Abrahamson and Ostroy, 1967). It was reported that opsin is more unstable towards urea denaturation than rhodopsin since urea begins to denature opsin based on decrease in absorbance at 500 nm at low concentration of 1 M (Hubbard, 1969). When compared to GuHCl, urea denatures opsin at much lower concentration than GuHCl, the latter begins to denature at 3.5 M (Hubbard, 1969). Recently, denaturation of opsin, the apo form of rhodopsin, in phospholipids bicelles with urea was reported (McKibbin et al., 2009). It was shown that denaturation of opsin in phospholipid/detergent mixed micelles of DMPC/CHAPS with 4M urea leads to an irreversible unfolding, corresponding to a decrease of 50% in helical content of opsin. A two-fold decrease in tryptophan fluorescence was also observed under the same conditions. Unfolding kinetics were measured from changes in tryptophan fluorescence with increase in urea concentration and the rate of unfolding was found to be dependent on urea concentration (McKibbin et al., 2009). Opsin in bicelles of different phospholipid/phospholipid mixtures

showed different stability towards urea denaturation. This suggests that lipid interaction of MPs is important in unfolding studies.

1.1.2   Membrane protein folding

1.1.2.1 Significance

In humans, MPs constitute one third of all proteins (Takeda et al., 2002). Important MP families are receptors, transporters, ion channels, pumps, and proteins with structural roles or enzymatic activity. Understanding folding mechanisms of such proteins is important from a fundamental perspective. In cells, folding pathways of MPs and soluble proteins begin to diverge from the time they emerge from the ribosome and pass through the translocon (von Heijne, 2006). The translocon is a channel in the endoplasmic reticulum (ER) membrane allowing the entry of proteins into the ER for post-translational modifications and then to be transported throughout the cell (Crowley et al., 1994; Alder and Johnson, 2004; Rapoport et al., 2004). MPs remain associated with the translocon for translocation to the ER membrane while soluble proteins pass through it to enter into the lumen of the ER for further events in their folding process. It is still not clear whether MPs begin to fold in the translocon and if they are partially or completely folded before entering into the ER membrane. It is very difficult to study folding pathways of MPs inside the complex environment of the cell, particularly with the participation of the translocon. A more tractable way to study folding of MPs is to denature them using chemicals or temperature and study their unfolding pathway *in vitro*. This also enables structural characterization of denatured states. Such studies are only possible *in vitro* and can give insights into early folding states of a protein. Through these studies, propensities of unfolded states to either remain completely unfolded or to form non-native interactions can be determined. Such *in*

vitro studies can then be correlated with *in vivo* findings. Such a correlation has been reported previously for rhodopsin where molecular findings probing structural aspects of certain RP mutants were shown to be related to the severity of the disease seen in patients (Iannaccone et al., 2006).

From a pharmacological point of view, an understanding of the folding mechanism of MPs may help in identifying avenues for the treatment of misfolding diseases that are caused by MPs (Sanders and Myers, 2004). In the field of soluble proteins, characterization of unfolded states has been crucial in understanding mechanisms of folding and indeed has shed light also on misfolding diseases (Dobson, 2001; Chiti and Dobson, 2009). An important conclusion is that even under strongly denaturing conditions some inter-residue interactions, either native-like or non-native and especially those among hydrophobic residues, are present in the unfolded state (Klein-Seetharaman et al., 2002a). Such interactions constitute residual structure in denatured states and are assumed to form during the early stages of folding of a protein, playing a crucial role for folding by acting as a folding nucleus (Klein-Seetharaman et al., 2002a). Non-native interactions of unstructured peptide fragments for example are believed to play a major role in amyloid formation in Alzheimer's disease (Harper and Lansbury, 1997). In principle, any protein sequence has an intrinsic propensity to aggregate, and even form amyloid fibrils (Dobson, 2001), but point mutations can enhance this propensity as has been shown for example for transthyretin and lysozyme (Booth et al., 1997; Sekijima et al., 2005). While these mutations do not alter the structure of the folded state, they change structure and stability of unfolded states and result in accumulation of folding intermediates (Booth et al., 1997; Canet et al., 1999). Based on the characterization of these folding intermediates, therapeutic strategies have been proposed such as blocking fibrillar growth by β-sheet breaker peptides (Soto et al., 1998) and stabilizing native

structure of these proteins by small molecules (Johnson et al., 2005; Ray et al., 2005; Soldi et al., 2006).

In the case of MPs, there are several pathological conditions that are related and possibly causally linked to their misfolding such as cystic fibrosis, Charcot-Marie-Tooth disease, hearing loss, and RP (Sanders and Myers, 2004). The strongest molecular evidence for misfolding as the underlying disease mechanism is for RP, a retinal degenerative disease. *In vitro* data testing folding and stability of certain RP mutations were shown to correlate with the severity of the disease in RP patients (Iannaccone et al., 2006). Mutations in rhodopsin, which is responsible for dim light vision, account for RP in 25% of patients (Hartong et al., 2006). No cures for RP or any other MP misfolding disease have yet emerged, highlighting the urgency in enhancing our understanding of folding pathways of MPs.

1.1.2.2 Challenges

How the three dimensional structure of a protein is formed as it emerges from the ribosome in an unstructured or partially structured state has always been the most intriguing question in biochemistry. Tremendous progress has been made in answering this question for soluble proteins (see Section 1.1.3). However, it still remains challenging to address this issue for MPs. Why has progress towards understanding folding mechanisms of MPs greatly lagged behind that of soluble proteins? *In vitro* folding/unfolding studies of proteins usually involve denaturing them, analyzing the denatured structure and then refolding them back to their native state. Each of these steps has its own set of challenges in the case of MPs.

a) Denaturation – The first step of perturbing such protein systems, i.e. unfolding or denaturing them with chemicals or other means, is difficult due to their high stability in the hydrophobic environment of the membrane. In order to accommodate the hydrophobic nature of

MPs *in vitro*, they need to be reconstituted in a detergent or lipid environment to maintain their functionality. This, in turn, renders them resistant towards denaturation. Hence, *in vitro* folding/unfolding studies of MPs require optimization of denaturing conditions that would lead to a significant degree of unfolding. Chemical denaturants such as urea and GuHCl that are effective in unfolding soluble proteins may not be effective against MPs. On the other hand, denaturants such as SDS and organic solvents such as trifluoroethanol which have the potential to solubilize hydrophobic stretches may prove to be more effective. However, these unfolded states are very prone to irreversible aggregation. TM regions of MPs on unfolding show tendency to aggregate due to exposure of large regions of hydrophobicity. A denaturing condition that leads to a large extent of unfolding may not be suitable if it also leads to aggregation of the protein. Thus, screening different denaturing conditions to identify optimal unfolding that does not lead to aggregation is very important; otherwise experiments characterizing the denatured states will suffer from aggregation artifacts.

b) Biophysical characterization – The second step of folding studies which involves characterization of denatured states requires application of biophysical methods. Conducting biophysical studies with MPs in general has been challenging due to the large size of MPs and the associated lipids or detergents; lipids and detergents furthermore add background noise to the protein spectra. These factors can also interfere during characterization of denatured states of MPs. Further, the interaction of denaturants with lipid and detergent molecules and/or with biophysical probes may complicate interpretation of biophysical measurements.

c) Refolding – The third step of folding studies is refolding from denatured states. Reversibility of an unfolding process confirms that intermediates observed during unfolding are on-pathway and the unfolded state obtained is a state from which the native protein can be

formed. Reversibility also enables reliable measurement of thermodynamic parameters such as enthalpy and free energy of folding and also provides greater detail about the nature of transition states. While reversibility of unfolding is crucial for kinetic and thermodynamic studies of folding, it is not a requirement for biophysical characterization of denatured states where the goal is to determine the propensities of interaction among residues in a largely unfolded state. The primary requirement for the study of unfolded states is long-term stability of these denatured states of interest, i.e. absence of aggregation. Further, the extent of unfolding is important. In order to catch a glimpse of the earliest stages in folding, proteins should be denatured to the maximum possible extent and then characterized.

1.1.2.3 Denaturation studies of helical membrane proteins other than rhodopsin

Seminal work on folding of MPs was carried out with bR (Huang et al., 1981). bR is a light driven proton pump in the purple membrane of *Halobacteria salinaria*. It consists of seven TM α-helices that are connected by short loops and a retinal chromophore covalently bound to a lysine residue. bR is the first MP to be successfully refolded into phospholipids via transfer into sodium dodecyl sulfate (SDS) micelles after denaturation by trifluoroacetic acid (TFA) (Huang et al., 1981). The possibility of refolding bR *in vitro* from denatured states has established bR as a model system for studying thermodynamic and kinetics of folding of helical MPs (Booth and Curnow, 2006). However, subsequent studies have refolded bR from a partially SDS denatured state which retain a large amount of residual helical structure (Curnow and Booth, 2007). Free energy of unfolding of bR by SDS was estimated from both kinetic and thermodynamic studies and were found to be similar (Curnow and Booth, 2007). Thus, it was concluded that refolding from an SDS induced denatured state is a two-state process (Curnow and Booth, 2007). Both free energy of unfolding and logarithm of rates of folding and unfolding were reported to be linear

with SDS concentration (Curnow and Booth, 2007). The latter again supports a two-state folding process.

Kinetic studies of refolding bR from an SDS-denatured state into lipid/detergent micelles have enabled detection of folding intermediates in its folding pathway (Booth et al., 1995; Booth et al., 1996; Booth and Farooq, 1997; Riley et al., 1997; Allen et al., 2004b; Curnow and Booth, 2007). Kinetic studies also showed that the transition state during SDS unfolding is close to the unfolded state. A detailed picture of the transition state was provided by Φ value analysis which investigates the folding transition. Φ values represent the effect of a single point mutation on the extent of folded and unfolded regions in the transition state of folding by measuring the change in the overall free energy change of folding (Fersht et al., 1992; Daggett and Fersht, 2003). bR is the only α-helical MP so far to satisfy the requirements of Φ value analysis since it can be reversibly unfolded (Curnow and Booth, 2009). Such studies have been done on a single helix, the second TM helix, of bR so far (Curnow and Booth, 2009). The second TM was selected because it is implicated to form early during folding of bR and is not involved in extensive contacts with retinal. Both equilibrium and kinetic measurements of free energy of unfolding of an alanine scan of the second TM helix were carried out (Curnow and Booth, 2009). High Φ values were observed for most parts of this helix indicating native interactions in this helix in the transition state (Curnow and Booth, 2009). Folding energetics of bR were also studied by means of double mutant cycle analysis to determine the contribution of H-bonds to stability of MPs (Joh et al., 2008). H-bonds are considered to be important intramolecular forces in membranes due to the absence of competition from water molecules and the low dielectric constant of the membrane environment (White, 2005). H-bonds may therefore play an important role in MP folding and stability. Eight positions involved in inter-helical H-bonds in the bR crystal structure

and single and double mutants of these sites which could be expressed and purified were studied (Joh et al., 2008). The contribution of each of the H-bonds individually is variable depending on the location of the H-bonds but the strength of the H-bond is not strongly correlated with its location. The average contribution of these interactions was found to be low, that of 0.6 kcal mol^{-1}. Thus, H-bond interactions have a modest contribution in stabilizing bR.

Efforts on elucidating the folding pathways of other MPs are underway. The focus is mostly on unfolding and refolding the proteins and an in-depth characterization of the intermediates is lacking. Bacterial helical MPs for which refolding has been possible are KcsA, from a trifluoroethanol (TFE)-denatured state (Barrera et al., 2005); DAGK from SDS (Lau and Bowie, 1997), urea and GuHCl (Nagy et al., 2001), DsbB from SDS denatured state (Otzen, 2003), EmrE from a SDS + urea denatured state (Miller et al., 2009), CopA from a GuHCl denatured state (Roman et al., 2010) and LHCII complex in higher plants from a SDS-denatured state (Plumley and Schmidt, 1987; Dockter et al., 2009). In most of these cases except in bR and CopA, refolding was accomplished only from a partially unfolded, near native state. Recently, studies with opsin in phospholipid bicelles revealed a significant decrease of 50% of helical content in the presence of urea, but it could not be refolded from such a largely unfolded state (McKibbin et al., 2009). However, GuHCl denaturation of CopA that led to a substantial decrease in MRE at 222 nm by about 75% could be refolded into the native state (Roman et al., 2010). Therefore, refolding of MPs, except bR and CopA, has been feasible only from a minimally denatured state which is structurally similar to the native state but refolding becomes difficult when large portions of the structure are unfolded.

1.1.2.4 Current models of folding of membrane proteins

The field of MP folding is still at a nascent stage due to the difficulties described above. So far, folding studies on bacteriorhodopsin (bR), a bacterial MP, and rhodopsin, a mammalian MP, have led to the formulation of two different models describing helical MP folding. These are the "two-stage hypothesis" (Popot and Engelman, 1990) and "long-range interactions hypothesis" (Klein-Seetharaman, 2005; Tastan et al., 2007).

Two-stage model of folding

The two-stage model of folding is based on folding studies on bR. It was observed that bR could be refolded from independent helical fragments in lipid-detergent mixtures (Marti, 1998). Each of these fragments consisted of different sets of TM helices of bR and was expressed independently in E. coli. These fragments when combined with their complimentary sets reconstituted to form the entire functional protein in a micellar environment. This indicated that the EC and CP loops of bR, which form regions of discontinuity between the different fragments, are dispensable for the folding of the protein. However, some of the loops do contribute to the stability of bR. There are also reports on chemical synthesis of individual helices of bR, where 4 of the seven helices have been synthesized, and their reconstitution with complementary fragments to form the fully functional protein (Hunt et al., 1997). Thus, the native structure of bR can be formed from either independent fragments expressed *in vivo* or individual helices synthesized *in vitro* in presence of lipids or detergents. Reconstitution from independent helical fragments is also seen in other α-helical MPs such as β-adrenergic receptor

(Kobilka et al., 1988), muscarinic receptor (Maggio et al., 1993), rhodopsin (Ridge et al., 1995b; Yu et al., 1995), NK1 receptor (Nielsen et al., 1998), α-factor STE2 receptor (Martin et al., 1999) and lac permease (Bibi and Kaback, 1990; Wrubel et al., 1990; Wrubel et al., 1994; Zen et al., 1994). All these studies, particularly those on bR, indicate that each TM fragment acts as an independent folding domain. Thus, the two-stage folding model for helical MPs was formulated. According to this model, helices are formed independently in the first stage and formation of tertiary contacts among them occur in the second stage of folding to generate the three-dimensional structure of a helical transmembrane protein (Popot and Engelman, 1990) (Figure 3). This view is also supported by the fact that insertion of single α-helices in a membrane is thermodynamically feasible.

Following the formulation of the two-stage hypothesis, questions began to be raised about the events that occur after the second stage of folding such as folding of loops, binding of prosthetic groups and oligomerization. These events are included as a third stage of folding in the three-stage hypothesis (Engelman et al., 2003). However, it should be kept in mind that this is a very simplified model explaining folding of helical MPs. It is possible that proteins do not fold in exactly three stages with independent folding of each of the helices as explained above. This was seen in folding of rhodopsin from independent fragments where one fragment with at least three helices is required for complete reconstitution of the native protein (Ridge et al., 1995a). This and other evidences, described below, necessitated the formulation of an alternative hypothesis for MP folding, the long-range interaction model.

Two-stage hypothesis

Long-range interaction model

Folding proceeds through grafting of tertiary structure onto stable helix elements

Folding involves tertiary interactions within and between helices and loops

Folded bacteriorhodopsin

Folded mammalian rhodopsin
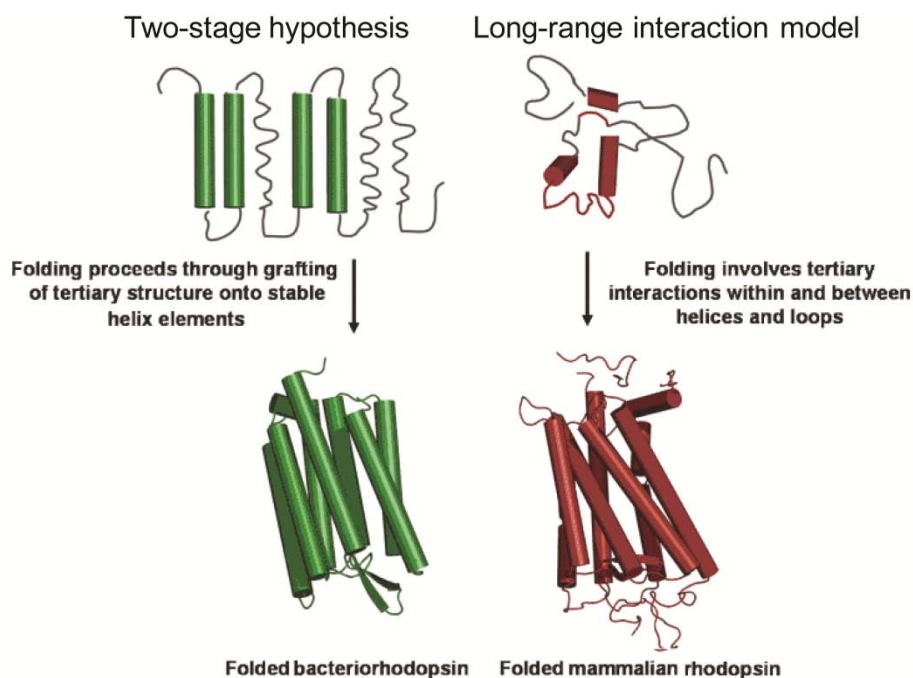
Figure 3: Models describing folding of helical MPs.

Two-stage theory of folding depicting the formation of independent helices followed by formation of their tertiary contacts to form the native structure. Long-range interaction theory of folding depicting the formation of tertiary interactions between different regions of a protein to form a non-native structure that triggers folding of the whole protein. As these folding models are largely based on folding studies of bR and rhodopsin, these protein structures are shown here as representative MPs (Tastan et al., 2007).

LRI model

Rhodopsin shares structural similarity but no sequence similarity with bR. However, in contrast to bR, its folding cannot be fully explained by the two- and three-stage hypotheses. *In vitro*, cell based and computational folding studies with this protein have suggested that interactions between EC and TM domains are important in the early stages of folding (Ridge et al., 1995a; Rader et al., 2004; Klein-Seetharaman, 2005; Tastan et al., 2007; Sapra et al., 2008). Folding studies of rhodopsin that are not consistent with the two-stage theory are described below.

a) Cell based studies

i) Rhodopsin cannot be refolded from individual helical fragments, unlike bR, and it is possible to refold it only in cells from a subset of fragments containing at least three helices (Ridge et al., 1995a). Therefore, helices in rhodopsin do not act as independent folding domains but inter-helical interactions along with participation of loops are necessary during folding.

ii) Refolding of rhodopsin from helical fragments has only been shown from fragments that are separated in the second and third CP loops indicating the indispensability of the remaining loops in the folding process (Ridge et al., 1995a).

iii) The fact that mutations in the loop regions of rhodopsin cause complete misfolding cannot be explained if it is considered that the loops fold only after formation of the helices, which is proposed in the three-stage hypothesis. Thus, loops appear to be indispensable for folding. Extensive mutation data are available for EC loop residues showing that mutations are not well tolerated in this domain (Doi et al., 1990; Anukanth and Khorana, 1994). Many of the point mutations that cause RP occur in EC loops and not in CP loops indicating the importance of the former region in folding of rhodopsin (a list of such mutations are provided in (Tastan et al., 2007)). This contrasting behavior of the two domains indicates the importance of EC loops in folding of rhodopsin.

iv) A disulfide bond present at the junction of EC and TM domains is crucial for stability of rhodopsin (Karnik and Khorana, 1990). Further, mutations in the TM and EC domains leading to misfolding also carry a wrong disulfide bond (Garriga et al., 1996; Hwa et al., 1997). Both these evidences indicate that TM helices and EC domain are structurally coupled.

b) In silico studies

A computational method, Floppy Inclusion and Rigid Substructure Topography (FIRST), was used to predict interresidue interactions that may be important in early stages of folding of MP (Rader et al., 2004; Tastan et al., 2007). The FIRST method involves breaking H-bonds in a protein in order of their increasing strength and identifying rigid and flexible regions in the protein at each step (Jacobs et al., 2001). The most rigid cluster that remains towards the end of denaturation is defined as the cluster containing at least three residues that are part of two or more secondary structures. This cluster is representative of a 'folding core' which is a structure that is formed in the early stages of folding of a protein to help initiate the process of folding. This computational simulation of thermal denaturation was reported for rhodopsin (Figure 4.A.) where it was shown that TM helices in rhodopsin do not unfold independently of each other and at the end of the unfolding process rigid regions remain, the largest of such regions consist of residues from EC loops and TM helices (the last line in the dilution plot in Fig. 4.A.). The folding core, when mapped onto the crystal structure of rhodopsin (PDB ID 1L9H), lies at the interface of the EC and the TM domains and includes the disulfide bond, indicating the potential importance of these regions in folding of rhodopsin (Figure 5). Mutations of more than 90% of the residues in the folding core cause misfolding of rhodopsin, underlining the importance of the core (Rader et al., 2004). These studies support the theory that interactions between EC and TM domains are necessary for forming a stable core that then triggers formation of the native structure of rhodopsin. On the other hand FIRST studies of bR showed that each helix unfolds as an independent domain (Figure 4.B.).
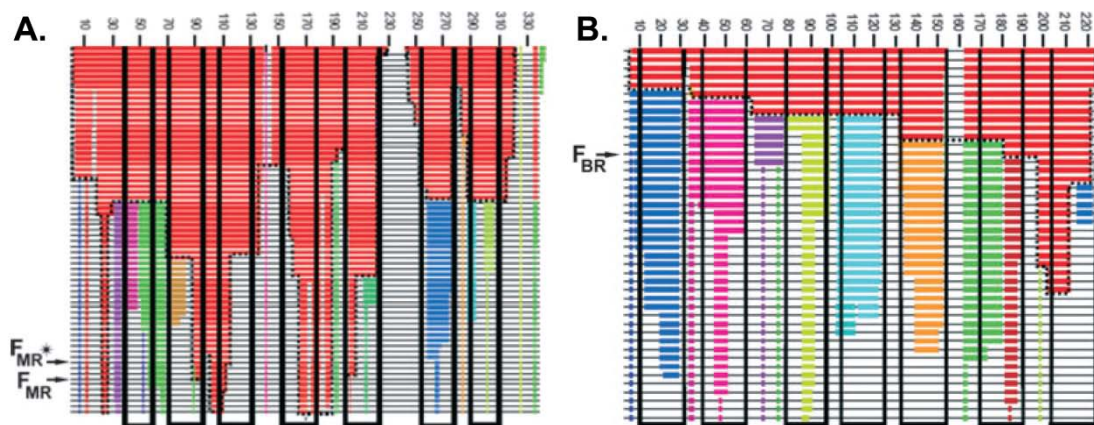
Figure 4: Dilution plots for rhodopsin and bacteriorhodopsin.

Dilution plots for rhodopsin (A) and bR (B) are shown (Tastan et al., 2007). Each thin black line represents residues with a flexible backbone, and each colored block identifies which rigid cluster a residue belongs to. Red color represents the largest rigid cluster in both the dilution plots. As one moves down these dilution plot, hydrogen bonds are removed one at a time based on energy. Lines are shown only when there is a change in the backbone rigid clusters. TM helices are shown as thick black outlines. The lines of the folding cores of bR and mammalian rhodopsin are marked as F_{BR} and F_{MR} respectively.
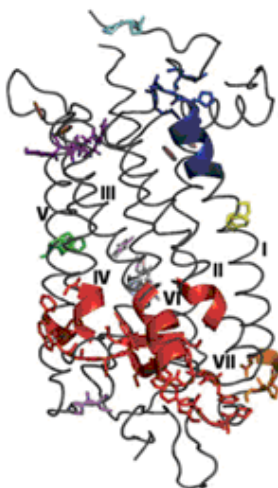
Figure 5: Folding core residues mapped onto 3D structure of rhodopsin.

Helices are numbered from I to VIII. Each color represents a set of equally rigid regions. The largest cluster of rigid residues is shown in red (Tastan et al., 2007). These colors correspond to the colors shown in the dilution plot in Figure 4.

c) In vitro studies

In vitro folding studies have been done with rod outer segment membranes using single molecule force spectroscopy and dynamic force spectroscopy (Sapra et al., 2006; Sapra et al., 2008). These methods involve unfolding a protein by pulling it from one end with a cantilever and measuring the resulting deflections of the cantilever. From the deflections, a force-distance curve is obtained showing the force required to pull a particular protein segment which in turn reflects the rigidity or stability of the segment. Different segments get unfolded with different force as the pulling continues from one end to the other depending on the strength of their intermolecular interactions. Single molecule force spectroscopy studies indicated the role of loops in structuring TM helices in rhodopsin (Sapra et al., 2006). The N-terminal region shows two independent segments with a high degree of stability, not seen in any other MP in a comparable region. Most of the stable structural segments observed on pulling span across both TM helices and loops. Rigid structural segments discovered by dynamic force spectroscopy were found to agree with that of the folding core residues identified by FIRST.

Based on all these evidences in sections a), b) and c) supporting the participation of EC loops along with TM helices in folding, a new theory, the LRI theory of folding, has been formulated. According to this theory, interactions between residues far apart in sequence are established to form a folding core during the initial stages of folding of a MP (Klein-Seetharaman, 2005) (Figure 3). These interactions may be helix-helix, helix-loop and/or loop-loop contacts that initiate the process of folding.

1.1.3 Comparison of the folding of membrane and soluble proteins

The Levinthal's paradox states that a polypeptide chain has innumerable possible conformations and if it was to search systematically the entire conformational space to attain a native state then this would take an astronomical length of time (Levinthal, 1968). Therefore, there are discrete pathways that are followed to simplify the search for the native state. For the folding pathways of soluble proteins mainly three folding models have been formulated: framework model, hydrophobic collapse model and nucleation-condensation model (Daggett and Fersht, 2003). The framework model depicts formation of independent secondary structure elements by local interactions during folding (Kim and Baldwin, 1982). In the hydrophobic collapse model, folding is triggered by the hydrophobic effect leading to interaction among hydrophobic residues to form the protein interior core and subsequent folding of the entire protein (Rackovsky and Scheraga, 1977; Dill, 1985). These two classical models of folding were combined by the nucleation-condensation model whereby a nucleus consisting of inter-residue contacts is formed that initiates folding (Abkevich et al., 1994). The "two-stage hypothesis" of folding of MPs described in Section 1.1.2.2 (Popot and Engelman, 1990) which postulates formation of independent TM helices as a first step in folding of helical MPs bears similarity to the framework model. The LRI model (Klein-Seetharaman, 2005) described in Section 1.1.2.4. that postulates a folding core in MPs bears similarities to the nucleation-condensation model.

A 'new view' of folding of soluble proteins was formed based on statistical mechanical models of folding whereby folding is considered to occur in a funnel shaped energy landscape (Bryngelson et al., 1995). The concept of energy landscape describing free energy of a polypeptide chain as a function of protein conformation and that folding occurs in discrete pathways down the funnel arises from the above Levinthal's paradox (Levinthal, 1968). The

25

funnel shape of this landscape indicates the large number of conformations accessible to a polypeptide chain as it begins to fold at the top of the funnel and a decrease in the number of possible conformations as the native state is approached at the bottom of the funnel. Such a folding funnel has been shown for soluble proteins so far. MP folding can be considered as proceeding down a funnel (Bowie, 2005) as is indicated by multiple folding pathways of bR (Lu and Booth, 2000). Presence of different unfolded states, as in the top of a folding funnel, was also hinted at during FIRST simulated unfolding of bR where different helices from different bR crystal structures unfolded early (Tastan et al., 2007). The major difference as compared to the soluble protein folding funnel is that folding of MPs begins from a more structured unfolded state than that of soluble proteins as shown by the difficulties in obtaining a completely unfolded state *in vitro* for most MPs (Bowie, 2005). Therefore, unfolded states in MPs are further towards the bottom of the funnel, closer to the native state. An additional factor that is different in MP folding funnels is the effect of the lipid bilayer on the properties of the former since it has been shown that composition of the bilayer influences folding pathways of bR (Allen et al., 2004a).

For soluble proteins, folding pathway down the funnel is either thermodynamically or kinetically controlled (Baker and Agard, 1994). For many soluble proteins the native structure is thermodynamically stable i.e. the native structure of a protein is the most stable structure and folding proceeds in a direction to attain a global free energy minimum (Anfinsen, 1973). However, Levinthal pointed out that protein folding occurs very fast and in a small fraction of time it is not possible to scan all possible conformations (Levinthal, 1968). Therefore, in the large conformational space available to a polypeptide chain, there may be kinetically inaccessible conformations where the protein is more stable leading to formation of a native state which may not be the most stable thermodynamically, in which case folding is said to be

kinetically controlled (Baker and Agard, 1994). Compared to soluble protein folding, very few studies on MP folding have been done to generalize their folding and ascertain into kinetic or thermodynamic control. Experimental studies on the kinetics and thermodynamics of folding are discussed below in Sections 1.1.3.1. and 1.1.3.2.

1.1.3.1 Kinetic studies

Similar to soluble proteins, a linear dependence of the folding and unfolding rate on denaturant concentration is observed during SDS induced unfolding of bR (Curnow and Booth, 2007). However, a Chevron plot of bR where the dependence of the log of folding and unfolding rate constants on SDS concentration are depicted is asymmetric as compared to that of soluble proteins. In these plots, there is a large dependence of the unfolding rate and a small dependence of the refolding rate on SDS concentration (Curnow and Booth, 2007). This low rate of unfolding in absence of denaturant in contrast to soluble proteins indicates high kinetic stability of bR (Curnow and Booth, 2007).

Another contrasting aspect of the kinetics of bR folding is the β value which is the ratio of m_u or m_f (measure of dependence of unfolding or folding rate on SDS) to the overall m (sum of m_u and m_f) and it reflects the extent of solvent accessibility and position of the transition state relative to the unfolded or folded state. The β value was found to be 0.1 for bR indicating a diffuse transition state that is closer to the SDS unfolded state (Curnow and Booth, 2007). A diffused transition state may help in binding of SDS molecules to the protein to enable its unfolding. In contrast, the β value for soluble proteins is 0.6-0.9 indicating that transition states of soluble proteins are closer to the folded state (Jackson, 1998). Φ value analysis of the second TM helix of bR showed that destabilizing mutations in this helix shifted the transition state to the unfolded state with an increase in folding activation energy (Curnow and Booth, 2009). This is in

contrast to that seen in soluble proteins where destabilizing mutations shift the transition state towards the folded state. This was explained by a possible effect of the mutations on SDS denatured states of bR since these states have considerable amount of structure, unlike the unfolded states of soluble proteins.

1.1.3.2 Thermodynamic studies

The free energy of unfolding of soluble proteins is similar to that of MPs of comparable size (Booth and Curnow, 2009). The dependence of free energy of unfolding on the denaturant concentration, given by the *m* value, is comparable between soluble proteins and MPs except where SDS has been used as a denaturant due to difficulty in excluding the effect of SDS interacting with micelles associated with MPs from that of its interaction with the MP (Booth and Curnow, 2009).

Considering the kind of forces that stabilize MPs, H-bonds were suspected to be more important than for soluble proteins due to reasons mentioned in Section 1.1.2.3. (White, 2005). However, it was shown by double mutant cycle analysis of bR that H-bonds in fact have only a modest contribution towards stability of MPs (Joh et al., 2008). This contribution is similar to that in soluble proteins with the length of the H-bonds also being similar (Joh et al., 2008; Booth and Curnow, 2009).

A computational study was done to predict changes in stability of rhodopsin by introducing known RP misfolding mutations in the available folded crystal structure of rhodopsin (Tastan et al., 2007). This was done to determine the effect of perturbation of local environment and change in physical property of the amino acids alone on the overall stability of rhodopsin. Low correlation was obtained between the computational stability data and *in vitro* folding and stability experiments of the mutants (Tastan et al., 2007). This indicates that little can be learnt

about effects of misfolding mutations from the native structure alone and the effect of such mutations on unfolded states and the folding pathway may provide more information about the contribution of individual amino acids to the stability of MPs.

1.2 SPECIFIC AIMS, ACCOMPLISHMENTS AND CONTRIBUTIONS

1.2.1 Specific aims

Folding studies of MPs is progressing at a very slow pace due to the difficulties in working with MPs described in Section 1.1.2.2. In the studies reported so far, establishing conditions for refolding and determining unfolding and refolding kinetics have been the primary aims. Little mechanistic insights has been gained and an in depth structural characterization of unfolded states of MPs has not been attempted. Yet it is the analysis of residual structure in denatured states that will provide much needed information on the nature of unfolded states and may provide mechanistic insights into understanding folding of MPs. In the long term, such studies may allow extending the concepts derived from these *in vitro* investigations to the folding of MPs *in vivo*. Finally, studies on mutations in rhodopsin causing RP in the context of the native structure have failed to explain their effects on misfolding (Tastan et al., 2007). This result demonstrates the need to better understand the molecular nature of unfolded states.

To increase our efforts in attacking the protein folding problem of helical MPs, in this thesis, we aim at structurally characterizing unfolded states of the helical MP, rhodopsin. Rhodopsin has been selected as a model system because it is a mammalian membrane protein, is well studied and its misfolding is implicated in disease. This study

will contribute to the fundamental understanding of MP folding in general, and can be used to test the new long-range interactions model in particular.

1.2.2   Outline of experimental approaches

In order to address the above aims, we extracted rhodopsin from natural and recombinant sources, purified and reconstituted it in detergent micelles. We then subjected the purified rhodopsin samples to a variety of biophysical studies, as outlined below.

1.2.2.1 Source

Rhodopsin is available in large quantities in bovine retina (>1 mg/retina), which therefore serve as the natural source for extraction of rhodopsin. Recombinant rhodopsin in the order of ~100-500 μg was from transient transfection of COS-1 cells (monkey kidney) with a vector carrying the opsin gene (Oprian et al., 1987). Purification of recombinant rhodopsin on the order of 2-10 mg was prepared from a stable cell line of suspension-adapted HEK293 (human embryonic kidney) cells (Reeves et al., 1996). Both expression systems performed the sufficient post-translational modifications to maintain structure and function of rhodopsin (see Fig. 3) (Oprian et al., 1987; Reeves et al., 1996).

1.2.2.2 Extraction

Rhodopsin purified from bovine retinae was extracted from their native membrane in detergent micelles of dodecyl maltoside (DM). Opsin expressed in cells was first treated with 11-*cis*-retinal to form rhodopsin before solubilizing in detergent. Rhodopsin can be extracted in different membrane mimetics such as lipid vesicles, bilayers, detergent micelles and mixed

micelles. The choice of a detergent environment is due to the relative ease of sample preparation. Detergents can also be removed to replace them with other detergents or reintroduce them into lipid environments of defined composition. Most importantly, there is less interference of detergent soubilized protein with spectroscopic techniques compared to other membrane mimetics. It has been shown previously that rhodopsin in DM, a non-ionic detergent, is functional on the basis of transducin activation assays (Bubis, 1998) and thermal stability of rhodopsin in DM is the same compared to that in native membranes (Knudsen and Hubbell, 1978; Ramon et al., 2003). While there are certain differences in the photochemical process of rhodopsin in DM versus in native membrane e.g. the conversion of Meta-I to Meta-II is faster in DM (Arnis and Hofmann, 1993), the Meta-II state structure and dynamics has been shown to be similar for rhodopsin in DM micelles versus membranes (Kusnetzow et al., 2006). Furthermore in this thesis we are primarily interested in the native and dentatured states of rhodopsin and not in the photoactivated state or the different intermediate involved in its activation. Thus, the choice of DM is highly appropriate.

1.2.2.3 Purification

Rhodopsin was purified in one step by selective binding of rhodopsin to the antirhodopsin-antibody Sepharose matrix (Oprian et al., 1987). The column consisted of anti-rhodopsin antibody, 1D4, which recognizes the C-terminal nonapeptide sequence of rhodopsin bound to Sepharose beads (Molday and Mackenzie, 1983). The pure protein was eluted by competing with a nonapeptide whose sequence corresponded to the epitope (Reeves et al., 1996). The buffer used for purification was 2 mM sodium phosphate, pH 6 + 0.05% DM such that only the correctly folded conformation is purified (Reeves et al., 1996). It has been seen previously that in high salt and/or high pH conditions the misfolded conformations are purified along with

the natively folded ones (Ridge et al., 1995b). With purified correctly folded and fully functional rhodopsin in DM micelles, the following folding studies were carried out.

1.2.2.4 Scheme of experiments for characterization of unfolded states

An overview of the experimental approaches to characterize unfolded states of rhodopsin is provided in Figure 6. The different levels of resolution in the 3D structure of rhodopsin were targeted: global (Figure 6.A.), region-specific (Figure 6.B.) and site-specific (Figure 6.C.). Each color represents the region of rhodopsin that was probed during structural characterization of denatured states. Figure 6.A. shows different colors for different regions of rhodopsin, representing structural characterization done on a global scale. Figure 6.B. showing the extracellular and cytoplasmic regions in red and blue respectively, represents the regions probed on a local, domain-specific scale which provides a greater degree of structural detail than experiments done at the global scale. Figure 6.C. showing an example residue in green represents characterization done at a site-specific scale.

A. Global

Cytoplasmic (CP)
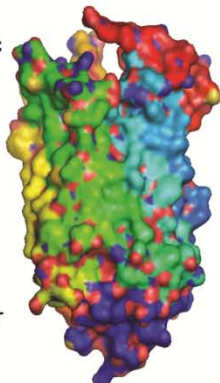
Extracellular (EC)

Circular Dichroism

Retinal-protein interaction

Fluorescence spectroscopy

Cysteine accessibility

^{1}H NMR spectroscopy

Terahertz spectroscopy*

Dynamic Light scattering

Mid-IR spectroscopy

B. Domain or residue type specific

Cytoplasmic (CP)
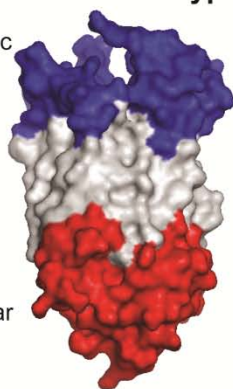
Extracellular (EC)

NMR spectroscopy of Lysine and Tryptophan isotope labeled protein

Cysteine accessibility

Retinal-protein interaction

C. Residue-specific

Cytoplasmic (CP)
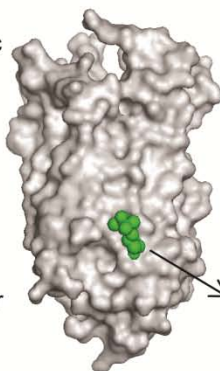
Extracellular (EC)

T108C

EPR spectroscopy

^{19}F NMR spectroscopy*

Figure 6: 3D structure representation of rhodopsin summarizing the experimental approaches

3D rendering of crystal structure of rhodopsin (PDB ID: 1L9H) representing A. the global B. local, domain specific structure changes and C. site-specific structural changes that are probed in the various experimental approches undertaken to probe denatured states. Each color signifies the region probed during structural characterization of denatured states. In C, the specific residue highlighted is T108C derivatized by an EPR spin label which is shown in green, ball and stick representation. * Methods under development, not yet applied to denatured states.

The approaches applied to these different scales from Figure 6 are summarized below.

1. Firstly, it was necessary to establish conditions under which rhodopsin could unfold to the largest extent possible without aggregation so that the earliest stages of folding can be characterized. The effects of the chemical denaturants, sodium dodecyl sulfate (SDS), urea, guanidine hydrochloride (GuHCl) and trifluoroacetic acid (TFA) on rhodopsin's secondary structure and propensity for aggregation were investigated. These results are described in Chapter 3.

2. To structurally characterize these largely unfolded states of rhodopsin, global changes upon denaturation represented by retinal-protein interactions, tryptophan fluorescence and cysteine accessibility, size of rhodopsin and overall protein flexibility were investigated. These studies are explained in Chapter 4.

3. Dynamics of specific regions were characterized with the long term goal of determining if a folding core like structure is formed in denatured states. It is expected that a core like structure involving interactions among various residues will lead to rigidity of that region compared to other regions where such interactions are not formed. We have therefore compared the motions of denatured rhodopsin by Nuclear magnetic resonance (NMR) in regions around the predicted folding core by probing tryptophans and that away from it by probing lysines. These are described in Chapter 5.

4. Residue specific information on motions of three residues within the predicted folding core was investigated in unfolded states of rhodopsin using electron paramagnetic resonance (EPR) spectroscopy. Flexible and rigid motions would reflect that either the predicted folding core residues are involved in interactions in denatured states or are part of a completely unfolded region respectively. These motions were compared with that of

three residues in the CP domain which is away from the folding core to show contrasting mobilities in regions in the folding core and that away from it. These results are discussed in Chapter 6.

5. In order to quantify motions in rhodopsin, ^{19}F NMR methods were developed for the attachment of novel monofluoro labels to cysteines in the CP domain and for measurement of relaxation rates. These were measured for the native state as proof of principle for the method as described in detail in Chapter 7.

6. We have developed a bulk method, terahertz (THz) spectroscopy, to determine global motions of rhodopsin as described in Chapter 8. This method was tested in the native dark and light activated states of rhodopsin to show application of this method in detecting conformational changes.

1.2.3   Summary of research accomplishments and contributions

1. Conditions for unfolding rhodopsin were optimized by screening different denaturing conditions so that maximum unfolding can be obtained without aggregation. Through these optimizations, we have provided a set of detailed approaches that can be undertaken for carrying out folding studies of any MP. Such elaborate descriptions for MPs were lacking in the literature which is a major reason for this field to be less advanced than soluble protein folding. 30% SDS and 3% SDS + 8M Urea (3S8U) were found to unfold rhodopsin by a significantly large extent without causing aggregation. Further, SDS denaturation curves showed four stages which correlated with structural changes of SDS micelles with increase in SDS concentration. This helped delineate the different stages of structural changes in rhodopsin during its unfolding.

2. Structural characterization of largely unfolded states of rhodopsin was achieved by first detecting global tertiary structure changes upon denaturation. Changes upon SDS denaturation showed four distinct stages of unfolding of rhodopsin based on the expected predominant micellar structures of SDS. Denatured states in SDS spheres and cylinders showed a relatively greater burial of cysteine and tryptophan residues and are more compact as compared to the states observed in mixed micellar structures. Overall backbone flexibility increased as compared to that of native rhodopsin with a concomitant increase in unfolding as indicated by 1D ^{1}H NMR. Such studies paved the way for designing and understanding higher resolution structural studies of denatured states.

3. Domain specific motions in denatured states were next examined by isotope labeling amino acid types that represent different domains so that they can be measured by NMR. We found that in denatured states, EC and TM domains (probed by Tryptophans) were less flexible than the CP regions (probed by Lysines). Thus, contrasting dynamics in these regions in the denatured states provided preliminary evidence for the validation of the folding core that was predicted to form in the EC-TM region.

4. To further increase the resolution of structural studies, residue specific motions in denatured states were detected by EPR spectroscopy. Similar to the differences seen in local motions of EC-TM and CP domains probed by NMR, a difference in residue specific dynamics was seen among residues in the EC and CP domains by EPR spectroscopy. The EC residues, selected from the predicted folding core residues, were more constrained in their motion than the CP residues. This agrees well with the long-range interaction theory of folding of rhodopsin according to which EC loops along with

TM regions are involved in interactions in the initial stages of folding that trigger folding of the whole protein.

5. Methods were developed to quantify motions of specific residues in rhodopsin by ^{19}F NMR. Such quantification of motions was not possible with trifluoro labels, such as trifluoroethylthiol (TET), which have been used so far for detecting conformational changes of protein by 1D ^{19}F NMR. Thus, fluoro-labeling of cysteines in rhodopsin using novel monofluoro labels was developed. Different monofluoro labels and their labeling conditions were tested to derivatize cysteines 140 and 316 in the CP domain in native state. Relaxation rates of these cysteines were measured to show the possibility of quantifying motions using monofluoro labels. Such a method can be applied in the future to measure residue specific motions in denatured states.

6. We developed the application of terahertz spectroscopy for detecting global motions in MPs by taking rhodopsin as the model system. Methods were established to measure motions in dark and light activated states of rhodopsin. The terahertz spectra of these states hinted at motions already reported in the literature, indicating the utility of this method for determining motions of MPs, which are often difficult by NMR. Further, this method provided new insights into changes in dynamics of rhodopsin upon activation. Thus, these studies can be considered as a big step towards developing this method for characterizing motions in denatured states.

2.0   CHAPTER 2: EXPERIMENTAL PROCEDURES

2.1   PREPARATION OF RHODOPSIN FROM BOVINE RETINAE

All operations involving rhodopsin were carried out under dim-red light illumination. Rhodopsin was prepared from frozen bovine retinae, purchsed from J. A. Lawson Co. (Lincoln, NE). Each retina yielded 1-1.5 mg of rhodopsin. Depending upon the amount of rhodopsin required, the corresponding number of retinae were taken. The retinae were thawed and then suspended in equal volume of buffer A. Retinae were mixed using a spatula and then transferred in small quantities to a Dounce homogenizer of appropriate dimensions depending on the volume in use. The retinae were then homogenized until no clumps were visible. After homogenization of the entire volume of retinae, dodecyl maltoside (DM) was added from a 10% stock to obtain a final concentration of 1%. This mixture was then end-over-end mixed at 4°C for 1.5-2 h. This was followed by centrifugation of DM solubilized retinae at 35,000 rpm in a 70Ti rotor using a Beckman ultracentrifuge to remove unsolubilized components. The pellet was discarded and an aliquot of the supernatant was used to quantify the amount of rhodopsin present by absorbance spectroscopy (described in Section 2.3.5.1.). Depending on the amount of rhodopsin estimated and the binding capacity of antibody (1D4) derivatized sepharose beads (described in Section 2.2.5.), which were used for purification of rhodopsin, beads were added to the supernatant. Solubilized retinae with 1D4 beads were then end-over-end mixed at 4°C for 4 h - 16 h.

Following this, purification of rhodopsin was carried out with a nonapeptide as described in Section 2.2.5.4.

2.2 RHODOPSIN: EXPRESSION AND PURIFICATION

All steps involving cells used as recombinant sources were performed under sterile conditions in the light until the addition of 11-*cis* retinal. Buffer designations are listed in the footnotes at the end of this chapter.

2.2.1 Expression in COS-1 cells

2.2.1.1 Construction of plasmids containing synthetic bovine opsin mutant gene in expression vector pMT4

Synthetic bovine opsin mutant genes were created in the expression vector pMT4 (Oprian et al., 1987). First, suitable fragments were prepared either by enzymatic restriction from existing vectors or from site directed mutagenesis as described in sections below for each mutant.

    a. A166C/C140S/C316S – QuikChange Multi-Site Mutagenesis kit from Stratagene (La Jolla, CA), was used to mutate these residues in wild type opsin gene. Primers were designed as per the specifications on the Strategene website using their QuikChange Primer Design tool (http://www.genomics.agilent.com). The sequences are shown in Table 1. Primers were ordered from Integrated DNA Technologies (IDT), USA. 200 μM master stock and 10 μM stocks in sterile water were prepared for each primer.

Table 1: Primer sequences

Mutation (Primer Name)	Primer Sequence
Forward, A166C (t418a)	5'-ggtacgtggtggtgagcaagcccatgagc-3'
Reverse, A166C (t418a_antisense)	5'-gctcatgggcttgctcaccaccacgtacc-3'
Forward, C140S (g496t_c497g)	5'-ggtcatggctctgtgctgtgcggccccg-3'
Reverse, C140S (g496t_c497g_antisense)	5'-cggggccgcacagcacagagccatgacc-3'
Forward, C316S (t946a)	5'-aagcagttccggaacagcatggtcaccactc-3'
Reverse, C316S (t946a_antisense)	5'-gagtggtgaccatgctgttccggaactgctt-3'

Protocol of PCR (polymerase chain reaction) amplification followed was according to the Stratagene manual for templates greater than 5 kb. Concentrations of the components used in the PCR mix are given in Table 2, the total volume was 25 μl. All the six primers listed above in Table 1 were added to the mix. The PCR cycle parameters are given in Table 3.

Table 2: PCR reaction mix for introducing A166C, C140S, C316S mutations

Materials	Concentration
10X QuikChange® Multi reaction buffer	2.5 μl
dNTP Mix	1 μl
Primers (above)	50 ng of each primer
DNA (wild type opsin)	128 ng
QuikSolution	0.75 μl
H$_2$O	16 μl
QuikChange® Multi enzyme blend (2.5 U/μl)	1 μl

Table 3: PCR cycling parameters for introducing A166C, C140S, C316S mutations

Segment	Cycles	Temperature (°C)	Time (minute)
1	1	95°C	1
2	30	95°C	1
		55°C	1
		65°C	13

Following PCR, 1 μl of DpnI enzyme was added to the PCR reaction products and incubated at 37°C for 1 h. After 1 h, the mixture was centrifuged briefly and then transformed into the supplied XL-10 Gold ultracompetent cells. For transformation, 2 μl

of β-mercaptoethanol provided with the kit was added to 45 μl of the competent cells and the contents were incubated on ice for 10 min, swirling gently every 2 min. Following this, 1.5 μl of the DpnI digested PCR product was added to the cells and incubated for 30 min following which a heat shock was given for 30 s in a 42°C water bath. After incubation on ice for 2 min, 0.5 ml of LB (Luria Bertani) media was added and the cells were incubated at 37°C with shaking at 250 rpm for 1 h. After 1 h, 100 μl of these cells were plated on LB-ampicillin agar plates, ampicillin concentration in the plates being 100 μg/ml.

b. C140S/C316S - A mutant containing the mutation F228C/C140S/C316S was obtained from Prof. H. Gobind Khorana's laboratory at MIT. C140S/C316S mutant was prepared by fragment replacement mutagenesis in the F228C/C140S/C316S mutant synthetic gene. Wild type and the triple mutant gene were obtained by EcoRI and NotI digestion from pMT4 vector extracted from were each digested with restriction enzymes XbaI and PstI to obtain oligonucleotides of sizes 176bp, 1705bp and 1881bp. The restriction digestion reactions were set up with the components at the concentrations described in Table 4. The 176bp of the triple mutant was substituted by the corresponding wild type fragment to remove F228C mutation from the triple mutant and obtain only C140S, C316S mutations.

c. S22C, E25C, T108C, V204, I205C, N151C, I154C, and M155C with C140S/C316S background. These mutants were obtained from Prof. Wayne Hubbell's laboratory at University of California, Los Angeles.

d. C222S/C140S/C316S, C264S/C140S/C316S – These mutants were prepared using the QuikChange Multi-Site Mutagenesis kit (Stratagene) as done for A166C/C140S/C316S mutant. C140S/C316S was used as a template DNA in which C222S and C264S

mutations were introduced. Primers were ordered from Integrated DNA Technologies (IDT), USA. 200 μM master stock and 10 μM stocks in sterile water were prepared for each primer. The primer sequences are given in Table 4.

Table 4: Primer sequence for introducing C222S and C264 mutations

Mutation (Primer Name)	Primer Sequence
Forward, C222S (t664a)	5'-tgattgtcatcttcttcagctatggccagctggtg-3'
Reverse, C22S (t664a_antisense)	5'-caccagctggccatagctgaagaagatgacaatca-3'
Forward, C264S (t790a)	5'-tggtcatcgctttcctaatcagctggctgccata-3'
Reverse, C264S (t790a_antisense)	5'-tatggcagccagctgattaggaaagcgatgacca-3'

The protocol for PCR (polymerase chain reaction) amplification was followed according to the Stratagene manual for templates greater than 5 kb. Concentrations of the components used in the PCR mix were same as in Table 2 except 100 ng of DNA was used. The primers are listed above in Table 4. The PCR cycle parameters were the same as those provided in Table 3.

e. W35F, W126F, W161F, W175F, W265F – These mutants were prepared in pMT4 vector by David Man previously in the lab. Further manipulations with these mutants were done as explained in Section 2.2.2.1.

f. T251C, Q244C, H65C and F146W/Q244C, all with a background of C140S/C316S/C322S/C323S – T251C, Q244C and H65C were obtained from the lab of Prof. H. Gobind Khorana at MIT. These were sequenced to confirm the mutations. The F146W/Q244C/C140S/C316S/C322S/C323S mutant was prepared by site directed PCR mutagenesis on the template Q244C/C140S/C316S/C322S/C323S. The primer was designed using the oligo design tool on the IDT, USA website (http://www.idtdna.com/Scitools/Applications/Primerquest/) and were ordered from IDT. The forward primer sequence is 5'- ATG AGC AAC TGG CGC TTC GGT GAG AA -3'.

The PCR reaction was set up using the components provided with KOD Hot Start DNA Polymerase (Novagen, NJ). The concentrations of each of the components are given in Table 5. The total volume of the mix was 50 μl. The starting DNA concentration was not mentioned on the tube obtained from MIT, 0.5 μl was used for the PCR. 200 μM and 20 μM stocks of the primers were prepared in H_2O. The PCR mix and cycles were set up following the suggested protocol on the Novagen website (www.novagen.com/KOD) for this enzyme.

Table 5: PCR mix for introducing F146W mutation

Materials	Concentration
10X KOD Hot Start Polymerase Buffer	5 μl
MgSO4 (25 mM)	3 μl
dNTP (2 mM each)	5 μl
DNA	0.5 μl
Primers	0.75 μl of each primer
H_2O	34 μl
KOD Hot Start Polymerase	1 μl

Table 6: PCR cycle for introducing F146W mutation

Segment	Cycles	Temperature (°C)	Time
1	1	94°C	2 min
2	30	94°C	15 sec
		57°C	2.5 min

The PCR products were subjected to DpnI digestion and then transformed into competent DH5α cells as explained for A166C mutant above.

2.2.1.2 Expression by transient transfection of COS-1 cells

COS-1 cells were transiently transfected with the above mutants as described in (Oprian et al., 1987) with the minor modifications described below.

Cells stored in liquid nitrogen were thawed as quickly as possible by placing vials in a 37°C water bath after removal from liquid nitrogen. The cells were transferred to a 15 ml Falcon tube and slowly (over 2 min) 10 ml of buffer B supplemented with L-glutamine/ Penicillin/Streptomycin (buffer C) and 10% bovine serum (buffer D) was added to allow slow diffusion of the cryo-preservative DMSO from the cell. Cells were pelleted at 1000 rpm for 10 min in a Sorvall Legend RT benchtop centrifuge, the supernatant was aspirated and 10 ml of fresh buffer D was added. The cells were resuspended and transferred to a 10 cm tissue culture dish and incubated at 37°C, 5% CO_2 (Nuaire DH Autoflow) in buffer D. Buffer B medium was purchased as a powder mixture (GIBCO). After dissolving, it was supplemented with 3.7g $NaHCO_3$ per liter of media. Cells were maintained at about 90% confluence maximum to avoid damage to the cells by overgrowth. Cells were fed every three to four days, until ~80-90% confluence was reached.

Cells were split 1:5 to 1:20. Plates (10 cm and 15 cm diameter) were washed with 10 ml of buffer A. 1 ml of 0.05% Trypsin-EDTA was added to a 10 cm dish and 2 ml to a 15 cm dish. After incubation at 37°C for 1 min, the plates were agitated until the cells detached from the surface (10 and 15 cm dishes). 9 ml (10 cm dish) and 8 ml (15 cm dish) of buffer D was added to inactivate trypsin. Cells were removed from the plates by pipetting up and down 3-10 times and transfer into new dishes of appropriate size followed by thorough mixing on the new plate by tilting.

For long-term storage of COS-1 cells, 70-90% confluent plates (15 cm) were trysinized as described above. After centrifugation at 1000 rpm for 10 min, the supernatant was discarded and the pellet was resuspended in 5 ml of 10% DMSO in buffer D medium. 1 ml aliquots were prepared in cryogenic storage vials (Nunc) and placed in cryofreezing container (Nalegene). The

boxes were kept at -70°C in freezers overnight where the cooling rate was 1°C/min. The following day, the vials were transferred to liquid nitrogen.

Cells on confluent 15 cm dishes were transiently transfected with the pMT4 vector as follows. All solutions were equilibrated at 37°C. 15 μg plasmid-DNA (pMT4) per plate was added to 10 ml of a solution of 0.25 mg/ml DEAE-dextran, 0.1 M Tris-HCl pH 8 in buffer C medium. The cells were aspirated, washed with 25 ml buffer C medium and incubated with the DNA-mixture for 6 h at 37°C. After 6 h of incubation, the DNA mix was removed and without washing 2 ml of shock buffer containing 10% DMSO and 6 mM Dextrose in buffer A was added and incubated for 2 min. Shock buffer was removed after 2 min and 15 ml 0.1 mM chloroquin in buffer C medium was added to the cells. The cells were then incubated for 2 h. After aspirating the chloroquin solution, and washing with 25 ml buffer C medium, the cells were incubated overnight with 30 ml buffer D medium. Total incubation time starting with the addition of DNA was 55-72 h. After aspirating the medium, cells were washed with 10 ml buffer A. They were then scratched off the plates in 2 ml buffer A per plate. Subsequent manipulations were performed on ice.

2.2.2 Expression in HEK293 cells

2.2.2.1 Construction of opsin expression plasmid using pACMV-tetO

W35F, W126F, W161F, W175F and W265F mutant opsin genes were created in pMT4 vector by David Man previously in the lab. These opsin genes needed to be moved from the pMT4 vector to the pACMV-tetO vector for stable transfection in HEK 293 cells. The pACMV-tetO vector, available in our lab, was originally developed by Dr. Philip Reeves (Reeves et al., 2002a; Reeves et al., 2002b) (Figure 7). A tetracycline (tet)-regulated gene expression system, in

mammalian cells was developed by fusing the bacterial tet repressor (TetR) with the activating domain of viral protein 16 (VP-16) (Gossen and Bujard, 1992), a tetracycline controlled transactivator was generated that enhanced transcripton of a gene from CMV-tetO promoter sequences. In another system developed by Yao et al. (Yao et al., 1998), a full-length CMV promoter is fused to two tetO sequences in tandem, which is tetracycline inducible and is based on TetR repression. Reeves et al. (Reeves et al., 2002b) modified this system to generate a new vector pACMV-tetO, to express mutant opsin genes.
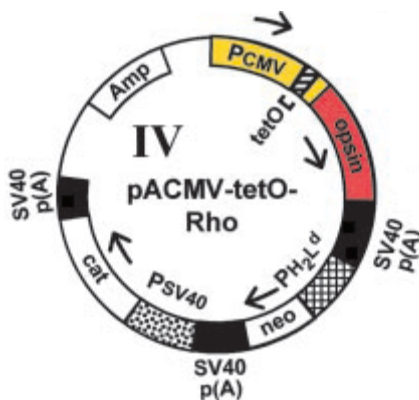
Figure 7: pACMV-tetO

Figure is taken from (Reeves et al., 2002b). The figure shows the promoter (CMV-tetO) and other important regions in the vector.

In order to excise the opsin gene from pMT4 vector, two unique restriction sites were required in pMT4 and pACMV vectors. Both the vectors had NotI and KpnI site in common. However, the unique KpnI site in pMT4 is a few bp away from the starting codon within the opsin gene fragment and thus had to be moved to the start of the opsin gene by site-directed mutagenesis (kit used was from Stratagene). This enabled excising the opsin gene by digesting with KpnI and NotI and then ligating into pACMV-tetO vector which is also cut by the same two enzymes. For the restriction digestion reactions, sequential digestion was set up with KpnI

followed by NotI as per the reaction mix on NEB website for each of these enzymes. For ligation reaction, different vector to insert ratios of 1:6, 1:9 and 1:12 were tested for each mutant. Quick ligase (NEB) was used to prepare the ligation mix that was kept at RT for 1 hour and then transformed into DH5α cells and grown on agar plates overnight in a 37°C incubator.

Colonies from the above step were picked and used to grow in a 1.5 ml LB media containing 100 μg/ml ampicillin. After growth at 37°C for 14 h, DNA was purified from the cultures using Qiaprep spin miniprep kit (Qiagen, MD). The steps for purification were followed exactly as given in the instruction manual and purified DNA was dissolved in sterile water. The purified DNA was subjected to restriction digestion with KpnI and NotI. The clones showing fragments of appropriate size corresponding to opsin and the vector backbone were selected and their sequences were confirmed by the core sequencing facility at University of Pittsburgh.

2.2.2.2 Preparation of HEK293 Stable Cell Lines Containing the Opsin Mutant Genes

pACMV-tetO vectors containing the mutant opsin genes were used to stably transfect HEK293 cells. Routine growth, splitting and trypsinization, long-term storage and reviving from frozen stocks were as described for COS-1 cells in Section 2.2.1.B. HEK293S cells were transfected by the method of Chen and Okayama (Chen and Okayama, 1987) as modified by O'Mahoney and Adams (O'Mahoney and Adams, 1994). Stable cell lines expressing the opsin genes at high levels were selected using elevated concentrations of geneticin (2-3 mg/ml) as described (Reeves et al., 1996).

Frozen HEK 293 cells were revived in buffer E media as described above for COS-1 cells (p. 69) and grown to 90% confluence on a 10 cm dish. The day before the transfection, this plate was split 1:10 in buffer D. On the second day (approx. 25 h later) in a 15 ml Falcon tube the following was mixed: 30 μg of DNA, 450 μl of water, 50 μl of 2.5 M $CaCl_2$, 500 μl of BES.

After the addition of BES, the mixture was incubated for exactly 1 min prior to addition of the solution to the plate. After gentle distribution of the solution on the cells, plates were incubated at 35°C, 3% CO_2 for 19 h. After 1 hour the efficiency of the transfection was checked by light microscopy. If the transfection was successful, the DNA precipitate looked like fine sand between the cells and sometimes red crystals formed after longer incubation. However, large colorless crystals formed in between the cells during the overnight incubation, were indicative of a failed or inefficient transfection. After 19 h incubation, the medium was removed and the plate was washed twice with 10 ml of buffer E. The cells were then fed with buffer E and the cells were returned to 37°C, 5% CO_2. At this stage and for all further operations, the pipettes were changed for each mutant and plate thus as to prevent any contamination of different transfected mutants with each other. After further 23 h, the plate was washed with buffer A, trypsinized and split 1:10. 6 plates for each transfected plate were prepared. To 1 ml of 1x trypsin (0.05%), 9 ml of buffer E was added and 10x pipetted up and down such that the cells did not clump. This was important for avoidance of mixed clones. 1 ml of this was diluted with 9 ml of buffer A. Of this diluted cell suspension, 40 μl was mixed with 40 μl of Trypan Blue. 10 ml was pipetted under a glass plate to a hemacytometer. Between 2-5 single cells should be counted under the microscope, corresponding to $0.5 – 1 \times 10^6$ cells per plate. After further 20 h, three of the plates were fed with buffer E media containing 2 mg/ml geneticin (G418) and three with buffer E containing 3 mg/ml geneticin. Media were replaced every 2-3 days with fresh media until colonies formed and reached workable size (in about 2 weeks). The medium was aspirated from a plate where the colonies that were being picked had been circled. 8 colonies could be picked per plate. Cloning rings together with vacuum grease had been autoclaved. Using sterile forceps, the cloning rings were dipped in vacuum grease until the ring was completely covered from the

bottom and were then placed on the colony. 40 ml of 1x trypsin (0.05%) was added to each of the 8 colonies in cloning rings. 1 min after the addition of trypsin to the first cloning ring, 40 ml of buffer E media was added to each cloning ring in the same sequence as the trypsin had been added. Using a 200 ml eppendorf pipette, the solutions were pipetted up and down 5 times before being transferred to a 24 well plate containing 1 ml of complete media with the appropriate amount of geneticin (2 or 3 mg/ml, see above). As soon as confluence was reached, the cells were trypsinized and transferred into two chambers in a 6-well dish with a difference in cell number of 1:4. The 4 times higher concentrated chamber was used to perform western blot analysis.

Western blot positive clones were split to one 10 cm dish and one 6-well chamber. After feeding the plates on day 3 or 4, the 10 cm dish was grown until confluent and harvested with 10 ml buffer A. Unlike COS-1 cell harvesting, HEK293 cell harvesting does not require scraping of the cells the plates. Rather, cells were detached by pipetting. The cells were spun down for 10 min at 5K at 4°C in 15 ml Falcon Tubes. Quantitation of the amount of rhodopsin was by difference spectroscopy as described below in Section 2.4.1. If the amount of rhodopsin per 10 cm dish was around 10 μg or more the corresponding 6-well chamber was split to one 15 cm dish. Upon reaching confluence, this plate was split into 5 plates, three of which contained 2 or 3 mg/ml geneticin, while two only contained 0.5 mg/ml geneticin. The three first plates were used to generate freeze downs for long-term storage. One of the 0.5 mg/ml geneticin containing plate was split 1:5, while the other plate was fed until confluence was reached. This plate was used for quantitation of rhodopsin production as described for the 10 cm dish, except for that 1 ml of 10 mM 11-*cis* retinal was used per plate and the cell pellet was solubilized in 1 ml of buffer A containing 1% DM. Multiplication of the rhodopsin amount per 10 cm dish with 40 yielded the

amount of rhodopsin that can theoretically be produced in the corresponding 1 liter suspension culture.

2.2.2.3 Expression of rhodopsin in HEK293 cells grown in suspension

Cells were kept frozen at -70°C. Growing cells were obtained as described for COS-1 cells (Section 2.3.1.). After approximately 3 days the confluent cells were split typically 1:5. After removal of the medium, plates are washed with 25 ml buffer A (15 cm dishes). 2 ml of 0.05% Trypsin-EDTA was added and the cells were left to detach from the plates. Cells were then transferred into the appropriate volume (25 ml medium per plate) of buffer D medium. Cells were confluent after approx. 3 days for a 1:5 dilution.

Suspension cultures were set up using 1 l spinner flasks containing 500 ml media as depending on whether isotope and non-isotope labeled material was to be prepared. For isotope labeled material, media were in composition according to buffer B media formulation. However, since certain amino acids had to be omitted, the media were prepared from individual components. Thus, all solutions were prepared as 100x concentrated stock solutions, except glucose, NaCl, glutamine and the isotope labeled amino acid, which were added as solids. Deviations from the buffer B media formulation were as follows. 1. The glutamine concentration was lowered by ½. The same amount was then added on day 5 or 6, together with the other additions described above. 2. The $CaCl_2$ concentration was lowered to 50 mg/l (Eilers et al., 1999). Isotope labeling also required the serum to be dialyzed to remove any amino acids. Thus, e.g. 500 ml fetal bovine serum was dialyzed 3-times against 10 l buffer A at 4^oC with a tubing cut off of 1 kDa as described (Eilers et al., 1999). For both, labeled and unlabeled material, the media were supplemented with 0.1% Pluronic F-68, 50 μg/ml heparin. Spinner flasks were

50

inoculated using three-four 15 cm tissue-culture dishes confluent with cells (6-9 x 10^7) per 500 ml of media and incubated at 37^oC in a humidified incubator. After 5-6 days, when the media turned yellow, the culture medium was further supplemented with 6 ml of 20% (w/v) glucose and 4 ml of 8% (w/v) $NaHCO_3$, 5 mM sodium butyrate. Cells were fed daily with glucose solution until the cells were harvested (usually on day 8). Cells were transferred to centrifuge vials equilibrated at 4^oC and the spinner flask was rinsed with 2x50 ml of ice-cold buffer A and combined with the main culture. After centrifugation for 10 min at 4K, 4^oC, in a Sorvall RC-3B centrifuge, the supernatant was immediately decanted and the cells kept on ice. 25 ml of ice-cold buffer A was added and the cells were resuspended. After transfer to a 50 ml Falcon tube, a further 25 ml was used to rinse the centrifuge pot and added to the Falcon tube. Cells were pelleted by centrifugation at 4^oC. The wet-weight of the pellet was recorded and the cells resuspended in a final volume of 20 ml buffer A.

2.2.3   Reconstitution of the opsin expressed in mammalian cells with 11-*cis* Retinal

Cell pellets from a 500 ml culture were resuspended in 20 ml of buffer A containing benzamidine (0.005%) and PMSF (0.7 mM). Cells harvested from plates were resuspended in 2 ml buffer A per plate. 11-*cis* Retinal was added to give 5 μM concentration and the suspension was incubated at 4ºC for at least 1.5 h. The concentration of reconstituted mutant rhodopsin was estimated by UV/Vis absorbance difference spectrum analysis of an aliquot solubilized in buffer A containing 1% DM. Addition of 11-*cis* retinal was repeated until no further increase at A_{500} was observed by difference spectroscopy.

2.2.4   Solubilization of cell pellets containing rhodopsin by use of detergents

For solubilization in DM, the rhodopsin containing cells or retinae were end-over-end mixed for 1-1.5 h in buffer A containing 1% DM. The volumes used for solubilization depended on the rhodopsin source. HEK293 cells were solubilized at 10 ml buffer/g wet pellet. COS-1 cells were solubilized at 2 ml buffer/plate. Unsolubilized material was removed by centrifugation for 30 min at 4°C, 35,000 rpm, rotor 60Ti or 45Ti, Beckmann Ultra Centrifuge. The supernatant was added to 1D4-Sepharose beads as described below in Section 2.2.5.2.

2.2.5   Affinity chromatography of rhodopsin using 1D4 sepharose

2.2.5.1 Preparation of 1D4 sepharose

Cyangen bromide (CNBr)-activated sepharose 4B was prepared from CNBr and sepharose 4B (Kuemel et al., 1979), based on the rapid reaction of cyangen halides with the hydroxyl groups of carbohydrates at high pH to form cyanate esters (Figure 8). The monoclonal anti-rhodopsin antibody 1D4 (Oprian et al., 1987) was then coupled to CNBr-activated sepharose 4B via its amino groups (Oprian et al., 1987) with minor modifications.
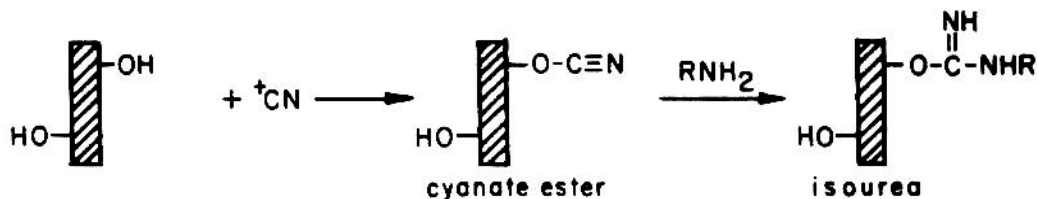
Figure 8: Activation of sepharose by CNBr and coupling of protein to the activated gel.

This figure is taken from (Kohn and Wilchek, 1978).

Prior to coupling, 1D4 was purified from a myeloma cell line provided by R.S. Molday (University of British Columbia) as follows. 1500 mg 1D4 antibody (stored at -20°C) was thawed. 300 ml of Protein A-sepharose 4B were packed and equilibrated with 5 times the bed volume of buffer F. All flow rates were between 0.5-1.5 ml/min, unless otherwise stated. The sample was diluted with 5 times its original volume of buffer F. The sample was loaded, followed by washing with buffer F until a straight baseline at 280 nm was reached. The sample was eluted with approximately 300 ml of buffer G. Fractions of 4 ml each were collected while monitoring 280 nm. In order to store the column for future use, it was regenerated with 300ml buffer H at a flow rate of 0.5ml/min. The column was stored at 4°C after washing with 2-10 times the bed-volume of buffer I. Due to the poor stability of 1D4 at pH 3, the pH of the fractions was immediately after elution adjusted to pH 8.3 using 0.5 M $NaHCO_3$ pH 10. Fractions containing 1D4 sepharose were combined and used directly for coupling, as long as the concentration of 1D4 was above 3 mg/ml. If the concentration was lower, the solution was first concentrated to up to 10 mg/ml before coupling. The concentration of antibody was determined using A_{280} ($A_{280} = 1.383$ is equal to a concentration of 1mg/ml). Dialysis tubes (Spectrapor, 14 kD cut-off, but could be higher) were washed thoroughly with *aqua dest*. and filled with the 1D4 solutions. Dialysis was against 5-10 l of buffer J 4 h to overnight. Dialysis buffer was subsequently changed at least 3 times. After dialysis, the concentration was determined using A_{280} as above.

The purified 1D4 antibody was coupled to CNBr sepharose as described below. First, 20 ml CNBr-Sepharose was prepared. 100-200 mg of 1D4 antibody can be bound to this amount of CNBr-Sepharose. If 100 mg of 1D4 was coupled the capacity of the final product was typically 1mg rhodopsin/ml of 1D4 sepharose. 500 µl acetonitrile was added per 1 g of CNBr (Sigma).

The volume increased after dissolving the CNBr, so that the final concentration was 1g/ml. This stock solution could be stored at -20°C. 20 g of Sepharose 4B slurry (Sigma) was washed three times with water in a filter funnel. 20 g of sepharose corresponds to 30 ml of slurry. Water was removed by vacuum and the sepharose was added to 30 ml of buffer K. While stirring vigorously with a regular stirring bar under the hood, 1 ml of BrCN-solution was added and stirred for exactly 2 min. The suspension was transferred quickly to the filter funnel that contained ice-cold water and was vacuum-filtered immediately. The beads were washed with 300 ml of ice-cold buffer L followed by 500 ml 1 mM HCl. All the washes were carried out extremely rapidly, i.e. such that vacuum-filtering of 100 ml took less than 30 seconds. Thus prepared CNBr-sepharose could not be stored. Coupling to 1D4 had to follow immediately after preparation, ideally within 2 min. If CNBr-sepharose was purchased from Pharmacia, 1 g of the dry powder CNBr-sepharose was equivalent to approx. 3.5 ml gel slurry. The dry CNBr sepharose was washed on a sintered glass filter with 500 ml of 1 mM HCl. All subsequent steps were the same for commercially available or self-made CNBr sepharose.

The coupling to 1D4 to CNBr sepharose was carried out at 3-10mg 1D4 per 1ml CNBr-sepharose 4B. 20 ml slurry was added to the concentrated sample of 1D4 containing 100 mg 1D4 in buffer J. Coupling was allowed to proceed by end-over-end mixing at until the supernatant after spinning down the beads for 5 min contained less than 5% of the total protein (after 4-5 h at RT). The supernatant was discarded. A volume equal to that of the original supernatant of blocking agent (1 M ethanolamine pH 8) was added. Blocking was allowed to proceed for 2 h at RT or overnight at 4°C. The beads were washed on a sintered glass filter 4 times with alternating solutions of buffer J and buffer M. Buffer A containing 0.05% NaN_3 was added in equal volume as the beads. The coupled 1D4-sepharose was stored at 4°C.

The capacity of 1D4-Sepharose was determined as follows. 500 µg ROS membranes were solubilized using DM as described in Section 2.2.4. above and the exact concentration was determined spectroscopically (as described below in Section 2.4.5.1.) 200 µl of 1D4-sepharose were added and rhodopsin was purified as described in Section B below. The capacity was calculated using the ratio between the rhodopsin purified and the amount of rhodopsin originally solubilized. Typically the capacity was 1 mg rhodopsin per 1 mg 1D4-sepharose if 100 mg of 1D4 was coupled to 20 ml of CNBr-sepharose.

2.2.5.2 Binding of solubilized rhodopsin to 1D4 sepharose

After centrifugation of non-solubilized material (described in Section 2.2.4.), the supernatant was added to 1D4-Sepharose. The amount of beads necessary to bind quantitatively the rhodopsin present in the supernatant could be calculated from the 1D4 sepharose binding capacity, usually 1 mg of rhodopsin per ml settled beads. About 10% excess of 1D4-Sepharose over rhodopsin content was used. After end-over-end mixing for at least 6 h at 4°C, the suspension was packed into a column. For 10-15 mg of rhodopsin to be purified the dimensions of the column were 2.7 cm diameter x (2 to 3) cm. If smaller amounts were purified, i.e. 100-500 µg, Biorad disposable chromatographic columns were used. The packed beads were washed at RT with at least 50 column volumes of buffer A containing 0.05% DM, for purification in DM.

2.2.5.3 Derivatization of rhodopsin bound to 1D4 sepharose

(i) Mono-fluoro derivatives – After the washing with buffer A, described in the last section (Section 2.2.5.2. above), the beads were further washed with 10 column volumes of buffer N containing 0.05% DM. After washing, the total beads containing 2-10 mg bound rhodopsin mutants were resuspended in 8-40 ml of buffer N containing 0.05% DM and mono-

fluoro reagent at different concentrations depending on the type of the reagent (described in Chapter 7, Section 7.3.). After end-over-end mixing for 3 h at RT or overnight at 4°C, excess reagent was removed by multiple washing with ~40 column volumes of buffer N with 0.05% DM.

(ii) Selective labeling of C316 with mono-Fluoro Derivatives - After the washing described in the last section (Section 2.2.5.2. above), the beads were further washed with 10 column volumes of buffer N containing 0.05% DM. After washing, the total beads containing 2-10 mg bound rhodopsin mutants were resuspended in 8-40 ml of buffer N with 0.05% DM and 4,4'-dithiodipyrydine (4-PDS) was added from a 1 M stock solution in ethanol to give a final concentration of 1 mM. After end-over-end mixing for 2.5 min at RT, excess reagent was removed by multiple washing with 40 ml of buffer N with 0.05% DM. A total of at least 35 times the column volume of buffer N with 0.05% DM was used. Complete removal of 4-PDS was tested spectrophotometrically (see Section 2.3.1.). The beads were then resuspended in 6-30 ml of buffer N with 0.05% DM. Fluorinated label was added to the column to have the final desired concentration depending on the type of reagent used (described in Chapter 7, Section 7.3.). After end-over-end mixing for 3h at RT or overnight at 4°C, excess labeling reagent was removed using ~50 times the column volume of buffer N with 0.05% DM.

(iii) Nitroxide-Derivatives - After the washing described in the last section (Section 2.2.5.2. above), the beads were further washed with 10 column volumes of buffer O containing 0.05% DM. After the washing, the total beads containing 200-500 μg bound rhodopsin mutants were resuspended in 2-5 ml of buffer O with 0.05% DM containing 100 μM of spin label. After three h reaction at RT, the resin was washed with 30 bed volumes of buffer O containing 0.05% DM.

2.2.5.4 Elution of rhodopsin from 1D4 sepharose

Unlabeled and monofluoro labeled correctly folded rhodopsin mutants were eluted from 1D4-Sepharose using buffer N with 0.05% DM and 70 μM epitope nonapeptide. Nitroxide labeled rhodopsin mutants using buffer O with 0.05% DM containing 70 μM epitope nonapeptide at a flow rate of 0.3-0.35 ml/min, the effluent being monitored by UV/Vis absorption spectroscopy. Complete elution of the rhodopsin mutants usually required ~5 column volumes of elution buffer.

2.2.6   Concentration and buffer exchange of rhodopsin for solution NMR analysis

Fractions from 1D4-immunoaffinity chromatography containing >0.2 μM rhodopsin (A_{280}/A_{500}, 1.6-1.8) were pooled and concentrated using the 15 ml or 50 ml membrane filter tubes, Centricon 30 (Amicon). First, the membrane of the concentrator was wet by centrifuging 1 ml of buffer N through the filter at 3500 rpm in Sorvall Legend RT centrifuge for 3 min or until most of the buffer filtered through. Following this, 4 ml (for 15 ml concentrators) and 8 ml (for 50 ml concentrators) of the pooled rhodopsin elution fractions were added to the concentrator and centrifuged at 3500 rpm for 10 min or until ~300 μl of the solution remains above the filter. The remaining elution volume was concentrated in this way taking care to resuspend the volume above the filter each time after centrifugation. After concentrating the entire volume of rhodopsin elutions, the final volume was spun down to 250 μl. After concentrating the protein, the buffer was exchanged to buffer P by adding 1 ml of buffer P and centrifuging to get a volume of ~250 μl. The buffer exchange step was repeated 6 times and the final volume was centrifuged to 100 μl. 250 μl of buffer P was then added to extract the protein from the concentrator. For analysis of

^{19}F NMR spectroscopy, after the above steps, TFA was added to the sample as an external standard.

2.3   ANALYTICAL PROCEDURES AND SPECTROSCOPIC TECHNIQUES

2.3.1   Quantitation of free sulfhydryl groups in rhodopsin by 4-PDS labeling

0.5 µM rhodopsin (mutant or labeled with fluorinated reagents or spin labels) in buffer N with 0.05% DM was treated with 4-PDS so that final concentration of PDS is 25 µM. The reaction was followed by development of absorption at 323 nm using the same concentration of 4-PDS as a reference. The absorption at 323 nm was corrected for the contribution of the rhodopsin β-band, obtained from a rhodopsin spectrum at identical concentration in the absence of 4-PDS. The molar extinction co-efficient of 4-thiopyridone at 323 nm is 19,000 $M^{-1}cm^{-1}$ (Grassetti and Murray, 1967). Cysteines react with 4-PDS in a 1:1 stoichiometric ratio and hence the number of cysteines reacting with 4-PDS was calculated from the 323 nm peak.

2.3.2   Crosslinking by glutaraldehyde

The terminal aldehyde groups of glutaraldehyde (Pentane-1,5-dial) react with the backbone amine groups of amino acids and thereby cross-link proteins that are close to each other in space. For the cross-linking reaction, rhodopsin and glutaraldehyde are mixed in a 1:10 molar ratio. The reaction was carried out at 25ºC and 37ºC for varying times in the range of 2 min to 15 min. The reaction was stopped by addition of 0.1M Tris, pH 8. The same reaction was also carried out at

4ºC for 1 hour to ensure completion of reaction. A different stopping solution of 0.2 M glycine was also tested. The samples were then run on a SDS-polyacrylamide gel as described below in Section 2.3.3.1.

2.3.3   Protein gel electrophoresis

2.3.3.1 SDS-PAGE

SDS-Polyacrylamide gel electrophoresis (PAGE) was carried out according to (Laemmli, 1970). Resolving gels (12% acrylamide) were poured after mixing 4 ml of 30% acrylamide, 2.5 ml of buffer Q, 3.4 ml of water, 75 µl APS (10%) and 10 µl TEMED. Stacking gels (3.75% acrylamide) were poured after mixing 0.5 ml 30% acrylamide, 1ml buffer R, 2.5 ml water, 30 µl APS (10%) and 7.5 µl TEMED. Laemmli protein loading dye (Biorad, Hercules, CA) consisting of 62.5 mM Tris, pH 6.8, 2% SDS, 25% Glycerol, 10mM β-mercaptoethanol and 0.01% Bromophenol Blue was used in 1:1 ratio to load native rhodopsin on the gel. Non-reducing Laemmli dye, which is the same as Laemmli dye but without mercaptoethanol, was used in some cases. Native gel loading dye containing only 25% glycerol and 0.01% bromophenol blue was also used. The use of dyes depended on the type and amount of denaturant in the sample and the kind of dye used has been mentioned in Chapter 3 wherever appropriate. Gels were run at 200 V till the dye front reached the bottom of the gel.

Coomassie staining was done by heating the polyacrylamide gel with a mixture of 45% methanol, 9% acetic acid, 0.2% Coomassie blue three times for 10 minutes in a microwave. The gel was then destained with 25% methanol, 10% acetic acid. Silver staining was done following the instruction sheet in SilverSNAP Stain kit (Thermo Scientific, Waltham, MA).

2.3.3.2 Native PAGE

Native PAGE was run for rhodopsin containing different denaturants. Gel and buffer compositions were the same as that of SDS-PAGE except no SDS was added to either of them. Additionally, native sample loading dye was prepared as follows: a 5 ml dye solution contained 1.25 ml of 0.5 M Tris, pH 6.8, 1 ml glycerol and 0.01% bromophenol blue. The most optimized condition of running the gel was found to be at 70 V at 4°C for about 4 h or till the dye front reached the bottom of the gel. Gels were run under both light and dark conditions.

Another type of native-PAGE, following the protocol in Current Protocols in Protein Science (Unit 10.3), was prepared. Two phosphate nondenaturing polyacrylamide gels with pH of 6.3 and 8.4 were tested. 10%, 7.5% and 5% gels were prepared. Two Tris nondenaturing polyacrylamide gels were also tested at pH of 8 and 8.8. Sample and electrophoresis buffers and condition for running the gels were followed as given in the protocol in Current Protocols in Protein Science.

Blue-native (BN-PAGE) was another kind of native PAGE that was tested. The protocol was modified from (Schagger and von Jagow, 1991; Schagger et al., 1994; Wittig et al., 2006). The gel buffer was prepared in 3X concentration and comprised of 75 mM imidazole with pH adjusted to 7 with HCl. 4% stacking gel was prepared from 0.8 ml of 30% acrylamide/bisacrylamide, 2 ml of 3X gel buffer, 50 μl of ammonium persulfate, 5 ul TEMED, 3.2 ml water. 7.5% separating gel was made from a mix of 3 ml of 30% acrylamide/bisacrylamide, 4 ml of 3X gel buffer, 72 μl of ammonium persulfate, 7.2 μl TEMED, 5 ml water. The cathode buffer consisted of 50 mM tricine, 7.5 mM imidazole, 0.002% Coomassie blue, pH7. Anode buffer was 25 mM imidazole at pH 7. Sample loading dye consisted of 0.01% bromophenol blue and 20% glycerol. The gel was run for 100 V for 50 min

or till the dye front reached the end of the stacking gel and then run for 300 V for 2-3 h or till the dye front reached the bottom of the gel. The gel was run in the dark at 4°C.

2.3.3.3 Urea-PAGE

The protocol followed for preparing urea-PAGE was the same as described in Current Protocols of Protein Science. In brief, gel components are same as that in SDS-PAGE, the only difference being 8 M urea was present in the gel instead of SDS. The running buffers have no SDS or urea. Use of native or Laemmli sample loading buffer depended on the type of sample, their use is mentioned in Chapter 3. The gel was run at 70 V at RT for 4 h.

Another way in which urea gels were prepared is as follows: for preparing 12 ml of 10% separating gel, 4 ml of 30% acrylamide/bisacrylamide solution (Biorad), 8 M urea, 1.2 ml of 0.5M tris-acetate, pH 8 or 1.2 ml of 0.5 M imidazole + 0.5 M MOPS, 1.5 ml of 0.04 mg/ml riboflavin and 14.4 μl of TEMED. For preparing 5 ml of 4% stacking gel, 0.66 ml of 30% acrylamide/bisacrylamide solution, 8 M urea, 0.5 ml of 0.5M tris-acetate, pH 8 or 0.5 ml of 0.5 M imidazole + 0.5 M MOPS, 0.625 ml of 0.04 mg/ml riboflavin and 6 μl of TEMED were mixed. Non-reducing Laemmli dye and native loading dyes were both used to load separate samples on urea gels depending on the sample as described in Chapter 3.

For a urea-SDS PAGE, the recipe of gel and buffers are the same as SDS-PAGE except that urea is dissolved in the gel buffer while making the separating and stacking gel.

2.3.4 Dynamic light scattering

Dynamic Light Scattering measurements were performed using a DynaPro-99-E-50 instrument (Protein Solutions Inc., Charlottesville, VA). 20 μl of sample was required to fill the cuvette for each reading. The buffer, 2 mM sodium phosphate pH 6, was filtered through 0.22 μm syringe filters. Filtration of DM and SDS detergent solutions in the presence and absence of rhodopsin was avoided as it resulted in peaks of large hydrodynamic radius due to non-specific reaction of the filter with the detergents. SDS solutions only in concentrations 0.05% - 3% could be measured using this instrument. Beyond 3% SDS, many large radius peaks appeared for the buffer solutions and hence it was difficult to test for aggregation in rhodopsin samples. While measuring urea samples, irreproducible results were obtained on the DynaPro instrument. For GuHCl containing buffer solutions, hydrodynamic radius of 0 nm was obtained on the DynaPro. Due to these problems, measurement of solutions that contained SDS in concentration greater than 3% and solutions containing urea and GuHCl were tested on different instruments. These were Zetasizer Nano (Malvern) and DynaPro plate reader (Wyatt Technology). However, the same problems described above were encountered with both these instruments.

Accurate measurement of diffusion co-efficient required the input of parameters, refractive index and viscosity co-efficient of the sample buffers. These vales were used in all the instruments tested.

2.3.4.1 Measurement of refractive index

Refractive indices of SDS in different concentrations dissolved in buffer N containing 0.05% DM were measured. Refractive index is a measure of the extent to which light can be bent by a solution as it passes from air to that solution. It is a ratio of the speed of light in air to that in

a solution. Refractive index of solutions was measured using Reichert Abbe Mark II Refractometer in the lab of Dr. Roger Hendrix (University of Pittsburgh). The measurements were done according to the instrument manufacturer's manual. In brief, the mode selector switch was positioned for measuring refractive index. Sample was placed on the prism surface after cleaning it gently with alcohol and distilled water. The prism cover was closed and the illuminator arm was moved so that the prism surface is illuminated. The adjustment controls were rotated while looking through the eyepiece to focus the crosshair and to get the shadow line at the bottom of the view. The view was adjusted so that no red or green color shows at the edge of the shadow line. The shadow line was then centered to the crosshair and the READ button was pressed to display the value of the refractive index. The temperature was controlled at 25°C. The values recorded for SDS containing solutions are shown in Table 7 below.

Table 7: Refractive index

Refractive indices of 1.5 μM rhodopsin solution in different concentrations of SDS.

% SDS	Refractive index		
0.5	1.3334	1.3335	1.3333
0.1	1.3333	1.3333	1.3333
0.3	1.3334	1.3334	1.3334
0.5	1.3336	1.3336	1.3336
1	1.3340	1.3340	1.3340
1.5	1.3350	1.3348	1.3348
2	1.3354	1.3354	1.3354
3	1.3367	1.3367	1.3367

2.3.4.2 Measurement of viscosity co-efficient

Viscosity coefficients of SDS solutions were obtained by measuring the diffusion co-efficient of silica beads of 50 nm radius (Polysciences Inc.) in water and in different SDS concentrations. 0.5 μl of a 5% solution of Si beads was used for measurements. Viscosity of any solution, according to Stoke-Einstein equation is given by

$$\eta = k_B \times T / 6 \times \pi \times D \times R \hspace{4cm} \text{Equation 1}$$

where

η is the viscosity

k_B is the Boltzman's constant $= 1.38 \times 10^{-23} \, m^2 \, kg \, s^{-2} \, K^{-1}$

T is the temperature

D is the diffusion constant

R is the hydrodynamic radius

Viscosity is inversely proportional to the diffusion constant. We first measure the diffusion constant of a species of known radius, Si beads in our case, in water and then in the solution whose viscosity we intend to measure. From the formula, $\eta_s / \eta_w = D_w / D_s$ where η_s and D_s are viscosity and diffusion constant of Si beads in any solution and η_w and D_w are the corresponding values of Si beads in water, we can calculate η_s.

Diffusion coefficients were obtained from the intensity autocorrelation function provided by the Dynamics V6 software supplied by the instrument manufacturer (Protein Solutions Inc., Charlottesville, VA). Viscosity coefficients were then calculated using the Stokes-Einstein equation (Equation 1). Hydrodynamic radii of 1.5 µM rhodopsin at varying concentrations of SDS were obtained by applying the Stokes-Einstein equation using Dynamics V6 software. All measurements were recorded at 25°C and are shown below in Table 8.

Table 8: Viscosity co-efficient

Viscosity co-efficients water, different concentrations of SDS, urea and GuHCl as measured by the diffusion of Si beads in these different solutions.

Solvent	η (centipoise)
Water	1
0.05% SDS	1
1% SDS	1
3% SDS	1.27
7% SDS	2.6
10% SDS	5
20% SDS	12

Solvent	η (centipoise)
Water	1
2M Urea	1.45
4M Urea	1.7
6M Urea	2.46
8M Urea	3

Solvent	η (centipoise)
Water	1
2M GuHCl	6.38
4M GuHCl	8.62
8M GuHCl	10

2.3.5 Steady-state absorbance spectroscopy

UV-visible absorption spectra were recorded with a Perkin–Elmer λ 25 spectrophotometer (PerkinElmer, Waltham, MA). All spectra were recorded with a bandwidth of 1 nm, response time of 1 sec and scan speed of 960 nm/min. Measurements were taken at $25^{o}C$ using a 10 mm path length cell.

2.3.5.1 Measurement of rhodopsin

Absorbance spectra of purified rhodopsin in buffer N containing 0.05% DM, pH 6 in absence and presence of SDS were measured. The molar extinction co-efficient used for rhodopsin at 500 nm is 40,600 $M^{-1}cm^{-1}$ (Wald and Brown, 1953b). Rhodopsin concentrations were calculated using a molar extinction coefficient of the 500 nm chromophore absorption of 40,600 $M^{-1}cm^{-1}$. A_{500} was determined either directly from absorbance spectra of pure rhodopsin solutions by absorbance difference spectroscopy. First, the dark spectrum was recorded. The rhodopsin solution was illuminated and the spectrum was again recorded. The difference between the two spectra allowed estimation of A_{500} and the concentration of rhodopsin was

calculated as above. For the photobleaching, the samples in the cuvette were illuminated with a 150-W fiber optic light (Fiber Lite A-200; Dolan-Jenner, Woburn, MA) equipped with a > 495 nm long-pass filter (Oriel) for 30 sec. A final full bleached spectrum (250-650 nm) was recorded immediately after illumination.

The time course of the appearance of the peak at 440 nm upon addition of 0.05% SDS was measured by repeated cycles which recorded each spectrum after every 2 min.

2.3.5.2 Measurement of nonapeptide

For accurate analyses of circular dichroism (CD) spectra, the protein spectra needed to be subtracted from buffer spectra containing nonapeptide in cases where rhodopsin was used from a stock of earlier elution fractions as discussed in 2.3.7. This was because of the contribution from the random coil structure of nonapeptide to the CD signal. To determine which elution fraction of rhodopsin has significant amounts of nonapeptide, the nonapeptide concentration in elutions was determined by absorbance spectroscopy. Buffer N containing 0.05% DM and 70 μM nonapeptide was passed through a 1D4 column and elution fractions were collected in the same way it would be done if rhodopsin was bound to the column. 70 μM nonapeptide was used since this is the concentration of nonapeptide used to elute rhodopsin. Absorbance spectra of these fractions are shown in Figure 9.A. and the plot of the maximum absorbance, which is at 196 nm, against the elution fraction number is shown in Figure 9.B. Note that the measurements were done after diluting all solutions by one-third their original concentration to keep the absorbance values below 1 so that Lambert-Beer's law can be followed. The red data point in Figure 9.B. is the absorbance of 70 μM nonapeptide containing solution. As shown in the figure, only the first elution fraction contained nonapeptide less than that 70 μM. This showed that only the first elution fraction contains less nonapeptide and all the following elutions contain the same amount

of nonapeptide as in the elution buffer. Hence, the effects of nonapeptide on the CD signal needs to be subtracted to obtain the true CD signal of rhodopsin.
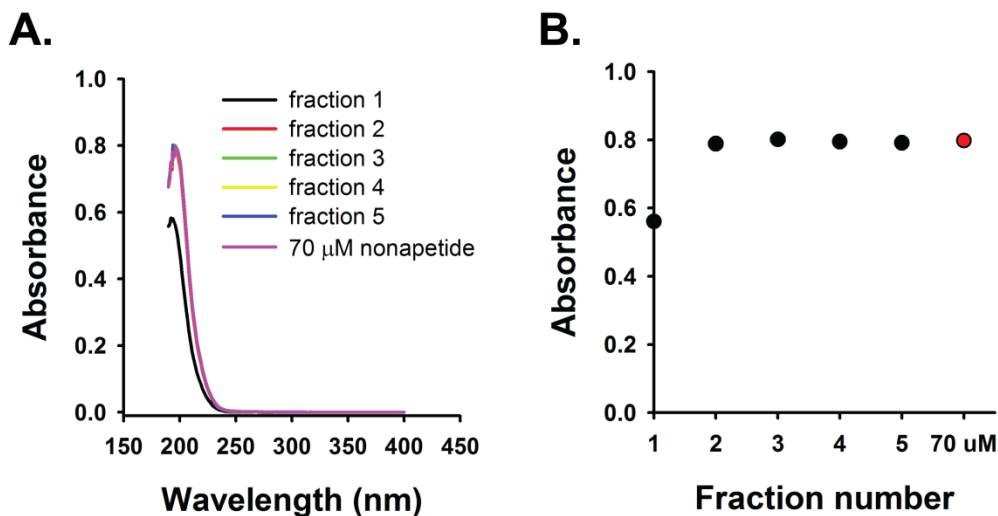
Figure 9: Concentration of nonapeptide in elution fractions.

A. Absorbance spectra of nonapeptide in successive elution fractions as it is collected from the 1D4 column. B. Plot of absorbance of these fractions with their corresponding fraction numbers. Red plot corresponds to absorbance of 70 µM nonapeptide, the concentration used for eluting rhodopsin from 1D4.

2.3.6 Stopped flow absorbance spectroscopy

Stopped flow absorbance measurements were carried out in Dr. Catalina Achim's lab at Carnegie Mellon University. For faster kinetics, the appearance of the 440 nm peak on addition of SDS was recorded for samples containing 1.5 µM rhodopsin as a function of time using a Biologic (Grenoble, France) MOS-450 spectrometer equipped with a SFM-20 stopped flow system. PMS-450 was used as the photomultiplier detector. The syringes were cleaned with double distilled water, ethanol and driend in air before starting an experiment and immediately after an experiment. O rings made of ethylene propylene diene M-class rubber were used which are required at the entrance of the cuvette in the observation head. Syringes containing water,

ethanol and air in that order were screwed into position and the flow lines and cuvette were flushed before the start of every experiment. Measurements were carried out at 25°C. A mixing ratio of 1:6 was used where rhodopsin was diluted to one-sixth its concentration by SDS. The initial rhodopsin concentration was 10 μM so that it reaches a final concentration of 1.5 μM after dilution with SDS. Appropriate intial concentrations of the SDS solutions were used for each titration point. These initial concentrations of SDS were either prepared from dilution of a master stock of 10% or 30% SDS depending on the final concentration required. For each shot to record each reading a total volume of 188 μl (rhodopsin+SDS) was prepared. The first two shots after every titration were required to flush the cell so that the previous sample was displaced with the new sample. Three spectra were recorded for each titration. A total of 8000 data points were recorded for each SDS titration. The time trace of each SDS concentration was fitted by a global fit of three spectra with a monoexponential function. In each case the error of the time constants was less than 4%.

2.3.7 Circular Dichroism spectroscopy

CD spectra were recorded using a Jasco J-810 spectrometer (Jasco Inc., Easton, MD) using a 1 mm quartz cell. All spectra were recorded at 25°C with a bandwidth of 1nm, scan speed of 100 nm/min and a response time of 1 second. Each spectrum reported was an average of ten spectra. Spectra recorded in the absence of denaturant and in the presence of up to 3% SDS, 3 M urea and 3 M GuHCl were subtracted from the corresponding buffer reference spectra containing 70 μM nonamer peptide used during rhodopsin purification. This is because rhodopsin is purified using a nonapeptide as described in Section 2.2.5.4. and the fractions eluted from the column have significant amounts of nonapeptide as described in Section 2.3.5.2. The random coil nature of the

nonapeptide may interfere with the CD signals of the protein and hence needs to be subtracted. CD spectra of nonapeptide were recorded at concentrations 70, 30 and 10 μM. 10 μM nonapeptide did not show any CD signal but 70 and 30 μM solutions significant and intermediate intensity CD signals respectively. For spectra of solutions containing more than 3% SDS, 3M urea, 3M GuHCl and all concentrations of TFA, sodium phosphate buffer containing 0.05% DM and appropriate denaturant concentration without nonamer were subtracted. This was because very small volumes of highly concentrated rhodopsin (~11 μM – 14 μM) were added to the working solution to achieve a final concentration of 1.5 μM resulting in dilution of the nonamer to levels undetectable by CD spectroscopy (nonapeptide levels estimated were below 10 μM). Note that while the subtraction of nonamer peptide affects MRE at 208 nm, the change in MRE at 222 nm is small and amounts to a maximum decrease in absolute MRE at 222 nm of about 5% (for 70 μM peptide, Figures 11.A. and B. in Chapter 3). Most solutions contained less concentrations of the peptide. The effect of denaturants over time was monitored by recording CD scans every 0.5 h for a period of 14 h.

All CD spectra were analyzed using CDPro software (Sreerama and Woody, 2000). The helicity was estimated by using CDPro by taking the basis set (# 10) containing both soluble proteins and MPs (Sreerama and Woody, 2000). A python script was developed in the lab as user interface for running CDPro. The script takes as input the CD spectra in millidegrees (θ), path length of cuvette (l in cm), concentration of protein (c in Molar units) and number of amino acids in protein (n) and calculates molar circular dichroism or delta epsilon

$\Delta\varepsilon = \theta /(10 \times l \times c \times n \times 3298)$ Equation 2

which is used as input to CDPro software. The script by default executes all the three secondary structure determining algorithms CONTIN/LL (Provencher and Glockner, 1981; Sreerama and

Woody, 2000), SELCON3 (Sreerama and Woody, 1993) and CDSSTR (Manavalan and Johnson, 1987) available with CDPro. There is also an option provided in the script for the user to choose either the basis set suggested by CDPro or to use all available basis sets for data processing. The script generates two plain text (comma separated value format) files: (1) wave length versus calculated MRE

$$[\theta] = \Delta\varepsilon \times 3298 \qquad \qquad \text{Equation 3}$$

and (2) re-formatted output of CDPro that can be opened by any spread sheet or plotting programs for further analysis. This script is available at http://jks-lab.structbio.pitt.edu/CD.

2.3.8   Steady-state fluorescence spectroscopy

Fluorescence measurements were carried out using a Varian Cary Eclipse fluorescence spectrophotometer (Varian Inc., Palo Alto, CA). Emission scans of 1.5 μM rhodopsin in 2 mM sodium phosphate buffer, pH 6 and 0.05% DM titrated with SDS in the presence and absence of 10 mM hydroxylamine were recorded in the wavelength range 310 nm-500 nm with an excitation wavelength of 295 nm. Excitation and emission slit widths were kept at 5 nm and 10 nm (bandpass), respectively. Medium photomultiplier voltage was applied and measurements were taken at a scan rate of 600 nm/min. For time course measurements, fluorescence emission at 330 nm was recorded every 30 min. All experiments were carried out at 25°C.

2.3.9   Stopped flow tryptophan fluorescence measurements

Stopped flow fluorescence measurements were carried out in Dr. Michael Trakselis' lab at the University of Pittsburgh. Rapid kinetics of the increase in fluorescence on adding SDS to 1.5 μM rhodopsin were measured using an Applied Photophysics SX18 spectrometer (Surrey, U.K.). All measurements were carried out at 25°C. The mixing ratio of rhodopsin and SDS used was 1:1. The initial rhodopsin concentration was 3 μM so that a 1.5 μM concentration can be obtained after dilution with SDS. Appropriate initial concentrations of SDS were used depending on the final concentration required. The total volume for each reaction mixture or each injection was 50 μl. For equilibriation and displacing the old sample from the cuvette with fresh samples, first three injections if the fresh sample were required. A total of 1000 data points were recorded for each SDS titration. Average of three scans was taken for each titration point. An excitation wavelength of 295 nm and an emission cut-off filter of 320 nm were used. Both, the emission and excitation slits were kept at 0.5 nm. All measurements were repeated three times. All curves were fitted with a sum of exponentials:

$$I(t) = \sum_{i=1} \alpha_i e^{-t/\tau_i} + c$$

Equation 4

where

α_i are the amplitudes,

τ_i are the lifetimes of each ith decay component and

c is the offset.

2.3.10 Terahertz spectroscopy

The THz spectroscopy experiments were carried by Dr. Kristina Woods at Carnegie Mellon University using a Jasco FTIR-6000 series spectrometer. A liquid helium cooled bolometer in the 15-250 cm^{-1} spectral range. The sample cell used in the experiments contained a 0.006 mm thickness polytetrafluoroethylene spacer (Specac Ltd., U.K.). For each transmission measurement a 25-mm-diameter region of the protein sample was illuminated with the THz beam to determine the absorbance. To maintain the hydration level of the protein solution constant during the experiment, the sample was placed in a sealed transmission cell consisting of two silicon windows. In the spectral measurements presented each scan consists of 16 averaged scans and the infrared data were collected with a spectral resolution of 4 cm^{-1}. The 15-120 cm^{-1} THz spectra were collected with a 25 micron beam splitter while the data in the 100-250 cm^{-1} spectral region were collected with a 12 micron beam splitter.

The molecular dynamics (MD) simulations were carried with the Gromacs package (Lindahl et al., 2001) version 3.2 using the Gromacs-96 forcefield. A starting structure of dark state of rhodopsin and the light state were initially downloaded from the protein databank. Both proteins were hydrated with water molecules and ions. In the simulations the SPC model of water was used. Energy minimization of the hydrated protein systems were carried out by using a steepest descent method to a convergence tolerance of 0.001 $kJ\ mol^{-1}$. The energy minimization was followed by a MD run with constraints for 200 ps in which an isotropic force constant of 100 $kJ\ mol^{-1}\ nm^{-1}$ was applied to the protein atoms. During the restrained dynamics simulation the temperature and pressure of the system were kept constant by weak coupling to Berendsen temperature and pressure baths (Berendsen et al., 1984). In all cases the protein, water, and ions have been coupled to the temperature and pressure baths separately. Particle

Mesh Ewald (PME) method (Darden et al., 1993; Essmann et al., 1995) was used to calculate the electrostatic interactions in the simulation, with a real-space cutoff of 1.0 nm, a fourth order B-spline interpolation, and a Fourier spacing of 0.12 nm.

2.3.11 Mid-IR spectroscopy

Mid-IR experiments were carried out with the help of Dr. Kristina Woods at Carnegie Mellon Institute. An absorption/transmission/reflectance (ATR) experiment was conducted due to the greater resolution than afforded by the regular transmission experiment. Spectra were collected in the 4000-650 cm^{-1} spectral region using a Midband MCT detector (MCT-B) operating in the 600-4000 cm^{-1} spectral range and a Ge/KBr beam splitter. Each sample scan contained 128 averaged scans with a spectral resolution of 4 cm^{-1}. All other parameters were set to default values. 10 μl of 1.5 μM rhodopsin in native or denatured states was placed in the sample window. The window was cleaned thoroughly with ethanol before adding every sample. A background spectrum without any sample was taken each time to confirm that the window was clean. A characteristic spectrum was obtained representative of a clean window. This background spectrum with air was also auto-subtracted from each sample spectrum. All the buffers were prepared in D_2O and deuterated SDS, urea and GuHCl were used. The final amount of D_2O in rhodopsin samples was 88.8%. This was done to reduce background signals from water in the amide I region of the spectrum. However, background signals from SDS and urea appeared in the amide I region and hence samples containing these denaturants could not be tested by mid-IR spectroscopy. Different concentrations of SDS and urea were tested but large signals appeared overlapping with the protein peaks in the amide I region.

2.3.12 NMR Spectroscopy

2.3.12.1   Parameters for recording 1D ^{1}H NMR spectra

Prameters pertaining to samples used for different experiments (eg. concentrations and buffer) are mentioned in the Results sections and figure legends where appropriate. DSS (2,2-Dimethyl-2-silapentane-5-sulfonic acid) was employed as external reference. 5 mm NMR tubes were used for measuring buffer spectra, 3 mm and 1.7 mm diameter NMR tubes were used for measuring denaturant containing rhodopsin samples. Data were acquired and analyzed using Topspin and Sparky software. 1D ^{1}H NMR spectra for determination of aggregation (Section 3.3.1.) were recorded on a 800 MHz spectrometer using selective excitation scheme with sculpting that utilizes a double pulse field gradient spin echo sequence (DPFGSE) (Hwang and Shaka, 1995; Stott, 1995). A total of 2048 scans were averaged to obtain the final spectrum at each condition. A line broadening of 1 Hz was used to process final spectra. 1D ^{1}H NMR spectra for detecting global changes on SDS denaturation (Section 4.6.) were recorded on a 900 MHz spectrometer using the p3919gp pulse program (Piotto et al., 1992) and a total of 1000 scans were collected for each sample.

2.3.12.2   Optimization of conditions to set up 2D heteronuclear single quantum correlation (HSQC) experiments

1D HSQC spectra were first recorded to optimize the conditions required to obtain a spectrum with suitable signal to noise ratio so that a 2D HSQC measurement with appropriate number of scans can be set up. Experiments were initially carried out on a 800 MHz spectrometer. The first sample tested was 50 μM α,ε-^{15}N-Tryptophan labeled rhodopsin denatured with 30% SDS in 5 mm NMR tubes. After recording 60,000 number of scans, high

intensity proton peaks from SDS appeared in 1-2 ppm region (Figure 10.A.) and low intensity proton peaks from protons attached to ^{15}N isotope in the protein appeared in the 8-10 ppm region (Figure 10.B., black spectrum). 1D HSQC pulseprogram with sensitivity enhancement (Morris, 1980) was also used but it did not show any improvement in protein signal intensity. Another reason for poor protein signals was a high p1 (proton, 90° pulse) value of ~27 that was obtained under these conditions. To prevent background signals of SDS buffer from appearing, deuterated SDS was used as denaturant and the sample was taken in a 3 mm NMR tube to reduce the p1 value. 1D HSQC spectrum of sample containing deuterated SDS was overlaid with that containing protonated SDS is shown in Figure 10. The p1 value reduced to ~18 and less background signals were observed (Figure 10.A., red spectrum) but the protein signals did not increase in intensity by a large amount (Figure 10.B., red spectrum). The same sample was then recorded on a 900 MHz spectrometer to see if there is any further increase in protein signal intensity. 1D HSQC at 37°C, 45°C and 55°C were recorded for 10,000 number of scans. However, no peaks were observed, even at higher temperatures. We therefore increased the protein concentration to 0.12 mM. The spectrum of 1000 number of scans of 0.12 mM rhodopsin denatured with 30% deuterated SDS and recorded on a 900 MHz instrument is overlaid with that of 50 μM rhodopsin denatured under the same condition and where 60,000 number of scans were collected on a 800 MHz instrument (Figure 10.B.). The former spectrum, with 2-fold increased protein concentration, showed similar signal intensity as the latter, despite using only 1/60th number of scans. The signals further improved by using 1.7 mm NMR tubes due to the decrease in p1 value to 12. Therefore, sample conditions were optimized to 0.12 mM rhodopsin, use of deuterated SDS and 1.7 mm NMR tubes at 37°C in a 900 MHz spectrometer. This indicated that the signals improved sufficiently with increase in rhodopsin concentration, change of NMR tube

to a narrower tube and with a higher magnetic field spectrometer. Similarly, for samples containing SDS and urea, deuterated forms of both denaturants were used. Moreover, for these samples, the pH had to be adjusted to pH 2 otherwise large background signals from the amide group of urea interfered with protein signals. For α-^{15}N-Lysine labeled rhodopsin, 50 μM of the protein was sufficient to obtain a good signal to noise ratio on a 900 MHz spectrometer at 37ºC.

2D HSQC spectra were set up under these optimized sample conditions for both ^{15}N-tryptophan and ^{15}N-lysine labeled samples. For the former sample, 2000 number of scans were recorded in the ^{1}H dimension was used to record 2D. The number of scans in the ^{15}N dimension was optimized by trial and error. Lower number of scans were required for the ^{15}N-lysine labeled sample which contained SDS. The number of scans after trial was set at 128 in the ^{1}H dimension and 48 in the ^{15}N dimension. However, a higher number of scans of 256 in the ^{1}H dimension and 80 in the ^{15}N dimension were required for the 3S8U, added in that order at pH 2 to the ^{15}N-lysine labeled sample.
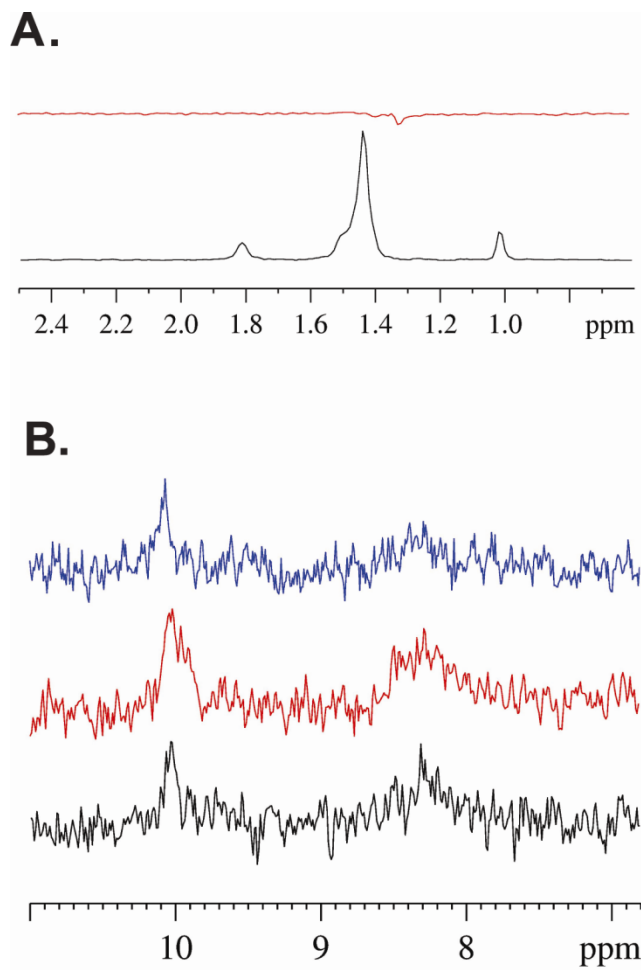
Figure 10: 1D HSQC spectra of 50 µM rhodopsin denatured with SDS.

A. Overlay of 1D HSQC spectra of A. 50 µM rhodopsin denatured with protonated 30% SDS (black) and deuterated SDS (red) in the region where SDS peaks appear. B. Overlay of 1D HSQC spectra of 50 µM rhodopsin denatured with protonated 30% SDS (black) and that with deuterated SDS (red) in the region where the amide proton peaks appear. Both these spectra were collected on a 800 MHz spectrometer. The blue spectrum is of 0.12 mM rhodopsin denatured with deuterated 30% SDS. The number of scans recorded are 60,000 for the 50 µM rhodopsin sample and 1000 for 0.12 mM rhodopsin sample. Since the number of scans is different for the blue spectrum, it is overlaid by adjusitng the noise level so that it is similar to the black and red spectra. Both spectra were collected on a 800 MHz spectrometer.

2.3.12.3 Parameters for recording ^{19}F NMR spectra and relaxation rate measurements

All ^{19}F NMR spectra were recorded on a Bruker ~600 MHz spectrometer equipped with a QNP probe at a ^{19}F resonance frequency of 564.686 MHz. Data acquisition and analysis were carried out using Topspin software. The sample was locked on deuterium. Samples were referenced to an internal standard, TFA. 5 mm tubes were used for measurements of free fluorine labels in solution and Shigemi tubes were used for rhodopsin samples. For samples containing glycerol, a co-axial glass insert tube (Wilmad lab Glass) filled with 100% D_2O was inserted into the 5 mm NMR tube for deuterium locking. Acquisition time, number of scans averaged and other specific parameters were as indicated in the text or legends in Chapter 7. Different pulse sequences were used as described below.

Relaxation rates of free fluorine labels in D_2O and glycerol and that of rhodopsin labeled with 4F at different temperatures were measured. To identify mechanisms dominant in monofluro methyl relaxation, R_2 of free label and that of label attached to rhodopsin was measured using different methods (also refer to Sections 7.5. and 7.8.). Since in monofluoro labels compared to trifluoro labels, two ^{19}F atoms are substituted to protons, effects of these protons on ^{19}F relaxation was studied using CPMG pulse sequences with a ^1H 180° pulse and with a composite proton pulse. Both these ways were aimed at suppressing cross-correlation between F-H dipolar interaction and fluorine CSA. Transverse relaxation rates (R_2) of free labels were determined using the following methods: 1) a Carr-Purcell-Meiboom-Gill (CPMG) experiment (Carr and Purcell, 1954; Meiboom and Gill, 1958) 2) CPMG experiment with a ^1H 180° pulse and 3) CPMG experiment with composite ^1H pulses, WALTZ (Shaka et al., 1983) and GARP (Shaka et al., 1985). WALTZ is a composite pulse which consists of 90° pulses with

phases x and –x and GARP is a composite pulse consisting of pulses with various durations with phases x and –x. All R_2 experiments were recorded by collecting a series of spectra with different relaxation delays in Tables 14 and 15 in Appendix A. Longitudinal relaxation rates (R_1) for free label were measured with and without ^{1}H 180° pulse using the Freeman-Hill method (Freeman and Hill, 1971) with the relaxation delays 0, 600, 1200, 1800, 2400, 3000, 3600, 4200, 5400 ms for 4F and 4F3 in D2O at 15, 25 and 35°C and in glycerol at 25°C the delays are 0, 40, 80, 120, 160, 200, 240, 280 ms for 4F3 and 0, 80, 160, 240, 320, 400, 480, 560 for 4F.

R_2 of 4F labeled rhodopsin was measured using 1) CPMG experiment 2) CPMG experiment with a ^{1}H 180° pulse, 3) a constant-time CPMG experiment by recording one reference spectrum at time zero and 4 repeated spectra at a constant relaxation delay of 3.6 ms with half durations between the pulses of 0.872, 0.422, 0.272 and 0.197 ms (R_{2disp}) and 4) a spin-lock experiment at a spin-lock radio-frequency field at 6.25 kHz with delays of 0, 1, 2, 3, 4, 5, 6 and 8 ms ($R_{1\rho}$). All experiments were conducted with ^{1}H decoupling during acquisition periods. Longitudinal relaxation rates (R_1) for rhodopsin sample was measured with and without ^{1}H 180° pulse using Freeman-Hill method with relaxation delays of 0.001, 0.0125, 0.025, 0.05, 0.07, 0.1, 0.15 and 0.2 ms. All relaxation experiments were carried out by recording a series of spectra with different relaxation delays and plotting the decrease in signal intensity over delay time. Relaxation rates were determined by fitting the relaxation rate curves to a mono-exponential function with 2 parameters,

$$y = y_0 e^{-Rt}$$
<div align="right">Equation 5</div>

where y is signal intensity at a given time t, y_0 is the initial signal intensity and R is relaxation rate. Decay curves were fit using Sigmaplot.

2.3.13 EPR spectroscopy

EPR experiments were performed in Dr. Wayne Hubbell's lab at University of California, Los Angeles (UCLA) with the help of Dr. Christian Altenbach and Sheryll Mangahas. EPR spectra were obtained on a Bruker ELEXSYS 580 using a High Sensitivity Resonator. The width of all spectra was 100G taken over a time frame of 30 s. The modulation amplitude was 1G with an incident microwave power of ~ 20 mW. If spectra appeared clipped, modulation amplitude was changes to 0.8G but in no case it was decreased lower than 0.8G. Attenuation was kept at 10 during measurements. All spectra were average of 25 scans. All experiments were carried out at 25°C. 6 μl sample in borosilicate capillary tubes of inner diameter 0.6 mm and outer diameter of 0.8 mm were used for each reading. Concentration of rhodopsin depended upon the type of mutant and the amount purified from transiently transfected COS-1 cells. Concentrations used were in the range of 50 μM – 100 μM rhodopsin. Continuous wave (CW) spectra of rhodopsin in dark, after light activation and in SDS denatured states were measured. Spectra were also recorded after 1 h of light activation. For denatured states, time points were taken after 1 h and overnight. LabVIEW programs (program name is Convert and Align) written by Dr. Christian Altenbach at University of California, Los Angeles were used to correct the offset, normalize and convert to a file usable by the baseline correction program.

[A] 137 mM NaCl, 2.7 mM KCl, 1.8 mM KH_2PO_4, 10 mM Na_2HPO_4 (pH 7.2)

[B] Amino Acid Composition of DMEM (Irvine Scientific):

Essential Amino Acid	mg/l	Non-essential Amino Acid	mg/l	Vitamins	mg/l	Inorganic Salts and other	mg/l
Arginine * HCl	84	Alanine	None	D-Ca pantothenate	4	$CaCl_2$	50
Histidine * HCl * H_2O	42	Asparagine	None	Choline Chloride	4	$Fe(NO_3)_3$ * 9 H2O	0.1
Isoleucine	105	Aspartate	None	Folic Acid	4	MgSO4	97.7
Leucine	105	Cystine* 2HCl	63	i-Inositol	7.2	KCl	400
Lysine * HCl	146	Glutamate	None	Niacinamide	4	NaCl	6400
Methionine	30	Glutamine	584	Pyridoxal*HCl	4	NaH_2PO_4 *H_2O	125
Phenylalanine	66	Glycine	30	Riboflavin	0.4		
Threonine	95	Proline	None	Thiamine*HCl	4		
Tryptophan	16	Serine	42			Phenol Red * Na^+	15
Valine	94	Tyrosine* 2 Na^+ * 2 H_2O	104			Glucose	4500

[C] buffer B with 100 units/ml Penicillin, 100 units/ml streptomycin

[D] buffer B and C with 10% FBS

[E] DMEM/F12: Ham's F-12/DME High Glucose (GIBCO) supplemented with 2 mM L-glutamine, 100 units/ml Penicillin, 100 units/ml Streptomycin, 10% fetal bovine serum

[F] 1.5 M glycine, 3M NaCl

[G] 0.1 M citric acid, 0.15M NaCl (pH 3)

[H] 6 M guanidinium-HCl

[I] 50 mM Na_2HPO_4/NaH_2PO_4 (pH 7), 0.01% thimerosol

[J] 0.25 M $NaHCO_3$, 0.5M NaCl (pH 8.3)

[K] 3.3 M K_3PO_4 (pH of 11.9 at 10-fold dilution)

[L] 0.25 M NaH_2PO_4/Na_2HPO_4 (pH 6)

[M] 0.1 M NaOAc, 0.5 M NaCl (pH 4)

[N] 2 mM Na_2HPO_4/NaH_2PO_4 (pH 6)

[O] 5 mM 2-(N-morpholino)ethanesulfonic acid (MES), pH 6.0

[P] 20 mM Na_2HPO_4/NaH_2PO_4 (pH 6), 10% D_2O

[Q] 1.5 M Tris, 0.4% SDS, pH 8.8

[R] 0.5 M Tris, 0.4% SDS, pH 6.8

3.0   CHAPTER 3: OPTIMIZATION OF DENATURING CONDITIONS TO MAXIMALLY UNFOLD RHODOPSIN

3.1   RATIONALE AND SUMMARY

Biophysical characterization of denatured states of a protein requires long-term stability of the denatured state without aggregation. Further, the extent of unfolding is important. In order to catch a glimpse of the earliest stages in folding, unfolding to a maximum extent is desirable. In this chapter, I therefore describe our efforts to chemically denature rhodopsin in DM detergent micelles by addition of the denaturants SDS, trifluoroacetic acid (TFA), urea and GuHCl and combinations thereof. MRE at 222nm, which represents the amount of helicity in a protein, was seen to decrease in the presence of maximum concentrations of denaturants in the order TFA > GuHCl > urea > SDS + urea > SDS. Through a combination of light scattering, SDS-PAGE, dependence of MRE at 222 nm on protein concentration and 1D ^{1}H NMR, I showed that rhodopsin aggregates when denatured by GuHCl, TFA and urea but not in any concentration of SDS, added over a range of 0.05% to 30%. Further, mixed denaturing conditions consisting of 3% SDS and 8M urea, added in this order, did not result in aggregation. SDS is able to prevent the exposure of large hydrophobic regions present in MPs which otherwise would lead to aggregation. Therefore, 30% SDS and 3S8U are the denaturing conditions of choice to study maximally unfolded rhodopsin without aggregation.

3.2   DETERMINING THE EFFICIENCY OF UNFOLDING

Secondary structure of rhodopsin in the presence of different chemical denaturants (SDS, urea, GuHCl, TFA, and combinations thereof) was assessed by CD. While solvent background precluded measurements at very low wavelengths for some of the conditions, at the very minimum the range including MRE at 222 nm - most important for assessment of helical structure content - was obtained for all conditions.

3.2.1   SDS as a denaturant of rhodopsin

To measure the loss of secondary structure in the presence of increasing amounts of SDS, rhodopsin was titrated with varying concentrations of SDS and the CD spectrum was recorded at each concentration. CD spectra of rhodopsin (1.5 μM) alone and in the presence of low concentrations of SDS up to 3% are shown in Figure 11.A. and those in the presence of high SDS concentrations up to 30% are shown in Figure 11.B. The corresponding plots of MRE at 222 nm are shown in Figure 11.C. and 11.D., respectively. The magnitude of MRE at 222 nm decreases abruptly at a concentration of 0.05% SDS and then remains essentially constant with increasing SDS concentrations until 3% (Figure 11.C.). The decrease in the magnitude of MRE at 222 nm at 3% SDS is $12\pm2\%$ which corresponds to an estimated ~19% decrease in helicity calculated using CDPro software (Sreerama and Woody, 2000). However, already at 2% SDS, a slight increase in the magnitude of MRE begins which reaches a maximum at 10% SDS (Figure 11.D.). Subsequently, a large decrease in the magnitude of MRE values at 222 nm is observed as the SDS concentration is raised beyond 10% up to 30% as shown in Figure 11.D. The change in MRE at 222 nm is $39\pm6\%$ at 30% SDS indicating loss of substantial amounts of native helical

regions. The corresponding decrease in helicity, as approximated using CDPro software, is ~45%. In order to ensure that the values recorded at each SDS concentration correspond to the maximal denaturation by SDS at that concentration, rhodopsin was incubated with 0.05%, 1.5%, 3% and 30% SDS overnight at 25°C. Loss of secondary structure was monitored by CD spectroscopy every 30 min during the incubation period but no time dependent further denaturation was observed (data not shown).

The changes in CD spectra (shown in Figure 11.A.) with increasingly higher concentrations of SDS added to rhodopsin are summarized in Figure 11.C. by MRE at 222 nm as a function of SDS concentration. SDS concentrations up to 3% show two distinct stages, an initial decrease in helicity followed by no change up to 3% SDS. The CD results at higher SDS concentrations are shown in Figure 11.B. and 11.D. A third stage over the range of SDS concentrations 3% to 10% SDS can be clearly seen in the CD spectrum in Figure 10.B. and summarized in Figure 11.D.: a distinct increase in the magnitude of MRE at 222 nm is observed in this range. In a fourth stage (15% to 30% SDS), a sudden decrease in helicity to a large extent is seen at concentrations beyond 15% SDS.
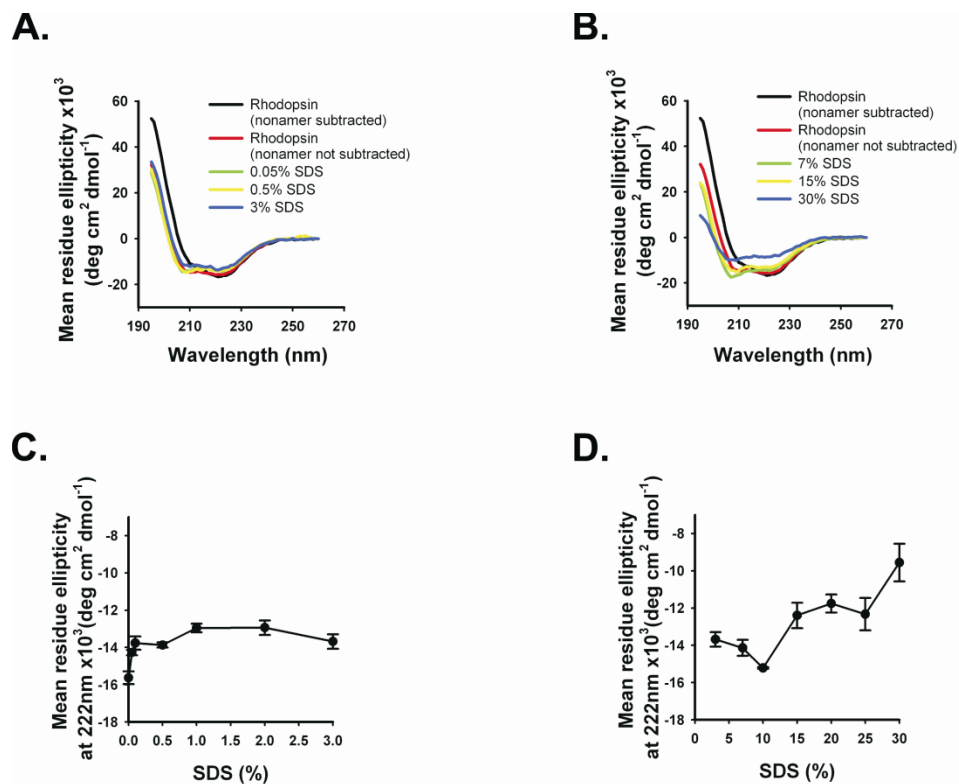
Figure 11: SDS induced denaturation of rhodopsin monitored by CD spectroscopy.

CD spectra of 1.5 μM rhodopsin (black line) alone and in presence of A. 0.05%-3% and B. 7%-30% SDS concentrations. Total MRE at 222 nm of rhodopsin in presence of C. 0.05%-3% SDS and that in presence of D. 7%-30% SDS. All CD spectra in A. are subtracted from the corresponding buffer spectrum containing 70 μM nonapeptide and those in Figure B. are subtracted from buffer alone because of reasons stated in the Experimental Procedures section. Spectra of rhodopsin (nonamer not subtracted) correspond to a concentration of 1.5 μM obtained after dilution from a very high concentrated protein sample thus resulting in amounts of nonamer undetectable by CD.

3.2.2 Thermal denaturation

Rhodopsin at 1.5 μM was subjected to thermal denaturation by increasing temperature from 25°C to 100°C. The extent of unfolding by temperature was measured by CD spectroscopy. The decrease in MRE at 222 nm with increase in temperature is shown in Figure 12. 50% decrease in

MRE at 222 nm was observed with the mid-point of the transition temperature (melting temperature) at 65°C. SDS denatured states were also subjected to temperature denaturation to determine if combined effects of SDS and temperature led to increased denaturation. A further 30%, 50% and 35% decreases in ellipticity were observed for 3%, 10% and 25% SDS denatured states. A shift in the melting temperature was observed with increase in SDS concentration. There is an increase in Tm values, starting at 65°C for native rhodopsin and rising to ~85°C for rhodopsin in the presence of 3% SDS indicating increase in stability of SDS denatured states with increase in SDS concentration. Beyond 3% SDS, melting temperature drops to 70°C at SDS concentration up to 30%. These values of Tm are qualitative since the melting curves could not be fit accurately to a two-state model due to the absence of a distinct second stage of unfolded state, particularly at high SDS concentrations. Further, as described in Section 3.3.2. rhodopsin begins to aggregate at 55°C and higher temperature complicating interpretations on changes in helicity or MRE at 222nm at these high temperatures in presence of SDS.
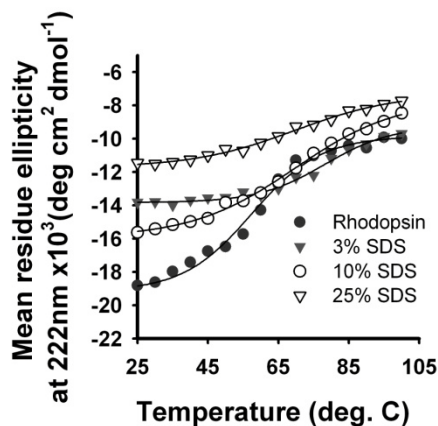
Figure 12: Change in secondary structure with temperature.

Plot of change in MRE at 222 nm with temperature of rhodopsin in presence and absence of SDS.

3.2.3   Urea as a denaturant of rhodopsin

Next, the effect of urea on rhodopsin was measured by CD spectroscopy. Rhodopsin (1.5 μM) was titrated with different concentrations of urea and the CD spectrum was recorded at each concentration, as shown in Figure 13.A. The change in MRE at 222 nm as a function of urea concentration is shown in Figure 13.B.

A two-stage unfolding behavior was observed. Essentially, no change in secondary structure of rhodopsin occurs up to 6 M urea. This is followed by a steep decrease by 57% in the magnitude of MRE at 222 nm in the range between 6 M and 10 M urea. This is greater than the extent of denaturation by 30% SDS. The mid-point of the unfolding transition is at 7 M urea. No time-dependent change in ellipticity was observed when rhodopsin was incubated with 10 M urea for 12 h (data not shown).
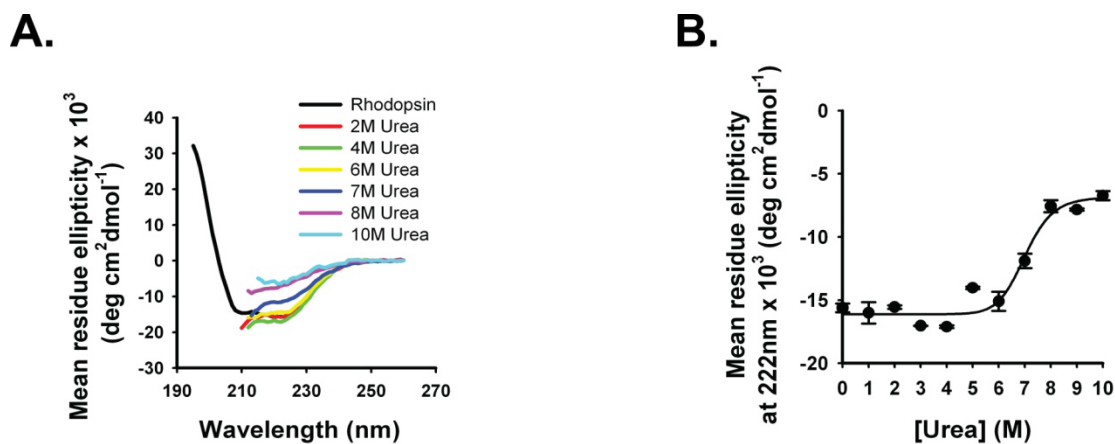
Figure 13: Urea induced denaturation of rhodopsin monitored by CD spectroscopy.

A. CD spectra of 1.5 μM rhodopsin (black line) alone and in presence of urea concentration from 2 M to 10 M. B. MRE at 222 nm of rhodopsin in presence of 1 M-10 M urea.

3.2.4   3% SDS+8M urea mixture as a denaturant of rhodopsin

SDS caused a significant extent of denaturation of rhodopsin without causing aggregates whereas urea denatured secondary structure of rhodopsin to a greater extent than SDS but caused aggregation (Section 3.3.3.). Therefore, if a mixed denaturant condition consisting of both, SDS and urea could result in an extent of denaturation similar or greater than that of urea but without aggregation was tested. Concentrations of 3% SDS and 8 M urea were chosen because addition of more than 3% SDS and 8 M urea led to large increase in the total volume and dilution of the protein concentration. Also, 8 M urea led to a similar degree of disruption of secondary structure as 10 M urea, the latter being the maximum urea concentration that can be used. A 44% decrease in MRE at 222 nm was observed when rhodopsin (1.5 μM) was treated with 3% SDS followed by addition of 8 M urea as indicated by the CD spectrum shown in Figure 14.A. A similar decrease in MRE at 222 nm was also observed when rhodopsin was first treated with 8 M urea followed by addition of 3% SDS (data not shown). Comparison of the extent of denaturation by 3% SDS (3S), 8 M urea (8U), 3% SDS+8 M urea (3S8U) and 30% SDS (30S) is shown in Figure 14.B.

As can be seen in this figure, addition of 8 M urea to 3% SDS denatured rhodopsin decreases the helicity to a much greater extent than that by 3% SDS alone. Also, the mixed denaturant leads to a similar extent of denaturation as that by 8 M urea and is slightly greater than that by 30% SDS.
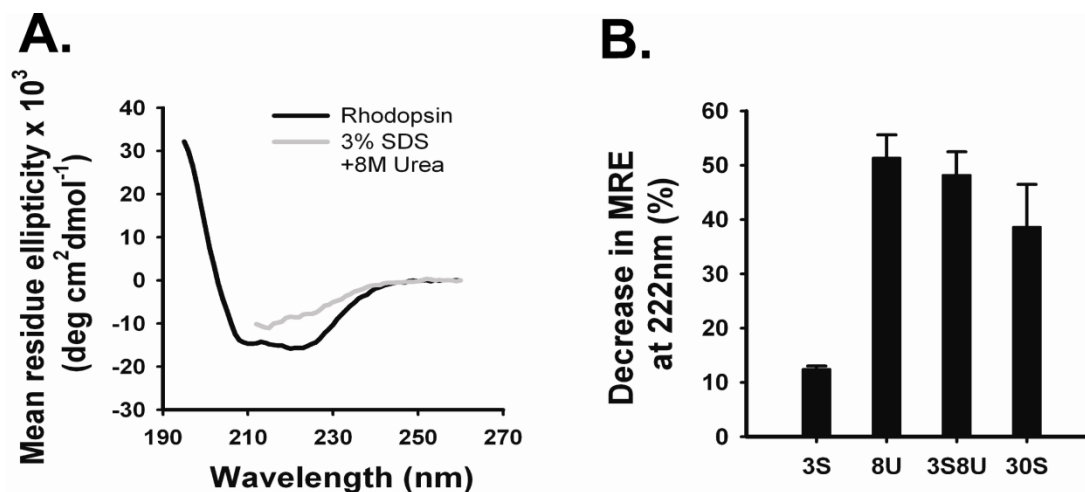
Figure 14: 3% SDS+8M urea induced denaturation of rhodopsin monitored by CD spectroscopy.
A. CD spectra of 1.5 μM rhodopsin (black line) alone and in presence of SDS+urea (grey line). B. Bar graph comparing percent decrease in MRE at 222 nm under different denaturing conditions of 3% SDS (3S), 8 M urea (8U), 3% SDS + 8 M urea (3S8U) and 30% SDS (30S).

3.2.5 GuHCl as denaturant of rhodopsin

Another denaturant, GuHCl, which is a common denaturant for soluble proteins was tested on rhodopsin. The CD spectra of rhodopsin (1.5 μM) titrated with different concentrations of GuHCl are shown in Figure 15.A. A plot of the change in MRE at 222 nm as a function of GuHCl concentration is shown in Figure 15.B. Similar to the urea-induced denaturation, a two-stage behavior is seen on GuHCl unfolding. Here, the mid-point of transition was at 4 M GuHCl, as compared to the mid-point of the unfolding transition in urea of 7 M (see Section 3.2.3.). The decrease in MRE at 222 nm at 8 M GuHCl is 66%; no time-dependent decrease in helicity was observed when rhodopsin was incubated with 8 M GuHCl for 12 h (data not shown).

A mixture of SDS and GuHCl was also considered for denaturation so that a hydrophobic environment is provided by SDS to mask the unfolded hydrophobic reigons of rhodopsin. However, SDS and GuHCl buffers when mixed together formed a precipitate, preventing further experiments with the protein.

3.2.6   TFA as denaturant of rhodopsin

Finally, an organic solvent, TFA, known for its strong denaturing properties and previous denaturation power in the case of bacteriorhodopsin (Huang et al., 1981) was tested. 4 M TFA was seen to disrupt rhodopsin almost completely as seen by the absence of a CD signal in the spectrum shown by the purple spectrum in Figure 15.A. However, 4 M TFA buffer alone gave a strong CD signal, making the quantification of the signal unreliable. Lower concentrations of TFA were also tested. For example, TFA at a concentration of 100 mM is the highest concentration with minimal signal background. However, this concentration led to a relatively small decrease of only ~12% in MRE at 222 nm (data not shown).
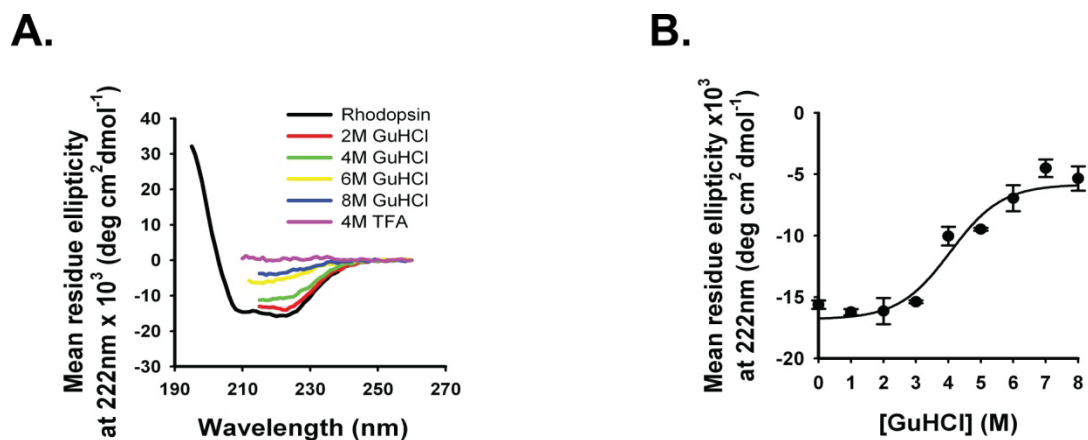
Figure 15: GuHCl and TFA induced denaturation of rhodopsin monitored by CD spectroscopy.

A. CD spectra of 1.5 μM rhodopsin (black line) alone and in presence of GuHCl concentration from 2 M to 8 M and 4 M TFA. B. MRE at 222 nm of rhodopsin in presence of 1-8 M GuHCl.

3.3   DETECTION OF AGGREGATES UNDER DIFFERENT DENATURING CONDITIONS

For each denaturant, presence or absence of aggregation was established. Here, the methods varied depending on the denaturant because some approaches are not applicable to some denaturants. The results are summarized in Table 9. and are described below in order of denaturant.

Table 9: Summary of biophysical techniques used to detect aggregates.

Denaturants	Concentration range	Techniques used for detection of aggregates					
		CD	SDS-PAGE	NMR	Trp fluorescence	Cys accessibility	By eye
SDS	0% - 30%	No dependence of MRE on [rhodopsin]	No oligomeric bands	No broad peaks representing aggregates	Shown in Chapter 4 for analyses of tertiary structure changes	Shown in Chapter 4 for analyses of tertiary structure changes	No precipitates detected
Urea	0M -10M	Not done since clear from SDS-PAGE and visual detection	Oligomeric bands	Cannot be done since aggregates are formed as seen by eye	Not done since sufficient evidence from SDS- PAGE and visual detection	Not done since sufficient evidence from SDS- PAGE and visual detection	Precipitates detected
SDS+Urea	3S8U	Not done since clear evidence from SDS-PAGE	No oligomeric bands, aggregation seen only when urea is added before adding SDS	Not done since clear evidence from SDS-PAGE	Not done since clear evidence from SDS-PAGE	Not done since clear evidence from SDS-PAGE	No precipitates detected
GuHCl	0M - 8M	Dependence of MRE on [rhodopsin]	GuHCl buffer alone precipitates on addition of Laemmlli dye	Cannot be done since aggregates are formed as seen by eye	Shows a decrease at 8M after an increase at 3M	Shows a decrease at 8M after an increase in 3M	Precipitates detected
TFA	100mM and 4M	Not done since precipitates were detected by eye and large background signals from buffer alone	Not done since precipitates were detected by eye	Cannot be done since aggregates are formed as seen by eye	Not done since precipitates were detected by eye	Not done since precipitates were detected by eye	Precipitates detected

3.3.1 SDS as a denaturant of rhodopsin

The studies described in Section 3.2.1. strongly suggest that high concentrations of SDS are very well suited to denature rhodopsin. In order to be able to characterize the molecular nature of such states, it is imperative that no aggregation occurs in the presence of SDS. Therefore, aggregation was tested by using multiple complementary methods, including SDS-PAGE, dependence of molar ellipticity on rhodopsin concentration, and ^{1}H NMR spectroscopy.

First, presence of aggregates was tested on native PAGE (Figure 16) to nullify the effects of SDS in the gel on denatured samples. Different native gels were tested. Firstly, non-denaturing gels made from phosphate buffer at pH 6.3 and 8.4 (Chapter 2, Section 2.3.3.2. for protocol) were tested. Rhodopsin in native state and that denatured with 3% SDS were run on a 10% gel but protein bands appeared stuck in the well upon Coomassie staining. 7.5% and 5% gels were then tested (Figure 16). The same samples were run and rhodopsin heated at 70°C was run as a positive control for aggregation. The 7.5% gel showed smears of SDS denatured samples running at the same position as that of rhodopsin except 3% SDS sample which ran lower than the rest. Thermally denatured sample was stuck in the well indicating aggregation. To clearly distinguish that rhodopsin samples were not stuck in the well, a lower percentage gel of 5% was tested to see if the protein samples can resolved on the gel. The thermally denatured sample remained stuck in the well while all the samples resolved on the gel with those containing greater SDS concentration running lower in the gel. The absence of any bands of molecular weight greater than rhodopsin in SDS denatured samples indicated absence of aggregation. However, to obtain a gel with stronger and discrete band, another buffer condition was tested. 10% gels containing tris were prepared as described in (Chapter 2, Section 2.3.3.2.) but the
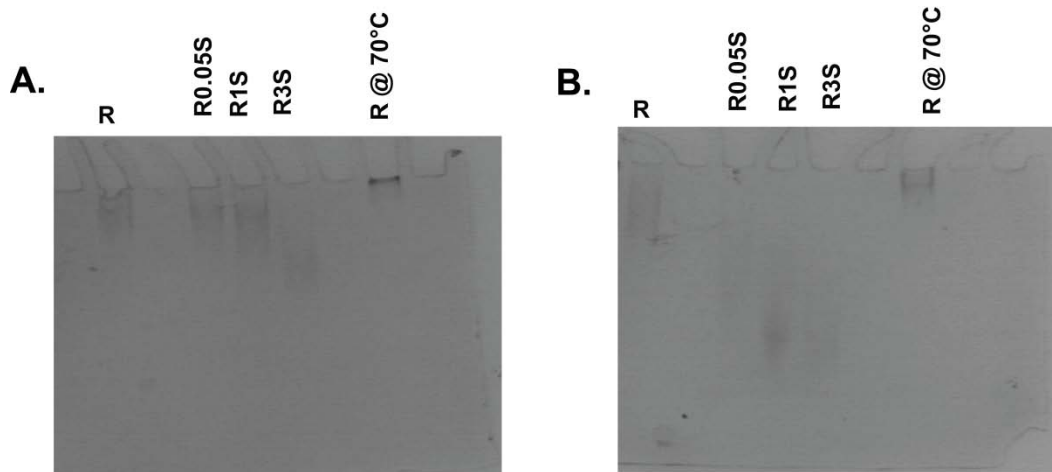
Figure 16: Native phosphate PAGE of SDS denatured rhodopsin

Coomassie stained A. 7.5% gel and B. 5% gel. Samples shown are rhodopsin in native state and denatured with 0.05% SDS (R0.05S), 1% SDS (R1S), 3% SDS (R3S) and 70°C (R@70°C).
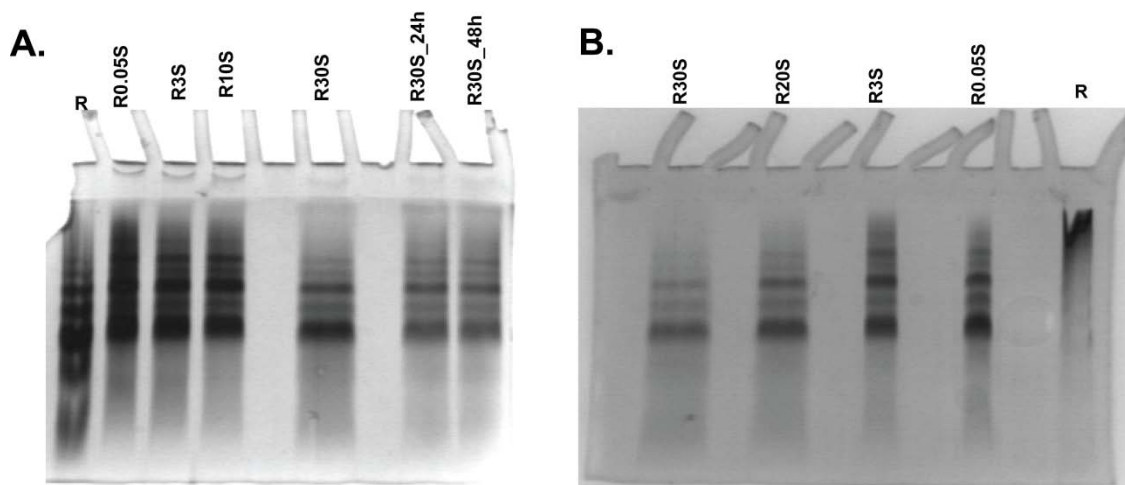
Figure 17: Native PAGE (without SDS) of SDS denatured rhodopsin

Silver stained 10% polyacrylamide gels prepared containing all the components of a SDS-PAGE but without SDS. Gels were run in the A. light and B. dark at 4°C, 120 V for 3 h. Samples shown are rhodopsin in native state and denatured with 0.05% SDS (R0.05S), 3% SDS (R3S), 10% SDS (R10S), 30% SDS (R30S), 30% SDS after 24 h and 48 h incubation.

protein bands did not run below the wells at all. Therefore, another kind of native PAGE was used. The composition of these gels was same as SDS-PAGE except no SDS was added. Gels were run with rhodopsin denatured in different concentrations of SDS as indicated in Figure 17.A. under light conditions according to the procedure described in Chapter 2, 2.3.3.2. and were stained with silver stain. Multiple bands were seen for all the samples, even for native rhodopsin. Such oligomeric bands were also seen in a previous report where opsin in disc membranes solubilized in 0.6% DM was run on blue native PAGE (Suda et al., 2004). The reason given for oligomerization of opsin was light-induced conformational change in rhodopsin. We tried to run blue native PAGE with our samples but a smear was obtained under the conditions tested. It is well established that for running blue native PAGE several parameters need to carefully optimized, particularly for MPs, such as protein detergent ratio and amount of Commassie dye which provides electrophoretic mobility to the protein in a native dye (Heuberger et al., 2002; Suda et al., 2004). The consideration of these factors while interpreting blue native PAGE has been discussed previously for rhodopsin (Heuberger et al., 2002). Hence, we did not proceed further with blue native PAGE. Appearance of oligomeric bands for native rhodopsin on native PAGE could be light-induced as previously observed. The same size of oligomeric bands also appeared in SDS denatured samples at all SDS concentrations. This is contrary to what was expected if aggregates were present, i.e. more intense bands of oligomers at higher SDS concentrations. Therefore, it was not clear if these bands appeared as a result of aggregation. Therefore, native PAGE was run in the dark (Figure 17.B.). Rhodopsin was stuck in the stacking gel whereas SDS denatured samples showed the same behavior as shown when the gel was run in presence of light. However, the extent of oligomerization did not worsen with increase in SDS concentration which is not expected if aggregation is caused due to SDS denaturation.

Next, SDS-PAGE was used to detect aggregation but with a modification that native loading dye was used so that no additional amount of SDS is introduced from the sample loading buffer and the result is not an effect of its addition. This is especially critical for the samples containing low concentrations of SDS such as 0.05%, 1% and 3%. The possibility that SDS present in the gel and running buffer (0.1% SDS in each) would dissolve the aggregates that are being detected is highly unlikely. This is because aggregates caused by SDS denaturation are being detecteds, i.e. the samples already contain SDS and if aggregates are present they would be dissolved in the sample even before loading on the gel. Further, the amount of SDS that have been used to denature rhodopsin is significantly higher than what is present in the gel and running buffer, thus ruling out the contribution of SDS in the gel system, other than that in the samples, to influence our results. Figure 18.A. shows a silver stained polyacrylamide gel with native rhodopsin in lane 2 (Rho). Native rhodopsin runs as a band between 37kDa and 25kDa on SDS-PAGE and the same gel shows rhodopsin denatured with 0.05%, 1% and 3% SDS in lanes 3, 4 and 5, respectively. These samples were loaded using native loading dye. As can be seen from these gels, a single band at the same position as native rhodopsin is observed for rhodopsin in the presence of different concentrations of SDS tested indicating no changes in electrophoretic mobility of SDS-denatured states compared to that of native rhodopsin. The adjacent gel shows rhodopsin denatured with 10%, 20% and 30% SDS in lanes 2, 3 and 4 respectively as compared to native rhodopsin (Rho) in lane 8. These samples were also loaded with native dye. To check the stability over time, rhodopsin was incubated with 30% SDS for 2h (lane 5), 12h (lane 6) and 24h (lane 7). A single band in the same position as that of native rhodopsin was also observed during longer incubation of rhodopsin in the presence of 30% SDS, suggesting that SDS-denatured rhodopsin is stable over long periods of time and no aggregation is observed even after
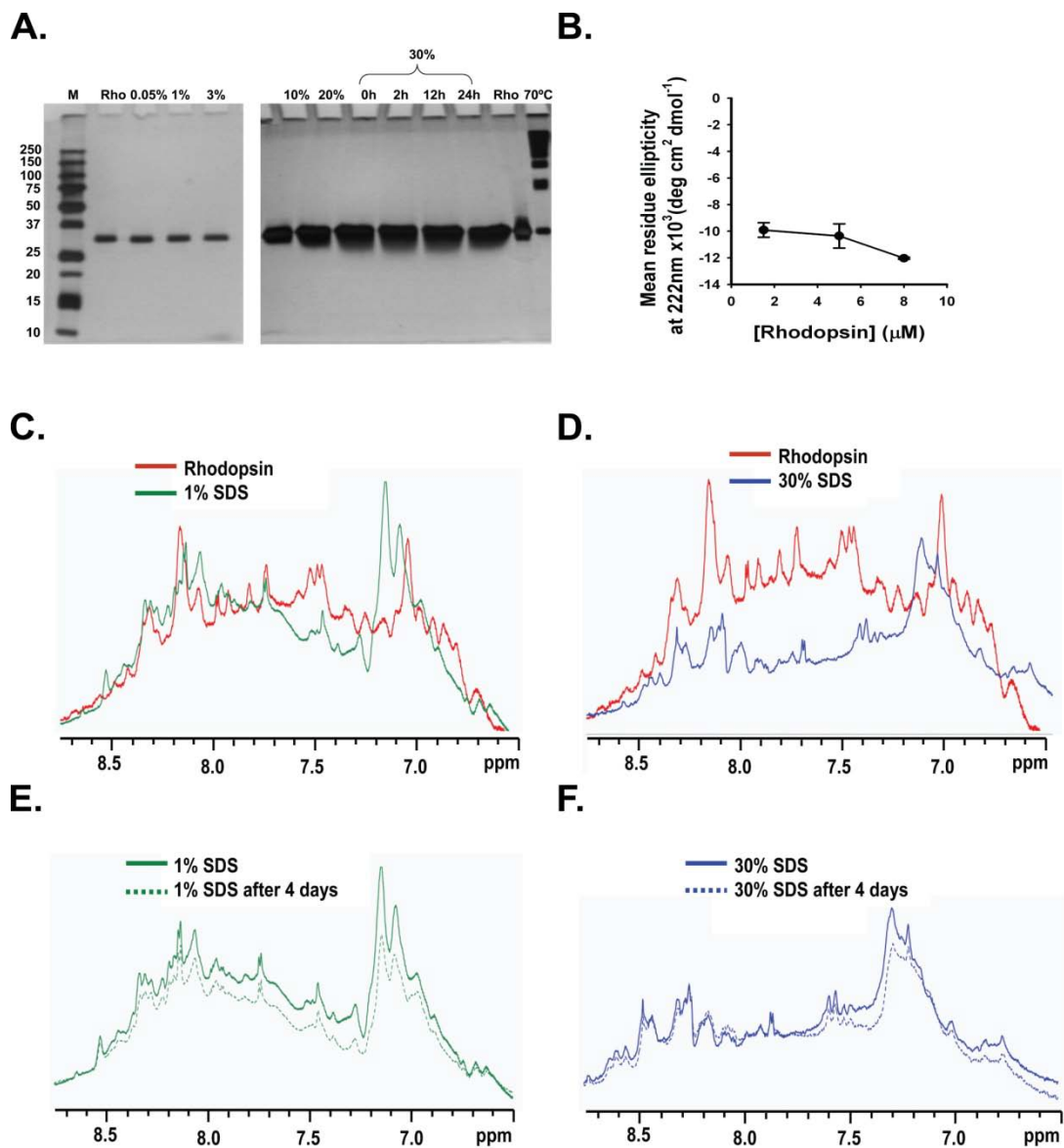
Figure 18: Detection of aggregation during SDS denaturation.

A. Silver stained 10% SDS-polyacrylamide gel of rhodopsin in presence of SDS – first gel, Lane 1: marker, Lane 2: native rhodopsin, Lanes 3, 4, 5: rhodopsin in 0.05% SDS, 1% SDS and 3% SDS respectively and second gel, Lanes 2 and 3: rhodopsin in 10% and 20% SDS respectively, Lanes 4, 5, 6 and 7: rhodopsin in 30% SDS at time t=0h, 2h, 12h, 24h respectively, Lane 8: rhodopsin, Lane 9: rhodopsin denatured at 70°C. B. Plot showing changes in MRE at 222nm on rhodopsin concentration during SDS denaturation. 1D proton spectra showing overlay of C. rhodopsin and rhodopsin in 1% SDS, D. overlay of rhodopsin and rhodopsin in 30% SDS, E. overlay of rhodopsin in 1% SDS and F. 30% SDS after 4 days of incubation with that after immediate SDS addition.

24 h of incubation. Rhodopsin denatured by heating at 70°C in lane 9 was run as a positive control for aggregation. In contrast to the lack of aggregation in the presence of SDS, the positive aggregation control shows higher molecular weight oligomeric bands.

To further confirm that rhodopsin denatured with SDS is not prone to oligomerization, cross-linking reaction with glutaraldehyde was carried out. It is expected that if monomers of rhodopsin are close enough to form dimmers or oligomers then they will cross-link via glutaraldehyde and show up as oligomeric bands on SDS-PAGE. Rhodopsin at increasing concentration of 1.5 μM, 5 μM and 10 μM was treated with glutaraldehyde in presence and absence of 30% SDS in different conditions described in Chapter 2, Section 2.4.2. No high molecular weight bands were seen in native state and in presence of 30% SDS indicating absence of oligomerization when denatured (Figure 19). Similar results were obtained even at different incubation times with glutaraldehyde.
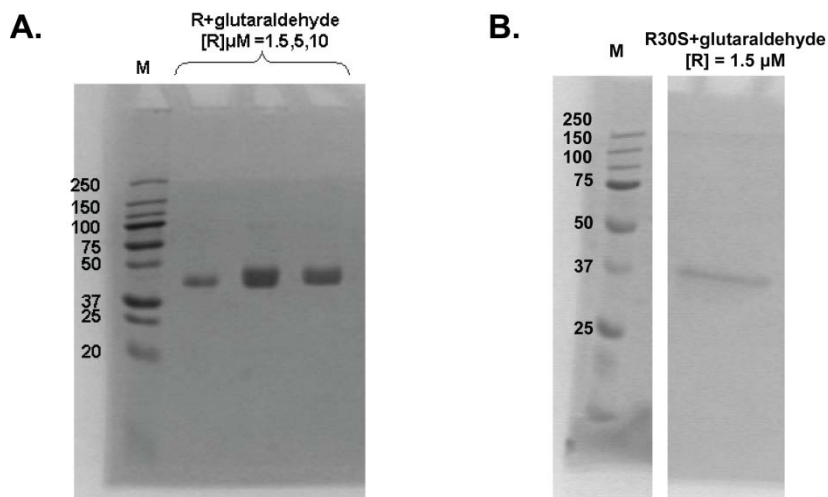
Figure 19: Glutaraldehyde cross-linking of SDS denatured states

Coomassie stained SDS-PAGE of A. rhodopsin in different concentrations of 1.5 μM, 5 μM and 10 μM and B. 1.5 μM rhodopsin denatured with 30% SDS treated with glutaraldehyde for 15 min at 37°C.

Since none of the SDS concentrations used showed evidence for aggregation and most denaturing conditions are of interest, the lack of aggregation at 30% SDS was further corroborated by testing if the CD spectra showed any sign of dependence on rhodopsin concentration. CD spectra of rhodopsin denatured with 30% SDS were recorded at increasing protein concentrations of 1.5 μM, 5 μM and 8 μM. No significant dependence of MRE at 222 nm on protein concentration was noted (Figure 18.B.). This further supports the absence of aggregation at the maximum SDS concentration used (30%), even at higher rhodopsin concentrations.

Finally, the lack of aggregation in SDS was further corroborated using ^{1}H NMR spectroscopy. Proton peaks arising from a natively folded protein are dispersed across the range of approximately -1 ppm to 10 ppm. Peaks corresponding to amide protons are found mainly in the region from 6.5 ppm to 10 ppm. For a disordered or completely unfolded protein, all amide protons in similar chemical environment cluster together around 8 ppm impairing resolution. In case of aggregated protein, loss of peak dispersion accompanied by an increase in line widths of proton peaks is expected. Thus, the lack of aggregation in SDS denatured states was tested by recording one dimensional proton NMR spectra of rhodopsin in the absence and presence of SDS. To avoid interference from detergent signals, these spectra were obtained by selective excitation of the protein backbone region by using a sculpting scheme as described in (Hwang and Shaka, 1995; Stott, 1995). Overlay of the proton spectra, showing the backbone region of rhodopsin alone and in the presence of 1% SDS is displayed in Figure 18.C. The peaks in native rhodopsin correspond mostly to the flexible regions of rhodopsin that become sharper on adding 1% SDS. The peaks between 7.2 ppm and 6.8 ppm in the native state coalesce to form a sharper peak in 1% SDS denatured state. Figure 18.D. shows the overlay between native rhodopsin and

that in presence of 30% SDS. Here again the peaks become sharper in presence of 30% SDS compared to the native state. Peaks between 7.2 ppm and 6.8 ppm appear to merge giving rise to a sharper peak in presence of 30% SDS. However, the overall peak intensity suffers a decrease in presence of 30% SDS when compared to that of native rhodopsin. This may be due to slow tumbling of the large cylindrical SDS micelles that are formed at 30% SDS. These 1D spectra show absence of aggregation since an aggregated protein sample would have given rise to broad peaks. No significant changes were seen in these spectra even after four days indicating absence of any time dependent aggregation (Figures 18.E. and 18.F.).

3.3.2   Thermal denaturation

Thermal denaturation curves measured by CD spectroscopy showed melting temperature of 65°C for native rhodopsin and even higher, of 85°C, for 3% SDS (Section 3.2.2.). These experiments also showed a significant decrease in secondary structure of rhodopsin by 50% and also further denatured SDS denatured states by a significant extent (shown in Figure 12). However, it was imperative to determine if aggregates are formed at such high temperatures and if rhodopsin unfolding as measured by CD is an artifact. Aggregates were measured by dynamic light scattering. 1.5 μM rhodopsin was heated to different temperatures and the distribution of hydrodynamic radius over a range was measured (Figure 20). It was seen that higher radius peaks begin to appear from 55°C onwards indicating aggregation from this temperature onwards. Therefore, CD spectra beyond 55°C suffer from aggregation artifacts and hence will not be considered for further studies.
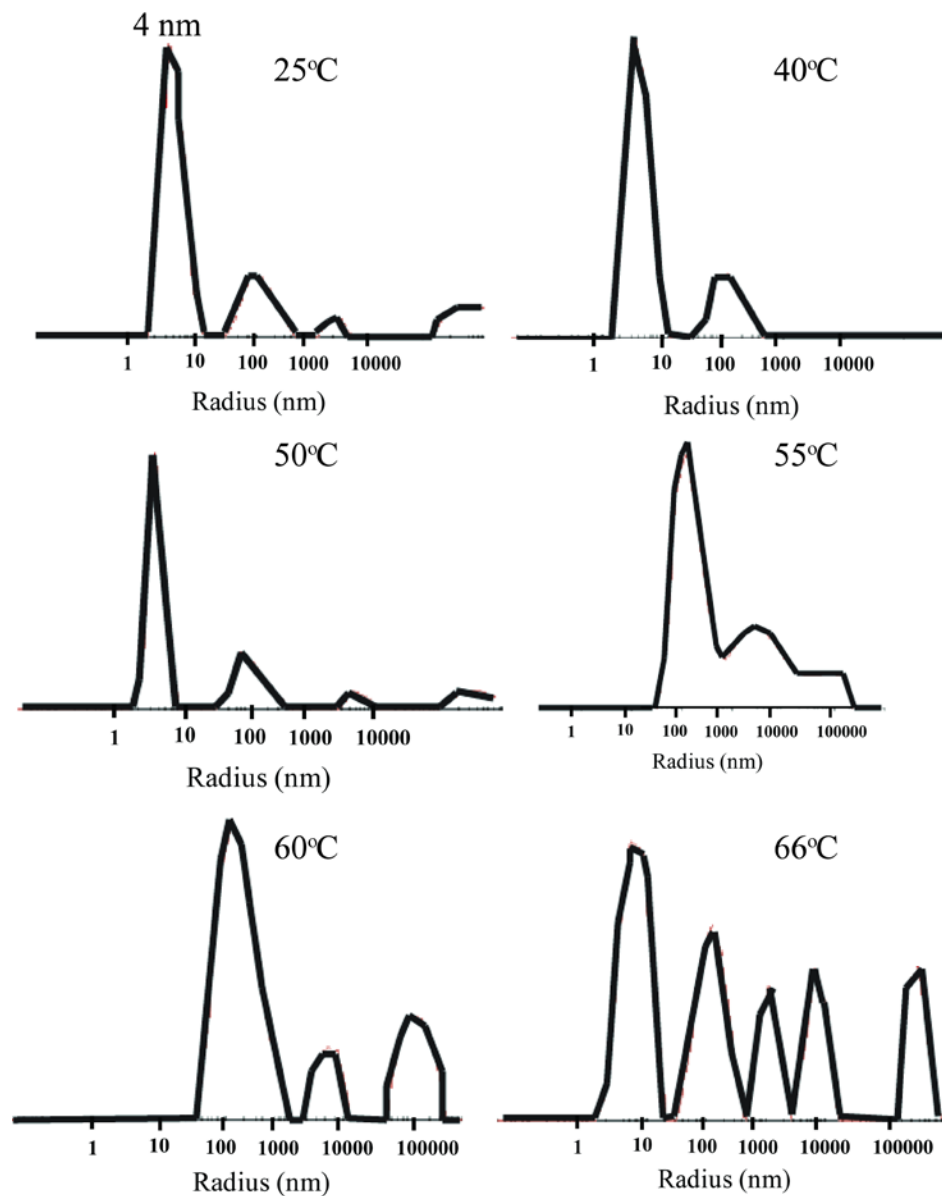
Figure 20: Dynamic light scattering of temperature denatured rhodopsin

Dynamic light scattering of rhodopsin denatured with increasing temperature showing appearance of 4 nm peak at 25°C without any peaks at larger radius. The latter peaks begin to appear from 55°C onwards.

3.3.3　Urea as a denaturant of rhodopsin

Urea denaturation disrupts helical content of rhodopsin to a large extent (see Section 3.2.3.). These largely unfolded states will be suitable for further analyses only if aggregation does not occur. Thus, aggregation in the presence of urea was investigated by two methods, SDS-PAGE and dependence of MRE at 222 nm on rhodopsin concentration.
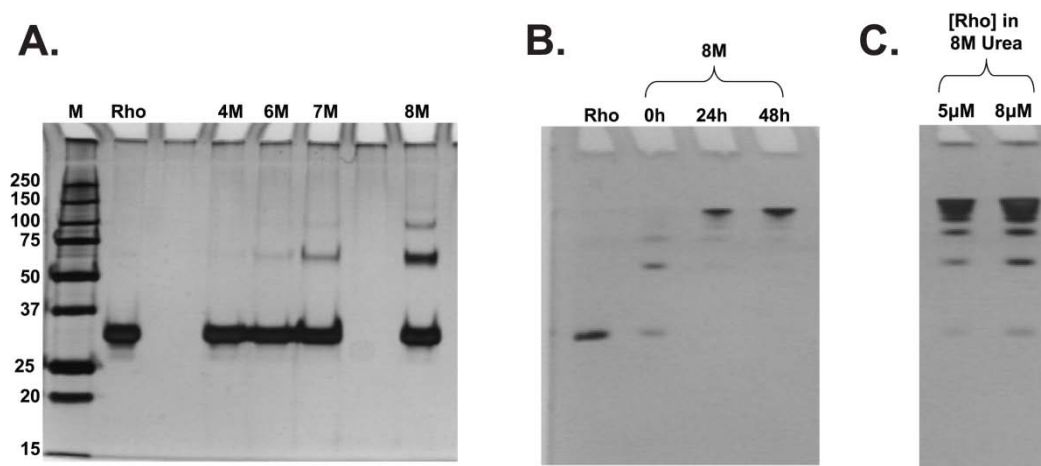
Figure 21: Detection of aggregation during urea denaturation.

Silver stained 10% SDS-polyacrylamide gel of rhodopsin in presence of different concentrations of urea. A. lane 1: marker, lane 2: native rhodopsin, lanes 3, 4, 5, 6: rhodopsin with 4M, 6M, 7M and 8M urea respectively after time t=0 of addition of urea. B. lane 2: native rhodopsin, lanes 3, 4, 5: 1.5μM rhodopsin in 8M urea after 0, 24h and 48h respectively. C. lanes 1 and 2: 5μM and 8μM rhodopsin with 8M urea respectively.

Rhodopsin treated with different concentrations of urea was run on SDS-PAGE to check for aggregation as shown in Figure 21. Native gel loading dye was used to run urea containing rhodopsin samples so that SDS present in Laemmli dye does not influence our results. The second lane in Figure 21.A. corresponds to native rhodopsin. In subsequent lanes, rhodopsin immediately after addition of 4 M, 6 M, 7 M and 8 M urea are shown. Oligomeric bands were seen from 7 M urea denaturation onwards. This is also the urea concentration at which urea

begins to significantly unfold rhodopsin (see Figure 13). Thus, rhodopsin begins to aggregate as soon as urea starts to unfold it. Stability of urea denatured states was determined by incubating 1.5 μM rhodopsin with 8 M urea for 0 h (lane 2), 24 h (lane 3) and 48 h (lane 4) (Figure 21.B.). The time course of urea denaturation clearly shows aggregation becoming worse with time. Increase in the extent of aggregation with increase in rhodopsin concentration denatured by 8M urea was seen by comparing lanes 1 (5 μM rhodopsin) and 2 (8 μM rhodopsin) in Figure 21.C. with that of rhodopsin at 1.5 μM in lane 2 in Figure 21.B. The same samples were also run with a non-reducing Laemmli dye and the same results were seen. Urea-SDS PAGE with 8 M urea dissolved in gel and buffer was also used to run urea denatured rhodopsin so that the same environment is maintained in the gel as is present in urea containing sample. Similar results as seen in SDS-PAGE were obtained. However, a urea-PAGE, i.e. gel containing only urea and not SDS, was also prepared but the samples were stuck in the well probably due to absence of migration to the positive electrode by the imidazole/MOPS buffer that was used (see Chapter 2, Section 2.3.3.3.).

Dependence of MRE at 222 nm on rhodopsin concentration in the presence of 8 M urea was analyzed also by CD spectroscopy. As shown above in Figure 21.A, aggregation is observed on the gel from 7 M urea denaturation onwards. Thus, 8 M urea was chosen for this experiment. Rhodopsin was denatured at increasing concentrations of 1.5 μM, 5 μM and 8 μM with 8 M urea. The CD spectrum at each of the rhodopsin concentrations was recorded (data not shown). However, precipitates were already detected by eye when 8 μM rhodopsin was treated with 8 M urea indicating aggregation of rhodopsin and thus making further analysis by CD unnecessary. The appearance of aggregates precludes the use of urea as a suitable denaturant for unfolding studies of rhodopsin.

3.3.4   3% SDS + 8M urea mixture as a denaturant of rhodopsin

As described in the CD experiments above in Section 3.2.4., the mixture of 3S8U as denaturants leads to a 44% decrease in MRE at 222 nm which is a significant decrease in the secondary structure content of rhodopsin. To determine if this condition leads to aggregation, the denatured samples were run on SDS-PAGE. In order to check for aggregation, SDS-PAGE analysis was performed as shown in Figure 22.

Samples were loaded using native dye. Lane 2 documents the presence of aggregates when rhodopsin is treated with 8 M urea first followed by 3% SDS. This indicates irreversible aggregation by 8 M urea that cannot be rescued by the addition of 3% SDS. However, no aggregates were detected on addition of 3% SDS followed by 8M urea to rhodopsin, as shown in lane 3. Therefore, 3% SDS + 8 M urea, added in this order, is a suitable condition for studying denatured states of rhodopsin.
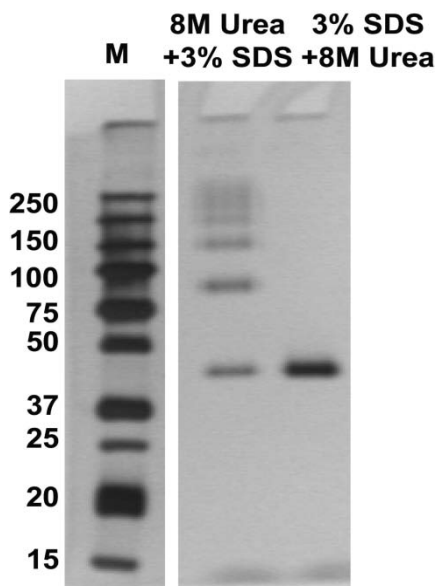

Figure 22: Detection of aggregation during SDS+urea denaturation

Silver stained 10% SDS-polyacrylamide gel of rhodopsin treated with 8M urea+3% SDS (8U3S) (lane 2) showing aggregation and 3% SDS+8M urea (3S8U) (lane 3) without any aggregates. Lane 1 shows the marker.

3.3.5 GuHCl as denaturant of rhodopsin

GuHCl denaturation results in a large decrease in MRE at 222 nm (66% at 8 M GuHCl) as seen from CD spectroscopy. Unlike for other denaturing conditions described above in Sections 3.3.1., 3.3.3. and 3.3.4., SDS-PAGE analysis could not be performed for GuHCl containing samples as precipitation was observed when Laemmlli buffer was added. Furthermore, native loading dye could not be used to run GuHCl denatured samples as they remained stuck in the wells of the gel. Aggregation was checked under both GuHCl and TFA denaturation conditions by determining the dependence of MRE at 222 nm on rhodopsin concentration. For GuHCl denaturation tryptophan fluorescence and accessibility of cysteine were measured in denatured states.

The CD spectra of rhodopsin at different concentrations of 1.5 μM, 3 μM, 5 μM, 6 μM, 7 μM and 8 μM each denatured with 6 M and that of 1.5 μM, 3 μM, 5 μM, 6 μM and 8 μM each denatured with 8 M GuHCl were recorded. Dependence of the MRE at 222 nm on protein concentration was observed at both 6 M and 8 M GuHCl concentrations tested (Figure 24.A.). This indicates that rhodopsin oligomerizes under these conditions and the greater decrease in MRE at 222nm that is observed in Figure 15 may be merely an aggregation effect.

Another supporting evidence for aggregates being formed during GuHCl denaturation was shown by mid-infrared spectrum. 1.5 μM rhodopsin was denatured with 3 M, 4 M and 6 M GuHCl and a mid-IR spectrum was recorded at each concentration. These spectra are shown in Figure 23 with the spectrum of native rhodopsin shown in the inset of the figure. An increase in peak intensity at 1625 cm^{-1} was seen with increase in GuHCl concentration indicating restriction in motion of bonds to a large degree which suggests presence of aggregates.
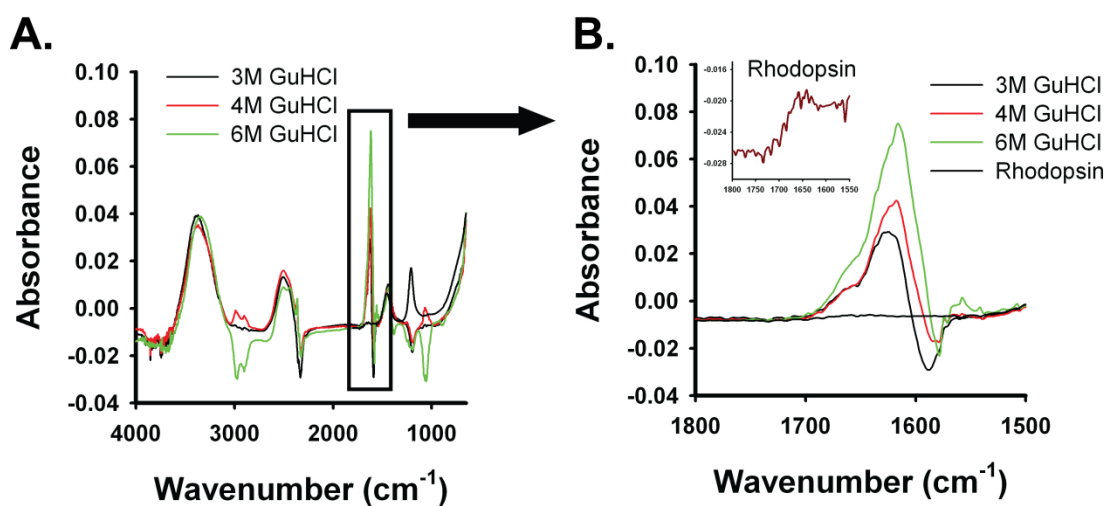
Figure 23: Mid-IR spectra of rhodopsin in native and GuHCl denatuerd states.

A. Mid-IR spectra of rhodopsin denatured with 3 M, 4 M and 6 M GuHCl (after subtraction from appropriate buffer spectra). B. Mid-IR spectra in the region 1800 cm^{-1} to 1500 cm^{-1} of rhodopsin in native state and that denatured with 3 M, 4 M and 6 M GuHCl. Native spectrum of rhodopsin is shown in the inset with the axes expanded for clarity.

Indirect evidence for aggregation in GuHCl also came from fluorescence spectroscopy. There are five tryptophan residues in rhodopsin. Their fluorescence in dark-adapted rhodopsin is quenched due to energy transfer to the retinal chromophore. The release of retinal, e.g. following light-activation and decay of the activated Metarhodopsin II species to free retinal and opsin, causes an increase in tryptophan fluorescence (Farrens and Khorana, 1995). Thus, fluorescence spectroscopy of rhodopsin is a sensitive probe for rhodopsin structure. Furthermore, aggregation would be expected to decrease rhodopsin fluorescence by way of quenching of tryptophan fluorescence through inter-molecular interactions. The changes in tryptophan fluorescence intensity at 330nm as a function of GuHCl concentration are plotted in Figure 24.B. An initial increase in tryptophan fluorescence was seen up to 3M GuHCl. This is consistent with the disruption of retinal-protein interaction as the protein begins to unfold, similar to what would be

106

seen by the retinal leaving the binding pocket after light-activation. With further increase in GuHCl concentration up to 8M, a decrease in fluorescence counts was observed. This is contrary to the significant unfolding of rhodopsin that occurs in the range 3M-8M GuHCl as judged by CD spectroscopy (see Section 3.2.5.). Therefore, this result supports the notion that rhodopsin aggregates under these conditions, which is expected to lead to a quenching of fluorescence. A similar pattern of change in fluorescence was also observed on longer incubation of rhodopsin with GuHCl (Figure 24.B.).

Aggregation was also investigated indirectly through protein accessibility measurements. Analogous to fluorescence measurements, tertiary structure and aggregation of rhodopsin can be probed by cysteine accessibility. Accessibility of cysteine residues was probed using the cysteine derivatizing agent, 4,4'-dithiodipyridine (4-PDS). 4-PDS reacts with the accessible free sulfydryl groups of cysteines releasing stoichiometric amounts of 4-thiopyridone which has an absorption maximum at 323 nm (Grassetti and Murray, 1967). Of the six free cysteines in rhodopsin, only two of them can be derivatized in the dark state whereas all six of them can be derivatized upon loss of 11-*cis* retinal on light activation (Chen and Hubbell, 1978). The effect on reactivity of cysteines to 4-PDS in GuHCl denatured states was checked. An increase in cysteine accessibility to four cysteines was seen up to 3 M GuHCl (Figure 24.C.). Further increase in GuHCl concentration to 8 M showed a decrease in the number of cysteines reacting with 4-PDS to three (Figure 24.C.). This pattern is similar to the decrease seen in tryptophan fluorescence. Burial of both tryptophans and cysteines, occurring at the same concentration of GuHCl, indicates formation of aggregates.

Taken together, these experiments suggest that although GuHCl unfolds rhodopsin significantly, it is not a desirable denaturant for studying unfolded states since it cases aggregation of the protein.
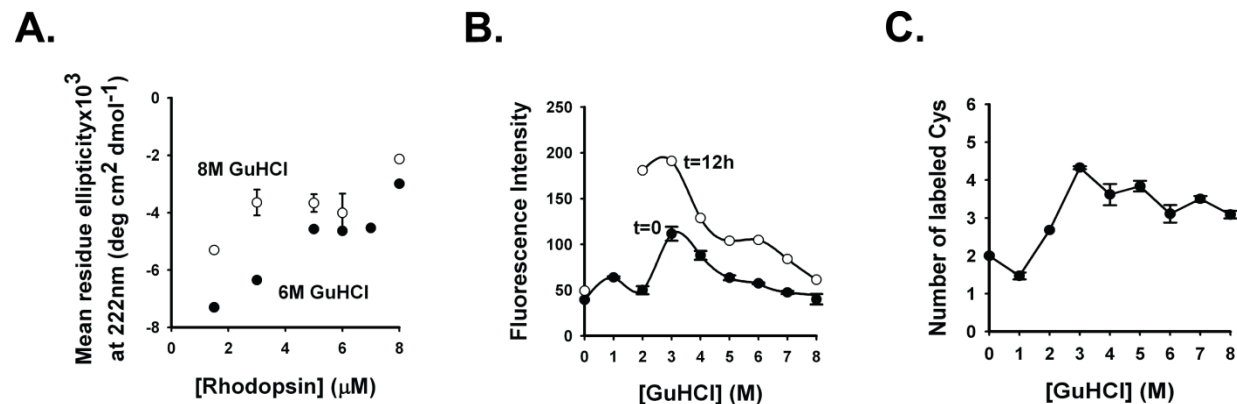
Figure 24: Detection of aggregation during GuHCl denaturation.

A. Plot showing dependence of MRE at 222 nm on rhodopsin concentration on adding 6 M (filled circle) and 8 M (open circle) GuHCl. B. Changes in fluorescence intensity at 330nm in presence of 0-8 M GuHCl immediately after its addition (filled circle) and after incubation for 12 h (open circle). C. Number of cysteines reactive to 4-PDS in different concentration of GuHCl ranging from 0-8 M.

3.3.6 TFA as denaturant of rhodopsin

TFA denaturation resulted in complete disappearance of the CD signal indicating complete disruption of secondary structure of rhodopsin. Thus, TFA could potentially be the best denaturant if it also does not cause aggregation.

To check for aggregation in TFA-denatured samples, different concentrations of rhodopsin at 1.5 μM, 5 μM and 8 μM were denatured with 4 M TFA and a CD spectrum was recorded for each of them. A dependence of MRE at 222 nm on rhodopsin concentration was seen but it could not be clearly determined due to high absorbance at 222 nm by buffer alone (data not shown). However, aggregates were clearly detected by eye after 3 days of preparing the

samples. Thus, TFA is not a suitable denaturant for characterizing unfolded states of rhodopsin due to their aggregation properties.

3.4 DISCUSSION

MPs are notoriously difficult to unfold (Booth and Curnow, 2006) due to the challenge of perturbing the surrounding stable membrane environment. The aim here was to achieve a largely denatured state of rhodopsin *in vitro* in order to mimic what might be corresponding to an *in vivo* early unfolded intermediate. Computational and single molecule studies with the mammalian MP rhodopsin have suggested that complex folding mechanisms may have to be considered to describe the folding of this protein (Rader et al., 2004; Klein-Seetharaman, 2005; Sapra et al., 2006; Tastan et al., 2007). Thus, in-depth studies of denatured states are needed to better understand these mechanisms. The characterization of unfolded states of rhodopsin, however, is still in a preliminary stage. Here, we report the results of screening different denaturants to arrive at conditions that lead to maximum unfolding of rhodopsin without causing its aggregation. The former was assessed by CD spectroscopy and the latter by different techniques depending on the suitability for the specific denaturant under investigation.

The use of CD spectroscopy for determining extent of denaturation was mostly qualitative because of the known interference of aggregation. Therefore, MRE at 222 nm was mainly used to report on the degree of disruption of secondary structure instead of calculating percent helicity by deconvoluting the CD spectra. MRE at 222 nm is strongly influenced by conformation of residues in a helix, length of helix, number of helices, distribution of residues in these helices, fluctuations of a helix and the dielectric constant of the surrounding medium (Hirst

and Brooks, 1994; Wallace et al., 2003). These parameters have an important contribution towards helicity estimation in the case of denatured proteins. However, in the absence of suitable basis sets for denatured MPs, compared to which software such as CDPro estimate the helicity (Sreerama and Woody, 2000), it is difficult to derive these parameters quantitatively from CD spectra. We therefore primarily relied on MRE at 222 nm values to describe secondary structure loss during denaturation in the Results section. Since it was found that basis sets in CDPro containing only soluble proteins when used for quantifying secondary structure of MPs yield reasonably accurate, albeit not quantitative results when considering α-helix content alone, we did estimate the extent of decrease in helicity as a qualitative indicator of the extent of unwinding of helices. This would provide the reader with some qualitative indication about the extent of denaturation being achieved.

3.4.1 SDS as a denaturant

SDS has been commonly used as a denaturant for both, MPs (London and Khorana, 1982; Dornmair et al., 1990; Lau and Bowie, 1997; Otzen, 2003) and soluble proteins (Jirgensons, 1967; Mattice et al., 1976; Rao and Argos, 1981; Mascher and Lundahl, 1989; Ibel et al., 1990). It was shown that the modes of unfolding depend on the SDS concentration range used and indeed SDS induced unfolding of soluble proteins correlates with changes in SDS micellar structure (Otzen, 2002; Otzen and Oliveberg, 2002). At low concentrations of up to 100 mM, SDS forms spherical micelles which convert into cylindrical micelles at concentrations above 6% where the aggregation number of SDS increases from 63 to 91 (Croonen et al., 1983). These cylindrical micelles, also referred to as "mode 2" micelles, are known to have more aggressive protein denaturation properties than the spherical micelles (Otzen and Oliveberg, 2002). Rapid

110

unfolding occurs in this mode due to the large number of SDS molecules interacting with the protein and enveloping it in its large cylindrical structures. Under high SDS concentration conditions, the transition state is stabilized and thus the energy barrier to unfolding is decreased.

Because native rhodopsin as a MP is maintained in DM detergent micelles, we propose that we expect four stages in detergent properties based on these published SDS properties. These stages are visualized schematically in Figure 25. At low concentrations of SDS, we expect that the SDS displaces the DM molecules in the micelles to form SDS/DM mixed micelles. Thus, stage 1 (0.05% to 0.3% SDS) represents spherical DM/SDS mixed micelles. As the SDS concentration increases, the contribution of the relatively small concentration of DM decreases, so that stage 2 (0.3% to 3% SDS) is dominated by the vast excess of SDS in the spherical micelles. Stage 3 (3% to 10% SDS) marks the transition from spherical to cylindrical SDS micelle shapes. Stage 4 (15% to 30% SDS) is then dominated by the cylindrical micellar structures of SDS. [Note that the use of the word "stages" merely intends to reference the different ranges in SDS concentration, and does not imply a temporal progression of rhodopsin structure during denaturation.]
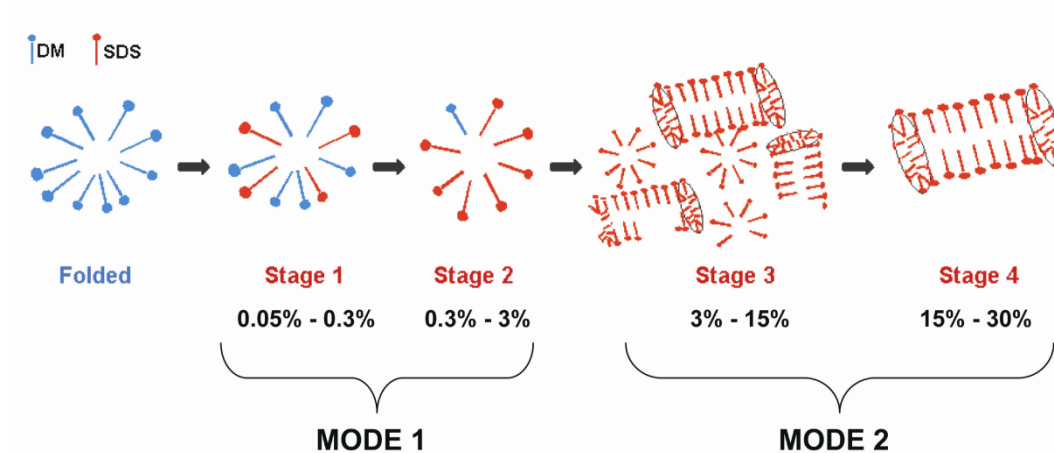
Figure 25: Model representing changes in SDS (in red) micellar structure on increasing addition of SDS to DM (in blue) micelles.

DM spherical micelles form DM/SDS mixed micelles in stage 1 upon SDS addition, stage 2 represents increase in SDS spherical micelles on further adding SDS, stage 3 represents transition to cylindrical micellar formation with further increase in [SDS], stage 4 represents formation of SDS cylindrical micelles.

Below, we discuss rhodopsin denaturation by SDS in light of these stages. In the first stage of unfolding, at low [SDS] of 0.05% to 0.3%, a modest decrease in the magnitude of MRE at 222nm was seen which saturated at a value of ~12% in stage 2 at [SDS] up to 3%, which corresponds to 100mM. Stage 3 is a transition, when SDS is going from spherical to cylindrical "mode 2" micelles (Croonen et al., 1983). SDS concentrations between 3% (100mM) and 15% (500mM) form this stage as the increase in aggregation number of SDS beyond 6% (200mM) leads to very large number of SDS molecules interacting with rhodopsin. As a result, we see an increase in the magnitude of MRE at 222nm at 10% SDS to a value close to the native state indicating that SDS is inducing non-native helices, a well-known property of SDS. Stage 4 is then dominated by cylindrical micellar structures of SDS that surround largely unfolded states of rhodopsin. Here, we see a ~40% decrease in MRE at 222 nm at 30% SDS (1 M). We estimate the extent of decrease in helicity on adding 30% SDS as a qualitative indicator of the extent of

112

unwinding of helices, and obtained a value of approximately 45%. This is consistent with "mode 2" unfolding in which SDS cylindrical micelles wrap around the MP and aggressively unfold it (Otzen, 2002; Otzen and Oliveberg, 2002). Formation of cylindrical micelles by SDS is also supported by 1D ^{1}H NMR experiments. A decrease in overall peak intensities of 30% SDS denatured rhodopsin as compared to the native form can be attributed to slow tumbling of the large cylindrical micelles that are formed at such high SDS concentrations.

In order for SDS denatured conditions to qualify for biophysical studies of denatured rhodopsin, we checked for aggregation. No aggregation of rhodopsin was detected based on multiple lines of evidences. SDS denatured rhodopsin did not show any oligomeric bands on SDS-PAGE. By using CD spectroscopy, a dependence of ellipticity at 222 nm on protein concentration would be expected if there are aggregates forming. Such dependence was not seen when rhodopsin at different concentrations was denatured by 30% SDS, the maximum concentration of SDS used here. Further, proton peaks on NMR spectrum of SDS denatured rhodopsin did not show any significant broadening compared to its native state, even after four days of incubation with 1% and 30% SDS the spectrum remained almost the same. However, there was a decrease in overall signal intensity of 30% SDS denatured state compared to the native state. This may be due to formation of cylindrical micelles of SDS which tumble slowly or technical difficulties due to the high buffer concentrations or protein aggregation. Since, aggregation has been ruled out by SDS-PAGE and CD spectroscopy, and no peak broadening was seen on NMR spectra of SDS treated rhodopsin, we conclude that the decreased intensity of the proton peaks is not due to aggregation. This is consistent with the notion that aggregation of rhodopsin, being a MP, is less likely in the presence of SDS because even though SDS is denaturing, it does provide a hydrophobic environment. Here, the hydrophobic amino acids that

will be exposed due to unfolding still remain surrounded by the hydrophobic tails of SDS and thus are shielded from the aqueous medium preventing aggregation. These results indicate that the maximum concentration of SDS of 30% is a desirable condition for future unfolding studies of rhodopsin.

3.4.2 Urea as a denaturant

Urea has been used very recently to study denaturation of opsin, a retinal-free form of rhodopsin, in phospholipid/detergent bicelles where it was shown to irreversibly unfold opsin to a significant extent (McKibbin et al., 2009). It was shown that 4 M urea could denature opsin to a significant extent as measured by a decrease in MRE at 222 nm by ~50%. In our study also, a significant degree of unfolding of rhodopsin in DM micelles with urea is seen but at a much higher concentration of urea, i.e. 8 M urea could decrease MRE at 222 nm by 57%. This is mostly due to differences in the degree of intrinsic stability of opsin and rhodopsin which is also influenced by the micellar system in which they are reconstituted. It appears that the native state of opsin is less stable than that of rhodopsin. It is also possible that urea-denatured opsin is less prone to aggregation because no precipitates by eye and change in sample absorbance, reported by voltage changes in the photomultiplier tube, occurred during time course studies by CD. These data indicate an absence of light scattering and hence aggregation (McKibbin et al., 2009). We found this method to be less reliable in detecting aggregation in our studies because they only detect very large aggregates. While we also did not detect aggregation by these methods in our studies, we did detect them based on SDS-PAGE and analysis by eye at higher rhodopsin concentrations. It is likely that aggregation is caused by exposure of large hydrophobic regions of rhodopsin due to its unfolding in urea. A way to mask these hydrophobic parts of the protein

could prevent it from oligomerizing. For this reason, we tested a mixture of 8 M urea and 3% SDS as a denaturant so that SDS can be effective in screening the hydrophobic residues from water. While aggregates are detected when 3% SDS was added to 8 M urea denatured rhodopsin, no aggregates are detected on reversing the order of addition of the denaturants. This further supports our theory that the cause of aggregation of rhodopsin in 8M urea is exposure of hydrophobic parts, which if masked by SDS before being denatured by 8M urea does not lead to aggregation. The extent of denaturation in 3S8U is found to be similar to that by 8M urea and slightly greater than that by 30% SDS thus making it a favorable denaturing condition to study unfolded states.

3.4.3   GuHCl and TFA as denaturants

GuHCl denaturation leads to a decrease in MRE at 222 nm of rhodopsin by a greater extent compared to the other mentioned denaturing conditions, SDS, urea and SDS + urea. TFA, a strong denaturing condition, leads to the maximum decrease in MRE at 222 nm compared to all of the denaturants tested. It leads to a complete disappearance of CD signal indicating complete unfolding of secondary structure. However, both these conditions also lead to formation of aggregates thus impairing their use in further unfolding studies. For GuHCl denaturation, MRE at 222 nm depended on rhodopsin concentration indicating aggregation. Tryptophan fluorescence and cysteine accessibility were shown to decrease at high GuHCl concentrations followed by their increase at low GuHCl concentrations. Mid-IR TFA induced unfolding led to precipitation after 3 days of TFA addition to rhodopsin indicating aggregation. The cause of aggregation is again likely due to the exposure of hydrophobic residues as with urea. However, SDS could not

be added to mask exposed hydrophobic amino acids so that aggregation can be prevented, since precipitation occurred when SDS and GuHCl buffers were mixed together.

3.5   SUMMARY OF CONTRIBUTIONS

Studies on *in vitro* MP folding reported so far have focused mostly on unfolding conditions that lead to refolding of the protein without details on the effect of other denaturing conditions that might lead to large degree of unfolding but may not be suitable for refolding. These studies have been done with the aim of thermodynamic and kinetic characterizations of folding pathways of MPs for which reversibility is a requirement. However, such studies have limited the growth of this field since refolding MPs is a very challenging task. Therefore, one way to advance the field of MP folding is through characterization of unfolded states, for which reversible unfolding is not a stringent criterion. The challenges involved in this case are a) to obtain large degree of unfolding since MPs are resistant to denaturation and b) to find a condition where these largely denatured states do not aggregate. Methodical tests of different denaturing conditions to unfold MPs to a large extent and of detecting aggregation of MPs when subjected to denaturation are lacking in the literature. These voids have necessitated our initial studies, as described in this Chapter, to understand folding of rhodopsin.

We have screened different denaturing conditions, SDS, urea, SDS + urea, GuHCl and TFA, to find a condition that leads to maximum unfolding without aggregation of unfolded states of rhodopsin. The extent of secondary structure disruption was estimated by CD spectroscopy. To detect aggregation of rhodopsin under each denaturing condition, systematic tests were carried out and evidences were collected from multiple experiments. We found that SDS, either

alone or in combination with urea, is a very suitable denaturant, due to the large degree of unfolding of rhodopsin in its presence and due to its ability to mask exposed hydrophobic stretches of largely unfolded MP by its long hydrocarbon tails, thus preventing them from aggregation. The work described here outlines the systematic approach required to initiate folding studies of MPs in general.

4.0   CHAPTER 4: GLOBAL CHARACTERIZATION OF TERTIARY STRUCTURE

CHANGES UPON SDS DENATURATION OF RHODOPSIN

4.1   RATIONALE AND SUMMARY

Little is known about the molecular nature of residual structure in unfolded states of MPs. An understanding of such states can provide key insights into folding mechanisms of proteins. The screen of chemical denaturants to maximally unfold the mammalian MP and prototypic G protein coupled receptor rhodopsin, without interference from aggregation, described in Chapter 3, identified sodium dodecyl sulfate (SDS), alone or in combination with urea, as the most suitable denaturant. This allowed me to initiate the biophysical characterization of SDS-denatured states of rhodopsin and interpret the results in light of changes in SDS micellar structures with increasing concentrations of SDS. SDS-induced tertiary structure changes – time-resolved and steady-state – were followed using 1) the absorption of the chromophore retinal as an intrinsic protein core probe, 2) the accessibility of surface exposed and buried cysteines, 3) the emission changes of initially buried tryptophans, 4) change in the overall protein size and 5) changes in overall flexibility. Overall backbone motions of rhodopsin probed by tryptophans and lysines show an increase in flexibility with increase in extent of denaturation. Evidence from light-scattering suggests that SDS initially replaces DM molecules, initiating the formation of the environment needed to disrupt rhodopsin secondary and tertiary structure. I show by using

absorbance and fluorescence spectroscopy as well as stopped-flow measurements that a softening and initial opening of the helical bundle of rhodopsin, followed by disruption of retinal-protein interactions with full opening of the helix bundle are the first two steps in denaturation, the kinetics of which depend on the amount of SDS used. Fluorescence and cysteine reactivity measurements indicate burial of tryptophans and cysteine side chains in a compact intermediate. Compactness in overall size is also shown by light scattering. These studies constitute the first characterization of a stable unfolding intermediate of the MP rhodopsin.

4.2   DISRUPTION OF RETINAL-PROTEIN INTERACTIONS

4.2.1   Equilibrium studies

SDS induced disruption of secondary structure is described in detail in Chapter 3. To correlate these secondary structure changes with SDS induced disruption of tertiary structure, we measured changes in the interaction between the chromophore retinal and rhodopsin. 11-*cis* retinal is covalently linked to Lys296 in the native dark state via a protonated Schiff base. Retinal binding contributes to the stability of rhodopsin and is important for its function. Retinal binding gives rise to a chromophore band in the absorption spectrum of rhodopsin at 500nm and is used here as a tertiary structure probe. The absorption spectra of rhodopsin in the absence and presence of different amounts of SDS are shown in Figure 26.A.

The 500 nm peak characteristic of native rhodopsin shifts towards 440 nm with addition

of increasing concentrations of SDS. A plot of the absorbance intensity at 500 nm as a function

of SDS (Figure 26.B.) reveals a steep loss of 500 nm chromophore absorption, as the peak

already begins to decrease in intensity on addition of 0.05% SDS and completely disappears on

adding 0.1% SDS. The absorption maximum that forms at 440 nm (Figure 26.A.) instead is

characteristic of a protonated Schiff base in solution devoid of specific protein contacts. This

implies disruption of retinal-protein interactions on addition of relatively small concentrations of

SDS. Over time, the 440 nm peak shifts to 380 nm indicating formation of free retinal due to

hydrolysis of the Schiff base (data not shown).
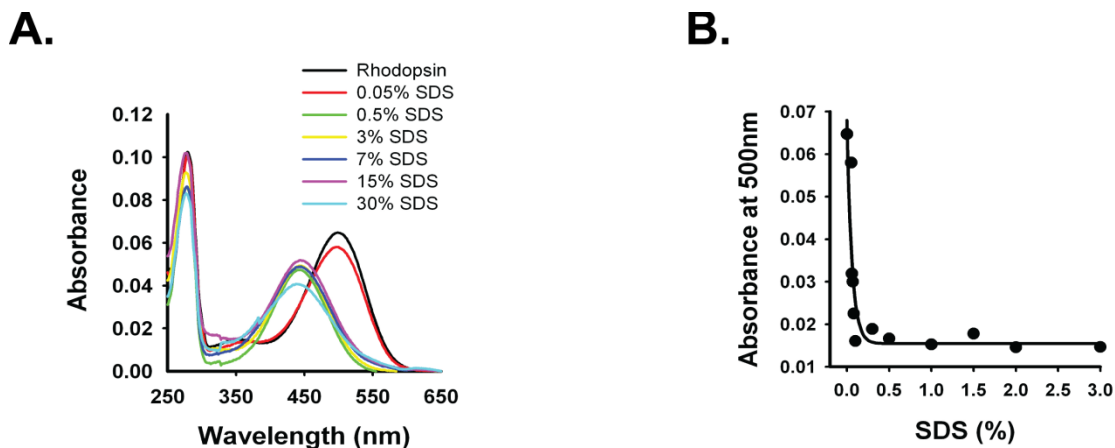
Figure 26: Stability of retinal-protein interactions.

A. Absorbance spectra of 1.5 μM rhodopsin alone (black line) and in different concentrations of SDS, as indicated in

the figure, showing the shift in the 500 nm peak to 440 nm. B. Plot showing decrease in absorbance at 500 nm with

increasing SDS concentration up to 3%.

4.2.2 Fast kinetics of the disruption of retinal-protein interactions

Only in the presence of 0.05% SDS, disruption of retinal-protein interactions occurs slowly, on the order of minutes. Above 0.05% SDS, formation of the 440 nm retinal band, indicative of rhodopsin denaturation, takes place in second and sub-second time scales. For these concentrations, we therefore measured the kinetics of the loss of native retinal-protein interactions using a stopped-flow apparatus. Stopped flow instrument in the laboratory of Dr. Catalina Achim in Dept. of Chemistry at Carnegie Mellon University was used. Absorbance spectrum of dark state rhodopsin was first collected to confirm that rhodopsin is not bleached when exposed to the lamp of the instrument. It was possible to mix rhodopsin and SDS in various mixing ratios. A ratio of 1:6 of rhodopsin and SDS was used for all experiments. Absorbance at 440 nm was collected over the times described below.

An exponential increase in absorbance at 440 nm was observed for all SDS concentrations tested and time traces are shown exemplary for some concentrations in Figure 27.A. Time constants of the increase for all of the measurements made are plotted as a function of SDS concentration in Figure 27.B. The loss of retinal-protein contacts proceeded drastically faster when going from 0.05% SDS (630±20 s) to 1% SDS (0.32±0.01 s) and indeed is the fastest at this concentration. Beyond 1% SDS, the time constant becomes slower with 2.04±0.03 s at 10% SDS, 4.74±0.06 s at 15% SDS and finally with 31.8±0.4 s at 26% SDS. These results indicate that the helical bundle is most rapidly opened around 1% SDS as compared to other SDS concentrations allowing fast disruption of retinal-protein interactions and resulting in a protonated Schiff base devoid of protein contacts.
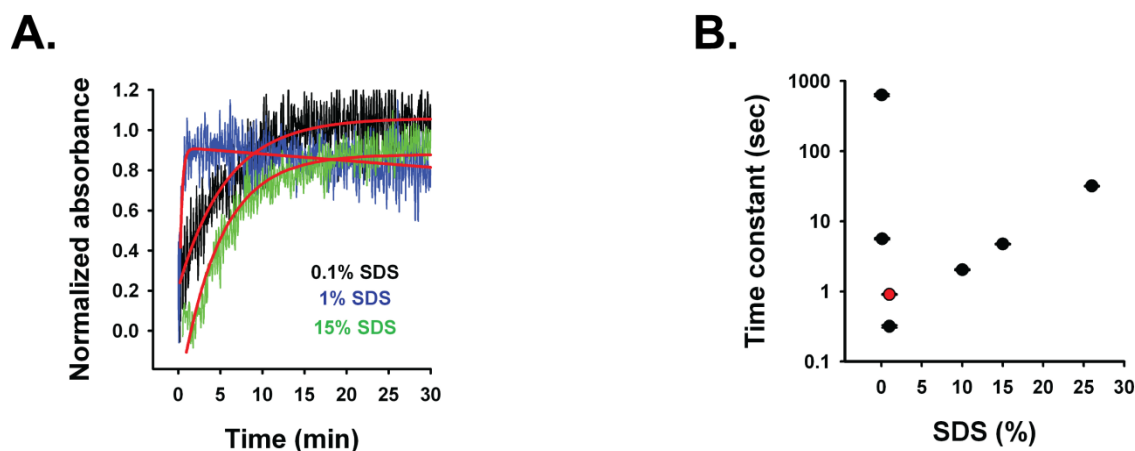
Figure 27: Stopped-flow kinetics of disruption of retinal-protein interactions.

Absorbance at 440 nm of rhodopsin denatured with SDS at concentrations of 0.1%, 1%, and 15% is plotted against time. Each curve was fitted to a monoexponential equation. B. Time constants obtained from the curve fittings of the absorbance kinetics obtained upon addition of 0.05%, 0.1%, 1%, 10%, 15%, and 26% SDS are plotted against each respective SDS concentration.

4.3   CHANGES IN TRYPTOPHAN FLUORESCENCE

4.3.1   Equilibrium studies

Unfolding of native helices and breaking of retinal-protein interactions are expected to result in changes in native tertiary interactions extending globally to disruption of the overall tertiary structure of rhodopsin. To characterize these structural changes, tryptophan fluorescence was employed as another internal tertiary structure probe. There are five tryptophan residues in rhodopsin, mainly located in close vicinity to the retinal chromophore. Their fluorescence in dark-adapted rhodopsin is quenched due to energy transfer to the retinal. The release of retinal, e.g. following light-activation and decay of the activated Metarhodopsin II species to free retinal

122

and opsin, causes an increase in tryptophan fluorescence (Farrens and Khorana, 1995). Figure 28.A. and 28.B. show changes in the fluorescence emission spectra of rhodopsin when titrated with SDS at low concentrations up to 3% and high concentrations up to 30%, respectively. Changes in fluorescence intensity at 330nm as a function of SDS concentration are plotted in Figures 28.C. and 28.D. There is a slight red shift in the wavelength of maximum emission from 330nm to 335nm when going from 0% to 30% SDS (Figures 28.A. and 28.B.). This shift indicates exposure of tryptophan side chains to a polar environment consistent with rhodopsin denaturation and is not due to non-specific solvent induced effects because free N-acetyl tryptophan with increasing concentration of SDS shows a blue shift (data not shown).

The addition of 0.05% SDS causes a 3-fold increase in tryptophan fluorescence (Figure 28.A. and 28.C.). Further increases in SDS concentration resulted in lesser increases in fluorescence intensity as compared to the native state. Fluorescence in SDS remained essentially constant when comparing concentrations starting from 0.5% up to 2-3% SDS. The fluorescence intensity at these concentrations was still 2.5-fold greater than that of native rhodopsin. The result mirrors the relatively constant values observed in MRE over the range 0.5%-3% SDS (see Chapter 3). At SDS concentrations beyond 3%, illustrated in Figure 28.D., there is a slight rise in fluorescence that maximizes at 15% SDS, where it is 1.5-fold higher as compared to the fluorescence at 3% SDS. Further increase in SDS up to 30% reverses this trend: a decrease in fluorescence is observed. To discriminate between protein and solvent induced effects leading to these changes in tryptophan fluorescence, fluorescence of free N-acetyl tryptophan was recorded over the same SDS concentration range of 0.05%-30%. A constant decrease in free N-acetyl tryptophan fluorescence was observed from 0.05%-3% SDS and the pattern of change beyond 3% SDS and up to 30% SDS was the same as that seen with rhodopsin but only at a lower
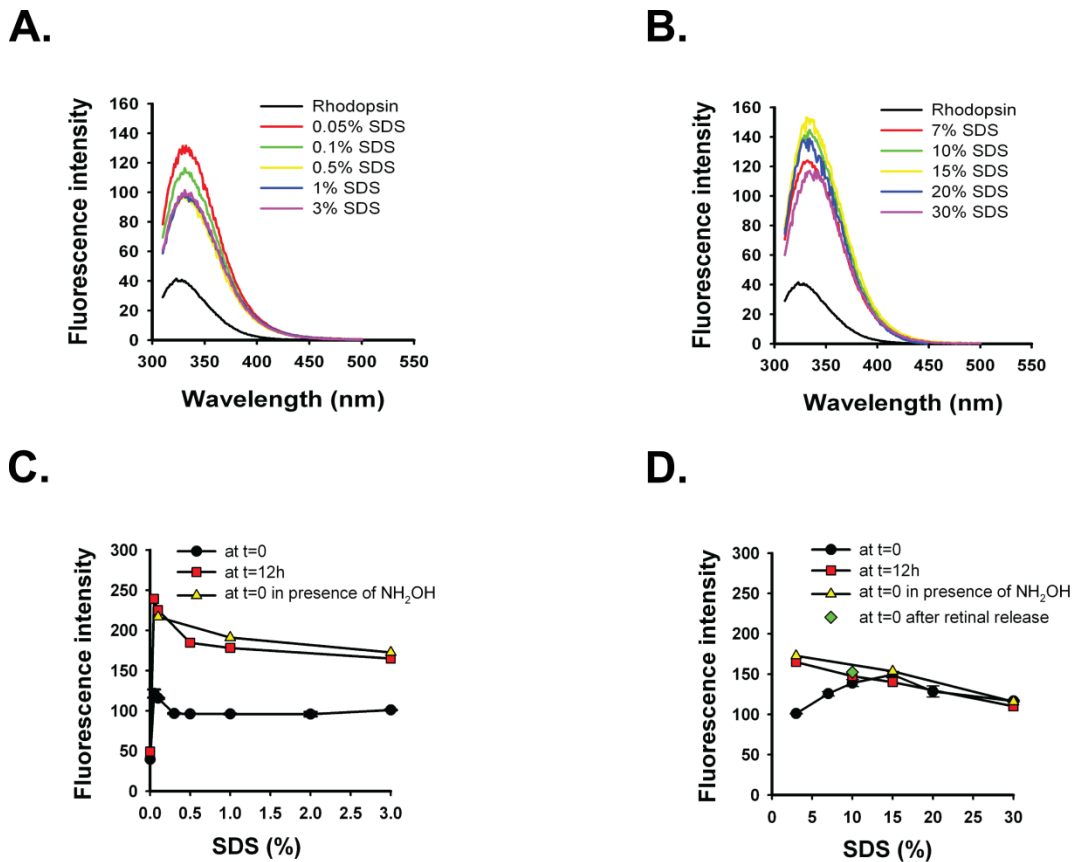
Figure 28: Changes in tryptophan fluorescence.

Emission spectra of 1.5μM rhodopsin upon titration with A. 0.05%-3% SDS and B. 7%-30% SDS in the wavelength range of 310nm-500nm. Changes in fluorescence intensity at 330nm at C. 0.05%-3% SDS and D. 7%-30% SDS concentrations immediately after its addition (t=0), after incubation for 12 h (t=12 h), immediately after its addition in presence of 10mM hydroxylamine (t=0 in presence of NH_2OH) and rhodopsin treated with 0.5% SDS in presence of 10mM hydroxylamine followed by increase in SDS concentration to 10% (t=0 after retinal release).

magnitude of intensity (data not shown). This shows that the initial increase in rhodopsin fluorescence on addition of 0.05% SDS is a protein mediated effect.

We also probed changes in fluorescence as a function of time. Rhodopsin was incubated with SDS at various concentrations and spectra were collected every 30 minutes. The fluorescence values at the end of 12 h of incubation time are plotted in Figure 28.C. and 28.D. (red squares). There was a drastic increase in fluorescence as compared to the results obtained at time zero. Even though non-covalent retinal-protein interactions are disrupted by the addition of SDS, we know that initially, the retinal is still covalently linked to rhodopsin. We therefore suspected that this difference is due to hydrolysis of the protonated Schiff base. Hydrolysis occurs on adding SDS which leads to the release of retinal over time (also see Section 4.2.1.). To test this hypothesis, we carried out SDS titrations in the presence of 10 mM of hydroxylamine which cleaves the retinal Schiff base bond (Wald and Brown, 1953a; Farrens and Khorana, 1995). In the presence of hydroxylamine the fluorescence measured immediately (t=0, yellow triangles in Figure 28.C. and 28.D.) was identical to that observed in the absence of hydroxylamine only after 12 h (t=12h, red squares in Figures 28.C. and 28.D.). This observation indicates that the spike in fluorescence increase at very low SDS concentrations (0.05%) followed by the slow decrease in fluorescence at intermediate SDS concentrations (between 0.05% and 3%) is a protein-mediated effect. Retinal quenching simply dampens the absolute fluorescence values. A difference is observed for concentrations 3% to 15%: here, in the presence of hydroxylamine and in its absence after 12 h, the same decreasing trend is followed, while in the absence of hydroxylamine at t=0 there is an increase in fluorescence until the two curves meet. To rule out that this is due to inaccessibility of retinal to hydroxylamine at increased SDS concentrations, we confirmed hydrolysis using absorbance spectroscopy.

Hydroxylamine reaction with the Schiff base results in formation of retinal oxime which gives a characteristic absorbance maximum at 360 nm (Wald and Brown, 1950). This peak was observed when rhodopsin in 10% SDS was incubated with hydroxylamine, confirming that retinal is hydrolysable under these conditions (data not shown). It was also observed that retinal hydrolysis occurred over time when rhodopsin is treated with 10% SDS (data not shown). To further confirm that the lack of increase in fluorescence in the presence of hydroxylamine at SDS concentrations greater than 3% is not due to retinal quenching, retinal was first removed by adding 0.5% SDS to rhodopsin in presence of hydroxylamine and then the SDS concentration was increased to 10%. The fluorescence counts of this experiment (shown as green diamond in Figure 28.D) was found to overlap with fluorescence counts of rhodopsin in 10% SDS at t=0, t=12 and that at t=0 in presence of hydroxylamine. Thus, the presence or absence of covalently linked retinal has no effect on the fluorescence of denatured rhodopsin in the presence of SDS concentrations in excess of 3% (Figure 28.D.), while at lower SDS concentrations, the presence of retinal quenches tryptophan fluorescence of rhodopsin.

It was shown by CD spectroscopy (Chapter 3, Section 3.2.4.) that addition of 8 M urea to 3% SDS denatured state led to a significant decrease in secondary structure content of rhodopsin. The net decrease in MRE at 222 nm was 44% which is similar to that denatured by 30% SDS. The effect of such a large degree of unfolding by a mixed denaturant on tryptophan fluorescence was determined. The fluorescence intensity at 330 nm in presence of 3S8U, pH6 was found to be similar to that of 15% SDS denatured state, i.e. much greater than that of the SDS denatured states at any other SDS concentration (Figure 29). This indicates that in the largely unfolded 3S8U state, disruption of tertiary interactions is greater than that in 30% SDS denatured state. The same mixed denaturant was also tested at a different pH of 2 since this condition was used in

NMR experiments to prevent background signals coming from urea amide protons at pH 6 as described in Chapter 5. 3S8U, pH2 decrease MRE at 222 nm of rhodopsin by ~28%, which is less than that denatured by 3S8U, pH6. Fluorescence intensity of 3S8U, pH2 was found to be similar to that in 0.05% SDS denatured state and is less than that in 3S8U, pH6 state. Lesser extent of decrease in tryptophan fluorescence by 3S8U at pH2 than at pH6 correlates with its lesser degree of disruption of secondary structure.
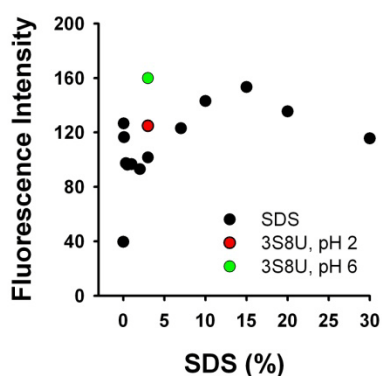
Figure 29: Changes in tryptophan fluorescence in presence of SDS and urea.

Plot showing changes in fluorescence intensity at 330 nm with SDS concentration and 3% SDS with 8 M urea at pH 2 and 6.

4.3.2   Fast kinetics of tertiary structure changes from tryptophan fluorescence

Steady state measurements of SDS denatured rhodopsin showed an increase in tryptophan fluorescence on addition of small amounts of SDS, i.e. 0.05% SDS. At higher concentrations of SDS, fluorescence counts were still higher than that in native state. At all these SDS concentrations, fluorescence increased further with longer incubation times with SDS, the rate of which was on the order of minutes and hence could be measured with a steady state spectrometer. However, the initial increase in fluorescence was on the order of seconds and

hence required the use of stopped flow instrument to determine its kinetics. Stopped flow fluorescence measurements were also carried out to complement the fast kinetics of disruption of retinal-protein interactions described in Section 4.2.2. These experiments were carried out in the laboratory of Dr. Michael Trakselis in Dept. of Chemistry, University of Pittsburgh. Mixing ratio of 1:1 was used to mix rhodopsin and SDS from the stopped flow syringes that were filled with double the required concentration of the protein and denaturant. A cut-off filter, with a wavelength cut-off of 320 nm, was used to collect emission fluorescence above 320 nm.

The fast kinetics of tryptophan fluorescence change with addition of SDS is shown in Figures 30.A.-D. In each case, there is a fast initial rise in fluorescence followed by a decrease (Figure 30.A., B.). The time constants of the two components as a function of SDS concentration are plotted for the initial rise in Figure 30.C. and for the subsequent decrease in Figure 30.D. The trends for both components are similar, with largest time constants observed at low concentrations and fast (!) time constants observed above 1%. It seems that below 1% different unfolding processes occur than above 1%. This is indicated by the two fluorescence decay components observed at 1%. The slower one agreeing with the data obtained at 0.05% SDS, while the fast time constant fits within the time constants obtained above 1%.
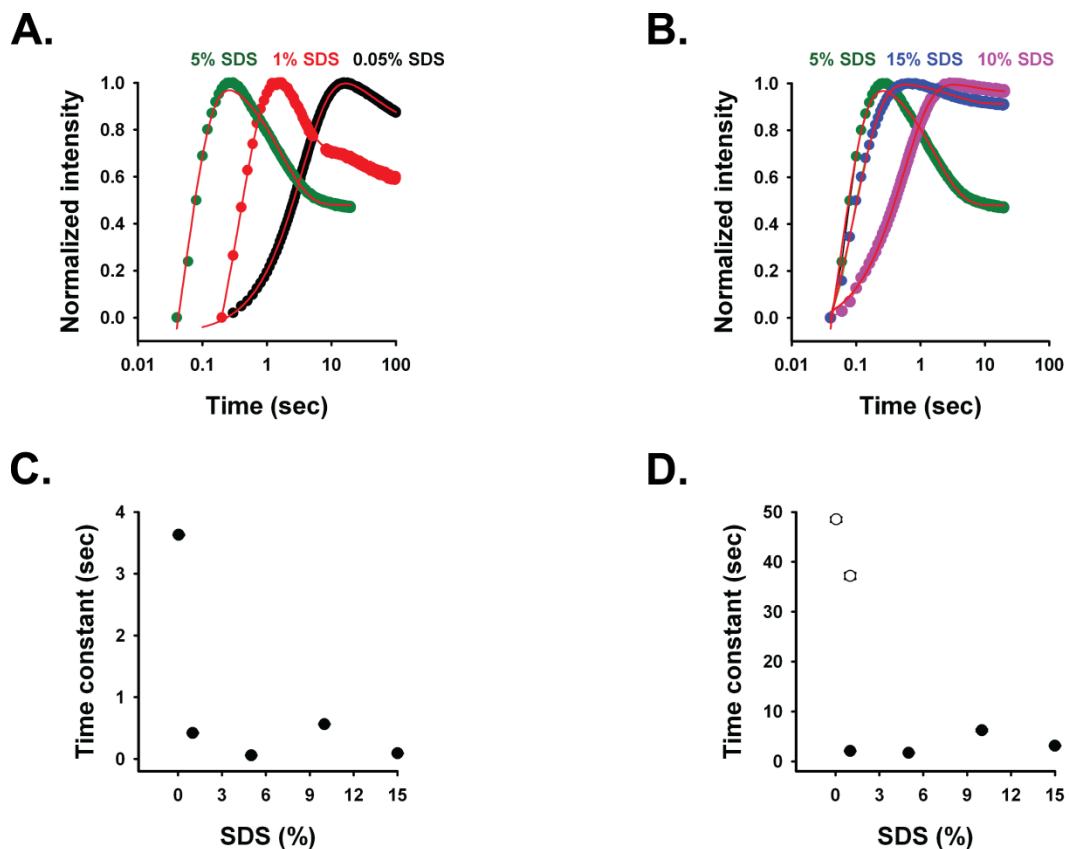
Figure 30: Stopped flow kinetics of trytophan fluorescence changes.

A. Stopped flow kinetics of fluorescence changes at SDS concentrations 5% and below. B. Stopped flow kinetics of fluorescence changes at SDS concentrations 5% and above. C. Time constants of the fast tryptophan fluorescence increase as a function of SDS concentration. Time constants were obtained from a multiexponential fitting. The first component of each fit represents the monoexponential increase in fluorescence. D. Time constants of the slow partial tryptophan fluorescence decrease as a function of SDS concentration. Except for 1% SDS all fluorescence decays were fitted monoexponentially. The data at 1% SDS were represented as biexponential decay.

4.4   CHANGES IN CYSTEINE REACTIVITY

Reactivity of cysteine residues was used as an additional global tertiary structure indicator. The native cysteine residues in rhodopsin are shown as blue circles in Figure 31.A. Accessibility of cysteine residues was probed using the cysteine derivatizing agent, 4,4'-dithiodipyridine (4-PDS). 4-PDS reacts with the accessible free sulfydryl groups of cysteines releasing stoichiometric amounts of 4-thiopyridone which has an absorption maximum at 323 nm (Grassetti and Murray, 1967). Of the six free cysteines in rhodopsin, only two of them, depicted by blue arrows in Figure 31.A., can be derivatized in the dark state whereas all six of them can be derivatized upon loss of 11-*cis* retinal on light activation (Chen and Hubbell, 1978). Rhodopsin (1.5 µM) was treated with different concentrations of SDS and then reacted with a 25-fold excess of 4-PDS. The reaction was followed spectrophotometrically by monitoring the increase in absorbance at 323 nm. Figure 31.B. shows the variation in the number of cysteines being labeled with 4-PDS with increasing SDS concentrations.
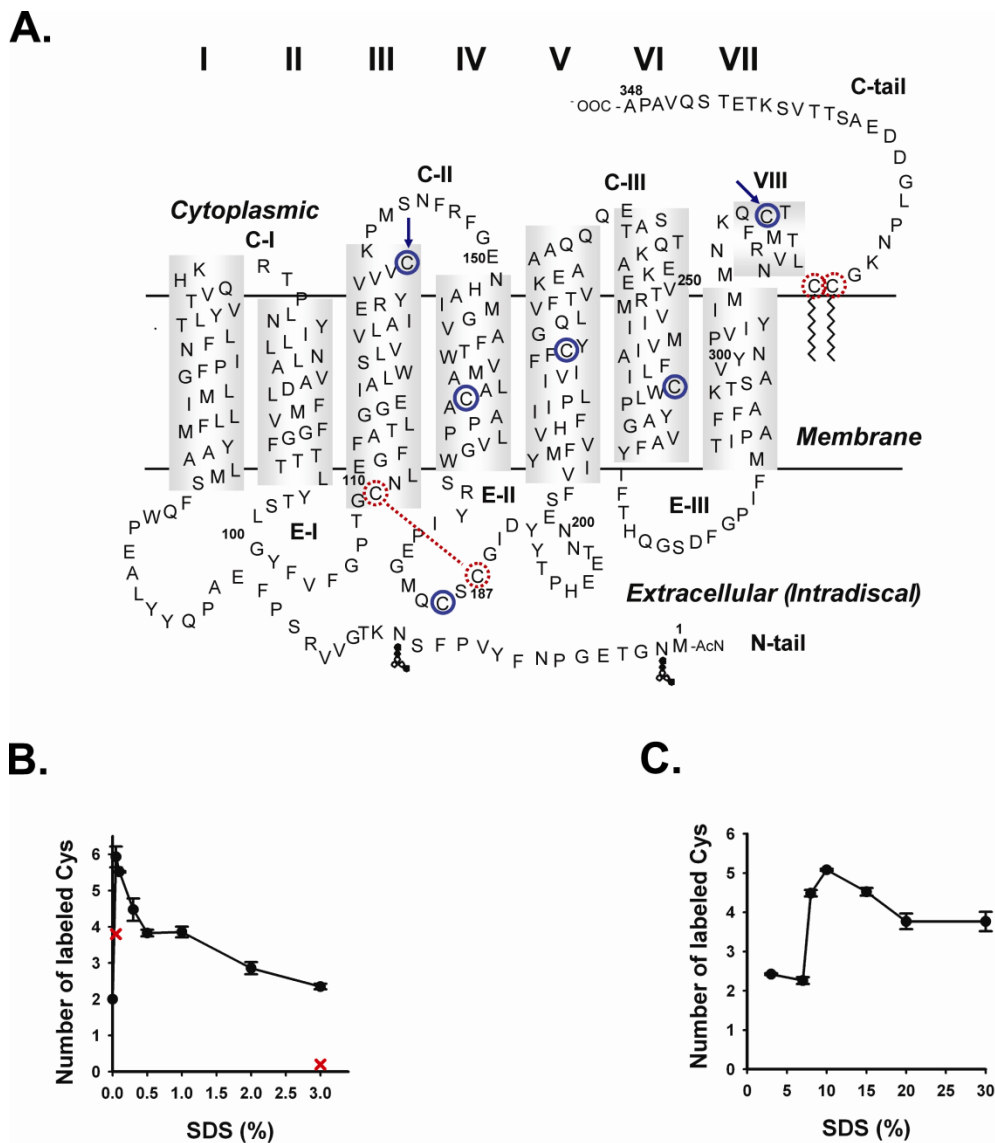
Figure 31: Changes in cysteine accessibility.

A. Secondary structure representation of rhodopsin showing the six cysteines that are reactive in the light-activated Meta II state of rhodopsin (blue solid circles). The positions of C140 and C316 are shown by blue arrows. Cysteines at positions 110 and 187 are engaged in a disulfide bond and cysteines at positions 321 and 322 are palmitoylated; they are therefore not reactive. These non-reactive cysteines are shown as red dotted circles and the disulfide bond is indicated as a red dotted line. B. Number of reactive cysteines against SDS concentration ranging from 0.05%-3% is plotted. The reactivity of cysteines in the C140S/C316S mutant is shown as crosses at 0.05% and 3% SDS. C. Number of cysteines accessible at higher SDS concentrations from 3%-30% are shown.

Denaturation of rhodopsin by 0.05% and 0.1% SDS resulted in all six cysteines becoming reactive to 4-PDS (Figure 31.B.). This indicates opening of the helical bundle of rhodopsin on SDS denaturation consistent with the tryptophan fluorescence data (Figure 28.A.). Subsequent increases in the SDS concentration decrease the accessibility of the cysteines to only two in the SDS concentration range of 3%-7%, as illustrated in Figures 31.B. and 31.C. In presence of both SDS and urea, i.e. in 3S8U at pH 6, the number of cysteines accessible to 4-PDS was found to be almost three.

In order to identify the two cysteines that are accessible at the elevated SDS concentrations of 3%, we replaced C140, in the second cytoplasmic loop, at the interface of the TM and the cytoplasmic domain, and C316, in the fourth cytoplasmic loop each with serine residues by site-directed mutagenesis. For reference, the locations of these cysteines in the rhodopsin structure are shown by blue arrows in Figure 31.A. The C140S/C316S double mutant was denatured with 3% SDS and the reactivity of the remaining four cysteines was assessed using 4-PDS, as described above for wild type. At low concentrations of SDS, four cysteines were labeled as expected (shown as red crosses in Figure 31.B.). In the presence of 3% SDS, no cysteines were labeled in the mutant (red crosses in Figure 31.B.). The absence of a 323 nm peak for the SDS denatured C140S/C316S double mutant at 3% SDS indicates that the two cysteines that were derivatized by 4-PDS in 3% SDS in the wild type are C140 and C316. These results point to the formation of a compact intermediate state at elevated SDS concentrations (around 3%), where only surface exposed cysteines are accessible.

At SDS concentrations greater than 7%, there is again a dramatic increase in cysteine reactivity resulting in five reactive cysteines at 10% SDS (Figure 31.C.). This observation is in concord with the increase in tryptophan fluorescence counts of rhodopsin treated with SDS in the

range of 3%-10% (Figure 28.D.). However, further increases in SDS concentration up to 30% decreases cysteine reactivity towards 4-PDS where four cysteines remain reactive (Figure 31.C.). This decrease in cysteine reactivity is again coherent with the decrease in tryptophan fluorescence intensity observed in the SDS concentration range of 15% to 30%. The coherence of the SDS concentration dependent changes in cysteine accessibility between 7% and 20% SDS with the tryptophan intensity changes suggests a specific SDS driven protein structural change in this SDS range.

4.5   DETERMINATION OF THE SIZE OF INTERMEDIATES DURING SDS
DENATURATION

The evidence described in Sections 4.3. and 4.4. indicate that tryptophan and cysteine residues become buried over the range 0.05%-3% SDS with the decrease in secondary structure content reflected by a 12% decrease in MRE at 222 nm at 3% SDS (see Section 3.2.1). We ruled out aggregation as a possible cause for the burial of tryptophans and cysteines as described in Chapter 3. To see if there are any changes in the size of denatured rhodopsin that may explain these results, this SDS concentration range from 0.05%-3% was further investigated by dynamic light scattering. SDS was titrated into 2 mM sodium phosphate buffer containing 0.05% DM as a control and into the same buffer containing rhodopsin (Figure 32.A). The size of the DM micelles in sodium phosphate buffer is estimated to be 3 nm (hydrodynamic radius) and that with rhodopsin is observed to be 4 nm as shown by black and grey bars respectively in Figure 32.A. SDS molecules have the same chain length as DM molecules. Therefore, addition of SDS to DM
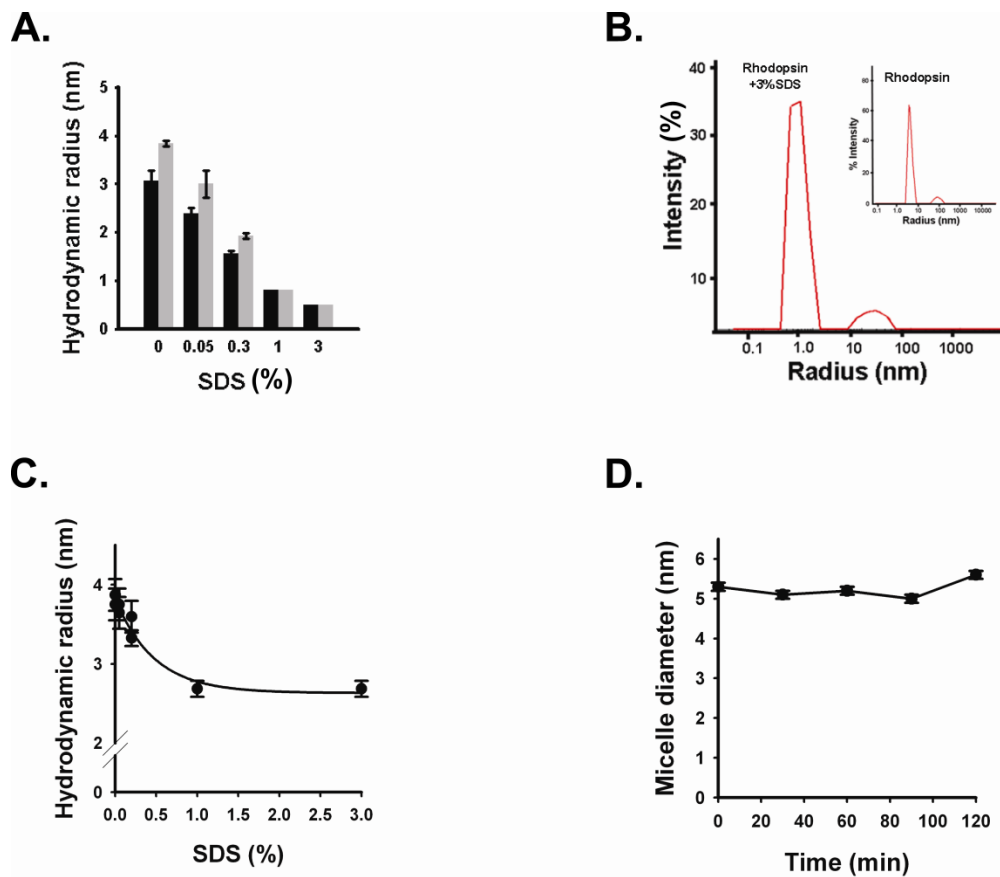
Figure 32: Probing rhodopsin by dynamic light scattering.

A. Decrease in hydrodynamic radius (R_h) of mixed DM-SDS micelle with (grey bars) and without (black bars) rhodopsin at increasing concentrations of SDS. B. Only one major peak at R_h=0.4nm was observed when 1.5μM rhodopsin was treated with 3% SDS. No other peak was observed. The inset shows that the hydrodynamic radius of rhodopsin in DM micelles is 4nm. C. Decrease in hydrodynamic radius (R_h) of mixed DM-SDS micelle containing rhodopsin at increasing concentrations of SDS (0.05% - 3%) as obtained from fluorescence depolarization. D. Stability of rhodopsin mixed micelle size at 1% SDS as a function of time.

micelles result in their entering into the DM micelles and forming mixed micelles (Bucci and Fagotti, 1991). The size of such mixed micelles was first tested in the absence of rhodopsin. A decrease in size from 3 nm to 0.4 nm was observed when 3% SDS was added to 0.05% DM (black bars in Figure 32.A.). These values were calculated after taking into account viscosity coefficients of SDS titrated buffer solutions. Viscosity coefficients of SDS solutions were obtained by measuring the diffusion co-efficient of silica beads of 50 nm radius in water and in different SDS concentrations. Diffusion coefficients were obtained from the intensity autocorrelation function as measured by the Dynamics V6 software supplied by the instrument manufacturer (Protein Solutions Inc., Charlottesville, VA). Viscosity coefficients were then calculated using the Stokes-Einstein equation. Hydrodynamic radii of 1.5 μM rhodopsin at varying concentrations of SDS were then obtained by applying the Stokes-Einstein equation using the Dynamics V6 software. The viscosity, η, of 0.05% to 2% SDS solutions was measured to be 1 cP (same as that of water) and that of 3% SDS solution was determined to be 1.27 cP. The hydrodynamic radius of rhodopsin in DM micelles was observed to decrease from 4nm in the absence of SDS to 0.4nm at 3% SDS (grey bars in Figure 32.A.). Since SDS is an anionic detergent, its aggregation number of 62 at its critical micellar concentration (Turro and Yekta, 1978), is smaller compared to that of DM which is 98 (Tummino and Gafni, 1993). Hence, the decrease in mixed micellar size on increasing SDS concentration in the lower SDS concentration range indicates that the DM molecules are increasingly getting replaced by SDS molecules both in the absence and presence of rhodopsin. Figure 32.B. shows a peak at 0.4 nm for rhodopsin micelles in 3% SDS. The radius of 0.4 nm reflects the size of the major species in solution which are the SDS micelles at 3% SDS and does not reflect the true size of rhodopsin. A small peak of very low intensity compared to the protein peak at 0.4 nm also appears but this peak is also seen

for rhodopsin alone in the absence of SDS (Figure 32.B. and inset of Figure 32.B.). This peak may originate from impurities in the solution since it was not filtered before the experiment. This is because when sodium phosphate buffer containing DM was filtered, highly intense peaks of large size were seen (data not shown). In collaboration with Dr. Ulrike Alexiev, fluorescence probes were placed on helix 8 of rhodopsin to carry out fluorescence depolarization experiment for calculating hydrodynamic radius of rhodopsin specifically (Dutta et al., 2010). A radius of 3.7 nm was obtained for the native state whereas a decrease in size to 2.6 nm was observed in presence of 1% SDS and remained the same till 3% SDS (Figure 32.C. and D.). Therefore, a decrease in hydrodynamic radius was observed in the size of rhodopsin with increase in SDS up to 3%. It was not possible to measure the hydrodynamic radius beyond 3% SDS concentrations due to quenching of the fluorophore.

4.6   CHANGES IN OVERALL PROTEIN FLEXIBILITY BY ^{1}H 1D NMR

The presence of a compact intermediate during denaturation of rhodopsin renders investigation into the dynamics of these states to enable identification of the regions of compactness. Therefore, we have studied qualitatively the global motions experienced by rhodopsin residues under denaturing conditions by measuring 1D ^{1}H NMR spectra in the presence and absence of different denaturants. At first, 1D proton NMR spectrum of native and denatured rhodopsin were compared to see if there are any significant global structural differences between the two. Figure 33.A. shows the 1D spectrum of native rhodopsin where broad and overlapping peaks are observed due to the presence of 348 amino acids which is too many to be resolved on a one dimensional proton spectrum. Further, it was observed previously that backbone amides of

tryptophans and lysines show more than the expected number of signals with varying intensities in the NMR spectrum of α-^{15}N-lysine-labeled and α,ε-^{15}N-tryptophan-labeled rhodopsin (Klein-Seetharaman et al., 2002b; Klein-Seetharaman et al., 2004). These observations indicated that there are conformational fluctuations on a μs-ms timescale leading to signal broadening (Klein-Seetharaman et al., 2002b; Klein-Seetharaman et al., 2004). With increase in denaturation, appearance of a greater number of proton peaks in the spectrum is expected due to a shift in timescale of motion from the μs-ms timescale to faster ns timescales of motion of the residues in unfolded regions of the protein. This shift to rapid motion in ns or faster timescales of unfolded regions in a protein will be henceforth referred to as increase in flexibility upon denaturation. In order to determine how this flexibility changes with unfolding of rhodopsin we obtained 1D proton NMR spectra of rhodopsin titrated with different concentrations of SDS. All these spectra are shown in Figure 33.

Figure 33.A. shows the comparison between the overall 1D spectra of native rhodopsin and 30% SDS denatured rhodopsin which is the maximally denatured state of rhodopsin. The number of peaks and resolution of the peaks have considerably increased after addition of 30% SDS. Greater number of backbone and aromatic side chains appears in the SDS denatured state, the latter peaks being non-existent in the native state. Peaks between 7-7.8 ppm coalesce to give a peak of high intensity. In Figures 33.B., C. and D. different regions of the 1D spectrum shown in Figure 33.A. are zoomed in for clarity and a better comparison. These regions are the aromatic region (around 10 ppm), the backbone region (around 8 ppm) and the further upfield region where protons of side chains and also backbone protons of some amino acids appear (around 6 ppm).

In Figure 33.B., peaks in the aromatic region that do not appear in native rhodopsin begin to appear on addition of SDS indicating enhanced flexibility in the ns or higher time regimes of the aromatic residues. A progressive increase in the number of peaks and their resolution is evident with increase in SDS concentration. The peaks around 8 ppm and 6 ppm shown in Figures 33.C. and 33.D. also show the same trend.
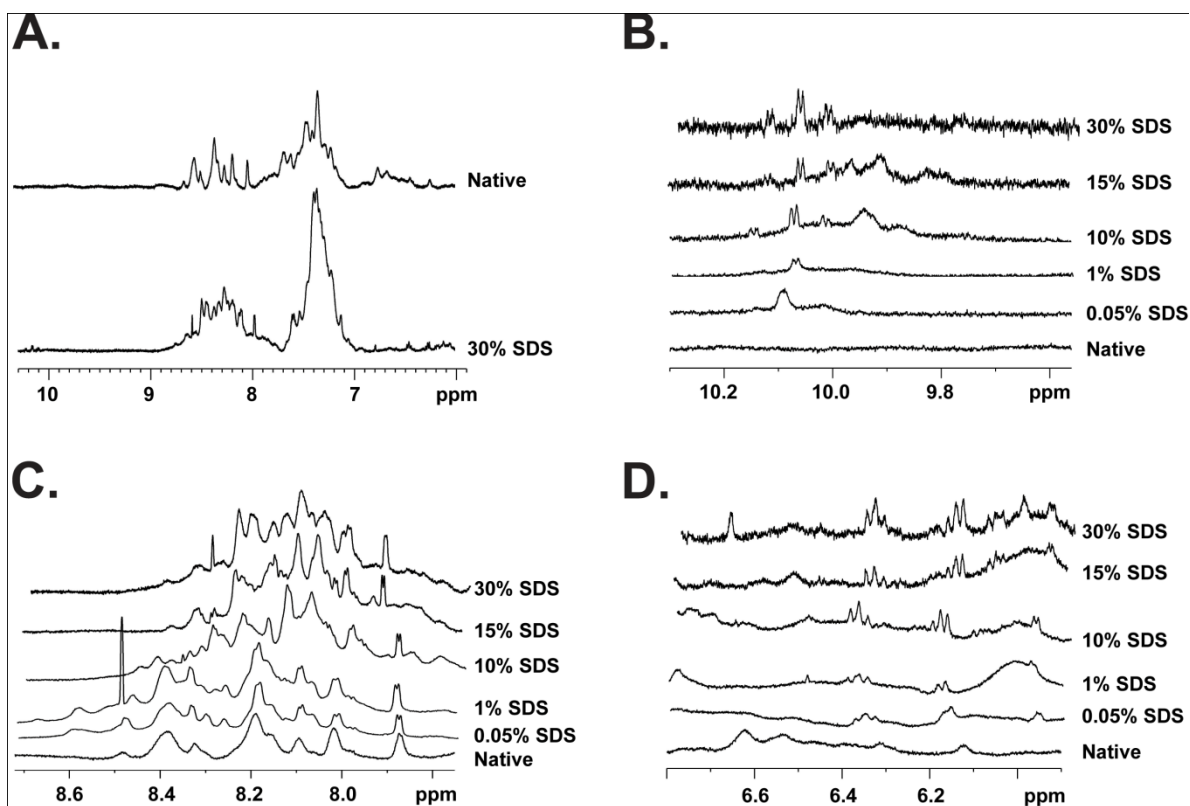
Figure 33: 1D ^{1}H spectra of native and denatured rhodopsin.

Overlay of native and 30% SDS denatured rhodopsin showing the region from 6 ppm to 10.3 ppm. (A.), overlays of native rhodopsin and 0.05%, 1%, 10%, 15% and 30% SDS denatured rhodopsin in the region around 10ppm (B.), 8 ppm (C.) and 6 ppm (D.). All spectra were collected at 37°C.

4.7   DISCUSSION

As described in Chapter 3, we deduced four denaturation stages based on CD measurements, which correlate with the types of SDS micellar structures expected at different concentrations. These are DM/SDS mixed micelles (stage 1, 0.05-0.3% SDS), SDS spheres (stage 2, 0.3-3% SDS), SDS spheres/cylindrical mixed micellar states (stage 3, 3-15 % SDS) and predominantly cylindrical micelles (stage 4, above 15% SDS). [Note that the use of the word "stages" does not imply a temporal progression, and is used in this context only to describe the respective conformational states observed at a particular SDS concentration range]. While stages 1 and 2 are characterized by a gradual loss in MP helicity of up to ~19%, stage 3 includes the formation of non-native helices, a well known property of SDS (Li and Deber, 1992; Rizo et al., 1993) when a very large number of detergent molecules interact with the MP and SDS is going from spherical to cylindrical shape. In stage 4, a ~40% decrease in helical content characterize the largely unfolded states of rhodopsin induced by SDS cylindrical micelles that aggressively unfold the MP at 30% SDS. The identification of these four denaturation stages is corroborated by the characterization of tertiary structure. We utilized four independent probes, retinal-rhodopsin interaction, cysteine reactivity towards 4-PDS, tryptophan fluorescence and hydrodynamic radius of denatured states.

4.7.1   Stage 1: Opening of helical bundle

In stage 1 of SDS-denaturation, at very low SDS concentrations (0.05%), initial opening of the helical bundle leads to an instantaneous increase in tryptophan fluorescence and cysteine accessibility in the protein core, while retinal-rhodopsin interactions only begin to be disrupted.

The tryptophan fluorescence increase takes place within seconds. In contrast, the partial loss of retinal-protein interactions occurs very slowly at 0.05% (in the minutes time range) indicating that there are not sufficient SDS molecules present at these concentrations to cause the breakage of native retinal-protein contacts. However, at 1% SDS, the loss of retinal contacts occurs very fast, in fact it reaches a peak indicating that at this stage optimal amounts of SDS are available to carry out this process. Beyond 1% SDS, i.e. at 10%, 15% and 26% SDS, the rates of the reaction slow down again indicating that the formation of cylindrical micelles at these concentrations of SDS is retarding the disruption of protein contacts including retinal-protein contacts. Thus, in stage 1 (at 0.05% SDS) there is a fast initial opening of the helical bundle, which is characterized by an increase in tryptophan and cysteine accessibility. This initial opening should be viewed as a softening of the helix bundle because it allows only partial loss of retinal-protein contacts leading to a slow "full" opening of the helical bundle (Figure 34.A.).

A similar trend in SDS dependence is also seen in measurements of cysteine reactivity towards 4-PDS, which has been previously utilized to study conformational changes in rhodopsin (Cai et al., 1999a; Klein-Seetharaman et al., 1999b). Here, this reaction was exploited to investigate tertiary structure changes under SDS denaturing conditions. While interpretation of cysteine accessibility results under denaturing conditions is qualitative due to possibilities such as disulfide exchange reactions in unfolded states, and effects of the hydrophobic environment on the molar extinction coefficient of 4-PDS, these factors are expected to influence the results mostly at high SDS concentrations beyond 3% (as seen in control studies of SDS+cysteine). At low concentrations of 0.05% and 0.1% SDS, all six free cysteines in rhodopsin react with 4-PDS compared to only two cysteines reacting in the native state. This may be triggered by perturbation of retinal interactions with rhodopsin at low SDS concentrations. The initial opening

of the helical bundle is accompanied by an increase in accessibility of the cysteine side chains to 4-PDS and an increase in tryptophan fluorescence. This supports the notion that the initial opening or softening of the helical bundle, probably mediated by surface-induced long-range effects, is the first stage of denaturation of tertiary structure by SDS. This interpretation is further corroborated by the decrease in steric hindrance of H8 mobility that was measured by fluorescence depolarization of fluorophore labeled C316 in H8 by our collaborator Dr. Ulrike Alexiev (Dutta et al., 2010). This is expected because opening of the helix bundle leaves more conformational space for individual proteins elements especially at the protein surface.

A. Stage 1 (SDS concentration range 0.05%-0.3%)

DM   SDS

Native state → **sec** → Initial opening (softening) of helix bundle (Trp fluorescence increase, cysteine accessibility, slow surface segment dynamics) → **min** → Full opening of helix bundle (loss of retinal-protein contacts)

B. Stage 2 (SDS concentration range 0.3%-3%)

DM   SDS

Native state → **msec** → Full helix bundle opening (loss of retinal-protein contacts, Trp fluorescence increase) → **sec** → Protein structural change and formation of compact state (partial Trp fluorescence decrease, burial of cysteines, micelle size)

Figure 34: Model depicting structural changes in rhodopsin in stages 1 and 2 of SDS denaturation.

A. Stage 1 represents addition of 0.05% SDS to rhodopsin whereby an initial slow opening of helical bundle on a time scale of seconds occurs. This is followed by complete opening of the bundle on a time scale of minutes. B. Stage 2 refers to denaturing concentration of SDS beyond 0.05% up to 3% whereby an opening of the helical bundle occurs in milliseconds followed by structural changes in rhodopsin leading to formation of a compact state is seen on a seconds time scale. The cartoon representations of rhodopsin are not drawn to scale and the decrease in the size of helices are only qualitative representations of the extent of denaturation.

142

4.7.2 Stage 2: Compact intermediate formation

In the second stage, in the range of 0.05%-3% SDS, the increase in SDS concentrations up to 0.5% decreases the tryptophan fluorescence counts, which then remain constant up to 3% SDS. Cysteine reactivity shows a continuous decrease, which plateau at two reactive cysteines in the presence of up to 3% SDS. The tryptophan fluorescence kinetics shows a biphasic behavior with fast increase and partial decrease for all SDS concentrations used. In contrast to stage 1, the kinetics of tryptophan fluorescence increase coincide with the kinetics of the disruption of native retinal contacts (0.4 s and 0.3 s at 1% SDS, respectively), indicating that the amount of SDS molecules is sufficient to break native retinal-protein contacts very fast leading to a full opening of the helix bundle. The kinetics of the partial fluorescence decrease is somewhat slower with values in the lower seconds range. Taking the development of a plateau between 0.5% and 3% SDS for both tryptophan fluorescence and cysteine accessibility into account, we associate the fluorescence decay kinetics in the seconds time range with a protein structural change leading to the burial of the cysteines (Figure 34.B.). This constitutes the second stage of unfolding. Several lines of evidence indicate that this second stage constitutes a stable compact intermediate state during SDS denaturation. The observed decreases in cysteine reactivity and tryptophan fluorescence from 0.05% to 3% SDS can be explained by the burial of four of the six cysteines and one or more of the tryptophan side chains during SDS denaturation in a compact intermediate state. In order to identify the cysteines that are getting buried and better characterize this intermediate, we carried out mutagenesis experiments whereby two cysteines, C140 and C316, near the cytoplasmic domain were mutated to serines. It is expected that denaturation will occur more favorably near the extramembranous domain causing the cysteines at this surface to be more accessible to derivatizing agents. The C140S/C316S double mutant showed no

reactivity towards 4-PDS at 3% SDS confirming that the two cysteines that remain reactive at 3% SDS in the wild type are indeed C140 and C316, located at the rhodopsin surface. The burial of the other cysteines could be due to either formation of a compact intermediate or masking by solvent molecules which are SDS micelles in this case. Hydrodynamic radius measurements by fluorescence depolarization strongly support the possibility of formation of a compact intermediate during the second stage of SDS unfolding. The hydrodynamic radius of the DM micelle with rhodopsin was estimated to be 4 nm. With increasing concentrations of SDS the radius decreases up to a value of 2.6 nm in 3% SDS. It should be noted that these values for the hydrodynamic radius are a qualitative measure of the size of rhodopsin since a spherical model has been assumed to estimate the hydrodynamic radius, both in the case of native and denatured rhodopsin. This was done to avoid complexity arising due to possible differential shapes of native and denatured states. Further, the native state of rhodopsin is known to have a complex shape based on crystal structures (see Figure 1.C.) (Teller et al., 2001), hence is difficult to be modeled. The shape of denatured states in 3% SDS is not known. Generally, for soluble proteins the hydrodynamic size increases on denaturation due to unfolding of the native structure. The contrary observed here for intermediate denatured states at 3% SDS indicates the possibility of formation of a compact intermediate which is surrounded by SDS molecules. Thus, at the second stage of unfolding, where the extent of denaturation corresponds to a 12% decrease in MRE at 222 nm, a decrease in size from the native state and burial of tryptophans and cysteines indicate formation of a compact protein core (Figure 34.B.).

4.7.3 Stage 3: Disruption of inter-helical interactions, cylindrical micelle formation

SDS concentrations between 3% (100 mM) and 15% (500 mM) form the third stage of unfolding as the increase in aggregation number of SDS beyond 6% (200 mM) leads to structural transition of SDS micelles from spherical to cylindrical (Croonen et al., 1983). The effect of a very large number of SDS molecules interacting with rhodopsin can be clearly seen in our CD experiment where there is an increase in the magnitude of MRE at 222 nm at 10% SDS to a value close to the native state indicating that SDS is inducing non-native helices, a well-known property of SDS (Li and Deber, 1992). However, these helices clearly lack inter-helical interactions within the cylindrical SDS micelles, as an increase in cysteine accessibility and tryptophan fluorescence is observed as compared to the previous stage. The time-dependence of the fluorescence counts and the analysis of fluorescence after treatment with hydroxylamine indicate that the retinal also lacks interactions with the rest of the protein that would lead to tryptophan quenching. Above 5% SDS, the kinetics of the formation of the 440 nm denatured rhodopsin species, indicative of the loss of retinal-protein contacts, becomes again slower than the internal protein conformational changes as measured by tryptophan fluorescence. The formation of cylindrical micelles at these concentrations of SDS is retarding the breakage of retinal-protein contacts probably due to the formation of stabilizing non-native protein structures.

4.7.4 Extensive denaturation, residual structure formation

The fourth stage of unfolding at SDS concentrations beyond 10% is characterized by a drastic disruption of helical structure: a ~40% decrease in MRE at 222 nm at 30% SDS (1 M) is observed. This corresponds approximately to a 45% decrease in helical content as estimated

using the CDPro software (Sreerama and Woody, 2000). This is consistent with so-called "mode 2" unfolding in which SDS cylindrical micelles wrap around the protein and aggressively unfold it (Otzen, 2002; Otzen and Oliveberg, 2002). However, despite the large degree of unfolding, we also see a decrease in fluorescence and in cysteine accessibility, where only four cysteines are reactive in the range of 15%-30% SDS as compared to five cysteines in stage 3. Therefore, it is likely that residual structure formed in the largely unfolded state of rhodopsin induced by 30% SDS is localised at a site that buries two cysteines and one or more tryptophan residues.

The possibility of formation of a folding core during folding of rhodopsin has been considered in the LRI model (Klein-Seetharaman, 2005). Computational modeling of denaturation of rhodopsin suggests that TM helices in rhodopsin do not unfold independently of each other and at the end of the unfolding process a rigid region remains that consists of residues from EC loops and TM helices (Rader et al., 2004). Our findings of a compact intermediate during denaturation of rhodopsin can be considered as preliminary evidence towards the presence of a folding core during its initial folding stages. However, correlating our studies of SDS denaturation with that of the above folding model will require identification of the location of the residual structure and its characterization in the future.

Global structural changes upon denaturation of rhodopsin were analyzed by recording 1D proton NMR spectra of rhodopsin titrated with different concentrations of SDS. Since, rhodopsin contains 348 amino acids, not all the protons can be resolved on a one dimensional proton NMR spectrum. The peaks that appear in the spectrum of native rhodopsin can be compared to those observed in the SDS denatured protein spectrum. We observed that the number of proton peaks appearing on the spectrum increased with increase in SDS concentration. This supports the notion that the structure of rhodopsin unfolds progressively with increase in SDS concentration

leading to highly flexible regions which appear as peaks on the 1D spectrum. The appearance of aromatic side chain peaks in the SDS denatured samples in the region around 10 ppm is particularly striking when compared to that of the native spectrum since no such peaks were seen in the native state. This clearly shows that significant changes occur in the environment of the side chains of aromatic amino acids upon denaturation making them more flexible.

4.8   SUMMARY OF CONTRIBUTIONS

Studies on understanding folding mechanisms of MPs are mostly associated with extracting thermodynamic and kinetic details of unfolding and refolding pathways, thus leaving behind very little information about the denatured state itself. Here, we have characterized global structural features of SDS denatured states of rhodopsin and also the process of unfolding using various spectroscopic techniques. However, often in such experiments, it becomes challenging to show that the readout is due to protein conformational changes and not due to solvent effects. We have taken care of these concerns by designing suitable controls such as effects of SDS on reactions of free cysteine with PDS and fluorescence of free tryptophan in SDS. We also carried out various fluorescence and absorbance experiments of rhodopsin in hydroxylamine to show that the changes in fluorescence are arising from protein mediated effects.

The studies described in the chapter have revealed the presence of a compact intermediate during denaturation of rhodopsin. This is in contrast to the widely expected and more commonly observed phenomenon with soluble proteins, which is an increase in their size upon denaturation. However, this compactness is isolated in a specific region as is indicated by the overall increase in flexibility of rhodopsin with denaturation which is shown to arise mainly

from the cytoplasmic domain (Dutta et al., 2010). Further, correlating our findings to the structural changes of SDS micelles with increase in SDS concentration has enabled understanding of the unfolding process of rhodopsin by SDS. This has helped us in sketching a model of the events that we believe is happening in the initial stages of unfolding of rhodopsin (Figure 34). Therefore, such characterizations necessitated further investigation of motions in a higher resolution which is described in the following chapters.

5.0 CHAPTER 5: IDENTIFICATION OF FLEXIBLE AND RIGID REGIONS IN UNFOLDED STATES OF RHODOPSIN

5.1 RATIONALE AND SUMMARY

The presence of residual structure in denatured states is well known for soluble proteins (Shortle, 1996; Daggett and Fersht, 2003; Cho et al., 2008). High resolution structural characterization of denatured states of proteins is one way to obtain information on the propensity of interactions among residues in early stages of folding. Determining motion of residues in denatured states is thus a direct measure of their involvement in interactions (Shortle and Ackerman, 2001; Klein-Seetharaman et al., 2002a). To what extent residual structure is retained in the denatured states of MPs and what is the putative nature of such residual structure in MPs is not known. *In vitro* unfolding studies of MPs uniformly show the difficulty in denaturing them; usually large regions of structure remain intact despite the presence of high concentrations of chemical denaturants (Plumley and Schmidt, 1987; Lau and Bowie, 1997; Otzen, 2003; Barrera et al., 2005; Dockter et al., 2009; Miller et al., 2009). In fact, bR (Huang et al., 1981) and CopA (Roman et al., 2010) are to date the only helical MPs that have been almost fully unfolded. This is because it is thermodynamically unlikely that MPs will be completely unfolded inside the membrane environment *in vivo* or in the membrane mimetics used to study these proteins *in vitro*. Thus, for MPs, residual structure may actually play an even more important role for folding than in soluble

proteins. Thus, it is critical for our understanding of MP folding mechanisms to characterize the molecular nature of denatured states in detail. No such in-depth characterization of the structure and dynamics in largely denatured states of MPs yet exists.

As described in Chapter 3, a screen of denaturing conditions that simultaneously maximize the extent of denaturation while preventing aggregation have identified 3S8U as suitable conditions to study largely denatured states of rhodopsin. Changes in global structure under these conditions have been characterized by time-resolved and steady-state spectroscopic measurements as described in Chapter 4. These studies indicated that a compact intermediate is formed in the denatured states. Cysteine reactivity and retinal-protein interaction studies indicated qualitatively that the location of compactness may involve TM regions and the interface between TM and EC domains. Compact intermediates have been predicted by the LRI theory of folding of MPs which proposes that interactions involving loops and TM helices form during early folding stages (Klein-Seetharaman, 2005). The model was based on computational analysis of predicted thermal denaturation of rhodopsin which had suggested the existence of a folding core involving loop and TM helices near the EC surface of rhodopsin (Rader et al., 2004).

To begin deciphering the molecular basis for compactness in unfolded rhodopsin, here I attempt to further approximate the position of residual structure in largely denatured states of rhodopsin. NMR spectroscopy has seen significant advances recently in studies of α-helical MPs (Oxenoid and Chou, 2005; Schnell and Chou, 2008; Zhou et al., 2008; Van Horn et al., 2009). Particularly for rhodopsin, extensive studies incorporating ^{15}N, ^{15}N/^{13}C and ^{19}F labels have been carried out showing the applicability of NMR to this system in the folded state (Klein-Seetharaman et al., 1999a; Loewen et al., 2001; Klein-Seetharaman et al., 2002b; Getmanova et

al., 2004; Klein-Seetharaman et al., 2004; Werner et al., 2007; Werner et al., 2008). Here, we use NMR spectroscopy of ^{15}N-α-lysine and ^{15}N-α,ε-tryptophan labeled rhodopsin to obtain a more in-depth characterization of denatured states of rhodopsin than is possible with global biophysical approaches such as circular dichroism and fluorescence spectroscopy described in Chapters 3 and 4. In this chapter, we describe our findings on the dynamics and local environment of different regions in the denatured states. We found that in these states the regions around EC and TM domains appear to be more rigid than the regions located at the CP side of rhodopsin. This has provided further, more detailed experimental support for the computational folding experiment in which a folding core involving TM helices and EC loops was predicted. Consequently, it has generated more evidence towards the LRI theory of folding which emphasizes the presence of interactions between loops and helices during initial stages of folding.

5.2   PROBING ENVIRONMENT OF SDS PROTONS WITH INCREASE IN SDS CONCENTRATION

In Chapter 3, I showed that SDS and 3S8U are optimum denaturing conditions for characterizing unfolded states of rhodopsin. Hence, I used these two conditions to denature rhodopsin and follow the changes in protein conformation with denaturation by NMR. In order to distinguish between protein mediated changes and non-specific changes due to solvent, I first measured ^{1}H 1D NMR spectrum of SDS at increasing concentrations. SDS micelles undergo changes in their shape with increase in SDS concentration as described in Chapter 3. Spherical micelles at low SDS concentrations change to cylindrical micelles beyond 6% SDS (Croonen et al., 1983). I

expected these micellar changes to be observed on the proton spectrum of SDS. Therefore, in order to test the effect of large cylindrical micelles on peak intensity, line width and chemical shift, we recorded 1D proton spectra at different SDS concentrations. I also recorded such a spectrum for 3S8U at pH 2 to see if there are any differences in proton peak width and chemical shift when compared to that of SDS containing solutions. Acidic pH of 2 was used for 3S8U denaturation to prevent background signals from amide protons in urea to appear on the 1D spectrum. Buffer used for the solutions is 20 mM sodium phosphate, pH 6. DM was added to all the solutions at a concentration of 0.6% as this amount was also present in rhodopsin containing solutions.
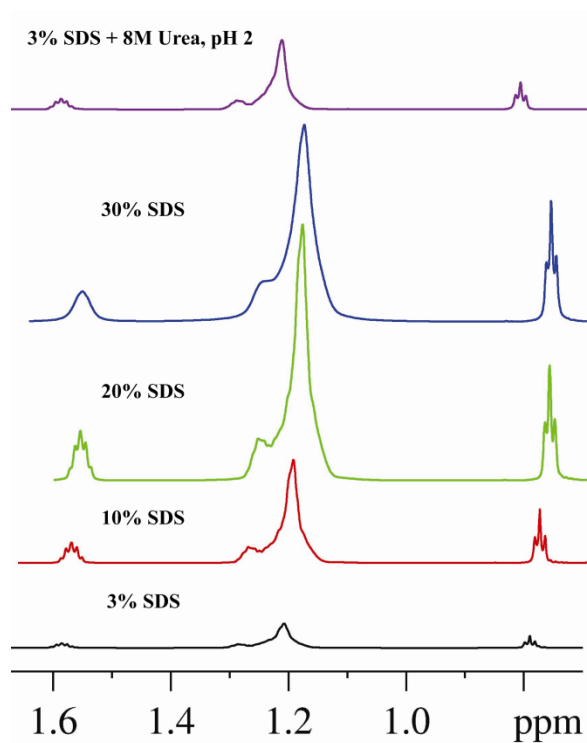
Figure 35: 1D ^{1}H spectra of SDS containing buffers.

Overlay of 1D 1H spectra of 3%, 10%, 20% and 30% SDS and 3S8U, pH 2. All spectra were collected at 37ºC and referenced to DSS. zgpr pulse sequence was used on a 800 MHz spectrometer. 60 scans were recorded for each spectrum.

Overlay of these 1D spectra is shown in Figure 35. The spectral region in Figure 35 shows peaks arising from protons in SDS alone and is free from proton peaks in DM. The overlay shows an increase in peak intensity with increase in SDS concentration from 3% to 20%. A slight broadening of all the peaks is seen at 30% SDS. However, overall peak dispersion remains the same without significant peak broadening with increase in SDS from 3% to 30% in spite of the change in micelle shape to cylindrical micelles beyond 6%. The peak dispersion remains the same for 3S8U, pH 2 solution as well. Therefore, change in micelle shape is not reflected as significant changes in chemical shift or line width of proton peaks of SDS.

5.3   PROBING DYNAMICS AND LOCAL ENVIRONMENT OF DEFINED REGIONS

In order to determine dynamics more specifically, I compared the motions of denatured regions of rhodopsin carrying isotope labels that preferentially label TM and EC versus CP residues. It is expected that if residual structure is formed in TM and EC domains as suggested by the results presented in Chapter 4 and based on the prediction of a folding core spanning these two domains (Rader et al., 2004), then these domains will have constrained motion due to inter-residue interactions. On the other hand, the CP domain which is away from the region of residual structure formation is expected to undergo rapid motion on ns or faster timescales or in other words will be more flexible due to greater extent of denaturation. Such differences in degrees of motion can be detected by using NMR. NMR detects motions of residues and exchange between different conformations on different timescales qualitatively in the appearance of spectra. The properties of NMR spectra depend on the rate of exchange. A fast exchange on the timescale of NMR measurement or a very flexible residue will appear as a single peak on the NMR spectrum

representing an average of all the conformations (Palmer, 2004). A slow exchange or a rigid residue will appear as several peaks, each peak corresponding to a particular conformation (Palmer, 2004). A residue with intermediate exchange, i.e. motion on timescales which is neither too fast nor too slow on the NMR timescale will appear as a coalescent peak with low signal to noise ratio (Palmer, 2004). Quantitatively, NMR can be used to measure the degree of motion of specific residues in terms of relaxation rates of their corresponding magnetization, these rates are determined by their motion (see Chapter 7 for a more detailed description of relaxation rates). Unfortunately, the large size of rhodopsin micelles makes accurate measurements of relaxation rates for protons not feasible due to their fast relaxation evidenced by the broad line widths.

Tryptophans, labeled with ^{15}N at its backbone and side chain nitrogens, and lysines, labeled with ^{15}N at its backbone nitrogen, were used as reporters of the TM-EC and CP domainsrespectively. This is because with the exception of Lys296, the TM attachment site for retinal, and one lysine near the N-terminus, all other lysine residues are located in the cytoplasmic domain (Figure 36, blue circles). In contrast, tryptophans are only observed in the TM and EC domains (Fig. 36, red circles). This allows us to obtain higher resolution structural information than with ^{1}H spectra alone.
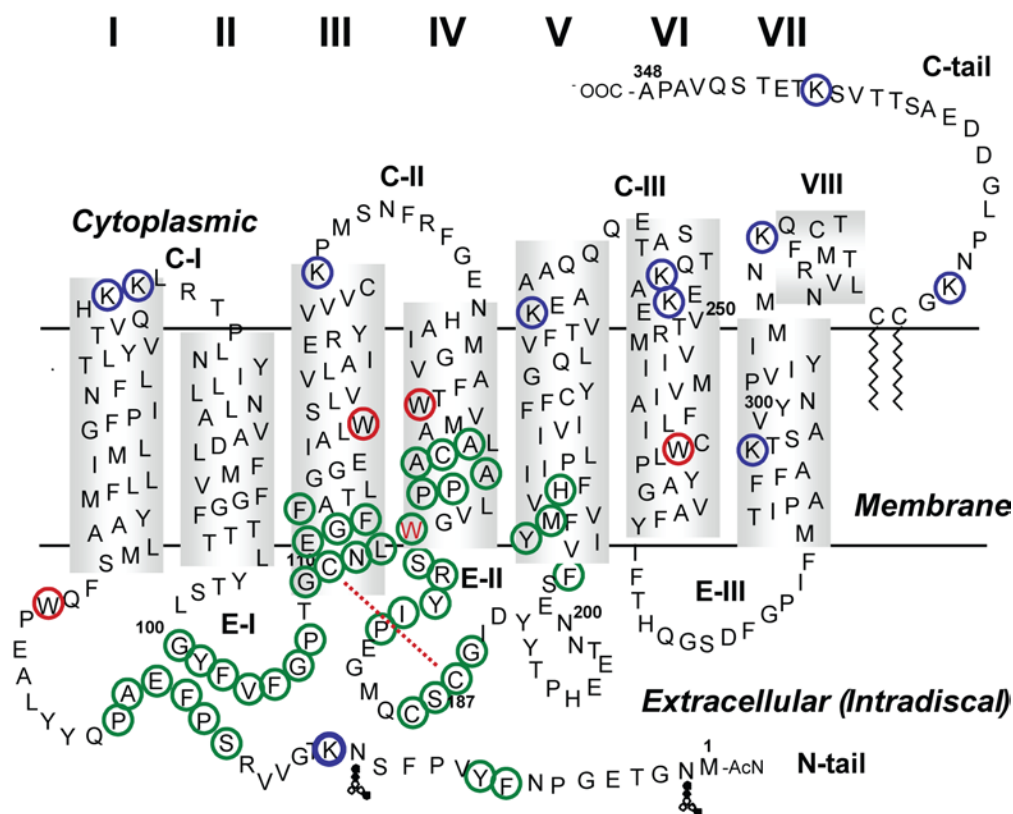
Figure 36: Secondary structure representation of rhodopsin.

Secondary structure representation of rhodopsin showing predicted folding core residues in green circles, tryptophans in red circles and lysines in blue circles.

5.3.1 NMR spectroscopy of α,ε-^{15}N-Tryptophan labeled rhodopsin

After optimizing sample conditions and data acquisition parameters (see Section 2.3.12.2.), 2D HSQC spectra of native, 1% SDS, 30% SDS and 3S8U denatured ^{15}N-α,ε-tryptophan labeled rhodopsin were acquired. The results are shown in Figure 37. The spectrum of native rhodopsin (Figure 37.A.) is identical to that reported earlier (Klein-Seetharaman et al., 2004). The native spectrum is characterized by a larger number of tryptophan backbone peaks than the number of tryptophans in the structure due to conformational heterogeneity, while the expected five side chain peaks are observed for the five tryptophan residues in rhodopsin (Klein-Seetharaman et al.,

155

2004). At 1% SDS (Figure 37.B.), fewer backbone peaks and clustering of the side chain peaks is observed compared to the native state. At 30% SDS, which maximally unfolds rhodopsin, very weak background signals were observed (Figure 37.C.). The side chain peaks remain clustered at a similar position but were significantly lower in intensity than that at 1% SDS.

To rule out that the overall low signal intensity at 30% SDS is due to slow tumbling of the large SDS cylindrical micelle, we tested another denaturing condition, 3S8U where no cylindrical micelles form (Nagarajan et al., 1982; Kumar et al., 2005). To avoid the urea background signal in the amide region of the spectrum, the pH was lowered to 2. Note that the denaturing efficiency of 3S8U at pH2 is less as compared to 3S8U alone. The former decreases the MRE at 222 nm of rhodopsin by ~25% as compared to ~45% by the latter and that by 30% SDS (see Sections 3.2.4.). As shown in the overlay in Figure 37.D., the backbone signals in 3S8U at pH2 are lesser in number and intensity than that in native and 1% SDS but are greater than that at 30% SDS. The side chain peaks appear to be less clustered compared to the spectra recorded in the native state and in the presence of 30% SDS indicating that a different denatured state is formed in 3S8U pH2 than in 30% SDS. The differences observed are in line with the intermediate denaturing capacity of this condition. This result indicates that the tryptophans are restricted in mobility, even under denaturing conditions.
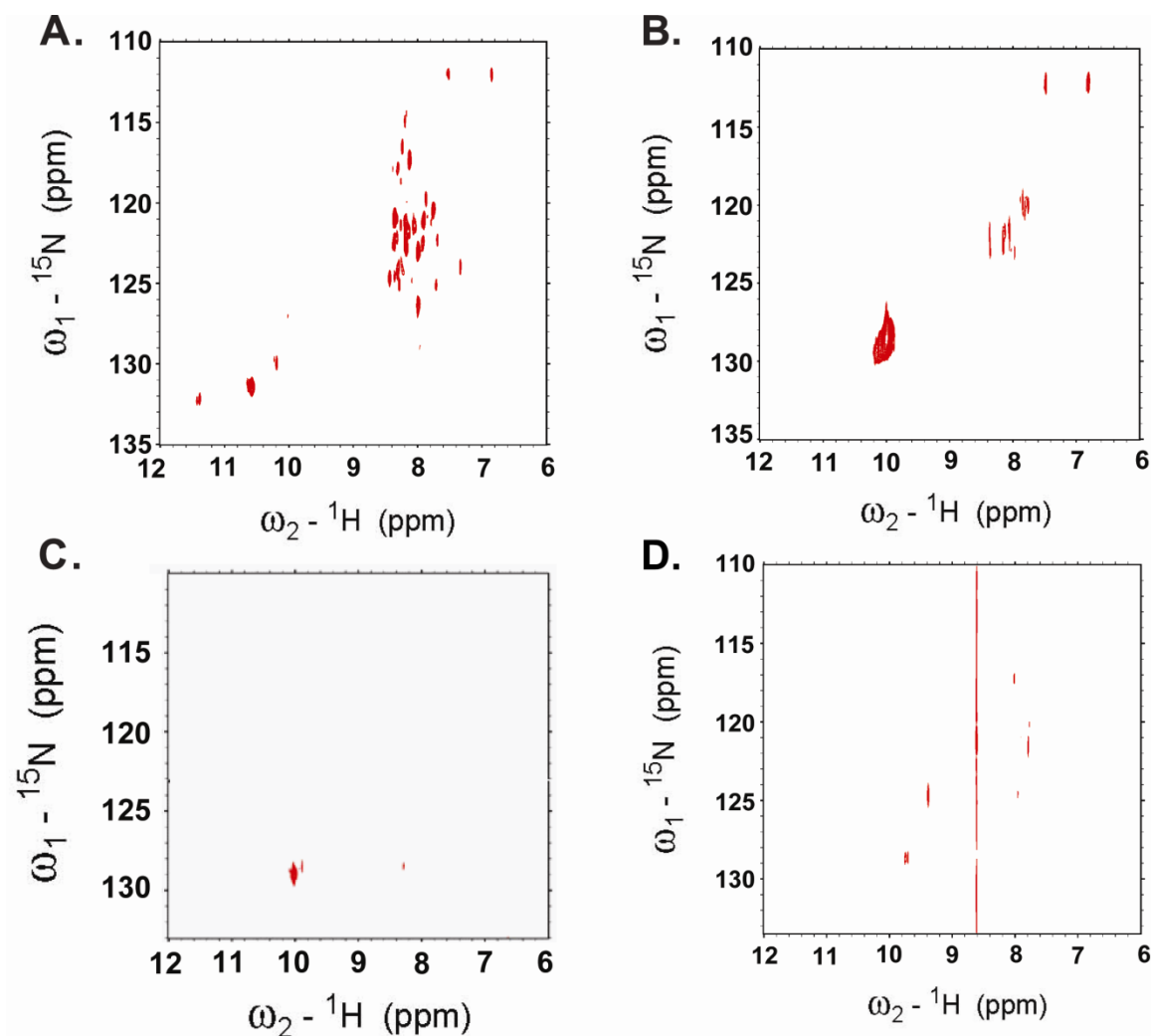
Figure 37: 2D HSQC spectra of native and SDS denatured 15N-α,ε-Tryptophan labeled rhodopsin.

2D HSQC spectra of rhodopsin in A. native state (data taken from Naveena Yanamala) and denatured with B. 1% SDS, C. 30% SDS and D. 3S8U. Native rhodopsin is at 0.15 mM concentration and denatured rhodopsin samples are all at 0.12 mM concentration. Number of scans recorded for native state is 1000 in ^{1}H dimension and 72 in ^{15}N dimension and for the denatured states is 2000 and 42 in ^{1}H and ^{15}N dimension respectively. The lowest positive value of contour is set at 10^7 for all the spectra shown.

To show that the decreased peak intensities of ^{15}N labeled tryptophans are not due to slow tumbling of the SDS micelles, we referred to 1D ^{1}H spectra of SDS buffers (Figure 35, Section 5.2.). This was done to check whether the large cylindrical micelles affected the intensity of the SDS proton peaks. However, as discussed in Section 5.2., the peak dispersion was not affected with increase in SDS concentration, even beyond the range where cylindrical micelles are known to exist. Therefore, large micelles did not affect peak intensity of SDS protons and hence it is unlikely that they would affect intensity of protein peaks.

5.3.2 NMR spectroscopy of α-^{15}N-Lysine labeled rhodopsin

In contrast to tryptophan residues, which probe the predicted folding core region, lysine residues are located mostly away from the predicted folding core. There are eleven lysines in rhodopsin. It has been seen earlier that the most intense peak originates from Lys339 in the C-terminal tail while other signals had intensities less than 10% that of Lys339 (Klein-Seetharaman et al., 2002b). Due to the low protein concentration used here of 50 μM, only the Lys339 resonance signal is observed (Figure 38.A.). In Figure 38.C. overlay of 2D HSQC spectra of 1%, 10% and 30% SDS denatured states is shown with the native spectrum shown in Figure 38.A. Comparing the HSQC spectra of the SDS titrated protein with that of the native state, the most intense peak that was observed in the native protein does not exist in SDS treated samples but other peaks begin to appear (Figure 38.B. and C.). The intensity and number of backbone peaks increase with increase in SDS concentration from 0.05% (Figure 38.B.) to 1% (in green, Figure 38.C.) and finally to 10% (in magenta, Figure 38.C) indicating increase in flexibility of the cytoplasmic domain, where most of the the lysines are located, due to their large extent of
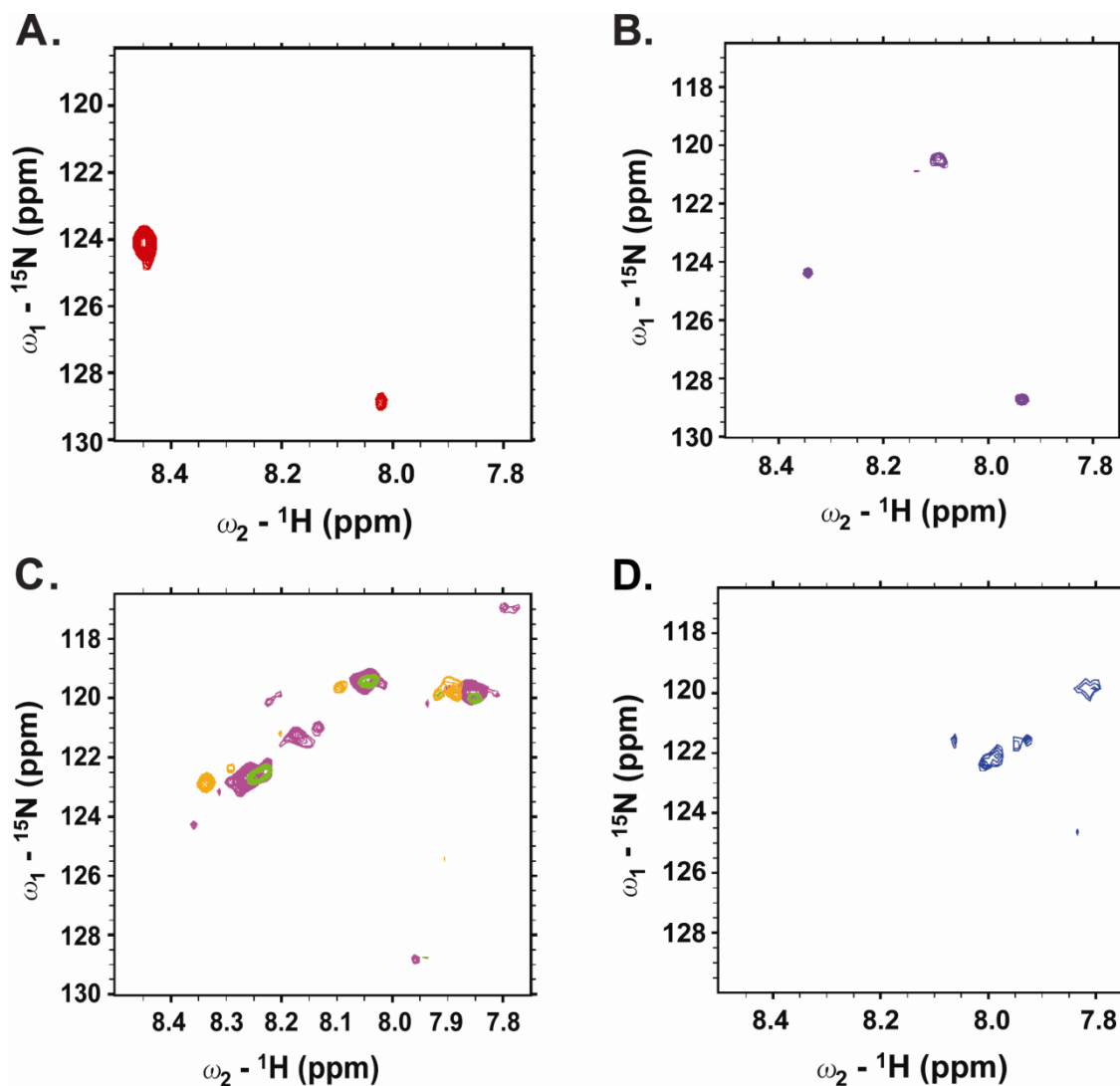
Figure 38: 2D HSQC spectra of native and SDS denatured 15N-α,ε-Lysine labeled rhodopsin.

2D HSQC spectra of rhodopsin in A. native state and denatured with B. 0.05% SDS, C. overlay of 1% SDS (green), 10% SDS (magenta) and 30% SDS (orange) denatured states and D. denatured with 3S8U, pH 2. The rhodopsin concentration in all samples is 50 μM. Number of scans for native rhodopsin was 128 and 48 in ^{1}H and ^{15}N dimension respectively, for SDS denatured rhodopsin was 256 and 80 in ^{1}H and ^{15}N dimension respectively and for 3S8U, pH 2 denatured state was 2000 and 48 in ^{1}H and ^{15}N dimension respectively. The lowest positive value of contour is set at 4.8×10^6 for native state, 2×10^6 for 0.05% SDS, 4.8×10^6 for 1%, 10% and 30% SDS and 9×10^6 for 3S8U pH 2.

unfolding. At 30% SDS (in orange, Figure 38.C.), peak intensities decreased compared to 10% SDS but appear similar to those observed in the 1% SDS denatured state except for the peaks around 120ppm/7.9ppm in $^{15}N/^{1}H$ dimensions respectively. These peaks appear to have a stronger intensity in the 30% SDS denatured state. Therefore, lysines are more mobile in 30% SDS than the tryptophans.

HSQC spectrum of rhodopsin in the presence of 3S8U at pH 2 was also recorded. The result is shown in Figure 38.D. Unlike with tryptophans, here larger numbers of scans were needed to obtain a suitable signal to noise ratio compared to the SDS titrated samples indicating formation of a different denatured state as compared to the SDS denatured samples.

5.4   DISCUSSION

With global information obtained from Chapter 4, here we proceeded to gather residue-type specific information (also see Figure 6.B.). The pattern of distribution of tryptophans and lysines gives us an advantage to study regions both around and away from the predicted folding core respectively. While probing tryptophans, I found that with increase in denaturation the side chain and backbone atoms behave differently in an HSQC spectrum. All five side chain peaks that were observed distinctly in the native rhodopsin spectrum, arising from each of the five tryptophans, are clustered together in a similar region in the 2D spectrum upon addition of SDS. This indicates that all the side chains experience a similar environment. The intensity of the cluster, however, decreased with increase in SDS concentration from 1% to 30%, contrary to the expected increase in intensity if a segment undergoes fast exchange on the ns timescale due to complete unfolding. Therefore, this result indicates that the motion of the side chains appears on

the intermediate exchange regime. The backbone peaks in native rhodopsin suffer from conformational heterogeneity in the slow exchange timescale and show more than five peaks in the 2D HSQC spectrum. Upon denaturation, the number of backbone peaks decreased significantly at 1% SDS and almost disappeared upon maximal denaturation at 30% SDS. This is contrary to the expected increase in signal intensity of protein peaks upon denaturation due to increase in mobility of completely unfolded regions in fast exchange timescales of ns or higher. Therefore, I hypothesize that the decrease in signal intensity of tryptophans indicates that motions of tryptophans are hindered in the denatured states, with the degree of motion lying in the intermediate time regime of exchange compared to the native state. Restriction of motion to intermediate timescales from fast exchange timescales is arising from interactions with other residues in the denatured state, thus forming a rigid structured region. This hypothesis is in concordance with our previous studies where formation of a compact state was seen under these denaturing conditions (see Chapter 4) since inter-residue interactions would hold the structure together decreasing its overall size as compared to a floppy unfolded protein with a larger effective size. Another reason for the decreased mobility of tryptophans could be due to slow tumbling of the large cylindrical micelles of SDS that are formed at 30%. Therefore, I tested a denaturing condition under which SDS does not form cylindrical micelles, i.e. 3S8U. Urea is known to increase the critical micelle concentration of SDS and disrupt rod-like micelles formed by SDS (Baglioni et al., 1990; Briganti et al., 1991; Kumar et al., 2005). Under this condition, tryptophan signal intensities were found to be intermediate between 1% SDS and 30% SDS which correlated with their corresponding degree of secondary structure disruption as described in Chapter 3. Thus, the absence of very intense signals under a denaturing condition where cylindrical micelles are not formed shows that the decrease in peak intensity at 30% SDS is not

due to slow tumbling of large micelles. There are also many reports on structure of peptides and small helical MPs in cylindrical micelle forming concentrations of SDS where tryptophans, in spite of being buried in the membrane region could be observed as peaks in the HSQC spectrum (McDonnell and Opella, 1993; McDonnell et al., 1993; Wang et al., 1996; Almeida and Opella, 1997; Schibli et al., 1999; Crowell et al., 2003; Franzin et al., 2007; Freitas et al., 2007). Therefore, the changes seen in tryptophan intensity in the presence of high SDS concentrations are due to changes in the protein and not induced by slow tumbling of cylindrical SDS micelles.

The rigidity observed in the TM-EC domain probed by tryptophans was compared with motions in the region away from the predicted folding core, i.e. in the CP domain, probed by lysines. The latter domain was found to be more mobile than the former domain indicating its greater extent of denaturation and hence faster exchange rate. This fits with the position of the predicted folding core which is around the TM and EC domains (Rader et al., 2004).

5.5   SUMMARY OF CONTRIBUTIONS

NMR has been extensively used in structural studies of soluble proteins both in folded and denatured states. To our knowledge, NMR based studies have not been reported so far to investigate the denatured state of helical MPs. I have, for the first time, gathered high-resolution structural information on denatured states of a helical MP, rhodopsin. Various conditions were optimized, such as buffer conditions, sample concentration, type of NMR tubes and strength of NMR spectrometer, before carrying out domain specific characterization of these states. Global structural characterization suggested formation of a compact intermediate during denaturation (described in Chapter 4). Compaction in structure as compared to an increase in size upon

unfolding indicates existence of non-native interactions in certain unfolded regions of the protein that decreases its overall size. I have determined the location of this compact region, using high-resolution structural studies, to EC and TM domains. My findings correlate with the location of the folding core predicted by the LRI model of folding of helical MPs. Thus, my studies can be considered preliminary evidence supporting this model which hypothesizes formation of a folding core in initial stages of folding of MPs.

6.0   CHAPTER 6: MOBILITY OF PREDICTED FOLDING CORE RESIDUES IN

DENATURED STATES OF RHODOPSIN

6.1   RATIONALE AND SUMMARY

I have shown by HSQC NMR of rhodopsin labeled by different amino acid types (Chapter 5) that the EC and TM domains are more rigid than the CP domain in denatured states of rhodopsin. Because assignment of the NMR signals is problematic, I obtained residue specific information alternatively by using EPR spectroscopy. This method has been very well established for studying changes in the CP domain of rhodopsin in its dark and light activated states by specifically mutating residues of interest to cysteines and labeling them with spin labels (Altenbach et al., 1999; Cai et al., 1999a; Cai et al., 1999b; Klein-Seetharaman et al., 1999b; Altenbach et al., 2001a; Altenbach et al., 2001b; Cai et al., 2001; Klein-Seetharaman et al., 2001). Here, I probed the differential dynamics of EC and CP domains in the denatured states by directly investigating residue specific motions in the predicted folding core, i.e. in the EC domain and comparing their mobility with residues away from this core, i.e. in the CP domain.

Denaturing conditions for unfolding rhodopsin to the maximum extent possible are 30% SDS and 3S8U (see Chapter 3). Since, the latter condition could not be used for NMR studies to characterize the denatured state of rhodopsin due to high background signals from urea, it was modified to 3S8U at pH2. This condition is almost half as good in denaturing rhodopsin as are

30% SDS and 3S8U. All the conditions have been tested for EPR spectroscopy. The studies reported here have been achieved by CW EPR measurements whereby rhodopsin, with residues of interest mutated to cysteines, is attached with a nitroxide spin label at the site of cysteine mutation and mobility information is derived from CW spectral line shapes of the attached nitroxide. TM-EC residues were selected from the predicted folding core with the aim to determine motions in the region of the predicted folding core. TM residue, A166C in TM4, was first tested for spin labeling. Different labels with high membrane permeating capabilities were tested to label A166C but none of them could successfully derivatize A166C. Instead, EC residues, T108C, V204C and I205C were successfully labeled with a spin label. Motions of these residues were compared with that of CP residues, N151, I154 and M155, to determine if contrasting motions occur between residues in the predicted folding core and that away from it. CW-EPR spectra indicate that although flexibility of EC and CP residues overall increases with increase in extent of denaturation, EC residues retain more rigidity in the denatured states than the CP residues. These results support the notion of residual structure in denatured states of rhodopsin which is localized near the predicted folding core in the EC domain and away from the distant CP domain.

6.2   SELECTION OF RESIDUES FOR SPIN LABELING

EPR has been extensively used to study conformational changes in rhodopsin on light activation (Altenbach et al., 1999; Cai et al., 1999a; Cai et al., 1999b; Klein-Seetharaman et al., 1999b; Altenbach et al., 2001a; Altenbach et al., 2001b; Cai et al., 2001; Klein-Seetharaman et al., 2001). Most of the residues that have been studied so far lie in the CP domain and were studied

by mutating them to cysteine for derivatization with EPR spin labels. My interest is in characterizing the TM and EC domain residues in denatured states since these residues have been predicted to be part of a folding core in rhodopsin (Rader et al., 2004). However, there are a number of considerations to be made in selecting residues in TM and EC domains for mutation to cysteine and derivatization by spin labels. In contrast to the CP residues, many misfolding mutations in rhodopsin are known to occur in the TM and EC domains (a list of such mutations are provided in (Tastan et al., 2007)). This low tolerance towards mutations leads to low expression levels of TM and EC domain cysteine mutants and of the expressed material, a significant fraction is misfolded, and cannot be used reliably for labeling. Even for correctly folded rhodopsin, accessibility of cysteines for labeling is an issue. Labeling amino acids in the TM domain is difficult since their side chains are buried either facing the helical bundle or in the membrane. EC residues are involved in tertiary structure more so than CP residues and are difficult to label, even when not affected by the membrane environment. Thus, the following mutants were selected for labeling.

i) Transmembrane domain mutants

A166 in TM4 was selected to test for labeling since its side chain faces away from the helical bundle and towards the membrane making it more likely to be labeled than side chains that face the bundle. I used this mutant to test more membrane permeable and reactive derivatization reagents.

ii) Extracellular domain mutants

Sheryll Mangahas in Dr. Wayne Hubbell's lab at University of California, Los Angeles had tested various mutants in the EC domain for expression, reconstitution with 11-*cis* retinal and labeling efficiency. Mutants at these positions: 14, 16, 22, 25, 36, 99, 108, 173, 191, 192,

193, 194, 195, 196, 197, 199, 202, 204, 205, 277 and 286 were obtained from Dr. Wayne Hubbell's lab at UCLA. Out of these residues, only 22, 25, 108, 204 and 205 were predicted folding core residues and were thus selected for my studies (Rader et al., 2004). We obtained DNA for mutants S22C, P25C, T108C, V204C and I205C from our collaborator Dr. Wayne Hubbell at UCLA. All the mutants have a background mutation of C140S and C316S, which are the endogenously free cysteines. However, S22C and P25C did not give any yields when transfected into COS-1 cells and hence could not be used for EPR experiments. Therefore, the EC domain residues, which are predicted to be part of the predicted folding core, studied were T108C, V204C and I205C. The positions of these residues are shown in Figure 39.A. in red along with the folding core residues in green. Spatial organization of the residues is shown in Figure 39.B.I. in red.

iii) Cytoplasmic domain mutants

As controls, CP domain residues that are at the same membrane depth as the EC domain residues tested were selected so that I can rule out the influence of differential positions of residues in these domains in the native state on our interpretations of mobility in the denatured state. It is very likely that a residue in an exposed loop region will behave differently upon denaturation as compared to a residue in the TM bundle. The former will be more likely to be in a flexible random coil like region than the latter in denatured states, thus making direct comparisons of their mobilities influenced by their position in the native state. Estimation of the membrane boundary was based on the OPM database (Lomize et al., 2006) and previous EPR
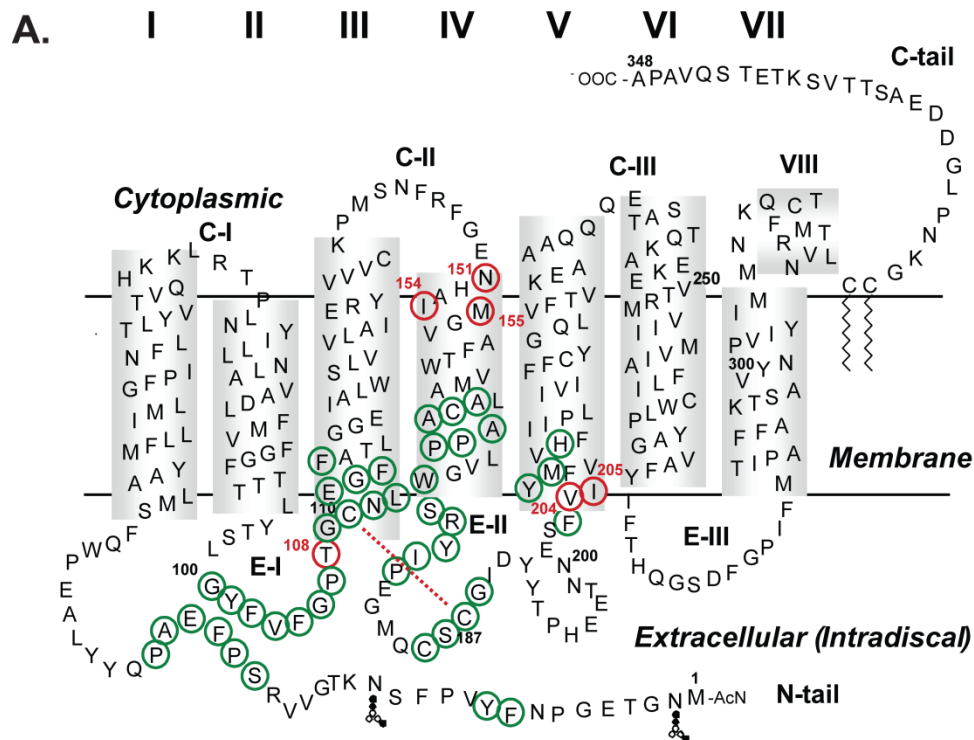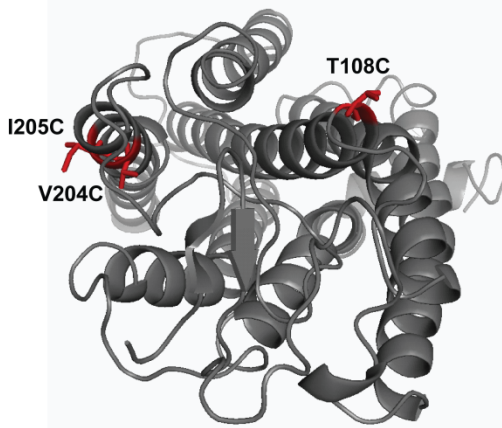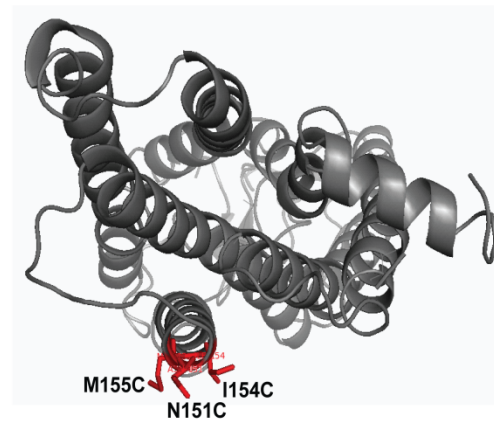
Figure 39: Secondary structure representation of rhodopsin showing resdiues studied by EPR.

Secondary structure representation of rhodopsin showing predicted folding core residues in green circles and the residues studied by EPR in red circles. B. Panel I. 3D structure of rhodopsin viewed from the EC face is shown with the EC residues studied by EPR shown in red sticks. B. Panel II. 3D structure of rhodopsin viewed from the CP face is shown with the CP residues studied by EPR shown in red sticks.

168

studies on accessibility of residues in rhodopsin (Altenbach et al., 1999; Cai et al., 1999a; Cai et al., 1999b; Klein-Seetharaman et al., 1999b; Altenbach et al., 2001a; Altenbach et al., 2001b; Cai et al., 2001; Klein-Seetharaman et al., 2001). In addition to selection of CP domain residues based on similar membrane depth as that of EC residues, I also considered similar position in a helix turn so that residues in both these domains would be expected to unfold to comparable extents and their motions can be compared. Thus, N151, I154 and M155 in the CP domain corresponding to I205, V204 and T108 in the EC domain were selected, respectively. The CP residues are highlighted in red in Figure 39.A. Spatial organization of the residues is shown in Figure 39.B.II. in red.

6.3   ATTACHMENT OF EPR SPIN LABELS

All cysteine mutants were expressed in COS-1 cells by transient transfection and were labeled on the 1D4 column during purification as described in Chapter 2. In the set of mutants studied here, all mutants formed a WT-like chromophore with λ_{max} at 498-502 nm. The spectral ratios (A_{280}/A_{500}) after elution from the 1D4 matrix at pH 6 gave ratios between 1.6 and 2.1. To facilitate EPR analysis of rhodopsin, a paramagnetic side chain was substituted at selected cysteine residues. Three different spin labels were tested, R1, 4-(2-Iodoacetamido)-TEMPO and 4-Maleimido-TEMPO. Chemical structures of these labels and strategy of labeling with R1 are shown in Figure 40. R1 has been extensively used in earlier studies of rhodopsin (Altenbach et al., 1999; Cai et al., 1999a; Cai et al., 1999b; Klein-Seetharaman et al., 1999b; Altenbach et al., 2001a; Altenbach et al., 2001b; Cai et al., 2001; Klein-Seetharaman et al., 2001). The other two

labels were used for their high membrane permeabilizing property and hence were used to label a residue buried in the TM domain.

The TM domain mutant, A166C, failed to be labeled with the commonly used spin label R1 (Figure 40.B.). Therefore, labels with greater membrane permeating ability, 4-(2-Iodoacetamido)-TEMPO and 4-Maleimido-TEMPO (Figure 40.A.), were tested. The protocol for labeling has been described in Chapter 2, Section 2.2.5.3. Neither of the two labels was able to derivatize A166C as no signals were detected in the CW-EPR spectrum. All other mutants in EC and CP domains could be labeled with R1.

A.

(1-oxy-2,2,5,5-tetramethylpyrroline-3-methyl)-methanethiosulfonate (R1)   4-(2-Iodoacetamido)-TEMPO   4-Maleimido-TEMPO

B.

+ protein-SH ⟶

side-chain R1
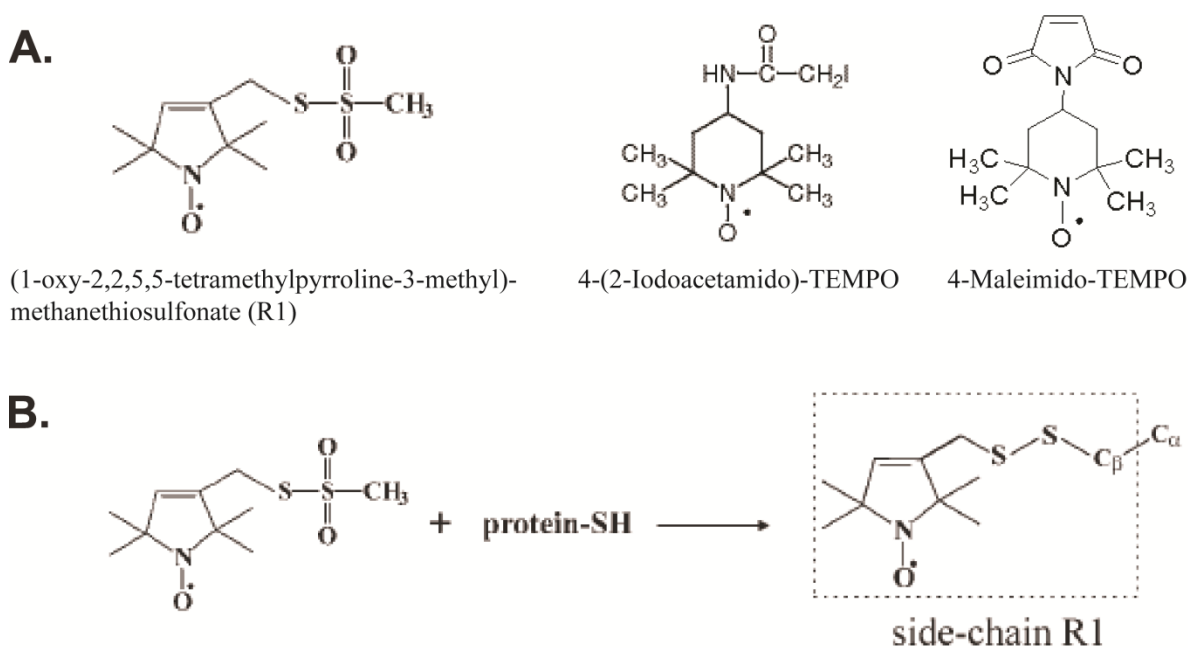
Figure 40: EPR spin labels.

A. Chemical structure of EPR spin labels tested. B. Chemical reaction of spin label, R1, with free sulfydryl groups of cysteines in protein.

6.4   MOBILITY OF EXTRACELLULAR RESIDUES IN DENATURED STATES

The line-shape of EPR spectra of spin labels attached to a protein contains information on mobility at these sites. Mobility is a qualitative descriptor of the dynamic state of the side chain, measured from the resonance line width and the second moment (McHaourab et al., 1996). Studies of spin labels in T4 lysozyme, a protein of known structure, showed that helix surface sites, buried sites, loop sites or tertiary contact sites can be resolved using side chain mobility (McHaourab et al., 1996). Following the indication from NMR spectroscopy that there is differential mobility upon denaturation when comparing CP versus TM/EC regions in rhodopsin, I collected residue specific information on motions of three residues within the predicted folding core in the EC domain, T108C, V204C, I205C (highlighted in red in Figures 39.A. and B.I.). CW-EPR spectra of these mutants in the native and denatured states were recorded (Figure 41). Since the shape of the spectrum is biased towards the most mobile component in all the spectra, the central line has been normalized to allow qualitative comparison of the immobile component. The native state of T108C shows two components of different mobilities. With addition of SDS in increasing concentrations, a gradual decrease in the immobile component was seen indicative of a direct relationship between higher residue flexibility with increasing denaturation. Similar decreases were seen for V204C and I205C mutants. Spectra of T108C, V204C and I205C denatured with 3S8U and 3S8U at pH2 are overlaid with that of the native and 30% SDS denatured proteins to compare the maximally denatured states in Figure 41.B. It is evident that 3S8U and 3S8U at pH2 denatured states retain a more immobile component than 30% SDS denatured state for all EC mutants. This difference is most clearly evident for I205C.
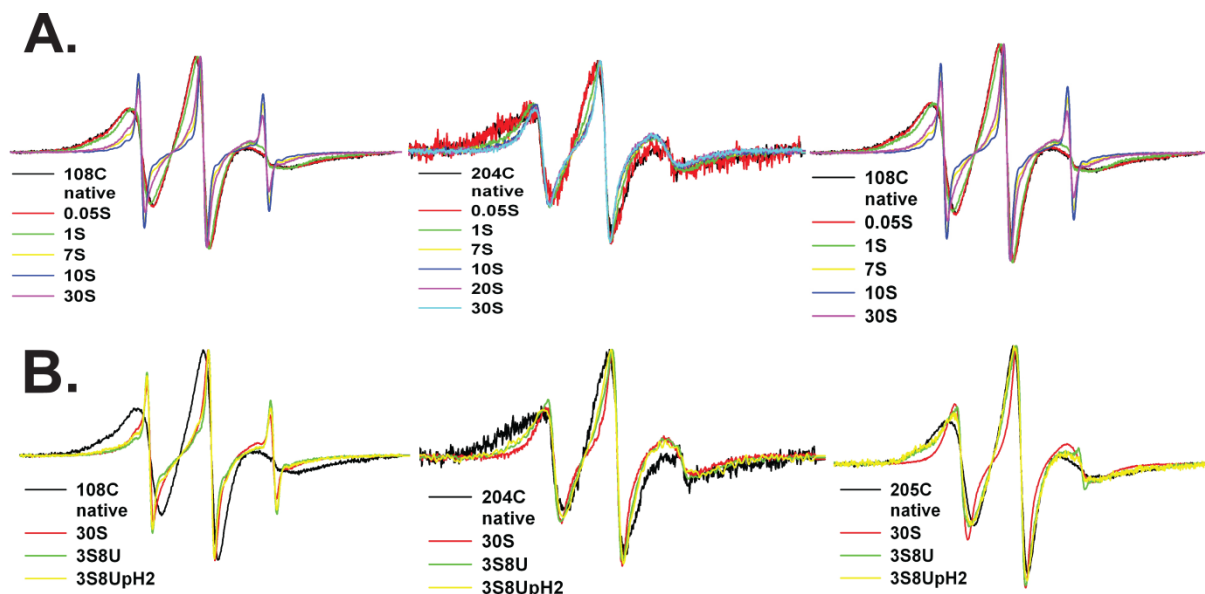
Figure 41: CW-EPR spectra of extracellular residues in native and maximally denatured states.

A. Overlay of CW-EPR spectra for T108C, V204C and I205C in the native state and treated with different SDS concentrations. B. Overlay of CW-EPR spectra for T108C, V204C and I205C in the native state and treated with 30% SDS, 3S8U and 3S8U at pH2.

6.5 MOBILITY OF CYTOPLASMIC RESIDUES IN DENATURED STATES

In order to compare the motions of folding core residues with that of residues away from the core, CW-EPR spectra of CP domain mutants, N151C, I154C and M155C (shown in red in Figures 39.A. and B.II.), in the native and denatured states were recorded. Comparing the native state spectra of N151C, I154C and M155C in Figure 42.A., the latter two mutants have a much stronger immobile component than N151C. This component only slightly decreases with increase in SDS for N151C as seen in Figure 42.A. since it is already mobile in the native state. However, for the I154C mutant, the immobile component disappears from 1% SDS onwards (Figure 42.A.) whereas for the M155C mutant a greater amount of immobile component is

retained at 1% SDS which completely disappears only at 10% SDS (Figure 42.A.). For all CP

mutants at 30% SDS, there is no immobile component indicating that the residues are completely

flexible in this state. This is in contrast with the results for the EC residues where an immobile

component was still retained in 1% SDS for all the residues tested and up to 7% for T108C and

V204C. In Figure 42.B., the spectra of CP mutants denatured with 3S8U and 3S8U at pH2 are

overlaid with that of native and 30% SDS denatured protein to compare the maximally denatured

states. Similar to what I observed for EC residues, the 3S8U and 3S8U at pH2 denatured states

retain more immobile components than the 30% SDS denatured state for all CP mutants.
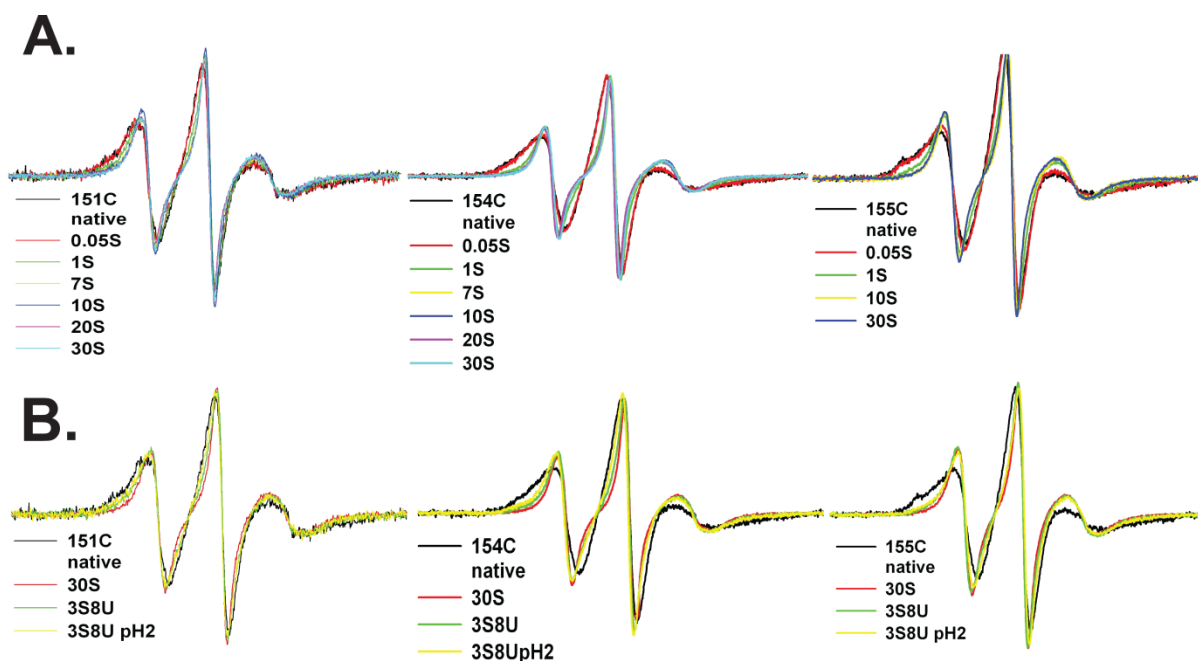
Figure 42: CW-EPR spectra of cytoplasmic residues in native and maximally denatured states.

A. Overlay of CW-EPR spectra for N151C, I154C and M155C in the native state and treated with different SDS

concentrations. B. Overlay of CW-EPR spectra for N151C, I154C and M155C in the native state and treated with

30% SDS, 3S8U and 3S8U at pH2.

6.6 COMPARISON OF MOBILITY OF EXTRACELLULAR AND CYTOPLASMIC DOMAINS IN DENATURED STATES

Next, I investigated if there are differences in the concentration of SDS required to mobilize residues to the same extent when comparing EC and CP residues. EPR data are provided in Figure 43.

Figure 43.A. shows the comparison of N151C (EC) and T108C (CP), residues located at the membrane interface, at the end of their helices and with their side chains facing the aqueous environment. T108C appears to be slightly more immobile than N151C which could be due to differences in backbone dynamics. At 1% SDS, this difference increases and T108C shows a greater immobile component than N151C. However, from 7% SDS onwards, T108C becomes very mobile. Spectra for 7% and 10% SDS denatured states for T108C were obtained after 5 h since this was the time taken for it to equilibrate. No time dependence changes were observed for N151C at any SDS concentration or for any other mutant under any denaturing condition. Even in SDS/urea mixtures, T108C showed much greater flexibility than N151C.

Figure 43.B. shows the comparison between I154C (CP) and V204C (EC). Both these residues are at the same membrane depth and at the same turn of the helix but the side chain of I154C is slightly more exposed than that of V204C. Similar to what I found for the T108C/N151C pair, V204C (EC) is more immobile than I154C (CP) in the native state. However, unlike T108C (EC) which gets flexible from 7% SDS onwards, immobility in V204C (EC) is retained more than in I154C upto 20% SDS. At 30% SDS, V204C is still slightly more immobile than I154C. For the combination of SDS and urea as denaturants, V204C again was more immobile than I154C. These results indicate that the EC residue, V204C, is showing more rigidity in the denatured states than the corresponding CP residue.

Figure 43.C. shows the comparison between M155C (CP) and I205C (EC). Both these residues are equivalently placed with regards to membrane depth and position in the helix. Here, M155C has a slight immobile component as compared to I205C in the native state. On increasing the SDS concentration to 0.05% and 1%, I205C becomes immobile than M155C, both showing a similar spectrum at 30% SDS. The immobility of I205C is significantly increased when the mixture of SDS and urea is used as a denaturant. Here again, it is seen that the EC residue is in a more rigid environment than the corresponding CP residue.
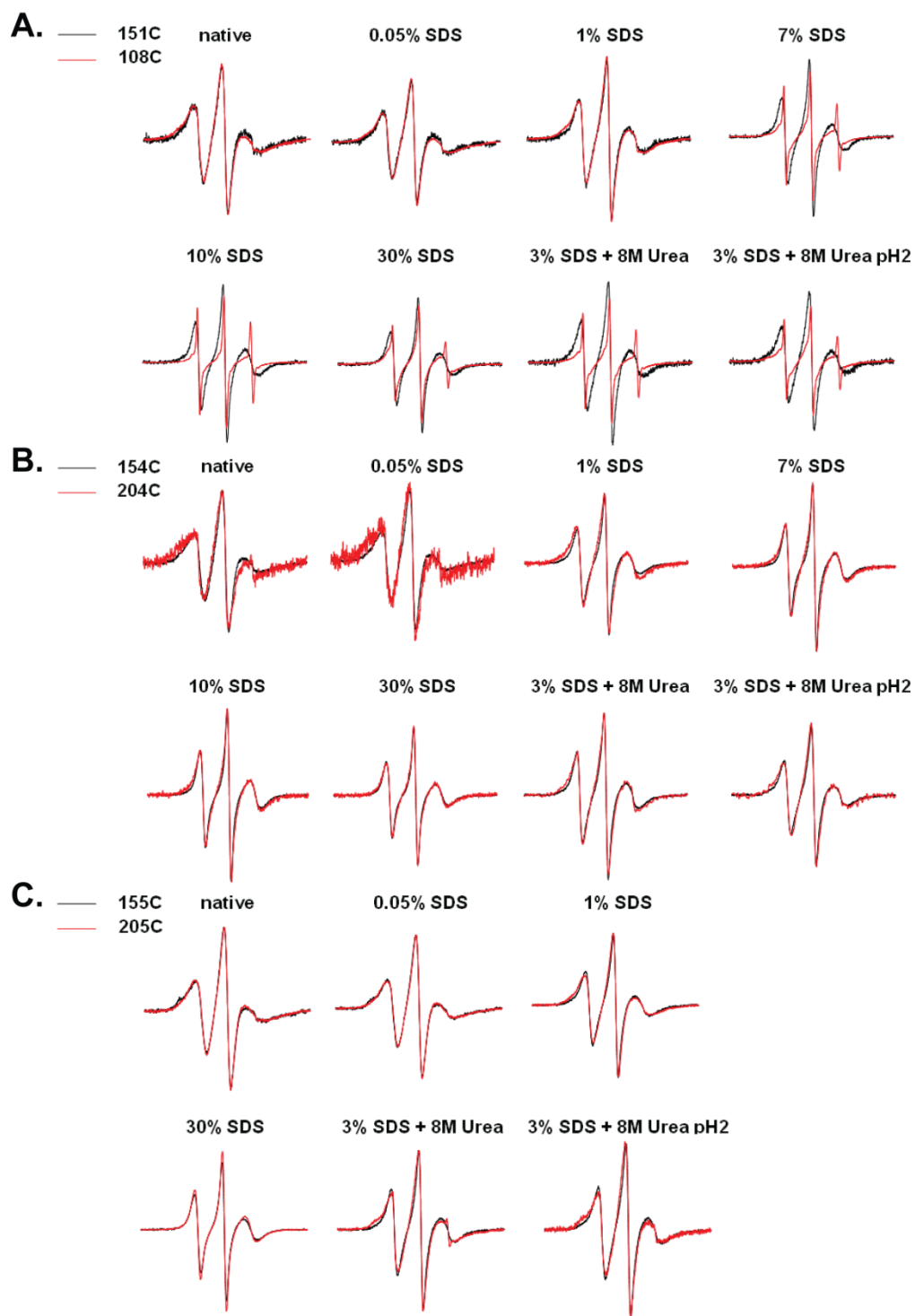
Figure 43: Comparison of CW-EPR spectra of extracellular and cytplasmic residues in native and denatured states.

Overlays of EPR spectra of T108C and N151C (A.), V204C and I154C (B.) and I205C and M155C (C.) where each mutant is treated with different concentrations of SDS and with 3S8U and 3S8U at pH2.

6.7   DISCUSSION

Having probed global changes and domain specific characterisitics of denatured rhodopsin, as described in Chapters 4 and 5, here I have gathered site-specific information on structural changes during denaturation of rhodopsin by using EPR spectroscopy (also see Figure 6.C.). In this way, I have investigated properties of the denatured states in three structural levels in increasing order of their degree of resolution. I have shown that in denatured states there is a difference in dynamics between the EC and CP residues, the former being more constrained in their motion than the latter. This suggests that the EC domain is involved in interactions in the denatured state that makes the EC residues less mobile. This finding also agrees well with the LRI theory of folding of rhodopsin where a folding core, consisting of interactions among residues in the EC and TM domains in the early stages of folding, has been predicted (Rader et al., 2004).

Based on global structural characterization of SDS denatured states, a model depicting structural changes during denaturation of rhodopsin was described in Chapter 4 (see Figure 34 and Section 4.7). It was also shown that these global structure changes correlate with SDS micellar structural changes (described in Figure 25, Section 3.4.1.) whereby in stage 1, mixed SDS/DM micelles are formed followed by formation of SDS spherical micelles in stage 2 which show a transition in stage 3 to form cylindrical micelles in stage 4 (Croonen et al., 1983). Now, with high resolution structural information available from domain specific (Chapter 5) and residue specific characterizations (described in this chapter), further details can be added to the model described in Chapter 4. This more detailed model is shown in Figure 44. It consists of SDS micellar structural changes (from Figure 25 in Chapter 3), global structural information (from the model in Figure 34 in Chapter 4) and site-specific information on dynamics (from this

177

chapter) in different SDS concentrations. This model shows that in low SDS concentration (0.05-0.3% SDS), where I saw initial opening of the helical bundle, I now know from EPR studies that the motions of the EC and CP domains are similar to that of the native state. In concentrations of SDS between 0.3-3%, where earlier studies had shown a compact state formation, current residue specific studies by EPR show the location of compactness to be in the EC region. The rigidity of this domain still remains in stage 3 (3-15% SDS) where further unfolding along with a transition of spherical SDS micelles to cylindrical ones occur. Finally, in maximally unfolded states, where a compact intermediate is suggested to form, although the CP and EC ends have become completely flexible based on EPR studies, residual structure still remains in the TM-EC regions as reported by tryptophans in NMR studies (Chapter 5).

Through this work, I have shown for the first time for MPs that mobility measurements by EPR spectroscopy can be useful in understanding structural changes during denaturation. This in turn provides details about possible interactions in unfolded states. The only other report of the use of EPR spectroscopy in MP folding studies is described during refolding LHCII, a helical MP, from a 50% lithium dodecyl sulfate denatured state (Dockter et al., 2009). In this report, distance measurements between two pairs of residues derivatized with EPR labels were carried out during equilibrium and kinetic unfolding and refolding studies. One pair was placed on either end of a TM helix and the other pair was placed in the luminal side of two different TM helices. Refolding kinetics showed that formation of tertiary contacts between the TM helices occurs after formation of TM helices. These findings are in accordance with the two-stage model of folding (Popot and Engelman, 1990). However, TM helix formation during LHCII refolding was observed to extend beyond the first stage of folding thereby not completely following the two-stage model. Again, as mentioned for almost all MP folding studies (Section 1.1.2.3.), the focus

in LHCII folding studies were on kinetics of folding rather than a detailed characterization of denatured states. The latter has been attempted in our studies where dynamics of specific residues in denatured states have been characterized in order to understand the possible interactions in unfolded states.
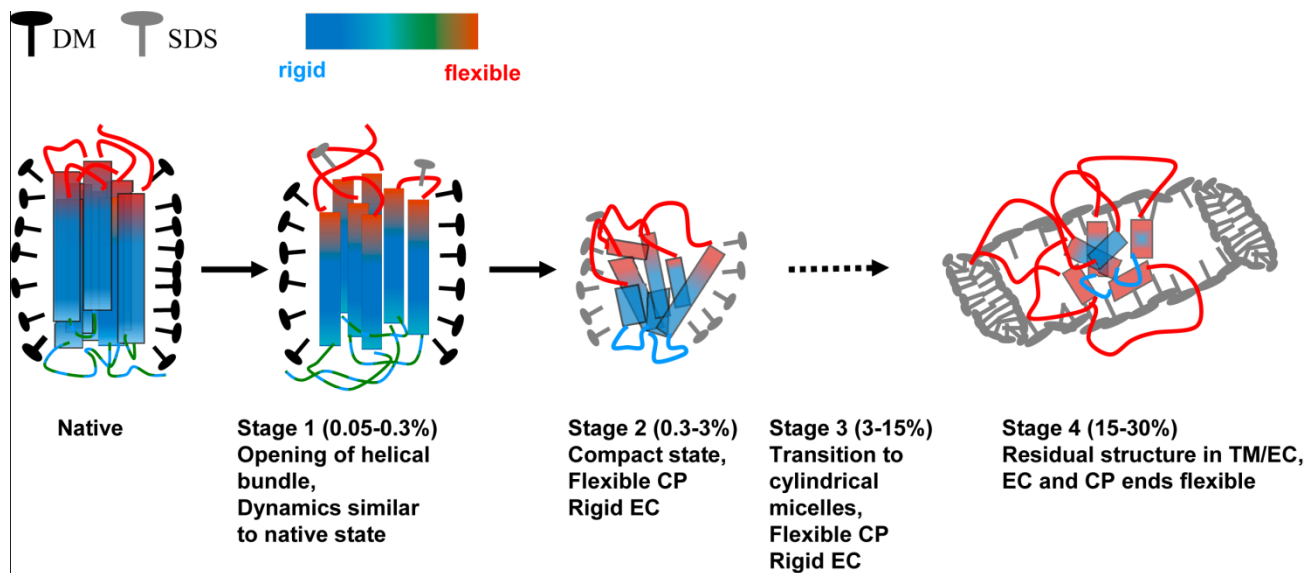
Figure 44: Model representing global and domain specific changes in denatured states.

TM regions of native rhodopsin are shown in cylinders with the colors corresponding to degree of flexibility of different regions as shown in the color bar. Stage 1 represents changes occurring in low SDS concentrations (0.05-0.3%) where opening of the helical bundle occurs. This is followed by stage 2 where on increase in SDS concentration to 3%, a compact state is formed with rigid regions in EC and TM domains. Beyond 3% SDS, transition to cylindrical micelles occurs followed by formation of compact states in cylindrical micelles in 30% SDS in stage 4, where residual structure is formed in the TM/EC region.

6.8   SUMMARY OF CONTRIBUTIONS

I have determined mobility of specific folding core residues in denatured states of rhodopsin by EPR spectroscopy. Such a site-specific characterization of denatured states of MPs had not been reported prior to this work. The only other instance where site-specific have been carried out is in a very recent report where distance measurements using EPR was used to follow refolding of LHCII, a MP (Dockter et al., 2009).

Through site-specific studies on mobilities, we have shown that the CP domain is more flexible and more susceptible to denaturation than the EC domain of rhodopsin. I have also mapped some of the residues that may participate in interactions forming a core of residual structure in denatured states. These are the residues in the EC domain predicted to be part of the predicted folding core that we found experimentally to be more immobile and hence involved in interactions with other residues. Thus, my studies provide direct experimental support for the earlier observation in computational analysis that a folding core is formed in the EC-TM region during initial stages of folding of rhodopsin (Rader et al., 2004). These studies, together with the NMR studies described in Chapter 5 also suggest the presence of rigid structured region in denatured states which together support the LRI model of rhodopsin folding.

7.0   CHAPTER 7: QUANTIFICATION OF RESIDUE SPECIFIC MOTIONS BY ^{19}F NMR SPECTROSCOPY

7.1   RATIONALE AND SUMMARY

As shown in Chapters 5 and 6, understanding the dynamics of unfolded states is crucial in identifying interactions among residues in these states. These interactions in denatured states are responsible for the formation of residual structure which can be considered as a folding nucleus that triggers folding of proteins. Hence, in order to understand protein folding pathways, it is important to investigate motional properties of residues in denatured states. Further, protein motions bring about conformational changes that are essential for protein function (Berendsen and Hayward, 2000; Wand, 2001; Fenimore et al., 2002; Bakan and Bahar, 2009; Tomita et al., 2009). The motions can range from femtoseconds to seconds and even to days. Therefore, in order to understand how proteins fold and carry out their function, we need to understand what these different motions are and where are they localized.

The methods mainly used to obtain high-resolution structure and dynamics information are X-ray crystallography, NMR and EPR spectroscopy. However, X-ray crystal structures only provide a snapshot of a particular protein conformation thereby limiting the information on motions within proteins in terms of B-factors which are not very descriptive and not representative of real time motions. NMR spectroscopy has proved to be the method of choice to

provide qualitative and quantitative insights into protein dynamics. However, for large MPs such measurements by NMR are at least very challenging and often impossible due to low expression levels, difficulty in assigning amino acid peaks, intrinsic conformational heterogeneity as seen for rhodopsin (Klein-Seetharaman et al., 2002b; Klein-Seetharaman et al., 2004) and poor signal to noise ratio due to large background signals from detergents or lipids and their large size (Yanamala et al., 2010). Further, the application use of NMR spectroscopy requires isotope labeling which can be expensive especially if mammalian cells are used for expression which is often the case for MPs. These limitations are also illustrated in the experiments discussed in Chapter 5, where 2D NMR analyses of rhodopsin, isotope labeled at tryptophan and lysine residues with ^{15}N were carried out under denaturing conditions. However, detailed dynamics experiments could not be performed due to rapid relaxation leading to low signal to noise ratios. EPR spectroscopy has been widely used for measuring dynamics of MPs, particularly for rhodopsin. However, this method involves mutagenesis of residues of interest and attachment of bulky labels. Moreover, the information obtained from EPR is largely qualitative based on spectral line shapes.

To overcome some of the above limitations for MPs, ^{19}F NMR spectroscopy was developed for rhodopsin paving the way for its application to MPs in general (Klein-Seetharaman et al., 1999a; Loewen et al., 2001; Yanamala et al., 2010). Site-specificity of this method abrogated the need for assignment of large number of peaks on the spectrum. Further, absence of ^{19}F background signals in detergent or protein, 100% natural abundance, presence of fluorinating reagents making it unnecessary to grow cells in expensive isotope media, enhanced signal intensity due to site specific labeling and enhanced sensitivity of fluorine atom are the main advantages of using ^{19}F NMR spectroscopy for MPs. This method has been successfully

applied in characterizing conformational changes of rhodopsin upon light activation (Klein-Seetharaman et al., 1999a; Loewen et al., 2001). This method requires mutation of residues of interest to cysteines and their derivatization with a fluorinating reagent. TET has been the label of choice for rhodopsin. However, the use of TET suffers from the following drawbacks. The chemical reaction of TET with cysteines is a reversible, two-step process, making it less convenient as compared to a single-step process. The reversibility of the reaction also leads to the possibility of the label detaching from its derivatized site over time. Further, a smaller label with fluorine attached directly to the sulfydryl group instead of after two -CH_2 groups as in TET would decrease the alteration in the environment of cysteines. Most importantly, estimation of dynamics of TET derivatized residues by NMR was complicated due to presence of three fluorine atoms and their interactions with each other. Therefore, limitations observed in the use of existing fluorine label for site-specific ^{19}F NMR indicate the immediate need for approaches suitable for characterizing motion of MPs. Towards this end, I helped develop the use of monofluro labels to overcome the existing hindrances for quantification of site-specific dynamics in rhodopsin by ^{19}F NMR spectroscopy.

7.2   FLUORINATING REAGENTS AND LABELING CHEMISTRY

Chemical structures of fluorine containing compounds that have been used in our studies are shown in Figure 45. Synthesis of CF3I was reported earlier in (Kieltsch et al., 2007). The fluorinating labels shown in Figure 45 apart from CF3I were synthesized by our collaborator Dr. Alex Doemling. Arbitrary names are given to each of these labels as indicated in the figure. Chemical reagents containing fluorine atom(s) were used to selectively label cysteine residues. The chemical reaction of a mono fluoro label with sulfydryl group of cysteine in rhodopsin is

Hypervalent Iodine(III)–CF3 Reagent (CF3I)

2-((2-fluoroethyl)disulfanyl)pyridine (2F)

4-((2-fluoroethyl)disulfanyl)pyridine (4F)

2-((2-fluoroethyl)disulfanyl)-5-nitropyridine (2NO2F)

4-((2,2,2-trifluoroethyl)disulfanyl)pyridine (4F3)

2-((2,2,2-trifluoroethyl)disulfanyl)-5-nitropyridine (2NO2F3)
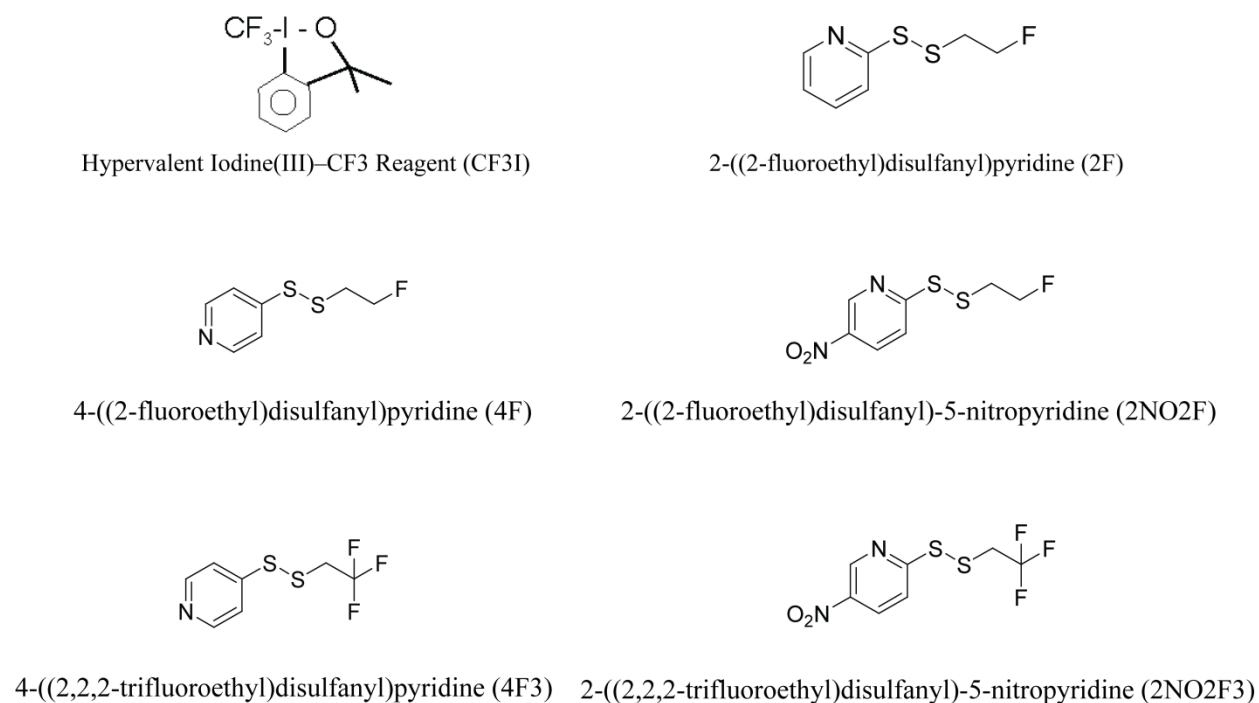
Figure 45: Chemical structures of fluorinating reagents

Chemical structures of all fluorine labels discussed in this chapter. Arbitrary names given for each label are mentioned in the brackets.

A.

$$FCH_2\text{-}CH_2\text{-}S\text{-}S\text{-}X + \boxed{Rho}\text{-}SH \longrightarrow \boxed{Rho}\text{-}S\text{-}S\text{-}CH_2\text{-}CH_2F + XSH$$

B.

Hypervalent Iodine(III)–CF3 Reagent (CF3I)

2-((2-fluoroethyl)disulfanyl)pyridine (2F)

4-((2-fluoroethyl)disulfanyl)pyridine (4F)

2-((2-fluoroethyl)disulfanyl)-5-nitropyridine (2NO2F)
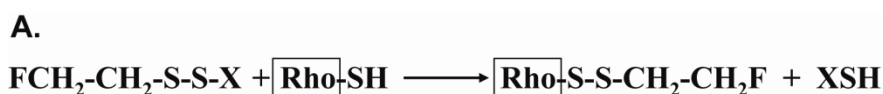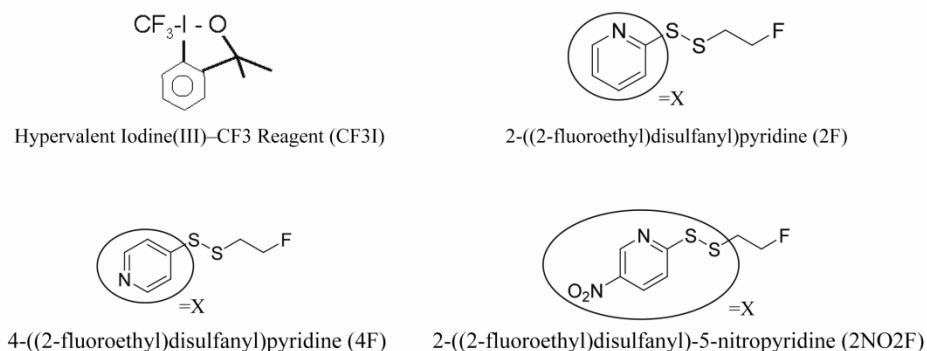
Figure 46: Reaction scheme and structures of ^{19}F reagents used for labeling rhodopsin

A. Labeling strategy of rhodopsin with monofluoro reagents. B. Fluorinating reagents used to label rhodopsin.

shown in Figure 46. These labels derivatize free sulfydryl groups of cystsines in proteins by means of disulfide exchange reaction. The reaction releases a by-product (XSH in Figure 46.A.) that has maximum absorbance at a specific wavelength and is used to track the progress of the reaction by recording increase in its intensity with time. The observed wavelength of maximum absorption depends on the reagent used and thus type of by-product formed during the reaction.

7.2.1 Shortening the fluorine label (-SCF$_3$ instead of -SCH$_2$CF$_3$)

To further minimize perturbation of protein structure by the ^{19}F label, I investigated smaller molecule alternatives for TET, the label that had been previously used for rhodopsin (Klein-Seetharaman et al., 1999a; Loewen et al., 2001). TET attaches –CF$_3$ group to cysteines via two –CH$_2$ groups and hence may be interfering with the native environment. Also, the chemical reaction of TET with cysteine is a two-step process and is reversible which may lead to inconvenience in labeling and the detachment of the label over time respectively. The latter has been observed in 1D ^{19}F NMR spectra as appearance of a free peak in TET labeled rhodopsin

sample with time. Therefore, I tested a label, CF3I (Figure 45) that attaches the $-CF_3$ group directly to the sulfydryl group of cysteine, thus minimizing structural perturbation. It also labels cysteines irreversibly and in a single-step process thereby simplifying the procedure of labeling and also ensuring integrity of the label after its attachment.

7.2.2   Replacing -CF$_3$ with -CFH$_2$

Novel monofluoro reagents, 2F, 4F and 2NO2F, were synthesized by our collaborator, Dr. Alex Doemling, to overcome the drawbacks of the commonly used fluorine label, TET, in characterization of residue specific dynamics of MPs. Derivatization of cysteine by these labels is a one-step reaction, thus better facilitating complete labeling of the reactive cysteines. Dynamics are conventionally measured by observing decay of transverse and longitudinal magnetization of nuclei of interest to equilibrium over time after application of a radiofrequency pulse. However, for labels such as TET with three fluorine atoms, such relaxation mechanisms are complicated due to interaction of such mechanisms of individual fluorine atoms with each other. Properties of single fluorine in monofluoro labels such as chemical shift and relaxation rates are expected to be more sensitive to structure and dynamics of residues compared to that of trifluroro label, TET which are more influenced by methyl rotation of the $-CF_3$ group. Therefore, in collaboration with Dr. Rieko Ishima we have studied the use of monofluoro labels with the motivation of quantification of motional parameters of specific residues in MPs.

7.2.3 Control trifluoro labels to compare with monofluoro labels

Trifluoro labels, 4F3 and 2NO2F3, were synthesized and studied as controls to compare their mechanism of relaxation with that of monofluoro labels. These trifluoro labels were designed as structural analogous of the monofluoro labels with the only difference being in the presence of three fluorine atoms instead of single fluorine. This was done to directly compare monofluoro labels with trifluoro labels.

7.3   FLUORINE LABELING STRATEGIES OF RHODOPSIN

The fluoro reagents, CF3I, 2F, 4F and 2NO2F, shown in Figure 46.B., were used for labeling accessible cysteines in rhodopsin. Rhodopsin has a total of ten cysteines, of which two cysteines, C140 and C316, are accessible in the dark (shown by blue arrows in Figure 47). Two cysteines C110 and C187 are disulfide bonded and C322 and C323 are palmitoylated (Ovchinnikov Yu et al., 1988; Papac et al., 1992). The remaining four cysteines become accessible only upon light activation (Chen and Hubbell, 1978). Labeling was carried out by two different methods. In method 1, purified rhodopsin was incubated with different concentrations of the label for different times depending on the labeling efficiency of the fluoro reagent. This method tested if the label can react with the exposed cysteines in rhodopsin. In method 2, rhodopsin, while bound to the 1D4 column, was incubated with the label and then purified as described in Chapter 2, Section 2.2.5.3.
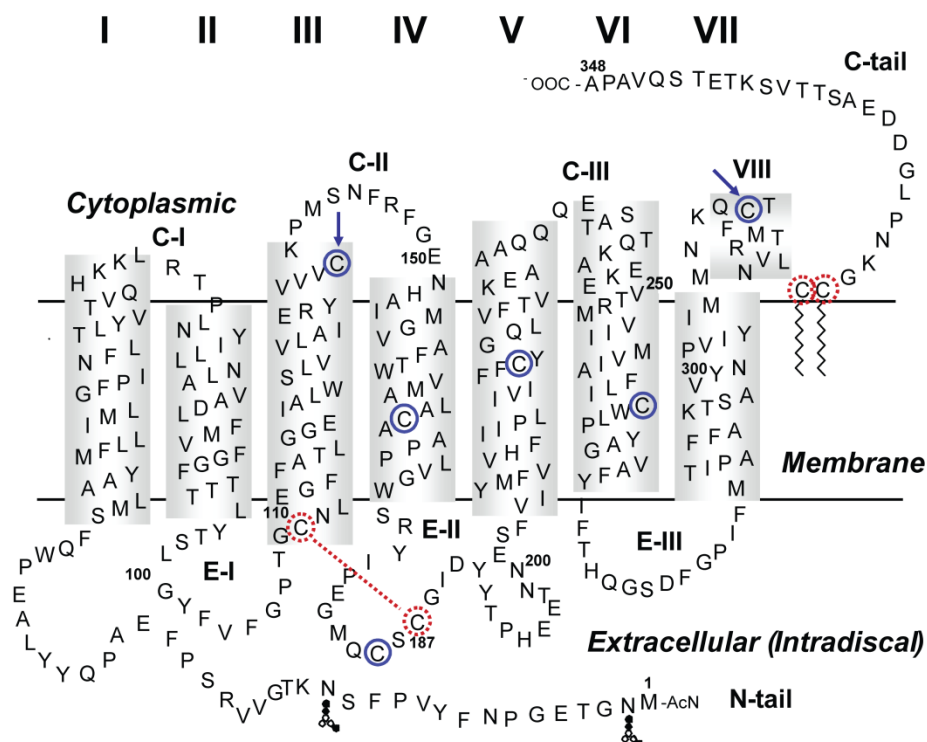
Figure 47: Secondary structure representation of rhodopsin showing endogenous cysteines

The cysteines reactive in the dark state, C140 and C316, are shown by blue arrows. The remaining cysteines shown in blue circles become solvent exposed upon light activation. Cysteines at positions 110 and 187 are engaged in a disulfide bond, and cysteines at positions 322 and 323 are palmitoylated; they are therefore not reactive. These nonreactive cysteines are shown as red dotted circles, and the disulfide bond is indicated as a red dotted line.

This method has been previously used to prepare NMR samples since it is easier for the excess label to be removed completely by washing the column extensively with buffer N containing 0.05% DM before eluting pure labeled rhodopsin. This ensures that no background signal from free label is observed on the NMR spectrum. Optimization of labeling conditions for each reagent is discussed below.

7.3.1   CF3I

CF3I was dissolved in Buffer N + 0.05% DM + 35% DMSO by overnight nutation at 4°C. CF3I was also found to dissolve in methanol. DMSO stock was used to test labeling. Using labeling method 1, as described above, 0.5 μM purified rhodopsin was incubated with CF3I overnight at 4°C with different concentrations of the label of 1 μM, 2.5 μM, 5 μM, 12.5 μM, 25 μM and 250 μM. The by-product of the reaction of CF3I with purified rhodopsin (reaction shown in Figure 48.A.) does not show any absorbance maximum in the wavelength region 220 nm – 650 nm. Hence, the extent of labeling by CF3I was tested by 4-PDS as described in Chapter 2, Section 2.3.1. The number of cysteines reacting with 4-PDS is indicative of the number of cysteines that did not react with CF3I. The number of cysteines accessible to 4-PDS after labeling with CF3I using concentrations 5, 25 and 250 μM is shown in Figure 48.B.I. One cysteine reacts with CF3I when 5 μM of the label is used. The extent of reactivity slightly increases (~1.5 cysteines) with increase in CF3I concentration up to 250 μM. This indicates the possibility of CF3I labeling two cysteines if higher concentrations are used.

Using method 2, two conditions were tested where rhodopsin bound to 1D4 column was incubated with a) 10 mM CF3I at 20°C for 0.5 h and b) 1mM CF3I at 4°C overnight. After incubation, the protocol for elution was followed as described in Chapter 2, Section 2.2.5.4. Labeling rhodopsin on the column with 10 mM CF3I for 0.5 h resulted in labeling of less than one cysteine (0.5 cysteines) but at a concentration of 1 mM and upon longer incubation time, one cysteine could be labeled (Figure 48.B.II.). Therefore, at least one cysteine could be labeled by CF3I by both the methods.
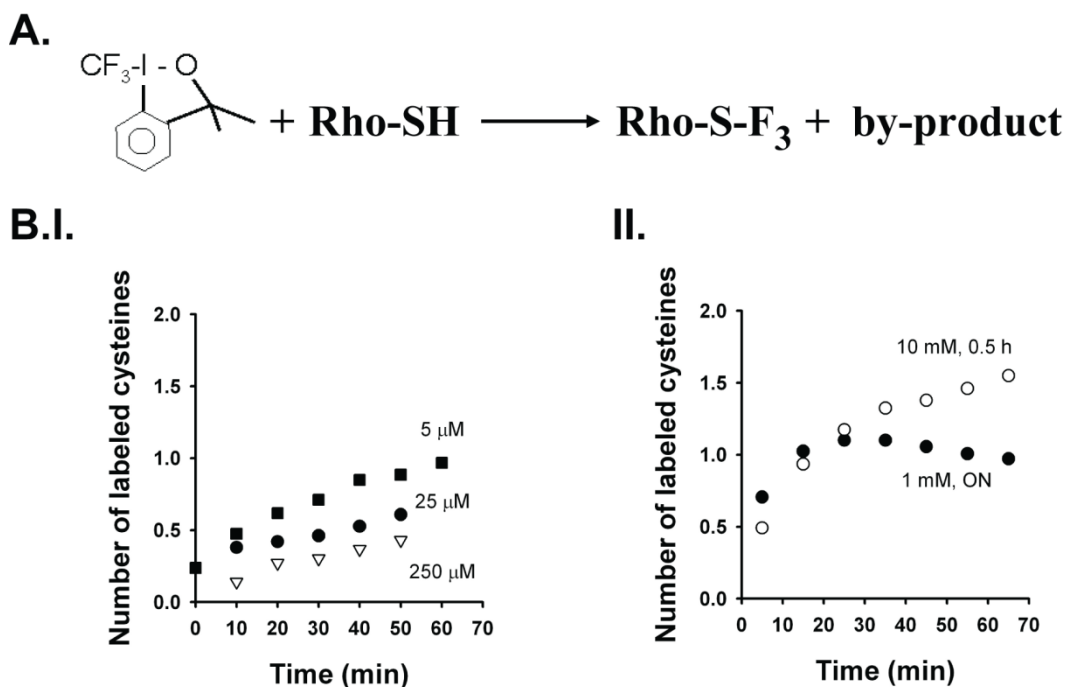
Figure 48: Number of cysteines accessible to CF3I

A. Chemical reaction of CF3I with cysteine SH in rhodopsin leading to derivatization of cysteine with CF_3 group and formation of a by-product. B. Plot of number of cysteines reacting with 4-PDS over time for I. pure rhodopsin incubated with increasing concentrations of CF3I and II. rhodopsin bound to 1D4 column incubated with 1 mM and 10 mM CF3I for overnight and 0.5 h respectively. All reactions are carried out in the dark.

To prepare the ^{19}F labeled NMR sample, rhodopsin bound to the 1D4 column was incubated overnight with 2 mM CF3I at 4°C. CF3I was added from a 70 mM stock in DMSO so that final concentration of DMSO is kept below 5% when added to the 1D4 column to prevent DMSO from damaging the column. However, only 2.6 mg instead of the expected 8-10 mg of CF3I labeled rhodopsin could be purified from 10 retinae. Thus, purification was repeated and again less than expected amount of rhodopsin was purified, only 5 mg instead of the expected 15-20 mg from 20 retinae, indicating interference of CF3I with rhodopsin purification. The remaining amount of rhodopsin that may be misfolded and/or stuck to the column was eluted with 50 mM Tris + 100 mM NaCl in pH 8 + 1mM DTT, 50 mM Tris + 100 mM NaCl in pH 8

190

and 0.1 M sodium acetate + 0.5 M NaCl in pH 4. The high salt and low pH conditions have been shown to elute misfolded rhodopsin (Ridge et al., 1995b). The pH 4 sample aggregated while concentrating and the aggregates were dissolved by adding 3% SDS. This was done because as we have described in Chapter 3, Section 3.3.4., aggregation did not occur in presence of SDS and 8 M urea did not cause aggregation when in presence of 3% SDS. Rhodopsin eluted with Tris, pH 8 with and without DTT was pooled together and concentrated. Concentration of rhodopsin in these samples could not be estimated since a small 500 nm peak was observed as these are misfolded samples where the ratio of 280 nm to 500 nm is much greater than 2. Therefore, CF3I adversely affected elution of rhodopsin from the column but the reason was not clear. Although some of the protein eluted from the column under conditions that would elute misfolded rhodopsin, it was still not clear if rhodopsin was irreversible bound to the column or was misfolded, or both.

7.3.2   2F

2F was dissolved in 70% DMSO to give a stock of 10 mM. Labeling property of 2F was first tested with free L-cysteine in solution. By means of this reaction, the absorbance maximum of the by-product was also determined. 2F alone in solution gave a peak at 280 nm and upon reacting 5 µM L-cysteine with 250 µM 2F, two peaks at 270 nm and 340 nm were observed corresponding to the by-product as shown in Figure 49.B. The two by-product peaks increase after 5 min of the reaction and saturate within 10 min. Absorbance spectra remains the same after 30 min is shown in Figure 49.B. confirming completion of the reaction. These absorbance maxima are similar to that seen by the by-product (2-thiopyridone) of the reaction between a previously known cysteine derivatizing reagent, 2-PDS and sulfydryl groups (Grassetti and

Murray, 1967). However, when 0.5 μM of pure rhodopsin was reacted with 25 μM and 100 μM 2F (the reaction is shown in Figure 49.A.), none of the by-product peaks were observed indicating that exposed cysteines in rhodopsin could not be labeled by 2F under the conditions tested. Therefore, further experiments were not carried out with this label.
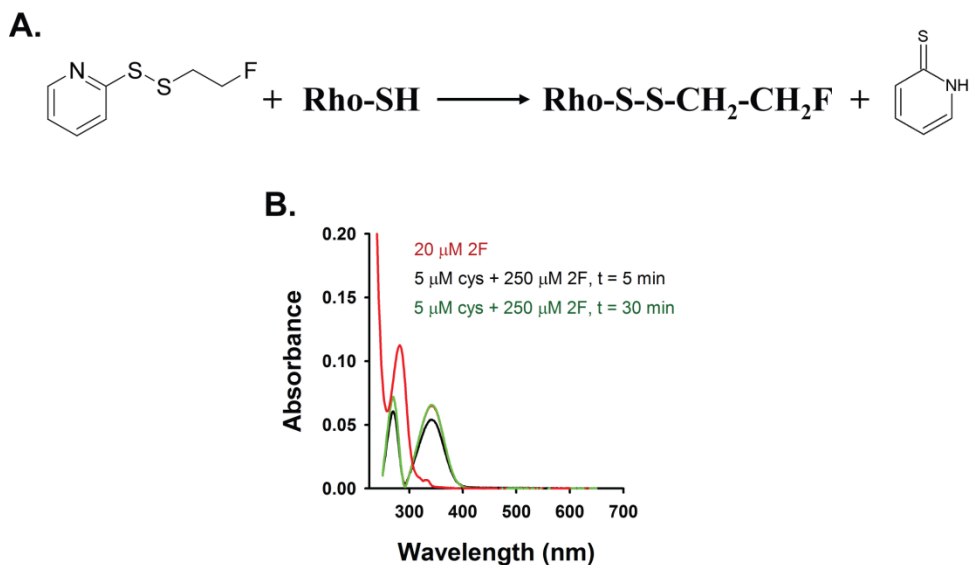
Figure 49: Absorbance spectra of 2F reacting with cysteine

A. Reaction of 2F label with cysteine SH in rhodopsin leading to the derivatization of cysteine with CH_2-CH_2F and formation of a by-product that absorbs at two wavelengths 270 nm and 340 nm. B. Reactivity of 2F with cysteine is shown. Absorbance spectra of free 2F at 20 μM (red), time course of reaction of 5 μM cysteine with 250 μM 2F after 5 min (black) and 30 min (green).

7.3.3 4F

4F was dissolved in 100% methanol to give a stock of 0.3 M. Its labeling property and absorbance maximum of the by-product were tested with L-cysteine. 4F alone in solution gave a peak at 246 nm and upon reacting 5 μM L-cysteine with 250 μM 4F, a peak at 323 nm was observed which corresponded to the by-product of the reaction. The by-product released in this

reaction is the same as that in 4-PDS reaction with sulfydryl groups, which is 4-thiopyridone (Grassetti and Murray, 1967). The reaction of 4F with cysteine SH group is shown in Figure 50.A. The extent of labeling was tested by following the peak at 323 nm over time and using the previously known molar extinction co-efficient of this molecule of 19000 $M^{-1}cm^{-1}$ (Grassetti and Murray, 1967), the number of cysteines in rhodopsin that react with 4F was calculated. 0.5 μM of pure rhodopsin was reacted with 125 μM 4F at 20°C which showed labeling of both cysteines in the dark after 100 min (Figure 50.B.). However, five out of six cysteines could be labeled after light activation. In order to test the temperature dependence of this reaction, 12.5 μM and 125 μM of 4F was reacted with 0.5 μM rhodopsin at 40°C. Both these conditions led to labeling of both the exposed cysteines in the dark whereas 12.5 μM of the label reacted with five cysteines and 125 μM label reacted will all six cysteines (Figure 50.B.). The reaction was fastest when 125 μM of label was used and slowest in presence of 125 μM of label at 20°C as shown in the table for reaction rate constants in Table 10. Therefore, 500 μM 4F at 20°C was used to test labeling of rhodopsin when bound to 1D4 column. The label was incubated with rhodopsin bound to the column for 2 h at room temperature before elution. Labeling efficiency of 4F was tested by reacting 4F-labeled rhodopsin with 4-PDS. No 323 nm peak, arising from the by-product of the reaction between 4-PDS and cysteine, was seen in the dark state of rhodopsin indicating that both the free cysteines are labeled by 4F. Thus, this condition was used to label rhodopsin to preparing samples for ^{19}F NMR experiments.

A.

B.
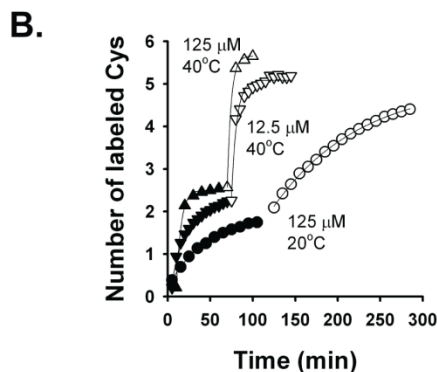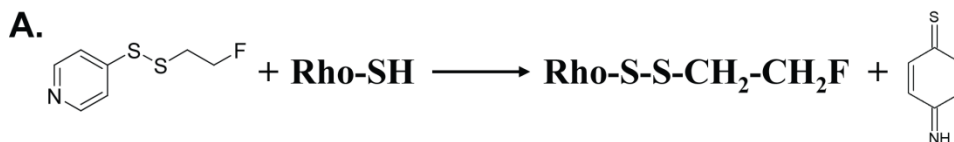
Figure 50: Number of cysteines accessible to 4F

A. Reaction of 4F label with cysteine SH in rhodopsin leading to the derivatization of cysteine with CH_2-CH_2F and formation of a by-product, 4-thiopyridone, that absorbs at 323 nm. B. Plot showing number of cysteines in rhodopsin reacting with 4F over time at different 4F concentrations of 125 μM and 12.5 μM and under different temperatures as indicated. Curves with open symbols are data points collected after illumination.

Table 10: Rate constants of cysteines reacting with 4F and 2NO2F under different conditions

(°C)	Label name, concentration (μM)	Rate constants (min^{-1})	
		Dark	Light
20	4F, 125	0.0125	0.0098
	2NO2F, 12.5	0.0269	0.0252
	2NO2F, 125	0.0154	0.2211
40	4F, 12.5	0.0587	0.1632
	4F, 125	0.1760	0.2164
	2NO2F, 125	0.1053	0.2254

7.3.4   2NO2F

2NO2F was dissolved in 100% methanol to give a stock of 0.16 M. Labeling property was first tested with L-cysteine. 2NO2F alone in solution gave a peak at 242 nm and upon reacting 5 μM L-cysteine with 250 μM of 2NO2F, a peak at 384 nm was observed corresponding to the by-product of the reaction. Next, the extinction co-efficient of the by-product was estimated so that the peak at 384 nm can be used to quantitate the number of cysteines reacting with 2NO2F. This was done by reacting 2NO2F with varying concentrations of L-cysteine and from slope of the plot of absorbance at 384 nm against cysteine concentration extinction co-efficient of the by-product of 17500 $M^{-1}cm^{-1}$ was obtained following Lambert-Beer's law (Figure 51.B.). 12.5 μM and 125 μM of 2NO2F were used to test labeling of 0.5 μM purified rhodopsin at 20°C. The reaction is shown in Figure 51.A. Both concentrations of the label led to labeling of only one of the two exposed cysteines in rhodopsin in the dark state and three of six cysteines in the light activated state (Figure 51.C.). Both the exposed cysteines were labeled in the dark with 125 μM of the label but only at a higher temperature of 40°C. The same condition labeled four cysteines in the light state. Thus, 500 μM of this label was used to label rhodopsin bound to 1D4 column after nutating for 2 h at room temperature. However, only one cysteine could be labeled in the dark (Figure 51.C.). Hence, this label was used to prepare single cysteine labeled sample for ^{19}F NMR.
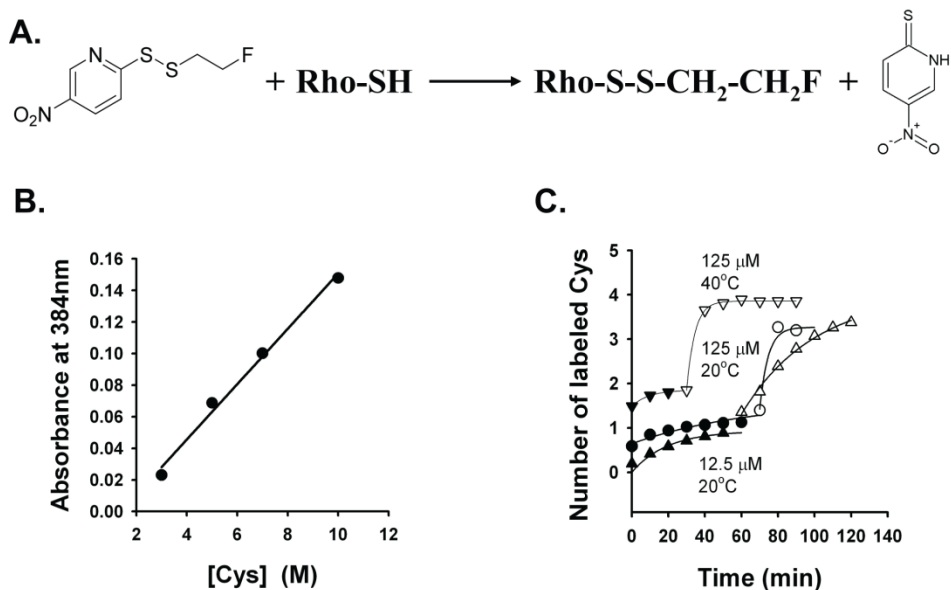
Figure 51: Number of cysteines accessible to 2NO2F

Plots showing A. absorbance maxima of the by-product of the reaction between 2NO2F and cysteine with increase in cysteine concentration and B. number of cysteines reacting with 2NO2F over time under different conditions as indicated. Curves with open symbols are data points collected after illumination.

7.4 ^{19}F NMR CHARACTERIZATION OF FLUORINE LABELS IN SOLUTION

1D ^{19}F NMR spectra and motion of free labels were measured under different conditions of temperature and buffer.

7.4.1.1 CF3I

1D spectra of 1 mM CF3I in H_2O in presence and absence of TFA are shown in Figure 52. TFA is added as an external reference for ^{19}F chemical shift. Two peaks at -24.7 ppm and -137.8 ppm are seen in presence of TFA whereas a single major peak at a different position of -38.2 ppm and a very small peak at -119.4 ppm are seen in the absence of TFA. Appearance of

more than one peak of CF3I and at different chemical shifts in the presence of TFA compared to that in its absence suggests that CF3I is either degrading in the presence of TFA or reacting with TFA. Thus, subsequent experiments with CF3I were carried out in the absence of TFA.
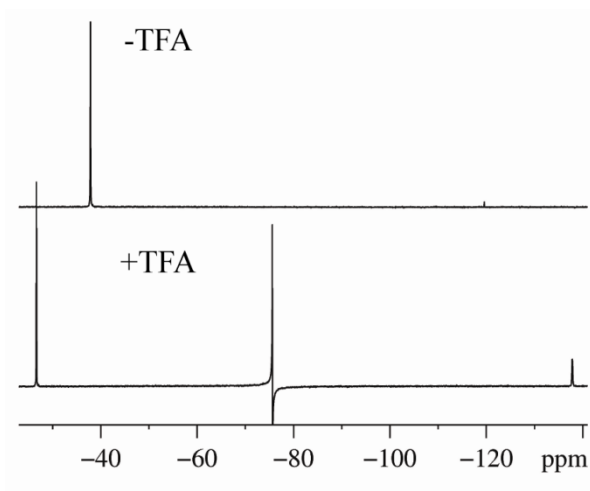
Figure 52: 1D ^{19}F NMR spectra of CF3I in water

1D ^{19}F NMR spectra of CF3I in water in presence and absence of TFA at 25°C. Number of scans collected in each spectrum is 64.

I tested if CF3I reacts non-specifically with functional groups in amino acids other than sulfydryl groups such as amines that are bonded to a –CH2 group as in lysine. This reaction is feasible since electronegativity of nitrogen is slightly more than that of sulfur in –SH group of cysteine and hence it can react with the electrophillic site of –CF3. To test this hypothesis, 1 mM CF3I was reacted with free 1 mM L-lysine and the reaction was followed by recording 1D NMR spectrum at different time intervals. A peak at -38.8 ppm, corresponding to free CF3I in solution in absence of TFA, was seen at time t = 0 which did not change in intensity and no other peak appeared over time up to 12 h (data not shown). Different concentrations of lysine were titrated into 1 mM CF3I to see the appearance of fluorinated lysine peak with increase in lysine concentration as the reaction proceeds. However, apart from the peak at -38.8 ppm, no other

peak appeared even at high lysine concentrations of up to 200 mM indicating that CF3I does not react with lysine.

In order to confirm that CF3I is able to derivatize sulfydryl group of cysteine, it was titrated with free cysteine in H_2O and appearance of fluoro cysteine peak was followed by 1D NMR spectra (Figure 53.A.). Two peaks, one major peak at -38.7 ppm and a very small peak at -120 ppm, were seen for the free label. With increase in cysteine concentration as indicated in the overlay, the peak at -120 ppm increased in intensity and shifted its position upfield beyond 1 mM cysteine. A small peak around -41.1 ppm appeared from 1 mM cysteine onwards and another peak at -30.7 ppm appeared from 10 mM cysteine onwards. These two small peaks increased in intensity up to 50 mM and then decreased at 200 mM. Small peaks were also seen around -78 ppm, these can be seen when the scales of the spectra in Figure 53.A. were expanded. Peak intensity of the free label at -38.7 ppm decreased up to 1 mM cysteine and then disappeared at higher cysteine concentrations. The area under the peaks that were increasing did not account for the decrease in the peak at -38.7 ppm. No systematic decrease in intensity of free label peak and corresponding increase in intensity of fluorinated cysteine peak were seen with increase in cysteine concentration. Further, appearance of several small peaks complicated the interpretation of these spectra. One caveat in performing these experiments is that cysteine is extremely susceptible to oxidation. Although care was taken in preparing the samples at 4°C and flushing sample tubes with argon, NMR experiments were carried out at room temperature in presence of oxygen. Thus, it was not clear from these experiments whether CF3I reacted with free –SH groups in cysteine.

Another positive control for reactivity of CF3I with –SH groups was tested by titrating CF3I with cysteine ester hydrochloride. This reaction was reported previously to give high yields of fluorinated product with CF3I (Kieltsch et al., 2007). Increasing concentrations of cysteine ester hydrochloride dissolved in methanol, as mentioned in the earlier report (Kieltsch et al., 2007), was titrated into 1 mM CF3I in H_2O and 1D NMR spectra were collected (Figure 53.B.). Free label peaks at -37.8 ppm and -119.5 ppm shifted downfield and upfield respectively with increase in cysteine ester hydrochloride concentration. A drastic decrease in the intensity of the former peak and an increase in the latter peak was observed on adding 100 μM cysteine ester hydrochloride. The -38.7 ppm peak stopped decreasing with further increase in cysteine ester concentration up to 10 mM beyond which it was undetected but the -120 ppm peak intensity continued to increase up to 50 mM. Several small peaks were seen at -73 ppm and -41.4 ppm. Again, no systematic increase in a peak that corresponds to fluorinated cysteine was seen in spite of the decrease in free label peak at -38.7 ppm. Moreover, the increase in the -120 ppm peak and appearance of small peaks could not be explained.
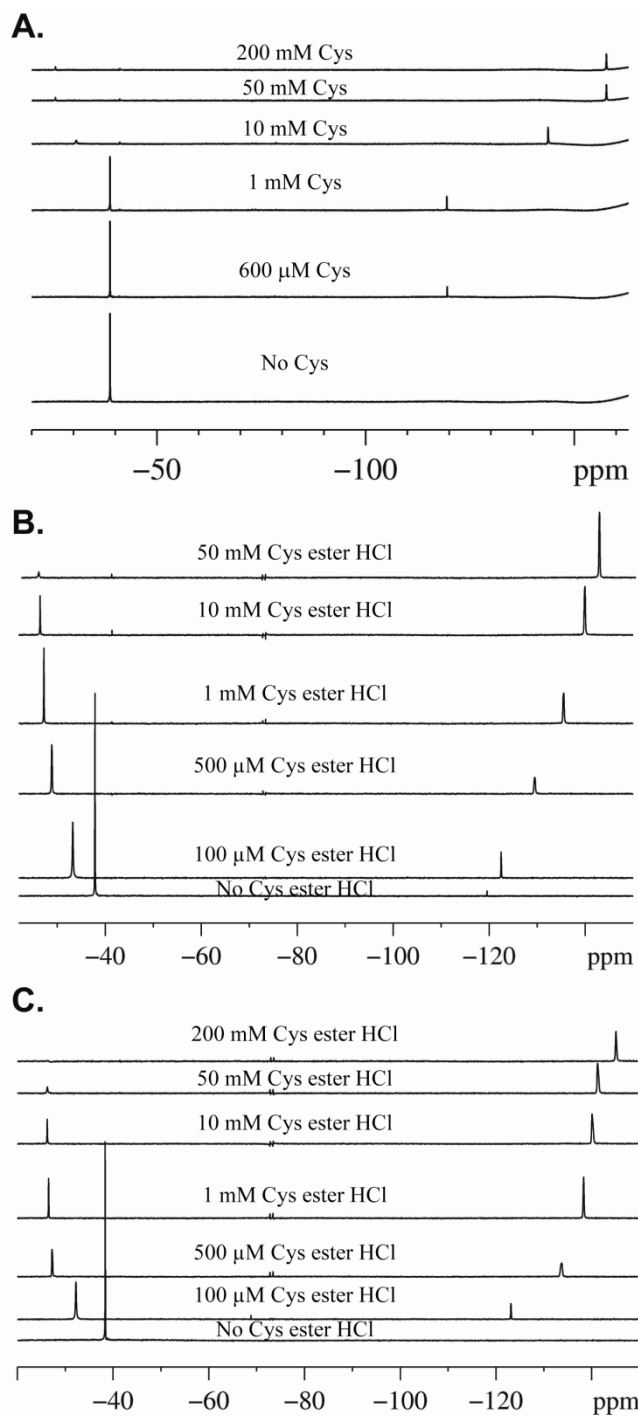
Figure 53: 1D ^{19}F NMR spectra following the reaction of CF3I with free sulfydryl groups

Titration of 1 mM CF3I with A. cysteine, B. and C. cysteine ester hydrochloride under different concentrations. All spectra in each overlay are aligned to the chemical shift of TFA. 64 scans were collected for each spectrum.

CF3I used in all these experiments was dissolved in DMSO, however, the earlier published report showed the use of CF3I dissolved in methanol (Kieltsch et al., 2007). Hence, cysteine ester hydrochloride titration into CF3I was repeated in H_2O but this time CF3I stock solution was prepared in methanol as described in the earlier published report. A single peak at -38.7 ppm was observed for CF3I which decreased in intensity when 100 μM of cysteine ester hydrochloride was added as shown in Figure 53.C. Under this condition, a peak at -123 ppm appeared but did not account for the decrease in intensity of -38.7 ppm peak. The -123 ppm peak continued to increase in intensity up to 1 mM and then remained unchanged up to 200 mM although it shifted upfield. There was no further significant decrease in -38.3 ppm peak up to 10 mM beyond which it disappeared up to 200 mM cysteine ester hydrochloride. Small peaks around -73 ppm appeared from 100 μM of cysteine ester hydrochloride onwards. Since, interpretation of these spectra was unclear and no clear evidence of CF3I reacting with free –SH group was obtained, we nevertheless tested its labeling with rhodopsin (see Section 7.3.1.).

One reason for the irreproducible nature of CF3I could be its instability. This was tested by recording 1D NMR spectra of the free label in different solutions over time. As shown in the overlay in Figure 54, a significant decrease in peak intensity was seen over 40 min indicating instability of CF3I. In the paper that reported its synthesis, reactions involving CF3I with small molecules having sulfydryl groups were carried out at -78°C (Kieltsch et al., 2007), which may have prevented such degradation of the label as we observe. Therefore, a possible explanation for all the experiments described above which were difficult to interpret could be that CF3I is not stable at room temperature over long periods of time. Labeling of proteins at -78°C is not practical and I conclude that CF3I is not a suitable derivatization reagent for proteins.
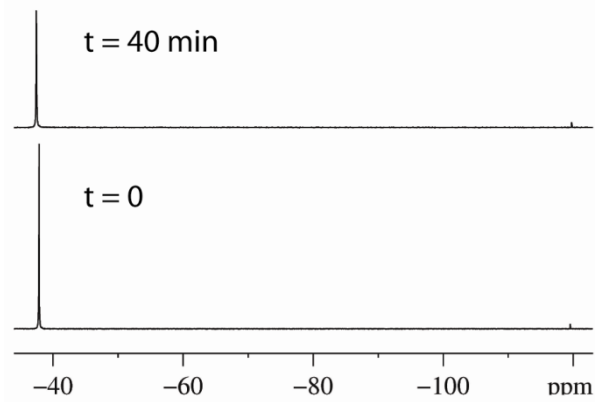
Figure 54: 1D ^{19}F spectra of CF3I in water over time

Both spectra are aligned relative to the chemical shift of TFA. 64 scans were collected for each spectrum.

7.4.1.2 4F and 4F3

1D ^{19}F NMR spectra of 6 mM free 4F label in 100% D_2O and in 100% glycerol solutions at different temperatures of 5°C, 10°C, 15°C, 25°C and 35°C were measured. Molecules in D_2O and glycerol undergo faster and slower tumbling respectively due to their different viscosities. Thus, D_2O and glycerol mimic conditions of tumbling of small and large molecules and will help in determining relaxation rates of labels free in solution and that attached to protein respectively. 1D spectra of 4F label were also measured in NMR buffer containing 3.6% and 9% DM to compare its chemical shifts with that of 4F labeled rhodopsin containing the same DM concentrations. Chemical shifts and peak widths of 4F under these different conditions are given in Appendix A in Table 18. All samples contained 0.46 mM TFA. Figure 55 shows the overlay of 1D spectra of 4F with and without F-H decoupling in D_2O and glycerol at 25°C where a septet of fluorine peak is observed due to the surrounding four protons in 4F with the decoupled peak centered at -216.6 ppm.
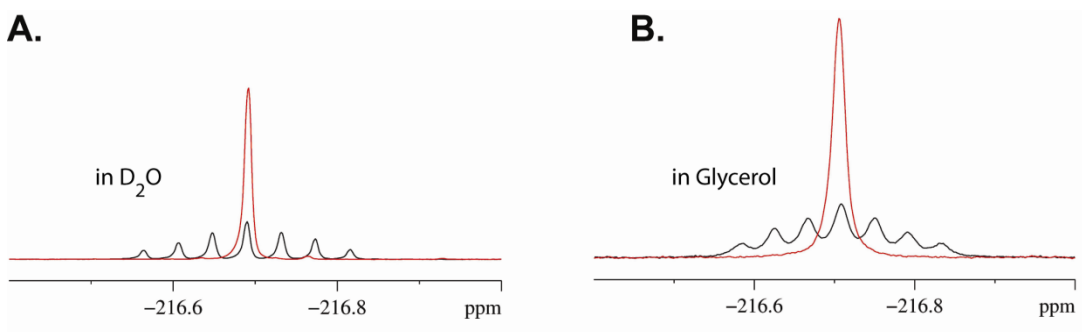
Figure 55: 1D ^{19}F NMR spectra of 4F in D2O and glycerol

1D ^{19}F NMR spectra of 4F in D_2O (8 scans) and glycerol (64 scans) with (red spectrum) and without (black spectrum) proton decoupling. Spectra in each overlay are aligned relative to TFA peak.

1D ^{19}F NMR spectra of 6 mM of free 4F3 label in 100% D_2O and in 100% glycerol solutions at different temperatures of 5°C, 10°C, 15°C, 25°C and 35°C were measured. All samples contained 0.46 mM TFA. Figure 56.A. shows the overlay of 1D spectrum of 4F3 in D_2O with and without F-H decoupling at 25°C where a triplet is observed with the decoupled peak centered at -66.17 ppm. The same experiment was carried out with 4F3 in glycerol, shown in Figure 56.B. The chemical shift and line width values of 4F3 peak in D_2O and glycerol at different temperatures are given in Appendix A in Table 17.
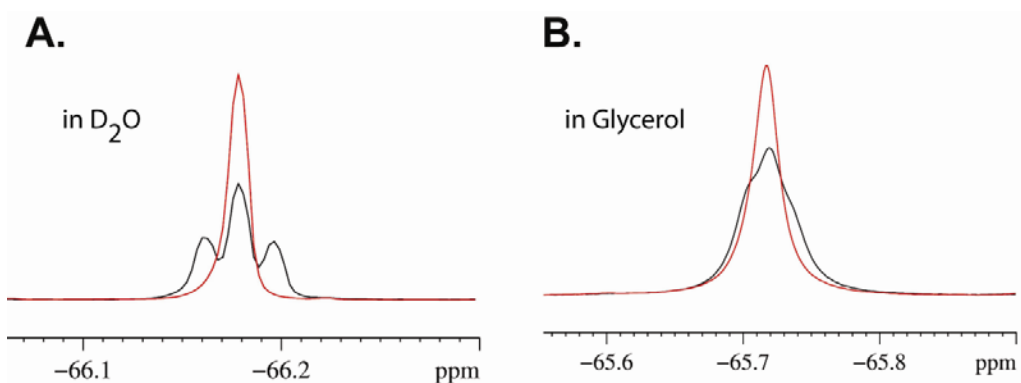
Figure 56: ^{19}F NMR spectrum of 4F3 in D2O and glycerol

1D ^{19}F NMR spectrum of 4F3 in D_2O (8 scans) and glycerol (32 scans) with (red spectrum) and without (black spectrum) proton decoupling. Spectra in each overlay are aligned to the chemical shift of TFA.

7.5 RELAXATION MEASUREMENTS OF FREE LABELS

Mobility of free labels was quantified by measuring relaxation rates. Relaxation is defined as the process by which net magnetization of a system (fluorine nuclei in the label in our case) reaches equilibrium, i.e. where no transverse magnetization in x-y plane exists and the net magnetization is along the z direction parallel to the applied magnetic field. The process by which z magnetization is restored to equilibrium is called longitudinal relaxation and the process by which x-y magnetization is restored to zero, i.e. equilibrium is called transverse relaxation. The mechanisms that trigger such relaxation processes are mainly dipolar interaction and chemical shift anisotropy (CSA). The former arises due to interaction between magnetic moments of two nuclei and the latter occurs due to a field induced by the electrons surrounding the nucleus which in turn influences its chemical shift. Therefore, the ways in which such relaxation processes occur depend on the properties of the system such as its shape and motion. Thus, using relaxation rates the environment of nuclei in a system and their nature of motion can be determined.

The factors that cause relaxation of fluorine atom in monofluoro labels are fluorine CSA, F-H dipole interaction, cross-correlation between H-F dipoles and cross-correlation between H-F dipole and fluorine CSA. These factors are different for trifluoro labels which are complicated due to cross-correlation between F-F dipoles (Werbelow and Marshall, 1973) and hence their relaxation mechanism is different from monofluoro labels. The factors that trigger relaxation of trifluoro labels are fluorine CSA, F-F dipole interaction, cross-correlation between three F-F dipoles and cross-correlation between F-F dipole and fluorine CSA (Werbelow and Marshall, 1973; Mehring, 1983; Goldman, 1984). As described in Section 2.3.12.3. in Chapter 2, different pulse programs were used to understand the mechanism of relaxation of monofluoro and trifluoro compounds.

7.5.1   4F and 4F3

Relaxation rates of labels 4F and 4F3 were measured to compare the mechanisms of relaxation of monofluoro labels and trifluoro labels. ^{19}F relaxation experiments in D_2O and glycerol for each label were carried out at different temperatures using different pulse programs as discussed in Section 2.4.12.3. in Chapter 2. The relaxation rates are given in Table 18 in Appendix A and and all the decay curves are shown in Figures 73 and 74 in Appendix A. Decay curves obtained from a CPMG experiment for 4F and 4F3 in D_2O look similar to each other at all temperatures. R_2 values are similar for both the labels (see Table 18 in Appendix A). However, at higher temperatures of 35°C where a composite ^{1}H 180° pulse is applied, the difference in decay curves for 4F and 4F3 is enhanced. The decay curves could not be fit to a monoexponential function, the curves fit better to a double exponential function. The reason for this is not very clear. However, we speculate that since a simple mono-exponential curve is not observed, the composite 180° pulse is unable to completely suppress cross-correlation effects between the two F-H dipoles (DD interaction) along with the cross-correlation between CSA and F-H dipolar interaction. R_2 of 4F at 35°C is higher than that of 4F3. This is because even though cross-correlation effects are supposed to be small under conditions of fast molecular tumbling, the effect appears to become significant under the conditionhere due to small auto-relaxation rates (mainly governed by diffusion). In presence of glycerol, which is intended to mimic large molecular tumbling such as motion of proteins, decay curves of 4F and 4F3 show complex behavior. Representative decay curves are shown in Figure 57. These were collected at 10°C using different pulse programs as indicated in the figure. All the decay curves recorded under different conditions of temperature using different pulse programs are shown in Figures 74 in Appendix A. However, the curves show a double exponential decay behavior. This is because at slower molecular tumbling, cross-

correlation is significant for both 4F and 4F3. Moreover, in CPMG experiment where no proton pulses are used, double exponential fits were required more evidently for 4F than for 4F3 indicating a slower decay of signals at longer times. Upon fitting to a double exponential curve, the decay curves for 4F show a slower second exponential decay than that for 4F3 indicating that greater signal intensity remains for 4F than 4F3 under all the conditions tested. This provides evidence for the advantage of 4F over 4F3 for use in studying protein dynamics.
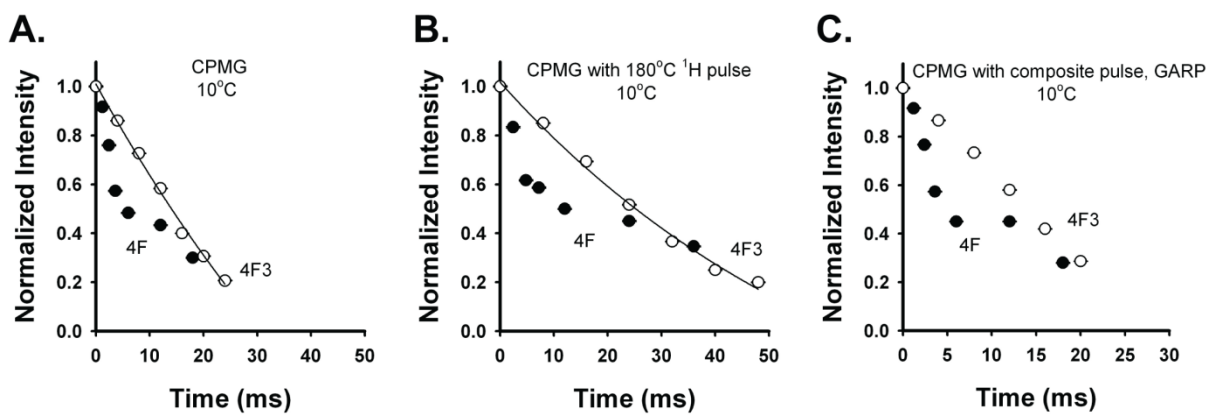
Figure 57: Comparison of the decay of transverse magnetization of 4F and 4F3 in glycerol

Decay of transverse magnetization of 4F (closed circle) and 4F3 (open circle) labels in glycerol at 25°C, 10°C and 15°C with the different pulse programs as indicated. Graphs were fit to a monoexponential decay.

Longitudinal relaxation experiment with and without ^{1}H 180° pulse were measured as a function of temperature for 4F. These values, summarized in Table 19 in Appendix A, were same in both presence and absence of ^{1}H 180° pulse. R_1 values of 4F are shorter than that of 4F3. Therefore, in terms of length of experiment, 4F free in solution has a longer T_1 (shorter R_1) means longer waiting time between repetition of pulses. However, when labels are attached to proteins, due to the surrounding protons from neighboring amino acids R_1 may become large by contribution from H-F cross-relaxation. Therefore, when labeled to proteins, R1 of 4F may become larger making it an appropriate label for protein dynamics studies.

206

7.5.2   2NO2F and 2NO2F3

1D NMR spectra of 2 mM 2NO2F label in 100% D_2O at 15°C, 25°C and 37°C were measured.

All samples contained 0.46 mM TFA. 6 mM concentration could not be used as was used for 4F

label since 2NO2F did not dissolve at such high concentration. Figure 58 shows the overlay of

1D spectra of 2NO2F with and without F-H decoupling at 25°C where a septet is observed with

the decoupled peak centered at -216.85 ppm. The chemical shift and line width values of 2NO2F

peak in D_2O at different temperatures are shown in Table 20 in Appendix A. 2NO2F in D_2O was

used to measure its relaxation rates in water to compare with that of 4F to determine which label

is advantageous for spectroscopic use.
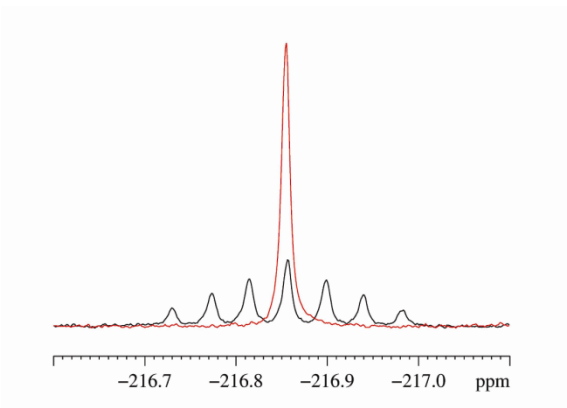
Figure 58: 1D ^{19}F NMR spectra of 2NO2F

Overlay of 1D ^{19}F NMR spectra of 2NO2F with and without proton decoupling. Spectra are aligned relative to the

chemical shift of TFA. 8 scans were collected.

Similar experiments were done with 2NO2F3 label in D_2O at 25°C. 1D spectra of 2NO2F3 with and without F-H decoupling is shown in Figure 59 where a triplet is observed with the decoupled peak centered at -66.16 ppm. Chemical shift and line width values of NO2F3 peak in D_2O and glycerol are shown in Table 20 in Appendix A. Relaxation rates of this label were then measured to compare with that of 4F3.
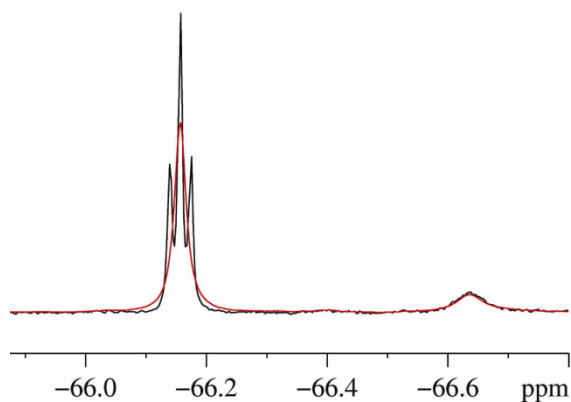
Figure 59: 1D ^{19}F NMR spectrum of 2NO2F3 in D_2O

1D ^{19}F NMR spectrum of 2NO2F3 in D_2O with (red spectrum) and without (black spectrum) proton decoupling. Spectra in each overlay are aligned to the chemical shift of TFA. 64 scans were collected for all spectra.

For 2NO2F and 2NO2F3 labels, relaxation experiments were carried out at temperatures 15°C, 25°C and 35°C for 2NOF and at 25°C for 2NOF3. All the decay curves fit to a monoexponential function as shown in Figure 75 in Appendix A. Comaprison of decay curves of 2NO2F and 2NO2F3 at 25°C is shown in Figure 60. R_2 values from CPMG experiment with 180° pulse are given in Table 11. These values were similar to CPMG where no 180° pulse was applied. Comparing the decay curves of 2NOF and 2NOF3 at 25°C, the former label, as seen for 4F, shows a slower second decay component than 2NOF3 indicating its advantage over 2NOF3. Comparing the relaxation rates of 4F and 2NOF, the former has lower values than the latter indicating advantage of the 4F as a label for protein measurements.

Longitudinal relaxation experiments with and without ^{1}H 180° pulse were measured as a function of temperature for both 2NOF and 2NO2F3. R_2 and R_1 values, summarized in Table 11, were identical in both presence and absence of ^{1}H 180° pulse.
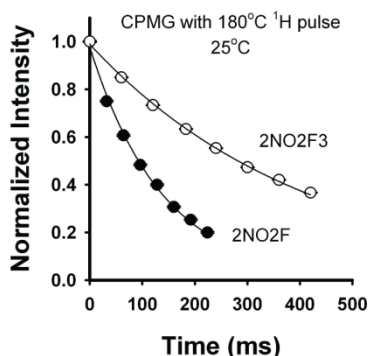
Figure 60: Comparison of decay of transverse magnetization of 2NO2F and 2NO2F3 in D$_2$O

Table 11: R$_2$ and R$_1$ values of 2NO2F and 2NO2F3 in D$_2$O

Label	Solvent	(°C)	R_2 (s^{-1}) with 180° pulse	R_1 (s^{-1}) with 180° pulse
2NO2F	D$_2$O	15	6.2742±0.2000	0.5973±0.0071
		25	7.2335±0.2000	0.4388±0.0052
		35	5.9172±0.2000	0.3043±0.0063
2NO2F3	D$_2$O	25	2.4202±0.0327	1.0878±0.0429

7.6 ^{19}F NMR CHARACTERIZATION OF -CF$_3$ LABELED RHODOPSIN

Among the fluorine reagents tested for labeling rhodopsin, CF3I showed labeling of one cysteine (see Section 7.3.1.). CF3I labeled rhodopsin was prepared for NMR experiments as described in Section 7.3.1. Due to interference of CF3I with rhodopsin purification, only 2.6 mg CF3I labeled rhodopsin (0.17 mM) could be prepared (see Section 7.3.1.). This sample showed no fluorine

peaks in a 1D spectrum recorded at 25°C and even at the higher temperatures of 37°C and 42°C tested. Therefore, SDS at concentrations of 0.3% and 10% were added to denature rhodopsin with the rationale that its flexibility increases upon unfolding (described in Chapters 5 and 6) and leading to an increase in signal to noise ratio. However, no peaks appeared even in the presence of SDS, nor when the temperature was increased to 42°C in the presence of SDS. Since, the rhodopsin concentration could be limiting for poor sensitivity, a higher concentration of CF3I labeled rhodopsin of 0.34 mM was prepared. 1D NMR spectra of this sample with and without decoupling pulse are shown in Figure 61.A. A broad peak with low intensity was seen in the range of -40 ppm to -43 ppm. Different spectral regions in the 1D spectrum were screened to see if this broad peak was the only one and a more intense peak of fluoro labeled rhodopsin exists elsewhere on the spectrum. The regions tested were from 140 ppm to 20 ppm and -20 ppm to -170 ppm but no peak other than the observed ~-40 ppm peak was seen indicating that the latter chemical shift is indeed the position where cysteines in rhodopsin fluorinated with CF3I will appear. Peak of free label in solution in presence of 6% DM, the same amount of DM as present in CF3I labeled rhodopsin sample, appears at -38.8 ppm, 1.2 ppm downfield from the shoulder of the rhodopsin peak at -40 ppm. In order to increase signal to noise ratio, the same spectrum was collected with 16k scans, without decoupling pulse, at a higher temperature of 37°C but only a slight increase in signal intensity was seen (Figure 61.B.).

Furthermore, 1D spectrum of denatured CF3I labeled rhodopsin samples, i.e. rhodopsin eluted in pH 4 buffer with 3% SDS was recorded. The spectrum is shown in Figure 61.C. It was expected that due to increased flexibility of the CP domain upon denaturation (as described in Chapter 5 and 6) the peak intensity of C140 and C316, both of which are in the CP region, would increase. However, a broad peak was observed at the same region as that of native rhodopsin, i.e.

in the range of -40 ppm to – 42 ppm. Further, the peak intensity of denatured rhodopsin even after 24k scans was much lower than that of the native state recorded after 12k scans. The low peak intensity of denatured state compared to native state did not correlate with increased flexibility of the CP domain upon denaturation as seen in other studies (Chapters 5 and 6) and therefore could be due to poor sensitivity of the label itself. Since a single broad peak with poor signal to noise ratio of was observed, this sample was not suitable for relaxation rate measurements. The poor signal to noise ratio correlates with the inability of CF3I to label free cysteine or cysteine ester hydrochloride as shown in Section 7.4.1.1. which could be due to instability of the label over time. Thus, the use of CF3I as a labeling reagent for sulfydryl groups has been shown only at very low temperature conditions of -78°C (Kieltsch et al., 2007). Protein NMR experiments usinf ^{19}F labels attached to cysteines are dependent on whether they can be labeled with fluoro reagents to probe conformational changes of proteins occurring at near physiological temperatures. Since, I are unable to extend its applicability to conditions suitable for maintaining the integrity of proteins, our studies show that this label is not suitable for protein NMR.
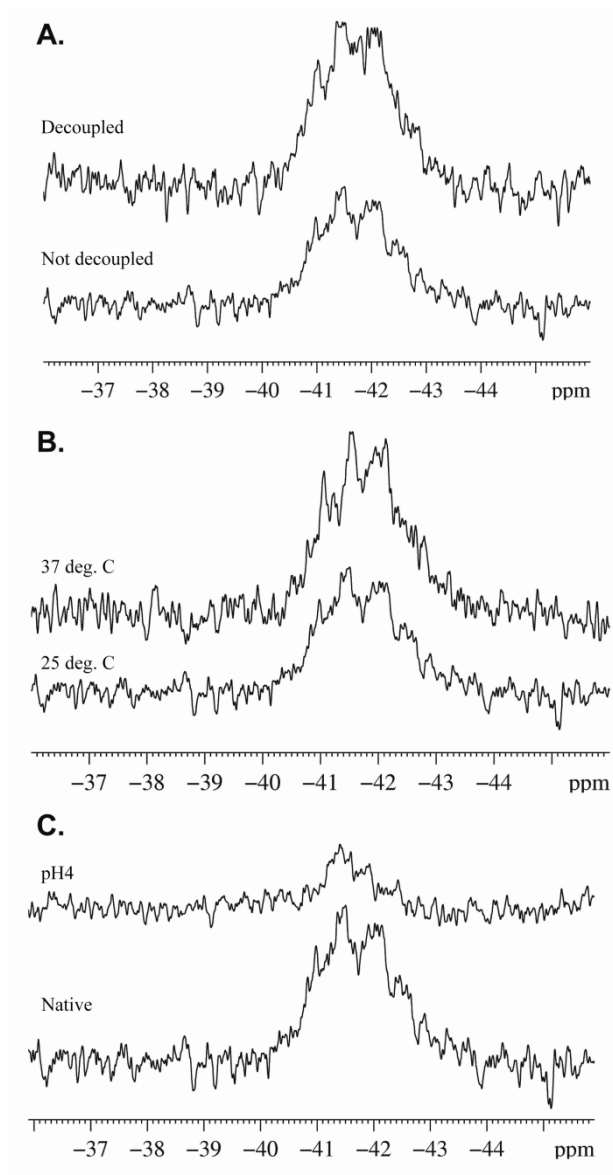
Figure 61: ^{19}F spectra of rhodopsin labeled with CF3I

A. Spectra recorded with (12k scans) and without proton decoupling (16k scans), B. Comparison of increasing temperature, 37°C (16k scans) as compared to 25°C (12k scans) and C. Comparison of samples eluted at pH 4 (28k scans) with native state (12k scans). Both spectra in each overlay are aligned relative to the chemical shift of TFA.

212

7.7 ^{19}F NMR CHARACTERIZATION OF -CH2-CFH2 LABELED RHODOPSIN

7.7.1 Rhodopsin labeled with 4F label

The 4F reagent labeled both free cysteines in rhodopsin in a small scale experiment as described in Section 7.3.3. Therefore, 4F was used to prepare monofluoro labeled rhodopsin for NMR experiments. 1D spectra of 0.7 mM 4F labeled rhodopsin containing 3.6% DM were measured at different temperatures as shown in Figure 62. Two peaks, at -215 ppm (peak 1) and -217.1 ppm (peak 2), corresponding to the two 4F derivatized cysteines at positions C140 and C316 in rhodopsin were observed. The former peak decreased in intensity with decrease in temperature but the latter did not show significant changes in peak intensity indicating that the cysteines corresponding to the two peaks have different motional regimes. Both the peaks moved upfield with decrease in temperature. Chemical shift values of the two peaks along with their peak widths are shown in Table 12.

In order to assign these two peaks to the two cysteines, C140 and C316, I selectively labeled one cysteine (C316) with 4F by selectively blocking the other cysteine (C140) with PDS. Labeling was carried out as described in Chapter 2, Section 2.2.5.3. The number of cysteines labeled in this process was tested by reacting 4F single cysteine labeled rhodopsin with 4-PDS. None of the cysteines labeled with 4-PDS and after light activation, only four of the six free cysteines reacted with 4-PDS indicating that two of the inaccessible cysteines were derivatized during purification, one with 4-PDS and the other with 4F. The 1D NMR spectrum of single 4F cysteine labeled rhodopsin was recorded (Figure 63). The NMR spectra showed a more intense peak at the position of peak 1 and a smaller peak at the position of peak 2 indicating that peak 1 corresponds to C316. Moreover, another peak at -215.3 ppm, adjacent to peak 1, was seen.

213

Therefore, instead of one peak, corresponding to C316 as expected, three peaks were observed at -217.2 ppm, -215.3 ppm and -215 ppm. It is not clear why a third peak appeared in the single cysteine labeled sample but not in the double cysteine 4F labeled sample. The appearance of more than the expected single peak in this sample indicated incomplete blocking of C140 with 4-PDS. Peak 1 being the most intense peak is tentatively assigned to C316.
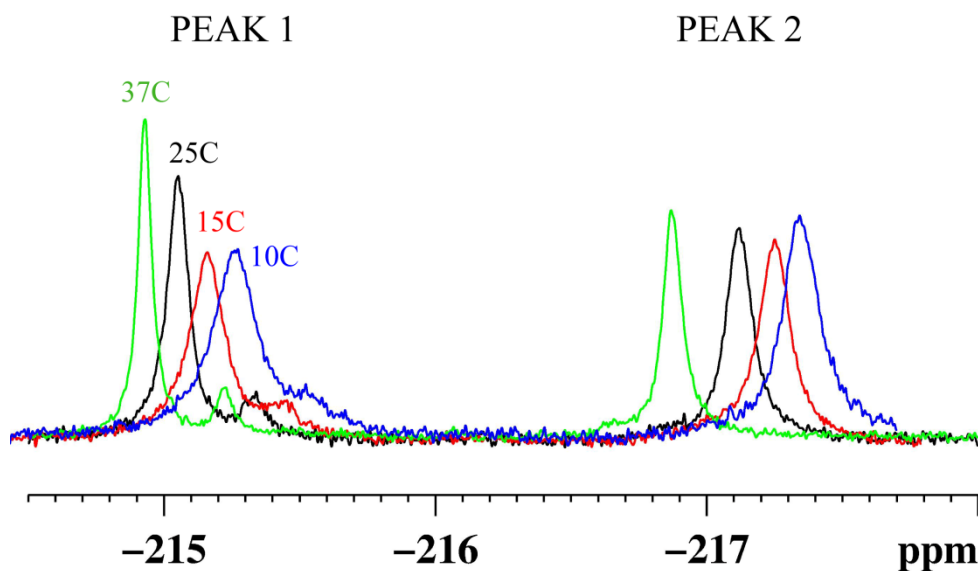
Figure 62: 1D ^{19}F NMR spectra of 4F labeled rhodopsin at different temperatures

Chemical shift and intensity of all spectra are aligned to that of TFA. 256 scans were collected for each spectrum.

The two peaks will be henceforth referred to as Peak 1 and Peak 2 as indicated in the figure.

Table 12: Peak widths and chemical shifts of fluorine labeled cysteines in rhodopsin at different

temperatures

Chemical shifts are obtained after aligning spectra to TFA.

(°C)	Peak 1 (ppm)	Peak 2 (ppm)	Peak 1 width (Hz)	Peak 2 width (Hz)
10	-215.253	-217.335	109.53	86.6
15	-215.168	-217.26	84.862	72.617
25	-215.053	-217.122	51.68	62.414
37	-214.926	-216.873	33.456	45.95
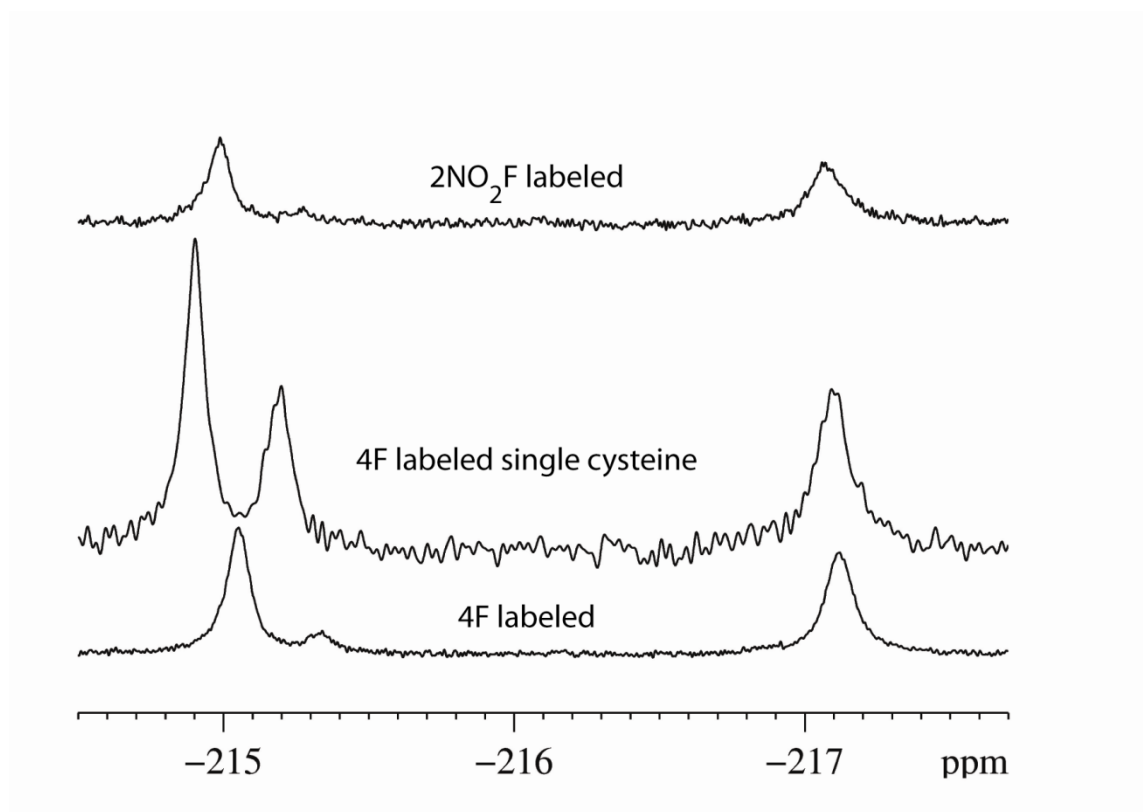
Figure 63: 1D ^{19}F NMR spectra of rhodopsin labeled with 4F and 2NO2F

Overlay of 1D ^{19}F NMR spectra of rhodopsin labeled with 4F (4F labeled), 4F after selectively labeling C140 with 4-PDS (4F labeled single cysteine) and 2NO2F (2NO2F labeled). Chemical shift of all spectra are aligned to that of TFA. 256 scans were collected for each spectrum. Peak intensities are not comparable since each sample has a different concentration of rhodopsin.

7.7.1.1 Effect of detergent concentrations

The effect of two different concentrations of detergent, DM, on 1D ^{19}F spectrum of 4F labeled rhodopsin was tested to determine the sensitivity of the 4F label towards changes in environment. 4F labeled rhodopsin used for NMR experiments described above contained 3.6% DM. We tested the effect of 9% DM added in different manner. 9% DM was selected because of reasons discussed in Section 7.7.1.3. In brief, I wanted to compare the signal to noise ratio of 4F labeled rhodopsin with that of TET labeled rhodopsin, the latter contained 9% DM. DM in 4F

215

labeled sample was increased to 9% by adding DM to increase the net concentration to 9%. The peak at -215 ppm remained unchanged (Figure 64.A.). However, the peak at -217.1 ppm decreased in intensity significantly in the sample compared to the sample containing 3.6% DM. This led me to test another sample in which DM concentration was increased to 9% in a different way, i.e. by concentrating the existing sample and then diluting it with NMR buffer so that final DM concentration is 9%. This was done so that the DM concentration was at least comparable even though not exactly the same. The sample preparation condition differed, however. TET labeled samples are preared such that elution fractions of rhodopsin were concentrated and a final DM concentration of 9% was achieved. The 1D spectrum of the 9% DM added sample showed a broad peak split into two with unequal intensities. One peak appeared at -215 ppm and a low intense broad peak appeared at -217.1 ppm compared to the 4F labeled sample containing 3.6% DM (Figure 64.A.). However, these large differences in peak shape of 4F labeled cysteines suggest that the environment of fluorine atoms attached to the cysteine groups is very sensitive to the DM concentration and the way of DM addition.

7.7.1.2 Changes with temperature

Changes in chemical shifts and peak intensities of 4F labeled rhodopsin with temperature are discussed in Section 7.7.1 where both these spectral parameters were observed to change with temperature. Further, the temperature dependence of samples containing different detergent concentrations was measured as shown in Figure 64.C. and D. to detect changes in peak shape and find a possible explanation for the spectra that were obtained at high DM concentration (see Section 7.7.1.1. above). The sample where DM was added to increase its concentration to 9% showed three peaks at -215, -216.2 and -217.4 ppm at 5°C with the latter two peaks decreasing in intensity with increase in temperature merging to appear as one peak at -216.6 ppm at 37°C and

simultaneously the peak at -215 ppm increases in intensity with increase in temperature and finally splits to appear as a doublet at 37°C (Figure 64.C.). This shows that the peaks at -215 ppm and -217 ppm have different degrees of flexibility at different temperatures. For the sample which was concentrated so that final the DM concentration was 9%, two peaks at -215.1 and -217.3 ppm and a very small peak at -216.3 ppm appeared at 15°C as shown in Figure 64.D. With increase in temperature, the peak at -217.3 ppm shifted downfield and increased slightly in intensity. The small peak at -216.3 ppm disappeared and the peak at -215.1 ppm bifurcated into a two peaks of unequal intensity with increase in temperature from 15°C to 37°C.

The reasons for the changes observed here are not clear. The assignment of the peaks to the two cysteines and hence their differential behavior under different conditions of detergent and temperature are discussed in Section 7.9. These results show that the 4F label is very sensitive to sample preparation details and temperature changes. Due to the absence of two discrete peaks in 4F labeled sample at high DM concentrations, the sample containing 3.6% DM was used for relaxation rate measurements.

7.7.1.3 Comparison with TET labeled sample

As described in Section 7.1, one of the aims of using 4F as a label was to compare the signal to noise ratio of 4F labeled rhodopsin with that of TET labeled rhodopsin to determine which label would be better for use. TET labeled rhodopsin was prepared and tested in our lab earlier by Naveena Yanamala. However, note that the sample conditions such as rhodopsin and DM concentrations were different from the 4F labeled sample described here. The latter sample contained 0.7 mM of rhodopsin and 3.6 % DM whereas the previous TET labeled sample contained 0.6 mM rhodopsin and 9% DM. Therefore, DM in 4F labeled sample was increased in ways discussed in Section 7.7.1.1. so that the same rhodopsin and DM concetrations are obtained

as that of TET labeled sample to decrease the influence of differences in DM concentration on comparison of signal intensities. However, due to the absence of two discrete peaks corresponding to two cysteines in high DM containing 4F labeled samples (Section 7.7.1.1.), lack of signal assignment and dissimilarities in sample preparations with TET labeled rhodopsin, signal to noise ratios of 4F labeled sample could not be compared to that of TET labeled rhodopsin.

A significant dependence on detergent concentration as seen in 4F labeled sample was not seen in the case of TET labeled rhodopsin as reported previously (Figure 64.B.) (Klein-Seetharaman et al., 1999a). Only small changes in chemical shift were observed in TET labeled rhodopsin with change in detergent type or concentration (Figure 64.B.). Further, TET labeled rhodopsin did not show significant changes in chemical shift, unlike that observed with 4F, with change in temperature (Figure 65.A.) (unpublished data from Naveena Yanamala). These comparisons show that 4F is much more sensitive to environmental changes than TET and hence can be used as a sensitive reporter of conformational changes in proteins. 4F also showed a larger chemical dispersion of 4F labeled cysteines compared to TET as shown in Figure 65.B. The two cysteine peaks in 4F labeled sample are seprated by more than 2 ppm whereas in TET labeled the separation is only 0.5 ppm. This is useful in detecting conformational changes as they will be better resolved on the spectrum. However, in these comparisons of 4F and TET, it should be kept in mind that the DM concentrations are different and hence may be reflected in the difference in spectral properties. This is especially beneficial when dark and light activated species or different denatured species are present in the sample.
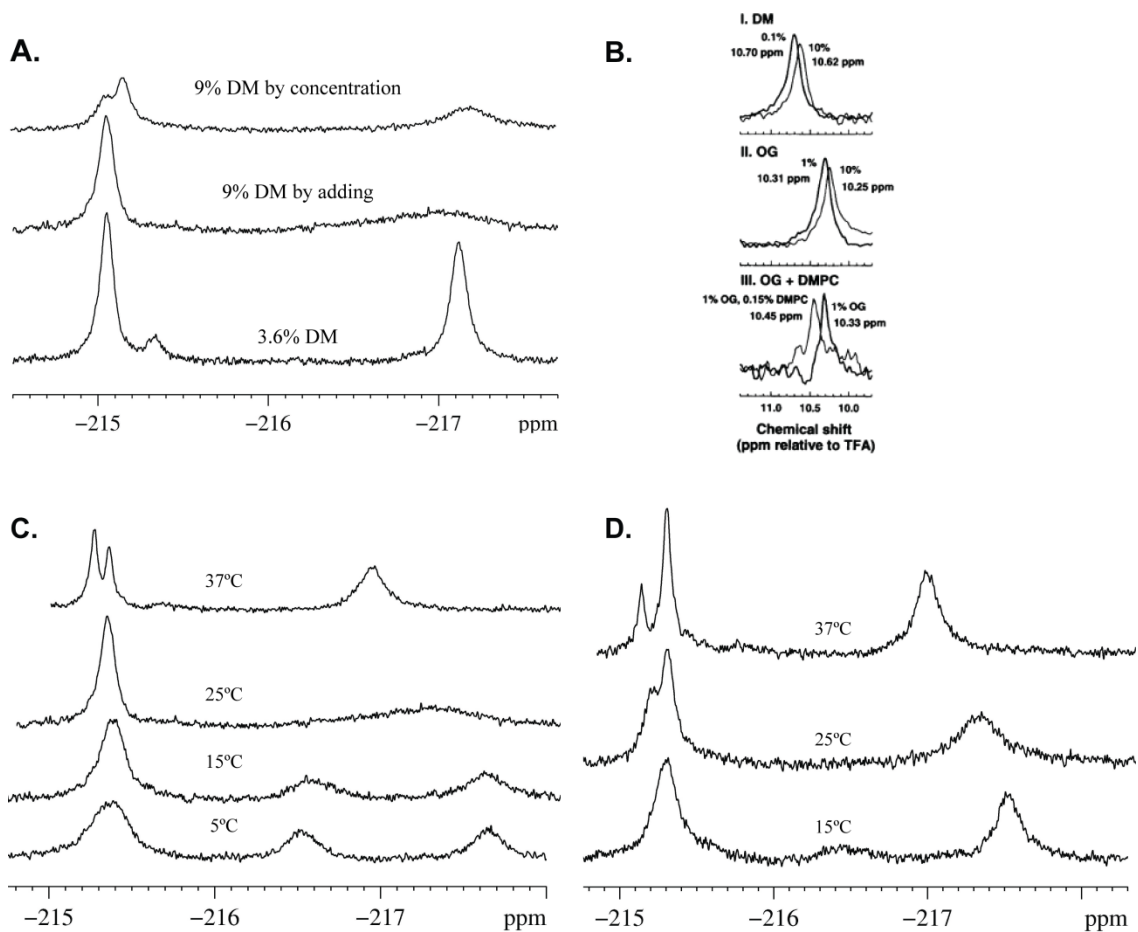
Figure 64: 1D ^{19}F NMR spectra of 4F labeled rhodopsin at different DM concentrations and temperature

A. Overlay of 1D ^{19}F NMR spectra of 4F labeled rhodopsin at different DM concentrations, B. Dependence of chemical shift of TET labeled rhodopsin on different detergents at different concetrations, figure taken from (Klein-Seetharaman et al., 1999a) C. Overlay of 1D ^{19}F NMR spectra of 4F labeled rhodopsin where DM has been added to increase its concentration to 9% at different temperatures and D. Overlay of 1D ^{19}F NMR spectra of 4F labeled rhodopsin where DM concentration was increased by concentrating the original NMR sample that contained 3.6% DM at different temperatures. Spectra in each overlay are aligned relative to the chemical shift of TFA. 256 scans were collected for all spectra.
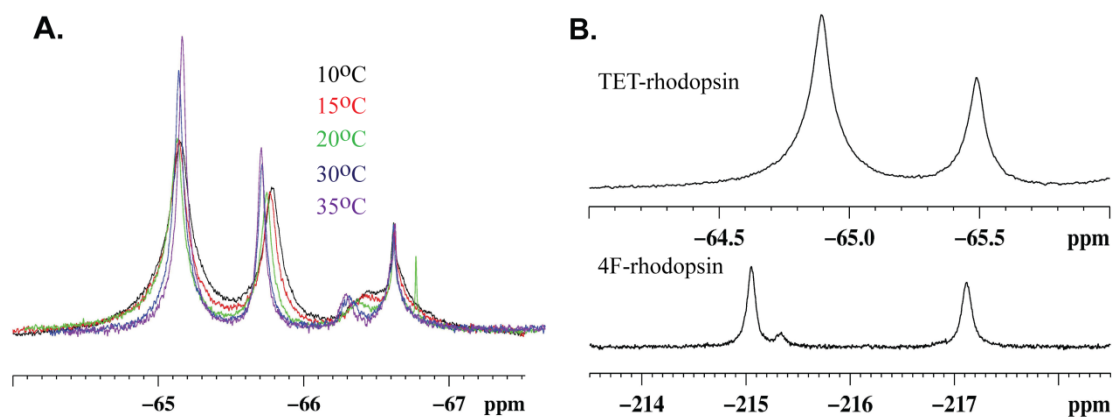
Figure 65: 1D ^{19}F NMR spectra of TET labeled rhodopsin

A. Overlay of 1D spectra of TET labeled rhodopsin at different temperatures (data from Naveena Yanamala). All spectra are aligned to the chemical shift of a contaminant peak at -66.6 ppm. B. Comparison of 1D 19F spectra of TET labeled rhodopsin (10k scans) and 4F labeled rhodopsin (256 scans). Spectral chemical shifts or intensities are not aligned to TFA.

7.7.2   Rhodopsin labeled with 2NO2F label

Efforts to assign cysteine peaks observed in the 1D spectrum of 4F labeled rhodopsin by selectively labeling one cysteine showed more than the expected single peak (discussed in Section 7.7.1.) and hence assignment could not be done with certainty. Here, 2NO2F was used to label single cysteine in rhodopsin. Due to the differential reactivity of different fluorine labels as shown in Section 7.3., 2NO2F had shown labeling of one cysteine in a small-scale experiment (see Section 7.3.4.). We studied this sample with the aim of assigning cysteine peaks. 0.2 mM 2NO2F labeled rhodopsin containing 2.14% DM was prepared. 1D spectrum of this sample is shown in Figure 63. The spectrum shows two equally intense peaks at the same positions as that of the two peaks seen in 4F labeled rhodopsin sample instead of the expected single peak corresponding to a single labeled cysteine. The line widths and chemical shift values are

220

provided in Table 13. Despite the small experiment showing labeling of one only cysteine, the appearance of two peaks in the NMR sample indicates labeling of both cysteines, C140 and C316, which are accessible in the dark state of rhodopsin. Therefore, assignment of cysteines could not be carried out by 2NO2F labeling.

Table 13: Peak widths and chemical shifts of 2NO2F labeled rhodopsin at different temperatures

Chemical shifts are obtained after aligning spectra to TFA chemical shift.

Sample	(°C)	Peak (ppm)		Peak width (Hz)	
2NO2F labeled rhodopsin	25	Peak 1	Peak 2	Peak 1	Peak 2
		-215.1	-217.129	54.14	75.569

7.8   RELAXATION MEASUREMENT OF 4F LABELED RHODOPSIN

4F labeled rhodopsin showed two peaks with high signal intensity corresponding to the two cysteines, C140 and C316, relaxation rates of the cysteines derivatized with 4F were measured. T_1 and T_2 relaxation experiments were carried out at different temperatures of 10°C, 15°C, 25°C and 37°C using different pulse sequences. As described in Section 2.3.12.3. in Chapter 2, different pulse programs were used to measure relaxation rates to understand the mechanism of relaxation of 4F label. R_{2disp} was measured to determine the effect of chemical exchange on transverse relaxation. If such effects exist then R_{2disp} values will depend on the pulse spacing in each constant time CPMG interval. $R_{1\rho}$ experiments were carried out to detect chemical exchanges occurring at a faster rate than that detected by R_{2disp}. In $R_{1\rho}$, a different magnetic field perpendicular and much weaker than the external magnetic field is applied and recovery of

magnetization along the former field is measured. Difference of $R_{1\rho}$ value from R_2 CPMG value will indicate exchange contributions.

For both peaks 1 and 2, R_2 values obtained from different experiments decreased with increase in temperature which was expected due to increase in flexibility with increase in temperature. Further, R_2 values across different pulse programs used at each temperature for each cysteine peak were similar to each other indicating that effects such as chemical exchange and F-H coupling may not contribute to relaxation mechanism of 4F derivatized cysteines. These values are given in Table 21 in Appendix A. A T_2disp experiment showing a decay of transverse magnetization at 10°C is shown for peak 1 in Figure 66 as an example. A similar curve is seen for peak 2. These curves did not show any dependence of transverse magnetization on the delays between pulses in the constant time CPMG interval at any temperatures indicating that chemical exchange is not contributing to this relaxation process under the conditions tested. Similar decay curves were obtained at the other temperatures and hence are not shown. At low temperatures of 10°C and 15°C, it is observed that peak 1 relaxes slightly faster than peak 2. However, at 37°C this trend reverses with peak 2 relaxing slower than peak 1. The transition occurs at 25°C where the R_2 of the two peaks become similar to each other. Figure 67 shows the plot of ln R_2 with the inverse of temperature showing this variation of R_2 of the two cysteines with temperature. The same trend in R_2 values for the two peaks was observed at both low and high temperatures when T_2 CPMG and $T_{1\rho}$ experiments were carried out. These decay curves showed a monoexponential decay. Dispersion experiments were also carried out in presence and absence of ^{1}H decoupling after acquisition to determine the effect of dipolar coupling on relaxation. The rates obtained in both these cases were not significantly different indicating that coupling contributions may not exist. Longitudinal relaxation rates (R_1) were also measured at different temperatures and the

rates are tabulated in Table 22 in Appendix A. Inversion recovery with protein decoupling was measured to calculate R_1 values.
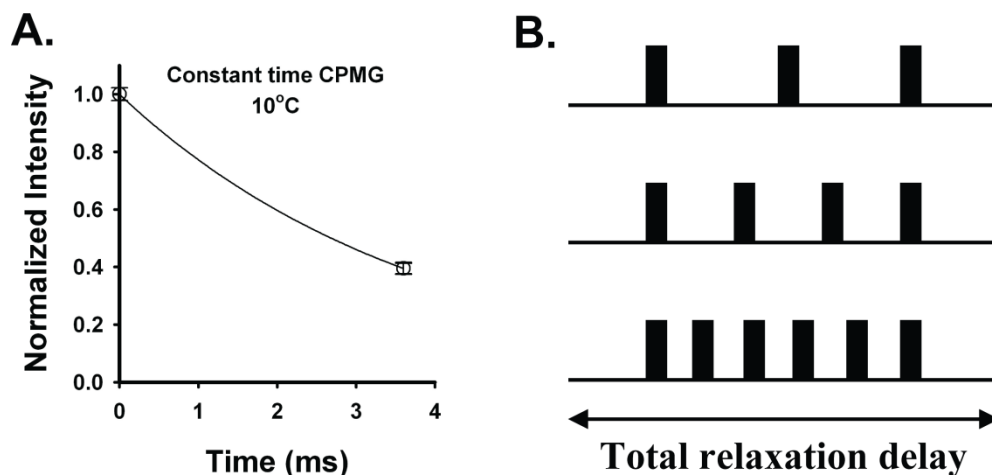
Figure 66: Constant-time CPMG relaxation of 4F labeled rhodopsin

A. Plot showing decay of transverse magnetization after a constant relaxation delay of 3.6 ms of 4F labeled rhodopsin at 10°C. Four experiments were done with the number of pulses increasing each time after every experiment. All the four decay curves are fit to a monoexponential equation. B. An example of constant-time CPMG pulse program used is shown in which the number of 180° pulses (shown as black bars) increases with every experiment within a fixed total relaxation delay.
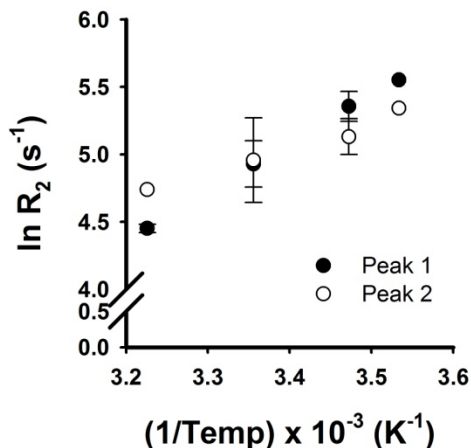
Figure 67: Dependence of R_2 on temperature of 4F labeled rhodopsin

Plot showing dependence of R_2 on temperature for the peaks 1 and 2 corresponding to the two cysteines, C140 and C316, of 4F labeled rhodopsin.

7.9   DISCUSSION

Characterizing dynamics of MPs has lagged behind that of soluble proteins due to challenges faced in using conventional spectroscopic methods (discussed in Section 7.1.). We have strengthened the existing method of ^{19}F NMR spectroscopy which has been so far used to detect conformational changes of rhodopsin to enable its application in quantification of site-specific dynamics of MPs. This has been done by testing novel fluorine labels with properties that may be more effective in measuring dynamics compared to that in the existing TET label. I have tested two kinds of labels, one that is directly attached to the sulphur atom of a cysteine and the other that attaches a single fluorine atom instead of three fluorine atoms as in TET.

7.9.1   Smaller label than TET

I tested labeling efficiency of the trifluoro label, CF3I, which derivatizes rhodopsin with –CF$_3$ instead of the –CH$_2$-CF$_3$ group. CF3I was tested with the aim to find a smaller label than TET so that perturbation in the environment of cysteines can be reduced. However, I found that CF3I labeling during purification interferes with elution of rhodopsin during purification from immunoaffinity column and also results in a broad peak in the NMR spectrum. Further characterization of the reaction of this label with free sulfydryl groups showed appearance of many peaks on the 1D spectrum raising doubts about the integrity of the reaction. I also found that the label degrades over time at room temperature. The paper that reported the synthesis and application of this label showed reaction with sulfydryl groups only at -78°C (Kieltsch et al., 2007), probably to prevent degradation of the label apart from preventing oxidation of sulfydryl groups. However, this temperature is not practical for carrying out labeling of proteins and

determining their conformational changes which occur at physiological temperatures of 37°C. Therefore, CF3I cannot be used as a fluorinating reagent for labeling proteins.

7.9.2 Monofluoro labels

Monofluoro labels 2F, 4F and 2NO2F were tested for labeling cysteines and labels free in solution and after labelig rhodopsin were characterized by NMR. The aim was to find a label containing a single fluorine atom, as opposed to three fluorine atoms in TET, since dynamics calculation of residues derivatized with a single fluorine by relxation rate measurements will be less complicated compared to labels with three fluorine atoms. Two trifluoro compounds, 4F3 and 2NO2F3, which are structurally analogous to the monofluroro reagents except for the number of fluorine atoms were also characterized by NMR to compare their motional properties with that of the monofluoro labels.

I analyzed labeling efficiency of three monofluoro reagents, 2F, 4F and 2NO2F, which were observed to label 0, 2, and 1 cysteine(s) respectively among the two free cysteines in native rhodopsin. 2F label did not derivatize cysteine residues and hence was not used for further characterization. NMR spectroscopy was used to obtain 1D spectral properties of free 4F and 2NO2F labels in solution. 4F also showed advantage for use as a probe to determine motion of specific residues by measuring their relaxation rates by ^{19}F NMR since it showed more retention of signal when compared to trifluoro labels in a slow molecular tumbling limit when measured free in glycerol solution. When labeled to rhodopsin, 4F labeled cysteines appeared as sharp peaks that were sensitive to temperature and detergent concentration and also to the way detergent was added. Such a sensitivity of a label to detergent environment was not observed with the previously used label, TET (Klein-Seetharaman et al., 1999a). 4F also showed larger

chemical shift dispersion for the two labeled cysteines in rhodopsin than TET. These properties indicate the advantages of using 4F as a label.

It was not possible to assign the peaks corresponding to fluorine labeled cysteines in rhodopsin. This is because 2NO2F labeling, which due to its differential reactivity showed labeling of one cysteine in a small scale experiment, showed two peaks on the 1D NMR spectrum. Moreover, selective labeling of one cysteine with 4F by blocking the other free cysteine with 4-PDS showed three peaks. Labeling of C140 apart from C316 with 4F is due to incomplete blocking of C140 with 4-PDS. Based on changes in peak intensities and chemical shifts with change in temperature and DM, I can speculate and assign the changes to particular cysteines. C140 is at the cytoplasmic end of helix 3 and C316 is in helix 8 which is parallel to the membrane. Assuming selective single cysteine labeling by 4F (C140 blocked by 4-PDS) to have labeled C316, peak 1, which shows greater intensity than peak 2, can be assigned to C316. This assignment fits with with the temperature changes seen for peak 1 where an increase in intensity of peak 1 was seen with increase in temperature. It has been shown by EPR and fluorescence depolarization studies that C316 is more mobile that C140 (Resek et al., 1993; Mielke et al., 2002) and hence its flexibility is expected to increase with increase in temperature, as is observed here for peak 1. Peak 2 does not show significant changes in intensity with increase in temperature. This behavior fits with C140 since it is more buried in the membrane than C316 and hence shows smaller changes in flexibility with temperature. In presence of higher concentrations of DM added in different ways, differential behavior is seen by these two peaks. This is expected since both the cysteines being probed are at the membrane-water interface and hence their motions are prone to be effected by even slight changes in micellar environment. These slight changes, detected by the 4F label, are discussed below.

226

Peak 2, tentatively assigned to C140, shows chemical exchange with increase in temperature which could arise due to conformational changes in the loop surrounding C140 or end of helix 3 that affects the environment of C140. Such an exchange phenomenon is seen in both the samples where DM concentration was increased in a different way. Changes in Peak 1 with temperature indicate presence of a different conformation as temperature is increased, thus giving rise to a split peak. This has also been seen in both the samples where DM concentration was increased in a different way. This could be due to the interaction of helix 8 with the surrounding micelle environment thereby giving rise to a different conformation at higher temperature. Further, differential temperature dependence of relaxation rate of the two cysteines show that motional differences exist in different regions of the cytoplasmic domain of rhodopsin. At low temperatures, the higher relaxation rate of peak 1 shows that it is surrounded by tertiary interactions which hinder its motion but with increase in temperature its lower relaxation rate indicates that it positions itself in a more flexible region compared to peak 2. This correlates with the assignment above of peak 1 being C316 and peak 2 being C140. Therefore, we have established that 4F can be used as a sensitive fluorine probe to detect conformational changes of MPs and also to quantify their dynamics.

7.10   SUMMARY OF CONTRIBUTIONS

I have established the use of novel monofluoro labels to enable quantification of site-specific dynamics of MPs by ^{19}F NMR spectroscopy. Such analyses were lacking for MPs since it was complicated to derive motional parameters for the commonly used trifluoro label by NMR. We have systematically carried out tests determining labeling efficiency of three monofluoro labels

and characterized their spectral properties and relaxation rates both free in solution and after labeling rhodopsin by ^{19}F NMR spectroscopy. The relaxation rates of free monofluoro labels were compared to structurally analogous trifluoro labels and were found to be advantageous for carrying out relaxation measurements with labeled proteins. This is due to thelonger retention of signals in the former label during relaxation measurements. I have shown that 4F is a suitable label for labeling both the free cysteines in rhodopsin. This is due to high signal to noise ratio, large chemical dispersion, strong sensitivity to small changes in environment and ease of a simplified model to explain motion of specific residues by means of relaxation rate measurements of the 4F label.

8.0   CHAPTER 8: DETECTION OF GLOBAL MOTIONS BY TERAHERTZ SPECTROSCOPY

8.1   RATIONALE AND SUMMARY

As discussed in Section 7.1., conventional methods for characterizing motion of proteins such as by NMR and EPR spectroscopy suffer from many limitations when applied to MPs. Low signal to noise ratio, difficulties in introducing probes and obtaining only qualitative information on dynamics are the main challenges. Therefore, I have investgated the applicability of a bulk method of THz spectroscopy, to characterize motions in MPs. THz spectroscopy investigates motions that lie in the the far infrared region of the electromagnetic spectrum spanning 1-200 cm^{-1}. Motions of large groups of atoms that occur in concert lie in this spectral region (Brooks et al., 1988; Hayward and Go, 1995). Frequencies in the THz region are believed to be important for determining mechanisms that trigger conformational changes in proteins (Jaaskelainen et al., 1998; Tama et al., 2000; Tama and Sanejouand, 2001; Knab et al., 2006). Commonly used methods to chafracterize low frequency vibrational motion of proteins are neutron scattering, far-infra red absorbance spectroscopy, THz spectroscopy, and normal mode analyses. However, for MPs, none of these methods have so far provided a detailed characterization of motions in different conformations. I have developed the use of THz spectroscopy to obtain information on global dynamics for MPs.

I have taken rhodopsin as a model system and characterized its dynamics in the THz region in the dark and light activated states. I have shown that this method provides high signal to noise ratio with sub micromolar concentrations of protein and along with spectral simulation techniques provides information on rapid motions in the timescales of picosecond to sub-picosecond. Such motions are believed to contribute to conformational changes important in protein function. These are vibrational motions that fall into two categories: high frequency vibrational motions that correspond to localized motions in proteins and low frequency vibrational motions that relate to global collective vibrational motions involving the entire protein.

8.2   THZ SPECTRA OF RHODOPSIN IN DARK AND LIGHT ACTIVATED STATES

THz spectra of rhodopsin were recorded in the dark (R) and after photobleaching (R*) to assess and compare dynamics of different structural regions in these two states. Peaks in the lower wavenumber region (40-90 cm^{-1}) represent vibrational modes on a global scale, i.e. of the entire protein and peaks in the higher wavenumber (90-175 cm^{-1}), apart from global motions, also provides information on vibrational fluctuations of specific types of amino acids. Molecular dynamics (MD) simulations using crystal structures of R (PDB ID: 1L9H) and R* (PDB ID: 3CAP) were also carried out and compared to predicted changes in the spectra to determine the regions on the protein that correspond to peaks observed on the spectrum.

8.2.1   THz region 40-90 cm^{-1}

Overlay of THz spectra of R and R* in the region 40-90 cm^{-1} is shown in Figure 68.A. Spectrum of R* shows a peak at 85 cm^{-1} which is indicative of side chain motions of nonpolar amino acids and also changes in H-bonds (Woods, 2010). This peak is absent in R. MD simulations indicate that this peak has contributions from H3 and E1 regions of R*. Moving to the lower frequency region in the spectrum, a peak at 70 cm^{-1} appears in the R spectrum but is absent in the R* spectrum. This peak corresponds to out of plane backbone modes coupled with side chain fluctuations (Woods, 2010). Further characterization of this peak was carried out to determine if the peak arises from backbone or side chain motions. This was done by recording the same spectrum of R as a function of temperature and hydration (data not shown). The increase in intensity of the 70 cm^{-1} peak at lower temperature (-180°C) and hydration (75% relative humidity) indicates that this peak arises from backbone motions (Woods, 2010). These are torsional motions and are contributed by E1, H3 and H6 (very small contribution) regions in R and C1 and C2 in R* as obtained from MD simulations. Another spectral change was seen at an even lower frequency of 63 cm^{-1}. This region depicts motions of basic amino acid side chain atoms such as Arg (Woods, 2010). From MD simulations, the main region in R responsible for this motion is predicted to be C2 (R147). H4 may also have a small contribution. In R*, there is slight shift of this peak to a higher frequency indicating damped side chain fluctuations or decreased mobility of these modes upon light activation. Further, there is a peak, at 57 cm^{-1}, which appears in R spectrum and is absent on the R* spectrum. This peak arises from backbone torsional motions (Woods, 2010). Motions in H5 are mainly responsible for this peak on the R spectrum with minor contributions from H2 and H3. For R*, mainly H1 motions and slight H5 motions are observed in simulations.
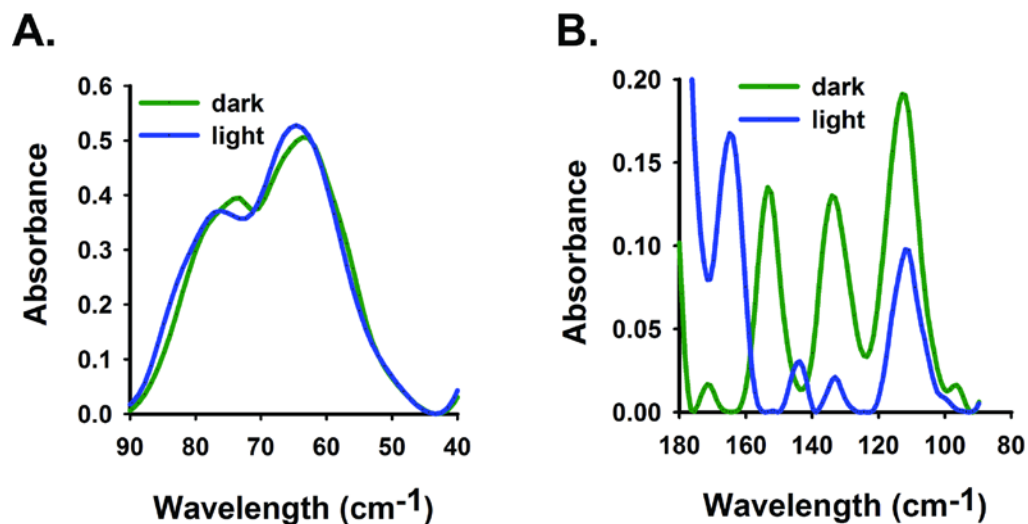
Figure 68: THz spectra of rhodopsin

THz spectra of rhodopsin at room temperature at different wave number regions: A. 40-90 cm^{-1}, B. 90-170 cm^{-1}.

8.2.2   THz region 90-175 cm^{-1}

From the low frequency region of the THz spectrum, we now move to the high frequency domain, i.e. from 90-175 cm^{-1}. Overlay of R and R* spectra within this range are shown in Figure 68.B. R shows a peak at 153 cm^{-1} which shifts to a higher frequency peak at 164 cm^{-1} upon bleaching. Peak at 153 cm^{-1} indicate side chain torsional motions of Phe (Woods, 2010). In R, H2 and H7 are mainly responsible for this peak as seen in simulations. The Phe residues in H2 are predicted to be F85, F88 and F91 and those in H7 are F287, F293 and F294. Minor contributions are from E1 (F103, F105), E2 (no F), H1 (F45, F52, F56) and H6 (F261, F273, F276) from simulations. In R*, shift of this peak to a higher frequency at 164 cm^{-1} indicates damping of Phe motions due to a twisting motion. From MD simulations, the regions corresponding to this peak were predicted to be H1, H2, H5 (F203, F208, F212, F220, F221) and

H6. The next peak that appears in the overlay is at 145 cm^{-1} in the R* spectrum which is absent in the R spectrum (Woods, 2010). The 145 cm^{-1} peak represents backbone motions of nonpolar amino acids and arises mainly from Ala residues in H2 (A80, A82) and H3 (A117, A124, A132) as seen from MD simulations. A peak at 135 cm^{-1} is observed in the R spectrum which indicates side chain motions of nonpolar amino acids (Woods, 2010) and mainly arises from H4 helix in R as obtained from simulations. Motions in H3, H6, E2 and C3 are responsible for this peak to a small extent. This peak shifts to a lower frequency of 130 cm^{-1} in R* and shows a much lesser intensity. The shift in the peak indicates movement of atoms to a polar environment. The regions corresponding to the vibrational motion at 130 cm^{-1} in R* are H4, H3 and H1 where H4 has the the main contribution to this motion as predicted by simulations. Another peak at 110 cm^{-1} appears in the R spectrum arising mainly from Ala residues in H4 as obtained from simulations. Ala residues in H4 are A153, A158, A164, A166, A168 and A169. This peak is commonly seen in different proteins and arises from backbone motions (Woods, 2010). Motions of other regions that correspond to this peak are small motions in E2, C3 and H6 from simulations. In R*, a peak at similar position, at 110 cm^{-1}, is observed but is at a lesser intensity than that in the R spectrum. The regions which show this backbone motion in R* are E1 and C1 from simulations. The last peak in the high frequency THz region appears at 96 cm^{-1} in the spectrum of R and this peak represents backbone fluctuations of basic amino acids. Such fluctuations arise from H1 (H65) and H3 (R135) regions in R according to simulations. This peak shows a very small shoulder in R* and the corresponding regions emerging from simulations are E2 and H2.

8.2.3   Overall helix and loop motions

From MD simulations, changes in overall motions in each helix and loop and their effect on THz spectra were predicted. Major changes in helix motions upon light activation are seen in helices H4 and H6 from simulations. Minor changes are seen in H1 and almost no changes are detected in the rest of the helices. Spectra showing changes in H4 in R and R* states are overlaid in Figure 69.A. Changes in H4 motions in R shows as a peak at 110 cm^{-1} which was also seen in the experimental spectrum where it represented backbone motions particularly of Ala residues in H4 (see Figure 68.B.). This peak shifts to 130 cm^{-1} upon light activation as shown in the simulated spectrum. This high frequency shift indicates that the side chain atoms of Ala in H4 corresponding to this motion experience a polar environment in R*. This correlates with the 130 cm^{-1} peak that was seen upon light activation in the experimental spectrum in Figure 68.B. and was believed to arise from H4 helix based on simulations. A similar shift of 110 cm^{-1} peak to 130 cm^{-1} peak upon bleaching was also seen for H6 helix as shown in Figure 68.B. However, simulations based on experimental spectra did not show contribution of H6 in motions detected at 130 cm^{-1} in R* but detected a small contribution of H6 in the motions corresponding to 110 cm^{-1} in R. Another peak of interest is 153 cm^{-1} that arises in the simulation spectra of R for all helices except H3 and H4. This peak, as discussed before, arises from side chain torsional motion of Phe residues and also appears in the experimental spectrum of R and is predicted to arise from H1, H2, H6 and H7 helices (Figure 66.B.). In the light activated state, this peak shifts for H1, H5 and H6 but does not shift for H2 and H7. Change in solvent accessible surface area (SAS) upon light activation was also determined from MD simulations. H6 is found to have a greater SAS in R* compared to R with mostly the hydrophobic regions becoming solvent exposed. H4 shows a small increase in SAS in R*.

234
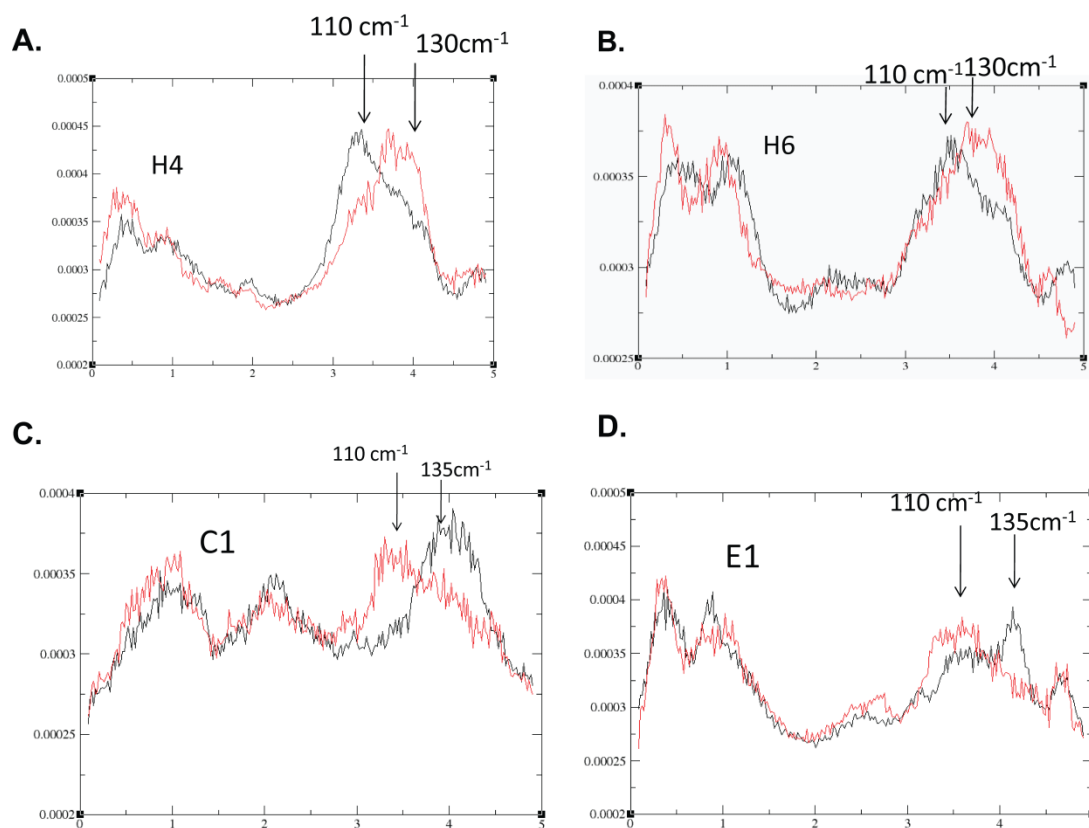
Figure 69: THz spectra from MD simulations, helix and loops

Dark state is shown in black spectrum and light state in red. H, C and E stand for helix, cytoplasmic loop and extracellular loop respectively.

Considering motion of the loop regions, we find significant changes in C1 and E1 upon light activation with almost no changes in the remaining loops. Changes in spectra of R and R* for C1 and E1 loops are shown in Figures 69.C. and 69.D. R spectra of both C1 (P71, L68) and E1 (G101, V104) show a peak at 135 cm^{-1} indicating side chain motions of nonpolar amino acids. However, L68 has been shown to fold into the protein and remain solvent inaccessible from biochemical studies. This peak shifts to 110 cm^{-1} in R* for both C1 and E1 indicating methyl group motions due to interaction of hydration molecules with backbone atoms in these regions. C1 and E1 also appear in simulations of the experimental spectrum of R* at 110 cm^{-1}.

235

Based on the simulations, C2 is found to be solvent exposed with increased motion of Phe side chains (F146, F148). Small motions in C3 are observed on THz experimental spectra as peaks at 135 cm^{-1} corresponding to nonpolar side chain motions and at 110 cm^{-1} corresponding to backbone motion. The 153 cm^{-1} peak which appears in spectra of all helices except H3 and H4 appears in the spectra of E1 (F103, F105), E2 (no F), E3 (F283) and C2 (F146, F148) in R state. E1 shows small backbone motions as a 70 cm^{-1} peak. Simulations also predict motion of Phe side chains and that of nonpolar side chains (G101, V104) for E1. E2 shows small motions of nonpolar side chains and backbone motion. In the R* state, this peak disappears for E2. SAS analyses for loop regions indicate a very large decrease in SAS for E3 in the R* state.

8.2.4   Backbone and side chain motions

From MD simulations, changes in backbone and side chain motions were predicted. Changes in backbone motions upon light activation are mainly seen in H2, H5 and H6 helices. Overlays of spectra of R and R* for each of these helices are shown in Figure 70. H1, H3 and H4 do not show changes in motion upon bleaching. A 63 cm^{-1} peak, absent in R spectra, can be seen in the R* spectra of H2 and H5 a shown in Figures 70.A. and 70.B. respectively. This peak represents Cβ-O bending motions arising from intramolecular hydrogen bonding. This peak is also seen in the R* experimental spectrum (Figure 68.A.) but is shown to arise from C2 (mainly) and H4 from simulations unlike from H2 and H5 as is predicted here. Another significant change is seen in motions of H6, shown in Figure 70.C., where a dramatic shift occurs from 80 cm^{-1} in R to 60 cm^{-1} in R*. The 80 cm^{-1} peak arises from backbone torsional motions that are induced by intramolecular hydrogen bonding. The 60 cm^{-1} peak represents torsional motion involving Cα-O atoms which is usually for helices interacting with aqueous solvent indicating solvent exposure

of H6 helix upon light activation of rhodopsin. However, the opposite is seen in the experimental spectra, where 80 cm^{-1} peak is observed only in the light state and 60 cm^{-1} peak is observed only in the dark state of rhodopsin (Figure 68.A.).

Change in motions of side chain atoms in all the helices is seen by a shift of 135 cm^{-1} peak to 130 cm^{-1}. This indicates exposure of side chains to aqueous environment in R* states.
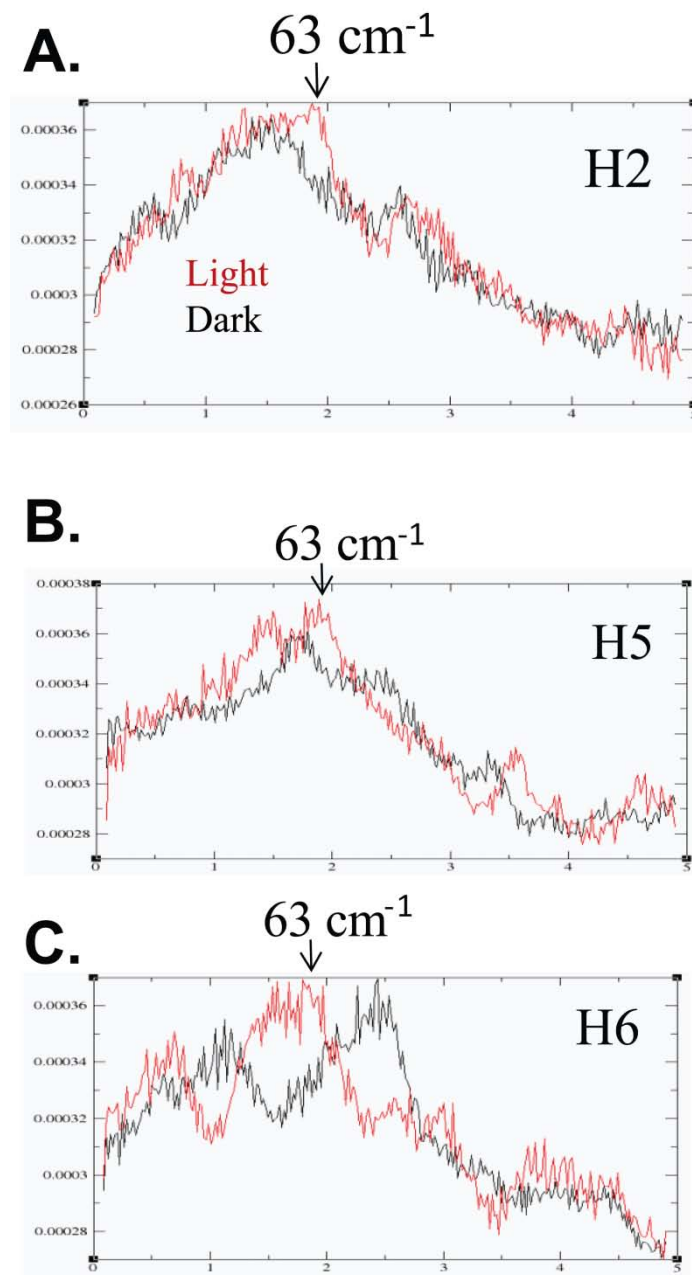
Figure 70: THz spectra from MD simulations, backbone and side chain

Dark state is shown in black spectrum and light state in red. H2, H5, H6 refer to helices 2,5 and 6 respectively.

8.2.5 Interhelical hydrogen bonds

MD simulations were used to predict changes in interhelical hydrogen bonds. Changes in hydrogen bonds among adjacent helices upon light activation are shown in Figure 71. The amount of intramolecular H-bonding is represented by the peak at 120 cm^{-1}. H-bonding is increased between H2 and H3 and H5 and H6 as shown by the increase in intensity of the peak at 120 cm^{-1} as shown in Figures 71.A. and 71.B. respectively. This correlates with the appearance of 63 cm^{-1} peak in the spectra of backbone motions of H2 and H5, which is a Cβ-O bending motion arising from intramolecular H-bonding (Figures 70A. and 70.B.). On the other hand, H-bonds between H1 and H2, H1 and H7, H4 and H5, H6 and H7 are reduced in R* as compared to R as shown in Figures 71.C, D, E and F. In the case of H3 and H4 interhelical H-bonding, there appears to be a correlation between intramolecular H-bonding and backbone motion of the helices that arises at 145 cm^{-1} (Figure 71.G.). This peak has also been seen in the experimental spectrum of R* (Figure 68.B.) and believed to arise from backbone motions of nonpolar residues, mainly from Ala residues in H2 and H3. This peak also appears in the backbone spectrum of the entire protein in the R* state indicating a significant contribution of this vibrational mode, arising from changes in intramolecular H bonding, to motions in the light activated state.
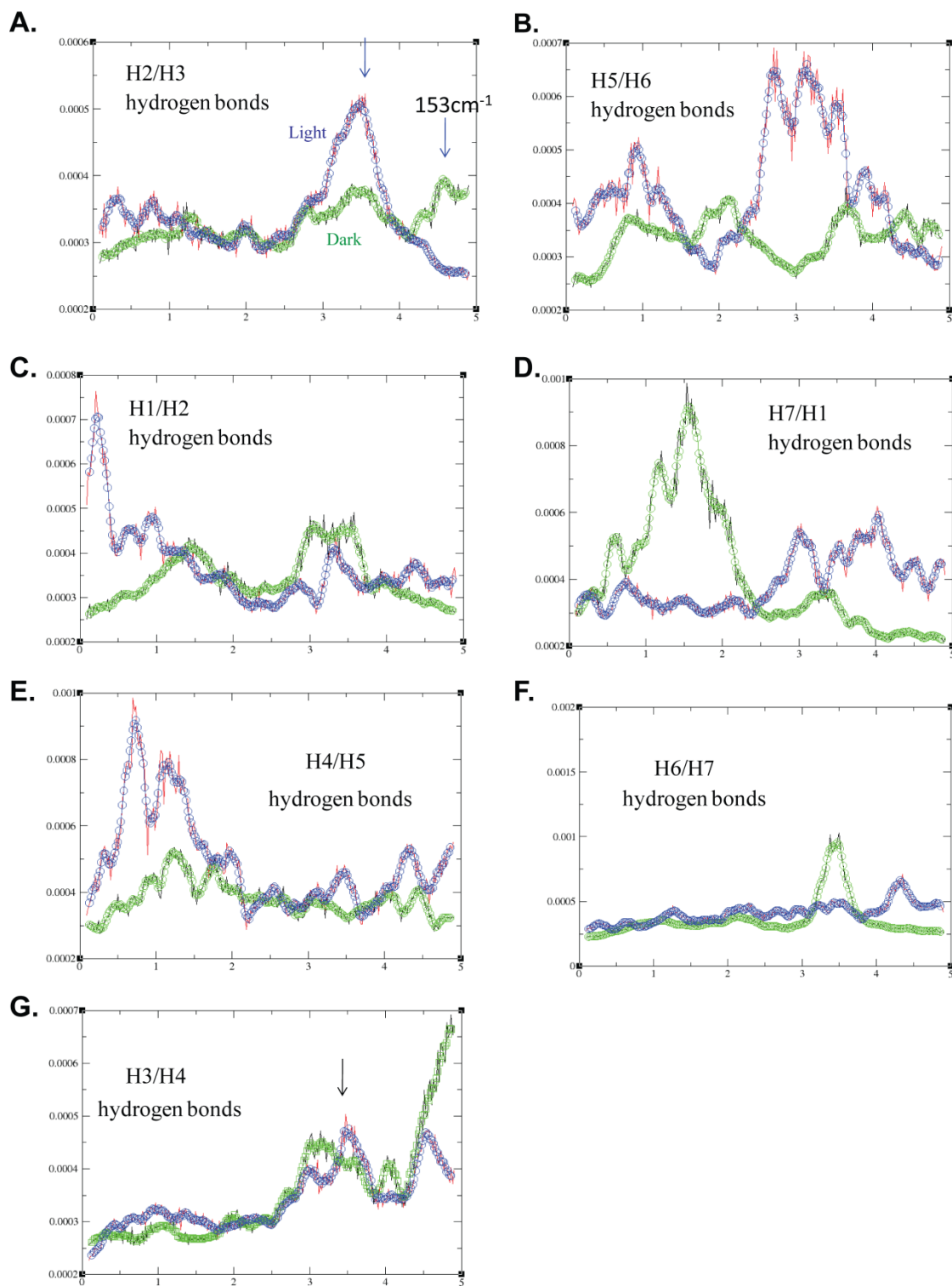
Figure 71: THz spectra from MD simulations, interhelical H-bonds

8.3   DISCUSSION

I have established the use of THz spectroscopy in obtaining information on collective vibrational motions of, rhodopsin as a model for MPs. I describe characterization of motions in rhodopsin in both its dark, inactive and active states. Several conformational characteristics were observed in the THz spectra of these states which corroborate with earlier biophysical and biochemical studies and also provide new insights into their motions.

8.3.1   Structural motions in the dark state of rhodopsin and comparison with previous studies

Crystal structures of the dark state of rhodopsin are available (Palczewski et al., 2000; Li et al., 2004; Okada et al., 2004), but not of the light-activated Meta-II state. Further, dynamic information is not quantitative from X-ray structures. NMR methods to study motions of large MPs are still at a development stage (see Chapter 5). Solution NMR studies with rhodopsin so far have shown line broadening due to conformational heterogeneity arising from µs-ms timescale fluctuations of backbone atoms thus making NMR analyses difficult (Klein-Seetharaman et al., 2002b; Klein-Seetharaman et al., 2004). Information on motions is largely deduced from EPR studies which have mainly focused on the CP ends of helices (Hubbell et al., 2003). THz spectroscopy is used here to gather more information on overall motions of helices and loops in the dark and light activated states of rhodopsin. I first disucss the dynamics observed in the dark state.

8.3.1.1 Helix motion

Overall flexibility of helices can be described by 153 cm^{-1} peak that appears both in the experimental spectrum and in MD simulations of rhodopsin. This peak is shown to arise from Phe side chain motion. H1, H2, H6 and H7 have this vibrational mode in the experimental spectra whereas all helices except for H3 and H4 show this mode in simulations. Phe residues are present in the center of the TM region in H1 and H2, mostly towards the EC end in H6 and H7 and in CP, TM and EC regions of H5. This shows that in the dark state TM and EC ends of most of the helices represented by Phe side chains are mobile which fits with the hypothesis that the dark state fluctuates among different conformations so that upon light activation it can find the right conformation fast since they are already flexible (Isin et al., 2006). This kind of motion has not been reported earlier due to the difficulties in perturbing the EC domain for its biophysical characterization (see Section 6.2. for discussion). Backbone motion of Arg in H3 (R135 of ERY motif) corresponding to 96 cm^{-1} peak has been detected. The ERY motif is highly conserved among GPCRs and is involved in an ionic lock interaction with H6 which preserves the dark state conformation (Teller et al., 2001). Flexibility of R135 in this motif could be advantageous when the bond in the ionic lock needs to be broken after light activation since the flexibility will make it easier to be broken. H4 also appears to be a flexible helix based on the appearance of 110 cm^{-1} peak in both experiments and simulations which denotes backbone motion of Ala residues in this helix. Further, motions in H4 are also seen by the peak at 135 cm^{-1} which arises from nonpolar side chain motion. CP end of H4 has been shown to be flexible based on EPR studies but overall helix motions are not yet reported (Farahbakhsh et al., 1995; Ridge et al., 1995c).

8.3.1.2 Loop motion

C1 loops show nonpolar side chain motions. Motions of side chains in C2, particularly those of Arg residues (R147) appear on the experimental spectrum. C2 is also found to be solvent exposed from simulations. The flexibility of C2 is in concordance with high mobility observed from crystal structure (Park et al., 2008; Scheerer et al., 2008) and high mobility and solvent accessibility of 146-148 amino acids from EPR studies (Farahbakhsh et al., 1995; Ridge et al., 1995c). C3 loop is the most flexible one compared to other CP loops, as evident from the incomplete crystal structure in this region (Palczewski et al., 2000; Li et al., 2004; Okada et al., 2004). High mobility is also observed for this loop from EPR studies especially for residues 232-245 and an increase in solvent accessibility is observed as well (Altenbach et al., 1996; Yang et al., 1996). The EC loops are characterized to a less extent. The experimental spectra predict very small motions in these loops. E1, E2 and E3 show small motions based on small motions of Phe side chains, backbone atoms and nonpolar side chains. This agrees well with the rigidity of EC loops observed in crystal structures of rhodopsin based on temperature factors (Palczewski et al., 2000; Li et al., 2004; Okada et al., 2004; Rader et al., 2004; Isin et al., 2006).

8.3.2 Structural changes in the light state of rhodopsin and comparison with previous studies

Until recently, information on conformational changes in rhodopsin after light activation was largely obtained from biochemical and EPR studies (Hubbell et al., 2003) and an ANM model of the MetaII state (Isin et al., 2006). These studies also provided information on the dynamics of different structural regions after photobleaching. The biochemical and EPR studies were mostly focused on changes in CP ends of transmembrane helices and CP loops since it is difficult to

introduce probes in the EC and TM domains for these studies without compromising stability of the protein. From these studies, mobility of H1, H2, H3, H6 and H7 was seen to increase upon light activation indicating reduced packing of the helical bundle (Farahbakhsh et al., 1993; Resek et al., 1993; Farahbakhsh et al., 1995; Yang et al., 1996; Altenbach et al., 1999). These studies also showed that the motion of H6 away from the helical bundle of rhodopsin is the main event that occurs after light activation (Altenbach et al., 1996; Hubbell et al., 2000). The remaining changes are not very large and are induced due to the motion of H6. These changes are mainly decreased mobility of H5, movement of H2 towards H4, movement of H7 and H3 away form the bundle and increased flexibility of C3 (Farahbakhsh et al., 1993; Resek et al., 1993; Farahbakhsh et al., 1995; Yang et al., 1996; Altenbach et al., 1999). However, the ANM structure of the light activated state predicts movement of H4 as a major structural change where large rigid body motions of H4 away from the bundle at the CP end stretching the C2 loop and thus exposing the ERY motif on H3 (Isin et al., 2006). The ANM structure also predicted larger motions in the CP side than the EC side with motions of the two ends being anti-correlated and a central region in the TM domain acting as a hinge. It also predicted a twisting or torsional motion for all the helices. Further, a movement of H1 and H2 away from H7 was seen. Very recently, opsin was crystallized in presence and absence of a peptide that corresponds to the carboxy terminus of α subunit of G-protein, believed to resemble the not yet experimentally determined light activated structure of rhodopsin (Park et al., 2008; Scheerer et al., 2008). Both crystal structures showed H6 tilted away from the helical bundle in concordance with the EPR results (Park et al., 2008; Scheerer et al., 2008). Additional significant changes that were seen in the crystal structures are movement of H5 such that it is parallel to H6, absence of ionic lock between H6 and H3 and formation of H-bond between residues in H6 participating in the ionic lock in dark state and H5.

Further, the crystal structure of opsin with the G-protein peptide bound to it shows a hydrophobic surface provided by the cytoplasmic ends of H5, H6, junction of H3 and C2 and L72 in C1 loop exposed for G-protein binding (Scheerer et al., 2008). However, these structures lack direct information on dynamics which is obtained by here THz spectroscopy.

8.3.2.1 Changes in helices

We attempted to provide structural characteristics, including information on dynamics, of all the three domains, CP, TM and EC, after light activation. Based on the THz experiments and simulations, H1, H4 and H6 show movements away from the helical bundle. H1 movement away from H7, based on reduced H-bonding with H7 and H2 from simulations, agrees with ANM studies (Isin et al., 2006). H7 movement away from H1 has been shown by EPR studies (Altenbach et al., 2001a). Motions of H4 showing movement of nonpolar side chains to face a polar environment are observed. This together with a small increase in solvent accessible surface area (SAS) upon photobleaching suggests motion of H4 away from the helical bundle. ANM model also shows H4 motion away from H3 at the CP end and towards the retinal at the EC end (Isin et al., 2006). The outward motion of H4 on light activation of rhodopsin is also seen in previous crosslinking studies where a large rigid body motion of H4 was observed whereby Ala169 in H4 which is 10A away from the ionone ring of retinal, which is towards the EC end, forms a crosslink with it after photoactivation (Borhan et al., 2000). This kind of rigid body motion of H4 causing its CP end to move away and the EC end to move closer to the retinal may be extrapolated from THz simulations in the following way. The simulations predicting a decrease in H4-H5 H-bonds on light activation and increase in SAS of H4 suggest changes in the position of H4 with respect to H5 which could be in the direction of bringing the EC end of H4 closer to retinal, thus agreeing with the biochemical results. H6 is also seen to move away from

the bundle based on these molecular dynamics simulations results. Firstly, appearance of a 130 cm^{-1} peak in the simulations suggests exposure of side chains of H6 to a polar environment which is also supported by an increase in SAS. Secondly, weakening of H-bonds between H6-H7 compared to the dark state and formation of H5-H6 H-bonds indicates motion of H6 away from H7 and towards H5. These findings can be correlated with the tilted position of H6 away from the helical bundle forming H-bonds with H5 in opsin crystal structures (Park et al., 2008; Scheerer et al., 2008) and motion of H6 away from H3 based on EPR studies (Altenbach et al., 1996; Hubbell et al., 2000). Based on both THz experiment and simulations, one common feature in all the helices is that they exhibit a twisting/ torsional motion which is also predicted by ANM in the light state (Isin et al., 2006) but it is not known whether the kind of motion is the same in both cases. Simulations show an increase in H2-H3 H-bonds and a decrease in H2-H1 H-bonds suggesting motion of H2 towards H3 which could also lead to movement of H2 away from H7 and towards H4 which have been reported by previous EPR studies (Altenbach et al., 1999) and ANM predictions (Isin et al., 2006). The increase in motion of Ala residues in H2 also supports the movement of H2 away from the helical bundle. The 96 cm^{-1} peak that is shown to arise from backbone motion of R135 in H3 disappears on light activation indicating loss of flexibility of such residues. This correlates with the stabilization of R135 by Y306 on H7 as seen in opsin crystal structures (Park et al., 2008; Scheerer et al., 2008). Moreover, H3 shows an exposure to polar/aqueous environment which correlates with crystal (Park et al., 2008; Scheerer et al., 2008) and ANM structures (Isin et al., 2006) where an exposure of hydrophobic regions in CP end of H3 for G-protein interaction is seen. Increase in solvent exposure of H3 can also be correlated with the outward movement of H3 on light activation from EPR studies (Farahbakhsh et al., 1995; Farrens et al., 1996). Increase in motion of Ala residues, which are spread out in H3,

246

represents flexibility of H3 and this correlates with all previous studies showing increase in its flexibility leading to a reduction in packing of protein core in the light state. H5 shows lower flexibility in the light state based on reduced motions of Phe side chains. There are five Phe residues in H5 spread out in the helix, thus motions of Phe reflects motion of the helix. These reduced motions of H5 are also seen in EPR studies but these studies were focused only on the CP end of helices (Altenbach et al., 1996; Hubbell et al., 2000). Decrease in Phe side chain motions indicates a decrease in motion of all helices towards the EC end on light activation, except for H3 and H4. This again correlates with the hypothesis that the inactive state fluctuates between different conformations, one of them being the active state conformer and that this fluctuation is advantageous when the protein needs to find and maintain the active conformation (Isin et al., 2006). Hence, inactive states are more flexible and active states are more rigid. This decrease in motion of EC and TM domains in light state has not been reported in earlier studies apart from the crystal structures of opsin which shows rigidity in these regions based on temperature factors (Park et al., 2008; Scheerer et al., 2008).

8.3.2.2 Changes in loops

Analyzing changes in CP loop motions on light activation shows that polar backbone motions are present in C1 loop (the polar residues in C1 are K66, K67, R69, T70) indicating that it is flexible. The only information on C1 we have from earlier studies is the crystal structure of opsin which shows L72 exposed for G-protein binding and formation of a short helix (Park et al., 2008; Scheerer et al., 2008). For C2 loop, decrease in mobility of basic amino acid side chains (R147, which is towards the side of H4), increase in motion of Phe side chains (F146, F148) and overall increase in backbone motion are observed. According to the ANM model of light activated state, H4 moves outwards leading to extension of C2 (Isin et al., 2006) which could be

the reason for increased mobility of residues towards H4 in the C2 loop seen in THz spectra. Regarding the EC loops, no significant changes are seen in E2 loop by THz spectroscopy on light activation except a decrease in side chain motion of Phe. However, there are no Phe residues in E2 loop. E1 shows small backbone motions and appears to be engaged in nonpolar side chain motions due to H-bond formation. From simulations, E1 shows increased solvent exposed regions and backbone motion of polar residue (Y102). The changes in E3 loop show as a decrease in SAS and a lower overall mobility except at F283.

8.4   SUMMARY OF CONTRIBUTIONS

We have reported a non-destructive, bulk method, THz spectroscopy, to report on dynamics of rhodopsin. This method is advantageous over the other conventional biophysical methods to study dynamics, in particular, NMR spectroscopy, since it has no limitation on the size of proteins to be probed and provides high signal to noise ratio at much lower protein concentrations. Moreover, it characterizes very fast sub-ps motions that are important contributors of motions in proteins required for their function but are difficult to be assessed by other methods for MPs. We selected rhodopsin as a model system to show the applicability of THz spectroscopy in studying MP dynamics. Rhodopsin is the best studied GPCR, its structure-function relationship on light activation has been investigated in great detail. Thus, in our studies of conformational changes upon light activation of rhodopsin using THz spectroscopy, we have observed changes that correlate with the existing literature. Further, new observations have been made by our studies of ps vibrational motion of different regions of rhodopsin and how they may possibly lead to formation of an activated state.

9.0   CHAPTER 9: FUTURE RESEARCH DIRECTIONS

9.1   OVERVIEW

The study of MP folding is very challenging since MPs are not easily amenable to denaturation in membrane environments and are prone to aggregate when denatured. I overcame these difficulties in the case of rhodopsin by screening different denaturing conditions so that maximum unfolding of the protein can be obtained without causing its aggregation (described in Chapter 3). My work has demonstrated that a suitable suite of complementary biophysical approaches can be used to identify conditions for studying MP folding *in vitro* in the case of rhodopsin. The difficulties in identifying solution conditions are a major reason for MP folding field to be less advanced than that of soluble proteins. My studies opened the door for detailed biophysical characterization of denatured states of rhodopsin which affords me with the opportunity to gain insights into the mechanism of folding and (potentially misfolding) of rhodopsin. I determined propensities for interactions among residues in unfolded states of rhodopsin, the first for MP for which such studies have been undertaken. Domain specific changes upon denaturation were detected by NMR spectroscopy (described in Chapter 5). These studies showed that there is disparity in dynamics among different structural domains of rhodopsin. It was observed that the CP domain, probed by lysines, is more flexible than the EC and TM domains, probed by tryptophans. This led me to further map the residues that make the

EC-TM domain rigid by detecting residue specific motions using EPR spectroscopy (described in Chapter 6). Among the CP and EC residues that were investigated, the latter were found to be more immobile than the former in denatured states.

These findings provide strong preliminary evidences towards supporting the LRI model of folding of rhodopsin. This model predicted that long-range interactions between EC and TM residues form a folding core during initial stages of folding of rhodopsin that triggers folding of the entire protein. To gather more evidence for this theory, more information on motions of amino acids in denatured states is required. Towards this goal, we initiated application of terahertz spectroscopy to characterize global motions in rhodopsin (described in Chapter 5). We studied motions of rhodopsin in the native state to show the applicability of this method. It is a new method in the field of biomolecular dynamics and can be particularly advantageous for studying dynamics of large proteins like rhodopsin that are difficult to study by NMR. Additionally, we also established an approach to quantify motions of specific residues in rhodopsin by ^{19}F NMR relaxation rate measurements (described in Chapter 5). For this, novel monofluoro labeling reagents were tested and conditions were optimized to label endogenous cysteines in rhodopsin.

This chapter describes the directions in which this thesis work can be advanced. It is divided into two sections – immediate future research goals and long-term goals. The representation below, Figure 72., shows these goals in bulleted format in context of their contribution to a) method development in general, b) understanding MP folding and c) specifically understanding folding of rhodopsin.

CONTRIBUTIONS

General Methods

⇩

• Developed ^{19}F NMR spectroscopic approach using novel mono-fluoro probes to quantify site-specific motions

• Developed terahertz spectroscopy to characterize global motions of proteins

Membrane Protein

⇩

• Provided a framework for conducting unfolding studies of MPs

• Established approaches to detect MP aggregation

• Gathered experimental evidence for long-range interaction model of MP folding

Rhodopsin

⇩

• Optimized denaturing conditions to carry out unfolding studies

• Carried out high-resolution structural studies of denatured states

• Determined location of possible folding core – supporting evidence for long-range interaction model of folding

• Determined dynamics of dark and light states by terahertz spectroscopy

• Quantified motion of cytoplasmic cysteines derivatized with novel mono-fluoro probes by ^{19}F NMR

FUTURE WORK

General Methods

⇩

• To characterize global and residue specific motion of MPs by terahertz and ^{19}F NMR spectroscopy

Membrane Protein

⇩

• To biophysically characterize unfolded states of MPs other than rhodopsin

• To compare and contrast between two-stage and long-range models of folding of MPs by studying bR

Rhodopsin

Immediate Goals

• To carry out more detailed structural studies of unfolded states to map more residues involved in possible folding core

• To characterize global dynamics of denatured state by terahertz spectroscopy

• To quantify motions of CP domain cysteines and compare with EC domain residues in denatured states by ^{19}F NMR

Long-term Goals

• To optimize refolding conditions

• To biophysically characterize denatured states of RP mutants

• To develop approaches to rescue RP mutants

• To characterize the role of translocon in rhodopsin folding

Figure 72: Summary of research contributions and future work

251

9.2   IMMEDIATE GOALS

9.2.1   Mapping residues involved in maintaining rigidity of extracellular-transmembrane domain in denatured states by NMR spectroscopy

Information on dynamics of tryptophans and lysines by NMR gave us qualitative insight into the location of structured and flexible regions in denatured states of rhodopsin (see Chapter 5). Tryptophans and lysines are present in the EC-TM and CP domains of rhodopsin respectively. The intensity of tryptophan backbone peaks decrease and completely vanish at the highest concentration of SDS used. This indicates that the motion of tryptophan backbone atoms is inhibited in unfolded states, possibly by getting buried in a structured region. Are tryptophan residues important in holding this structured region together? If so, then what is the contribution of each tryptophan residue to the stability of this rigid region? This can be analyzed by determining the effect of their mutation, to amino acid types such as alanine, on the HSQC spectrum of ^{15}N tryptophan labeled rhodopsin in denatured states. Among the five different tryptophan residues, of particular interest is W175 since it is present in the predicted folding core region. It will be interesting to see if its mutation prevents the decrease in intensity of tryptophan backbone amide signals with increase in denaturation. This would imply that mutation of W175 has disrupted the structured region thereby increasing flexibility of the tryptophan residues and consequently their signal intensities. This would indicate that W175 is critical for the formation of rigid structured region in the unfolded states. In this way, contribution of other tryptophans can also be determined. However, the following difficulties may be encountered while deconvoluting the contribution of each tryptophan to the HSQC spectral changes. The primary requirement for these studies is that these mutants have to correctly fold and express in levels

suitable to carry out structural studies. Further, global characterization of secondary and tertiary structure as described in Chapters 3 and 4 needs to be carried out for each mutant to determine if the denaturing conditions optimized for wild type are also suitable for characterizing the mutants. This is because the mutants may aggregate or may not unfold to a large extent under the denaturing conditions that are optimized for wild type. If this is the case, then further optimization of denaturing conditions for characterization of the unfolded states of the mutants is required. However, different denaturing conditions for the mutant and wild type could make comparison of their HSQC spectra difficult since the changes observed may be influenced by the nature of denaturant used and not by the mutation alone.

An alternative way to determine residue specific contributions is by using HNCO NMR experiments to assign specific residues. This can be done by labeling specific amino acids with the ^{15}N isotope in the backbone and the amino acid prior to it in sequence with ^{13}C isotope in the backbone. For a unique pair in the protein, this will result in a single peak in the HNCO spectrum corresponding to this pair. For example, W175, which lies in the predicted folding core and hence is an interesting residue to study, uniquely pairs with G174 and thus can be assigned by HNCO. The change in this peak in the HNCO spectrum representing changes in W175, can then be followed as a function of increasing denaturant concentration. Thus, site-specific conformational changes in W175 upon denaturation of rhodopsin can be probed. There are 17 unique pairs of amino acids among the 37 predicted folding core residues that can be assigned by HNCO and their motions characterized. In this way, the environment of more residues of the potential folding core can be mapped. However, assignment of residues may not be straightforward because of appearance of signals with low signal to noise ratio, appearance of more than one peak due to isotope scrambling and conformational heterogeneity as has been

reported in earlier efforts to assign tryptophan residues (Klein-Seetharaman et al., 2004; Werner et al., 2007). Assignment of tryptophan residues required the use of both solution state and solid state NMR methods (Werner et al., 2007).

Further, if assignment of residues can be achieved and good signal to noise ratio can be obtained in denatured states, then relaxation rate measurements become feasible to quantify their motions. This will help in mapping residues involved in formation of rigid regions and their extent of involvement since relaxation rates higher than that expected for a random coil will indicate rigidity of that residue, thus suggesting its participation in a structured region. Moreover, effect of mutation of these residues on the relaxation rate will indicate the importance of that residue in keeping the structured region intact and contributing to its rigidity.

9.2.2 Quantification of residue specific motion in denatured states by ^{19}F NMR

9.2.2.1 Assignment of cysteine residues

The contribution of this thesis is a set of experimental conditions suitable to quantify motions of specific residues in native rhodopsin by fluorine labeling endogenous cysteines, C140 and C316, that have free sulfydryl groups and then measuring their rate of relaxation using ^{19}F NMR relaxation experiments (see Chapter 7). Such quantification has not been possible previously with the trifluro label that has been extensively used for ^{19}F NMR studies of rhodopsin (Klein-Seetharaman et al., 1999a; Loewen et al., 2001). This is due to the complex mechanisms of relaxation of three fluorine atoms in the trifluoro label. To overcome this, we tested novel monofluoro labels that were synthesized by our collaborator Dr. Alex Doemling. The type of fluorinating reagents and their labeling conditions were optimized. What is required next is to assign the cysteine peaks that we observed in the 1D ^{19}F spectrum by mutation of either

of the two cysteines. Further, measurement of relaxation rates of C140 and C316 in denatured states need to be carried out to compare with that in native state. Characterizing motions of C140 and C316 will provide information on the degree of flexibility of CP domain.

9.2.2.2 Measurement of dynamics in denatured states

Next, we can ask the question: Is the extent of flexibility of CP residues greater than that of EC-TM residues selected from the predicted folding core? For this, motion of EC and TM residues need to be quantified by means of relaxation rate measurements. Firstly, EC and TM residues need to be screened for tolerating mutation to cysteine and secondly, for accessibility to fluorinating reagents. The challenge here is to find EC residues that tolerate a cysteine mutation since this domain is known to misfold upon mutations (Doi et al., 1990; Anukanth and Khorana, 1994). This is similar to the approach taken for EPR experiments in our studies (Chapter 6). However, it may be possible that residues that are not accessible or reactive to spin labels are reactive to fluoro labels. Further, quantification of motion is possible if ^{19}F NMR approach is used compared to EPR where mobility experiments provide largely qualitative information (as seen in Chapter 6). Comparison of motion of large number of predicted folding core residues and also residues surrounding the predicted folding core in the EC and TM domains with that of CP residues will help in understanding differences in motion in large regions of these domains. A more rigid EC and TM domain in denatured states will imply presence of structured regions thus providing more evidence towards the LRI theory of folding. Residues away from the folding core but in the EC domain need to be selected as well for such studies to see if these regions are rigid or flexible. If they are rigid, then quantification of motion of residues will greatly help in determining the extent of rigidity of these residues compared to the folding core residues. If a

structured region is detected in the region of the predicted folding core, then its degree of rigidity will be higher than other regions in the EC domain.

9.2.2.3 Introduction of fluorine probes by unnatural amino acid

Another way by which fluorine probes can be introduced in a protein is by incorporating unnatural amino acids that are fluorinated during protein synthesis in cells (Link et al., 2003; Hendrickson et al., 2004). The principle behind this method is that an amber stop codon on mRNA at a site corresponding to the amino acid of interest is read by a suppressor tRNA which is aminoacylated with an unnatural amino acid. However, it is not a site-specific method and results in all the amino acids of a particular type in the protein to be replaced by its fluorine analog. Advantages of this method are high signal to noise ratio due to fluorine, absence of background signals, both of which are big challenges in structural characterization of MPs by NMR and no cysteine mutation is required. The approach here is to replace amino acids such as tryptophans in rhodopsin with their fluorinated analogs to study their conformational changes upon denaturation in a 1D and 2D ^{19}F spectra. Due to their enhanced signal intensity, it could be possible to measure their relaxation rates to quantify their motions in denatured states. However, the process of incorporating fluorinated amino acids is tedious since it involves screening different mutants of aminoacyl tRNA synthetase, from *E. coli*, that can aminoacylate a suppressor tRNA, also from *E. coli*, with a fluorinated amino acid inside mammalian cells. This aminoacyl-tRNA synthetase/ suppressor tRNA pair should be highly specific for the unnatural amino acid to be incorporated so that the endogenous, natural amino acids are not wrongly incorporated. This methodology has been shown by expressing rhodopsin containing unnatural amino acids with a keto group in HEK 293T cells (Ye et al., 2008; Ye et al., 2009; Ye et al., 2010).

9.2.2.4 Direct comparison of monofluro with trifluoro labeled rhodopsin

As described in Chapter 7, TET labeling of rhodopsin suffers from a few limitations in terms of convenience of labeling and application in dynamics measurements. The former arises due to two-step procedure of labeling and the latter is due to complicated analyses of relaxation rates from the presence of three fluorine atoms. Hence, novel monofluoro reagents which react in a single step process were tested with rhodopsin to show the utility of monofluoro reagents over TET. However, due to differences in sample conditions between TET and 4F labeled rhodopsin, spectral properties such as line width and dynamics information from relaxation rates could not be compared directly. The immediate step required for comparison is to prepare TET labeled rhodopsin and 4F labeled rhodopsin for NMR experiments simultaneously and under identical conditions so that samples containing similar protein and detergent concentrations can be obtained. This will enable direct comparison between the two labels so that a label with characteristics suitable for NMR measurements can be obtained.

9.2.3   Characterization of motion of additional predicted folding core residues in denatured states by EPR spectroscopy

Motions of amino acids inside and away from the predicted folding core, i.e. in the EC and CP domains respectively were compared by EPR spectroscopy (see Chapter 6). The basis of selection of the EC residues was high expression yields of the cysteine mutants of the residues and their accessibility to spin labels. We found that the CP residues were more prone to become flexible than the EC residues when denatured and that the EC residues retained more immobility than the CP residues. However, we need to determine motions of additional residues in these domains in order to compare larger regions of these domains so that the findings can be

generalized. As controls, mobility of residues from the EC and TM domains which do not belong to the predicted folding core need to be studied as well and compared with that of folding core residues studied and CP residues.

Studying residues in the EC domain is generally challenging given the low tolerance of the EC domain towards mutations. Therefore, a systematic screen of expression of cysteine mutants of the folding core residues is required to determine the residues that can tolerate mutation and also get derivatized by spin labels. This may require optimization of conditions for labeling and purification of the labeled protein and also testing different spin labels of higher membrane permeability, the latter as described in Chapter 6.

9.2.4   Detection of long-range interactions among residues in extracellular-transmembrane domain in unfolded states by double electron-electron resonance (DEER) spectroscopy

In this thesis, we have discussed determining the existence of residual structure and mapping the residues involved in it. Additionally, we also need to define the extent/nature of interactions among these residues, particularly the predicted folding core residues to know which interactions are feasible. This can be achieved by measuring distances between residues that belong to the folding core but are far away in the primary structure using Double Electron-Electron Resonance (DEER) spectroscopy in denatured states. For example, distance between residues in EC loop and TM helix from the predicted folding core need to be measured. This experiment will require screening double cysteine mutants that express well and can be labeled by spin labels. The same limitations described in Section 8.2.3. also apply here.

9.2.5   Characterization of global motions in denatured states by terahertz spectroscopy

The use of THz spectroscopy has been mostly confined to the world of physics and it is being recently developed to understand biological systems. We in collaboration with Dr. Kristina Woods have started its application to understand global motions in MPs, by using rhodopsin as a model system (see Chapter 8). We aim to apply this method to understand motions in denatured states, which are often difficult to be monitored for large systems like rhodopsin by conventional spectroscopic techniques such as NMR. We have described the utility of this method by characterizing global motions of native rhodopsin in the dark state and that upon light activation. MD simulations of the structure of rhodopsin based on information from the THz spectra to understand motions of specific amino acid types has indicated that in the dark state helices in their TM and EC ends are flexible. Further, small motions were detected in the EC domain. This is a significant advancement in detecting motions in the TM and EC domains which are otherwise challenging to be determined by conventional spectroscopic methods such as NMR and EPR, as discussed in Chapters 5 and 6. Therefore, a bulk method that requires protein (as large as rhodopsin which is 42 kDa) as little as ~1 mg/l to characterize its motions on a 'semi-global' scale, i.e. motions of specific amino acid types in the entire protein, can be very useful for large MPs. Characterization of such motions in denatured states is crucial in discovering the presence of residual structure in these states which in turn helps in understanding the mechanisms by which proteins fold. We need to use this method to obtain information on global motions of denatured rhodopsin in order to compare with the motions detected in native state. THz spectra will be recorded at different concentrations of SDS and in presence of 3S8U to determine changes in motions of the helices from native state motions. If the EC ends of helices

become more rigid in denatured states than that in native state, then it would indicate that they are involved in forming rigid structured regions in unfolded states as observed in our studies.

9.3   LONG-TERM GOALS

9.3.1   Unfolding studies of additional helical membrane proteins

The work presented in this thesis takes rhodopsin as a model system to provide the framework for studying folding of MPs in general. The systematic work done in determining the extent of denaturation and aggregation has laid down the steps required to initiate folding studies of MPs in general. Structural characterization of denatured states of different MPs on the lines described here will enable comparison of the mechanistic details of folding of different MPs. Such studies will indicate whether there are general guidelines that are followed in MP folding or whether the rules are largely dependent on the nature of MPs or if MPs can be classified into different groups depending on the manner they fold.

A very interesting comparison of structural features of denatured states would be between rhodopsin and bR. Both proteins share a high structural similarity but are believed to fold by different mechanisms. Rhodopsin and bR are representative of different folding models, the LRI model and the two-stage folding model respectively. These two models are contrasting since the former model underscores the involvement of EC loops along with TM helices during folding of MPs whereas the latter model hypothesizes the participation of only TM helices and the indispensability of loops in MP folding. Therefore, carrying out structural characterization of

denatured states of bR by following the experiments done for rhodopsin will explain the differences, if any, in the folding pattern of these two proteins and hence explain the two models.

9.3.2   Refolding studies of rhodopsin

In Chapter 1, we have shown that 30% SDS and 3S8U are the two best conditions under which largely unfolded and aggregate-free denatured states of rhodopsin can be characterized. Under these denaturing conditions, we have shown that rigid structured region or a potential folding core is formed in the EC-TM region of rhodopsin. Refolding is not necessary to carry out the type of characterization we have described in this thesis. However, to show that the observed rigid, structured region in largely unfolded states is a core of structure that is competent to fold into the native state, refolding of rhodopsin from these unfolded states needs to be carried out. Further, refolding studies under the denaturing conditions that we optimized are also required for thermodynamic analyses of folding. It is very challenging to refold MPs since the majority of regions to be refolded are hydrophobic and hence need to be reconstituted into a membrane mimetic. Thus, the properties of detergents or lipids or detergent-lipid mixtures, such as lateral pressure, hydrophobic thickness and curvature, to name a few, are very critical (Booth and Curnow, 2009). Hence, refolding MPs is not trivial and requires extensive screening and optimization of different membrane mimetics. Refolding experiments have been reported for several MPs, bR (Huang et al., 1981), DsbB (Otzen, 2003), DAGK (Lau and Bowie, 1997; Nagy et al., 2001), KcsA (Barrera et al., 2005), LHCII (Plumley and Schmidt, 1987; Dockter et al., 2009), CopA (Roman et al., 2010) and EmrE (Miller et al., 2009). But, in most of these cases, refolding has been achieved from a slightly denatured state. Recently, denaturation studies of opsin in phospholipid bicelles with urea showed a significant decrease of 50% in its helical

content, but it could not be refolded from such a largely unfolded state (McKibbin et al., 2009). Refolding of MPs, except bR and CopA, is typically feasible only from a minimally denatured state which is structurally very similar to the native state but becomes difficult when large portions of the structure are unfolded. In the case of bR, different refolding conditions consisting of different detergent micelles, lipids and lipid-micelle mixtures have been screened depicting the role of different detergents and lipids when refolding MPs (Huang et al., 1981; London and Khorana, 1982; Allen et al., 2004b; Allen et al., 2004a). Taking cues from these studies, refolding of rhodopsin needs to be carried out from its 30% SDS denatured state. The method of removing the denaturants to allow refolding also needs to be optimized, i.e. whether to remove by diluting or by dialyzing in presence of DM (or other detergents or lipids) and 11-*cis* retinal. The time of incubation with micelles and 11-*cis* retinal also need to be optimized. In the case where rhodopsin does not refold from the 30% SDS denatured state, refolding could be attempted from less unfolded, intermediate states that are obtained by addition of lower SDS concentration.

We have used rhodopsin solubilized in DM for all our unfolding studies. Given this as the initial state, it is possible that the denatured states obtained from it cannot be refolded. In such a case, unfolding and refolding studies of rhodopsin reconstituted in different micelle systems could be carried out. Characterization of unfolded states in different solvent systems will also show whether the rigid residual structure seen in EC-TM domain in SDS unfolded states can exist irrespective of the nature of the membrane mimetic.

If refolding of rhodopsin can be attained then it will open up a range of opportunities to examine the transition states and final denatured states thermodynamically and kinetically. Thermodynamic parameters of folding such as free energy, enthalpy and entropy can then be

estimated from folding-refolding curves. Phi values, which will help to characterize the environment of specific residues in the transition states, can also be estimated, as has been done for bR (Curnow and Booth, 2009). In another study carried out with bR illustrating the importance of H-bonds in the stability of MPs, it was reported that the overall contribution of sidechain H-bond interactions is very small, only about 0.6 kcal mol^{-1} (Joh et al., 2008). This study was done only on bR and a generalization to all MPs was drawn. However, given that folding mechanisms may differ among different MPs it is difficult to conclude such generalizations. As described in Chapter 1, there are several differences in folding mechanisms of rhodopsin and bR which gave rise to two different folding hypotheses, the two-stage folding model and the LRI model. Thus, if rhodopsin can be refolded, then by the approaches used in (Joh et al., 2008) the contribution of its H-bonds to its overall stability, in particular, the difference in H-bond energies among the predicted folding core residues or those in the EC-TM domains and that of residues away from the core or in the CP domain can be determined. This study with rhodopsin can be carried out by double mutant cycle analysis of mutants of the predicted folding core residues that are involved in H-bond interactions in the native state as done for bR (Joh et al., 2008).

9.3.3 Biophysical characterization of unfolded states of Retinits Pigmentosa mutants

The study of the fundamental aspects of MP folding mechanisms has implications for understanding of MP misfolding diseases also. Rhodopsin is a good model system to study such disease mechanisms since there are many misfolding mutations in rhodopsin that cause a misfolding disease, RP (Berson, 1996). RP is a retinal degenerative disease; one cause is the misfolding of rhodopsin. Mutations in rhodopsin lead to its misfolding and retention in the ER

263

and a loss of photoreceptor in the retinal membrane. The mechanism by which rhodopsin misfolds is not fully understood. Our folding studies on wild type rhodopsin need to be implemented on RP mutants of rhodopsin to structurally characterize their denatured states of these mutants. The major challenge in studying these mutants is that their expression level is usually very low. However, there are some RP mutants, such as N15S, which can be expressed in quantities suitable for biophysical studies. Residue-specific characterization of unfolded states of RP mutants is needed to determine the presence or absence of residual structure or 'folding core' which may help in deciphering the mechanisms of misfolding. Moreover, with the bulk method of THz spectroscopy that requires low amounts of proteins (see Chapter 8), global dynamics of low expressing RP mutants can be characterized. Knowledge of structural features of these denatured states may help in designing strategies for curing RP and other related MP misfolding diseases.

9.3.4   Developing pharmacological chaperones to rescue misfolded Retinits Pigmentosa mutants

Several diseases are caused by misfolding of MPs. One way to limit misfolding is to design pharmacological chaperones that bind to misfolded regions or unstable, non-native, unfolded regions and shift the equilibrium towards folded states. Several studies have been published to rescue RP mutants by small molecule chaperones, which are retinal-like, where reconstitution of RP rhodopsin mutants is determined in the presence of such chaperones (Li et al., 1998; Saliba et al., 2002; Noorwez et al., 2003; Noorwez et al., 2004). Although there are some reports on the successful use of retinals in animal studies, the instability, photosensitivity and unwanted effects of metabolic by products do not make them therapeutically suitable (Ohgane et al., 2010). A

different approach can be to screen for small molecules that bind to denatured states of rhodopsin. However, the challenge here is to develop a binding assay. One way to determine binding is by using ^{19}F NMR spectroscopy whereby changes in either the chemical shift or peak width of fluorinated small molecules are determined. Isothermal calorimetric measurements can also be carried out to determine binding. Another way to detect binding is to test if rhodopsin refolds in the presence of such small molecules. This will also be a test of their chaperoning property. However, refolding may be very challenging as described in Section 8.3.5. Therefore, these small molecules need to be tested on RP mutants. *In vitro* experiments of binding as explained above for wild type rhodopsin need to be repeated for RP mutants. The best way to test their chaperoning property will be to determine if they can reconstitute misfolded rhodopsin in cells. Experiments in the cell will include growing cells expressing RP mutants in presence of these chaperones or incubating the cell supernatant with 11-*cis* retinal and these chaperones to determine if yield of rhodopsin increases.

9.3.5   Role of translocon in rhodopsin folding

Even for soluble proteins, there is still a lack of understanding of how proteins fold inside a cell since the complexity of the cell makes it a difficult experimental system. Further, simultaneous involvement of more than one factor in folding makes the system even less controllable to set up an experiment. Factors such as molecular crowding, the chaperone system, ER to Golgi trafficking, translocon and protein quality control influence protein folding in cells (Ruddon and Bedows, 1997). In the case of MPs, since all the action occurs in the ER membrane, the most important factor for folding appears to be the translocon. The translocon plays a key role in MP folding as it translocates TM segments from the translocon to the membrane. There have been

several reports using an *in vitro* transcription-translation system to probe the mechanism by which the translocon (Meacock et al., 2002; Isin et al., 2006; Ismail et al., 2008) partitions TM segments of opsin into the membrane. These studies showed that different TM helices associate with different components of the translocon. Although TM1-4 translocate to the membrane sequentially after each TM is synthesized, TM5-7 are retained in the translocon until opsin synthesis is complete. It was also shown that retention of the TM helix depends on the properties of the helix since replacement of TM7 with TM3 resulted in spontaneous exit of TM3 after its synthesis. These studies raise important questions concerning the folding mechanism of rhodopsin. Why is it necessary for some of the TM segments to be retained in the translocon until opsin synthesis is complete? Are the TM segments involved in some interactions required to trigger opsin folding? Is the translocon machinery just a gateway for MPs to enter the membrane as it is for soluble proteins to enter into the ER lumen for proper folding, or does folding of MPs begin inside the translocon? Future studies need to be focused in answering these questions as the translocon may be a potent chaperone-like component critical for MP folding. One approach to answer these questions is to characterize the structure of the TM segments inside the translocon in the *in vitro* transcription-translation system. However, this system is too complex and large for *in vitro* structural studies but is less complicated than the entire cell system. Recently, NMR studies have been published whereby structure and dynamics of large molecular weight systems such as that of nascent protein chains bound to ribosomes in an *in vitro* transcription-translation system have been carried out (Hsu et al., 2007; Hsu et al., 2009). ^{15}N and ^{13}C correlation spectroscopy were recorded to characterize structure of the nascent chain. Similar studies can be tested for studying structural features of proteins in the translocon. Another approach can be incorporating fluorinated amino acids at specific residues during

266

protein synthesis, as described in Section 9.2.2.3., and characterizing their environment inside the translocon by ^{19}F NMR.

1D NMR SPECTRAL PARAMETERS AND RELAXATION RATES OF FLUORINE

LABELS

Table 14: Parameters for measuring R_2 of 4F

Buffer	Pulse program	5°C	10°C	15°C	25°C	35°C
D_2O	CPMG with 180° pulse	0,60,120,180,240,300,360,420	0,60,120,180,240,300,360,420	0,120,240,360,480,600,720,840	0,120,240,360,480,600,720,840	0,120,240,360,480,600,720,840
	CPMG	0,60,120,180,240,300,360,420	0,60,120,180,240,300,360,420	0,120,240,360,480,600,720,840	0,120,240,360,480,600,720,840	0,120,240,360,480,600,720,840
	CPMG, WALTZ	NA	NA	NA	NA	0,8,40,60,100,200,300,400
	CPMG, GARP	NA	NA	NA	NA	0,8,40,60,100,200,300,400
Glycerol	CPMG with 180° pulse	0,2.4,4.8,7.2,9.6,10,14.4	0,2.4,4.8,7.2,12,24,36	0,8,16,24,32,40,48,56	0,16,32,48,64,80,96,112	0,8,20,40,80,160,200,240
	CPMG	0,1.2,2.4,3.6,4.8,6,7.2	0,1.2,2.4,3.6,4.8,6,12,18	0,4,8,12,16,20,24,28	0,8,16,24,32,40,48,56	0,4,10,40,80,100,120
	CPMG, WALTZ	NA	NA	0,2,4,6,8,10,12,14,16,18,20,24,28	0,16,32,48,64,80,96,112	0,2,4,8,28,40,50,60,90
	CPMG, GARP	0,1.2,2.4,3.6,4.8,6,7.2	0,1.2,2.4,3.6,4.8,6,12,18	0,2,4,6,8,10,12,14,16,18,	NA	0,4,8,16,20,40,80,100

Table 15: Parameters for measuring R$_2$ of 4F3

Buffer	Pulse program	5°C	10°C	15°C	25°C	35°C
D$_2$O	CPMG with 180° pulse	0,80,160,240,320,400,480,560	0,120,240,360,480,600,720,840	0,120,240,360,480,600,720,840	0,240,480,720,960,1200,1440,1680	0,120,240,360,480,600,720,840
	CPMG	NA	NA	0,120,240,360,480,600,720,840	0,320,640,960,1280,1600,1920,2240	0,120,240,360,480,600,720,840
	CPMG, WALTZ	NA	NA	0,8,40,60,100,200,300,400	NA	0,8,40,60,100,200,300,400
	CPMG, GARP	NA	NA	NA	NA	0,8,40,60,100,200,300,400
Glycerol	CPMG with 180° pulse	0,2.4,4,8,9.6,12,19,24	0,8,16,24,,32,40,48	0,8,16,24,32,40,48,56	0,16,32,48,64,80,96,112	0,32,64,96,128,160,240
	CPMG	0,1.2,2.4,3.6,4.8,9.6,12,18	0,4,8,12,16,20,24	0,4,8,12,16,20,24,28,32	0,8,16,24,32,40,48,56	0,16,32,48,64,80,120
	CPMG, WALTZ	NA	NA	NA	16,24,32,64,128,144,160,176,208	0,10,18,28,40,60,90,120
	CPMG, GARP	0,1.2,2.4,3.6,4.8,9.6,12	0,4,8,12,16,20	0,4,8,12,16,20,24,28,32	NA	0,32,64,96,128,160,240

Table 16: Peak widths and chemical shifts of 4F in D$_2$O, glycerol and different DM concentrations at different temperatures

Spectra for D$_2$O and glycerol are aligned to TFA chemical shift.

Solvent	(°C)	Peak (ppm)	Peak width (Hz)
D$_2$O	5	-216.6886	4.571
	10	-216.6818	4.343
	15	-216.6927	5
	25	-216.6886	5.621
	35	-216.687	13.00
Glycerol	5	-216.8744	40.063
	10	-216.8321	25.572
	15	-216.7815	17.225
	25	-216.6963	9.863
	35	-216.6229	7.19
3.6% DM	25	-216.62	5.1
9% DM	25	-216.67	12.85

Table 17: Peak widths and chemical shifts of 4F3 in D$_2$O and glycerol at different temperatures

Spectra for each sample are aligned to the chemical shift of TFA.

Sample	(°C)	Peak (ppm)	Peak width (Hz)
4F3 in D$_2$O	5	-66.234	12.898
	10	-66.2157	12.807
	25	-66.1707	13.396
	35	-66.1463	13.5
4F3 in Glycerol	5	-65.7722	26.052
	10	-65.7566	18.8
	25	-65.7083	9.7
	35	-65.6747	7.093
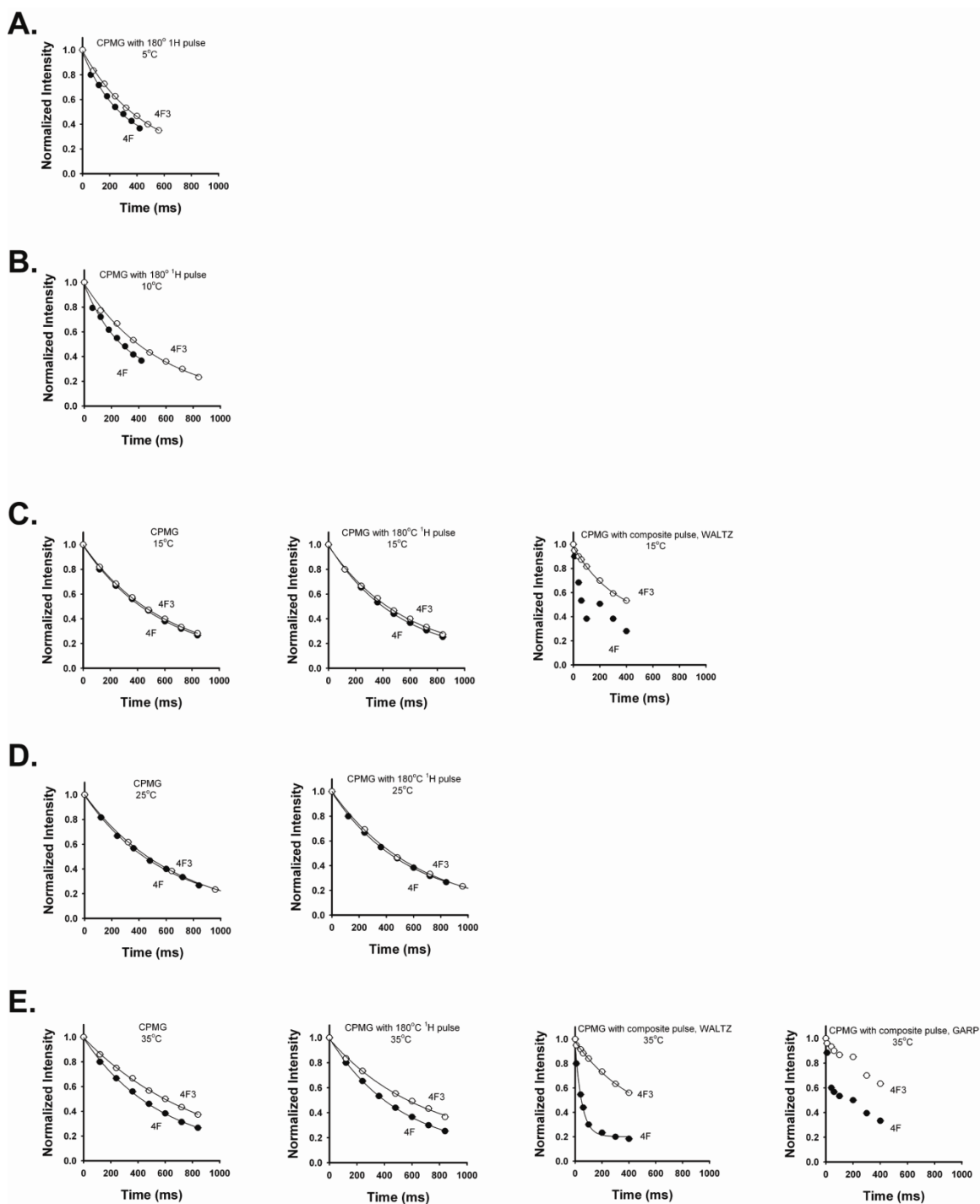
Figure 73: Decay of transverse magnetization of 4F and 4F3 over time in D$_2$O

Decay of transverse magnetization over time of 4F (filled circle) and 4F3 (open circle) labels in D$_2$O at A. 5°C, B. 10°C, C. 15°C, D. 25°C and E. 35°C. The different pulse programs used at each of these temperatures are indicated on the graphs. All graphs were fit to monoexponential decay.

271
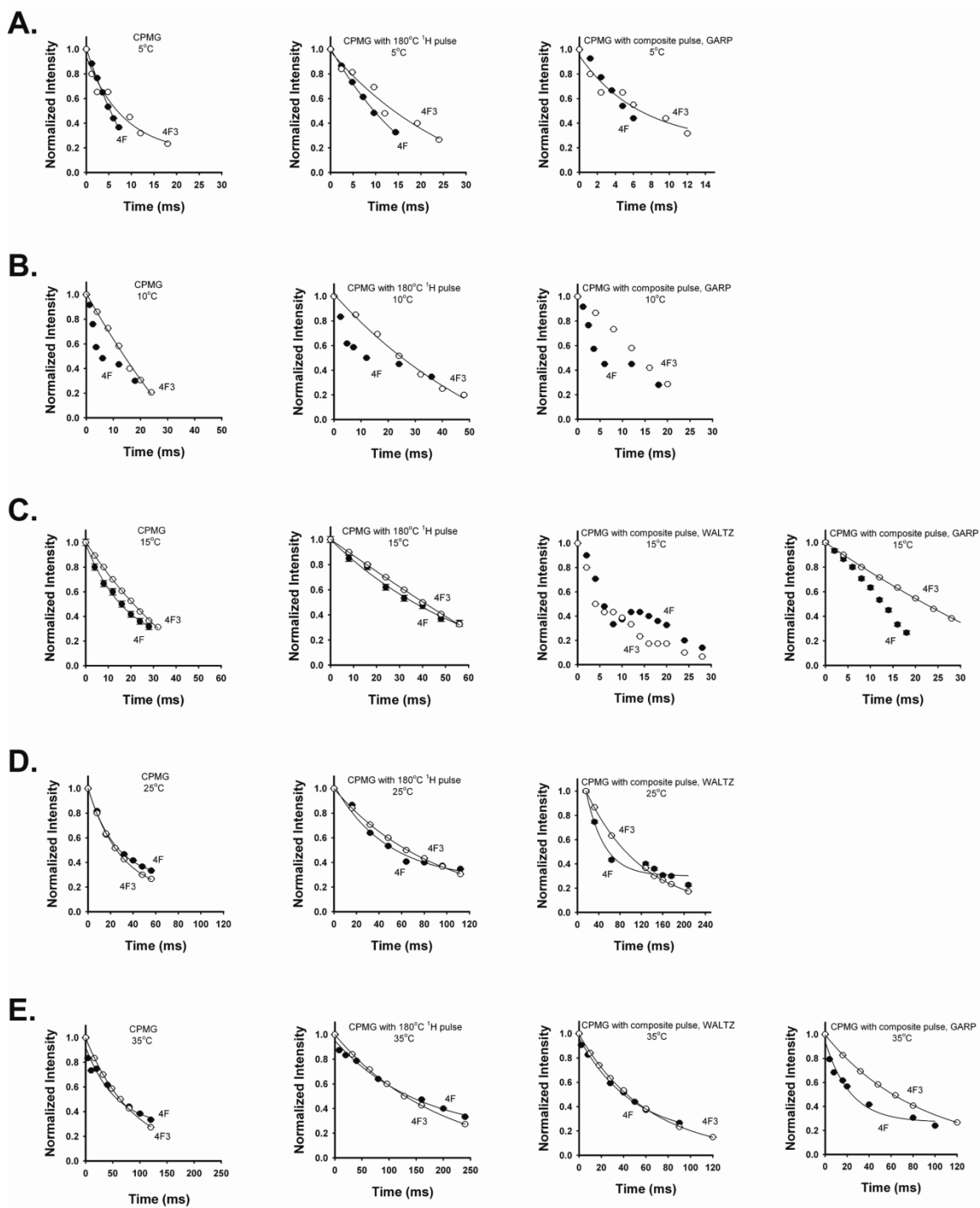
Figure 74: Decay of transverse magnetization over time of 4F and 4F3 in glycerol

Decay of transverse magnetization over time of 4F (filled circle) and 4F3 (open circle) labels in glycerol at A. 5°C, B. 10°C, C. 15°C, D. 25°C and E. 35°C. The different pulse programs used at each of these temperatures are indicated on the graphs. All graphs were fit to monoexponential decay.

Table 18: R$_2$ values of 4F in D$_2$O and glycerol at different temperatures using different pulse sequences

Solvent	(°C)	Experiment	R$_2$ s^{-1}	
			4F	4F3
D$_2$O	5	CPMG with 180° pulse	2.3570±0.1000	1.9000±0.0313
	10	CPMG with 180° pulse	2.3634±0.100	1.7000±0.0420
	15	CPMG with 180° pulse	1.7007±0.0257	1.5000±0.0321
		CPMG	1.5800±0.0257	1.5223±0.0149
		CPMG with composite pulse, WALTZ	NA	1.5870±0.0675
	25	CPMG with 180° pulse	1.6000±0.0256	1.5000±0.0168
		CPMG	1.5500±0.0250	1.498±0.0126
	35	CPMG with 180° pulse	1.7007±0.0247	1.1000±0.1000
		CPMG	1.5897±0.0247	1.1587±0.0131
		CPMG with composite pulse, GARP	Did not fit	Did not fit
		CPMG with composite pulse, WALTZ	8.914±2.2 (poor fit)	1.4173±0.0505
Glycerol	5	CPMG with 180° pulse	74.9±3.4	50.4±5.1
		CPMG	135.3±5.7	82.1±10.5
		CPMG with composite pulse, GARP	Did not fit	86.6±11.6
	10	CPMG with 180° pulse	32.9±8.7 (poor fit)	31.5±2.4
		CPMG	Did not fit	57±5.0
		CPMG with composite pulse, GARP	Did not fit	Did not fit
	15	CPMG with 180° pulse	19.7±0.8	18.3±1.0
		CPMG	41.9±1.5	34.6±1.2
		CPMG with composite pulse, GARP	Did not fit	33.2±1.4
		CPMG with composite pulse, WALTZ	Did not fit	Did not fit
	25	CPMG with 180° pulse	11.3±1.0	10.50±0.08
		CPMG	21.3±1.4	25.5±0.9
		CPMG with composite pulse, WALTZ	7.7±1.2 (poor fit)	9.18±0.09
	35	CPMG with 180° pulse	4.4±0.3	5.36±0.04
		CPMG	8.8±1.0	10.8±0.1
		CPMG with composite pulse, GARP	15.9±2.8	11.1±0.1
		CPMG with composite pulse, WALTZ	15.5±0.7	15.9±0.2

Table 19: R_1 values of 4F and 4F3 in D_2O and glycerol at different temperatures using different pulse sequences

Solvent	(°C)	R_1 (s⁻¹) with 180° pulse	
		4F	**4F3**
D_2O	15	0.3470±0.0029	0.9261±0.0075
	25	0.2805±0.0033	0.7113±0.0059
	35	0.2261±0.0053	0.5739±0.0036
Glycerol	25	2.5411±0.02747	4.1911±0.0349

Figure 75: Decay of transverse magnetization of 2NO2F and 2NO2F3 over time in D_2O

Decay of transverse magnetization over time of 2NO2F (filled circle) and 2NO2F3 (open circle) labels in D_2O at A. 15°C, B. 25°C and C. 35°C. The different pulse programs used at each of these temperatures are indicated on the graphs. All graphs were fit to monoexponential decay.
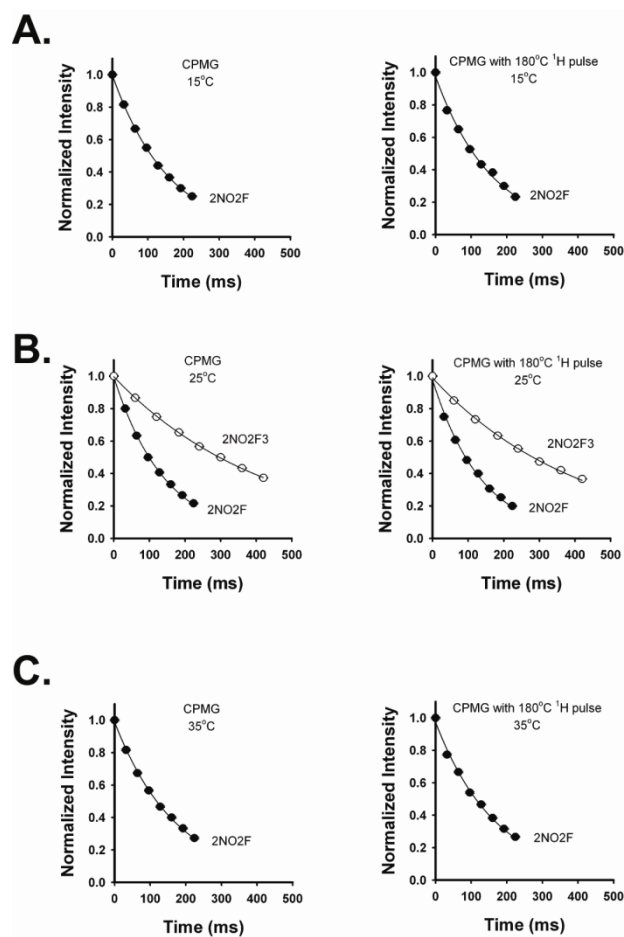
Table 20: Peak widths and chemical shifts of 2NO2F and 2NO2F3 in D_2O at different temperatures.

Chemical shifts are obtained after aligning spectra of free label in D_2O to that of TFA in D_2O.

Sample	(°C)	Peak (ppm)	Peak width (Hz)
2NO2F in D_2O	15	-216.8753	5.44
	25	-216.8548	6.017
	35	-216.8356	6.2
2NO2F3 in D_2O	25	-66.157	13.35

Table 21: R_2 values of both peaks 1 and 2 of 4F labeled rhodopsin at different temperatures in different experiments measuring transverse relaxation rate

(°C)	Experiment	R_2 (s^{-1})	
		Peak 1	Peak 2
10	T_2disp with ^{1}H decoupling	257.8±0.0	209.1±0.0
	T_2 CPMG with ^{1}H decoupling	260.8±18.0	199.6±9.0
	T_1rho with ^{1}H decoupling	283.0±12.9	220.9±10.3
15	T_2disp with ^{1}H decoupling	212.0±4.4	169.3±4.4
	T_2 CPMG with ^{1}H decoupling	217.1±10.8	165.0±6.4
	T_1rho with ^{1}H decoupling	240.1±11.6	177.1±13.0
25	T_2disp without ^{1}H decoupling	121.0±10.3	139.1±0.0
	T_2disp with ^{1}H decoupling	138.3±4.8	142.3±9.0
	T_2 CPMG without ^{1}H decoupling	120.1±3.9	133.3±3.4
	T_2 CPMG with ^{1}H decoupling	120.0±4.1	125.0±4.6
	T_2 CPMG with ^{1}H decoupling and [1]H 180° pulse	133.9±4.5	131.9±7.0
	T_1rho without ^{1}H decoupling	148.3±5.6	124.3±7.8
	T_1rho with ^{1}H decoupling	157.9±7.6	134.5±5.1
37	T_2disp with ^{1}H decoupling	85.8±0.6	114.3±0.0
	T_2 CPMG with ^{1}H decoupling	74.1±3.4	92.4±3.7
	T_1rho with ^{1}H decoupling	89.1±6.5	86.0±3.7

Table 22: R_1 values of peaks 1 and 2 of 4F labeled rhodopsin in different experiments at different temperatures.

(°C)	Experiment	R_1 (s^{-1})	
		Peak 1	**Peak 2**
10	T_1 with ^{1}H decoupling	1.6752±0.0664	1.8325±0.0227
15	T_1 with ^{1}H decoupling	1.6069±0.0444	1.7071±0.0462
25	T_1 with ^{1}H decoupling	1.3762±0.0284	1.5285±0.0129
	T_1 with ^{1}H decoupling and 180° ^{1}H pulse	1.4364±0.0584	1.5059±0.0367
37	T_1 with ^{1}H decoupling	1.3223±0.0269	1.2941±0.0451

APPENDIX B

PUBLICATIONS

B.1   MANUSCRIPTS PUBLISHED

1. Saxena K, **Dutta A**, Klein-Seetharaman J and Schwalbe H. (2010) Isotope labeling in insect and mammalian cells. Protein NMR Techniques (Methods in Molecular Biology), Third Edition, <u>accepted for publication</u>.

2. **Dutta A**, Tirupula KC, Alexiev U, Klein-Seetharaman J. (2010) Characterization of membrane protein non-native states. 1. Extent of unfolding and aggregation of rhodopsin in the presence of chemical denaturants. Biochemistry, 49(30), 6317-28.

3. **Dutta A**, Kim TY, Moeller M, Wu J, Alexiev U, Klein-Seetharaman J. (2010) Characterization of membrane protein non-native states. 2. The SDS-unfolded states of rhodopsin. Biochemistry, 49(30), 6329-40.

4. Yanamala N[†], **Dutta A**[†], Beck B, Fleet B, Hay K, Yazbak A, Ishima R, Doemling A and Klein-Seetharaman J. (2009) NMR-Based screening of membrane protein ligands. Chemical Biology and Drug Design, 75(3), 237-56. ([†] Joint first authors).

5. Qi Y, Dhiman HK, Bhola N, Budyak I, Kar S, Man D, **Dutta A**, Tirupula K, Carr BI, Grandis J, Bar-Joseph Z, Klein-Seetharaman J. (2009) Systematic prediction of human membrane receptor interactions, Proteomics 9(23), 5243-55.

B.2 MANUSCRIPTS IN PREPARATION

1. **Dutta A**, Altenbach C, Mangahas S, Yanamala N, Gardner E, Hubbell WL and Klein-Seetharaman J. (2010) Comparison of dynamics between extracellular and cytoplasmic domains in denatured states of rhodopsin by NMR and EPR spectroscopy.

2. **Dutta A,** Cao H, Doemling A, Ishima R, Klein-Seetharaman J. (2010) Synthesis and ^{19}F relaxation studies of a monofluoro labeling reagent for quantification of side chain dynamics in membrane proteins.

BIBLIOGRAPHY

Abkevich VI, Gutin AM, Shakhnovich EI (1994) Specific nucleus as the transition state for protein folding: evidence from the lattice model. *Biochemistry* **33**:10026-10036.

Abrahamson EW, Ostroy SE (1967) The photochemical and macromolecular aspects of vision. *Progress in biophysics and molecular biology* **17**:179-215.

Alder NN, Johnson AE (2004) Cotranslational membrane protein biogenesis at the endoplasmic reticulum. *The Journal of biological chemistry* **279**:22787-22790.

Allen SJ, Curran AR, Templer RH, Meijberg W, Booth PJ (2004a) Controlling the folding efficiency of an integral membrane protein. *Journal of molecular biology* **342**:1293-1304.

Allen SJ, Curran AR, Templer RH, Meijberg W, Booth PJ (2004b) Folding kinetics of an alpha helical membrane protein in phospholipid bilayer vesicles. *Journal of molecular biology* **342**:1279-1291.

Almeida FC, Opella SJ (1997) fd coat protein structure in membrane environments: structural dynamics of the loop between the hydrophobic trans-membrane helix and the amphipathic in-plane helix. *Journal of molecular biology* **270**:481-495.

Altenbach C, Cai K, Klein-Seetharaman J, Khorana HG, Hubbell WL (2001a) Structure and function in rhodopsin: mapping light-dependent changes in distance between residue 65 in helix TM1 and residues in the sequence 306-319 at the cytoplasmic end of helix TM7 and in helix H8. *Biochemistry* **40**:15483-15492.

Altenbach C, Klein-Seetharaman J, Cai K, Khorana HG, Hubbell WL (2001b) Structure and function in rhodopsin: mapping light-dependent changes in distance between residue 316 in helix 8 and residues in the sequence 60-75, covering the cytoplasmic end of helices TM1 and TM2 and their connection loop CL1. *Biochemistry* **40**:15493-15500.

Altenbach C, Klein-Seetharaman J, Hwa J, Khorana HG, Hubbell WL (1999) Structural features and light-dependent changes in the sequence 59-75 connecting helices I and II in rhodopsin: a site-directed spin-labeling study. *Biochemistry* **38**:7945-7949.

Altenbach C, Yang K, Farrens DL, Farahbakhsh ZT, Khorana HG, Hubbell WL (1996) Structural features and light-dependent changes in the cytoplasmic interhelical E-F loop region of rhodopsin: a site-directed spin-labeling study. *Biochemistry* **35**:12470-12478.

Anfinsen CB (1973) Principles that govern the folding of protein chains. *Science* **181**:223-230.

Anukanth A, Khorana HG (1994) Structure and function in rhodopsin. Requirements of a specific structure for the intradiscal domain. *The Journal of biological chemistry* **269**:19738-19744.

Arnis S, Hofmann KP (1993) Two different forms of metarhodopsin II: Schiff base deprotonation precedes proton uptake and signaling state. *Proceedings of the National Academy of Sciences of the United States of America* **90**:7849-7853.

Baglioni P, Rivara-Minten E, Dei L, Ferroni E (1990) ESR Study of Sodium Dodecyl Sulfate and Dodecyltrimethylammoium Bromide Micellar Solutions. Effect of Urea. *Journal of Physical Chemistry* **94**:8218-8222.

Bakan A, Bahar I (2009) The intrinsic dynamics of enzymes plays a dominant role in determining the structural changes induced upon inhibitor binding. *Proceedings of the National Academy of Sciences of the United States of America* **106**:14349-14354.

Baker D, Agard DA (1994) Kinetics versus thermodynamics in protein folding. *Biochemistry* **33**:7505-7509.

Barrera FN, Renart ML, Molina ML, Poveda JA, Encinar JA, Fernandez AM, Neira JL, Gonzalez-Ros JM (2005) Unfolding and refolding in vitro of a tetrameric, alpha-helical membrane protein: the prokaryotic potassium channel KcsA. *Biochemistry* **44**:14344-14352.

Berendsen HJ, Hayward S (2000) Collective protein dynamics in relation to function. *Current opinion in structural biology* **10**:165-169.

Berendsen HJC, Postma JPM, Gunsteren WFv, DiNola A, Haak JR (1984) Molecular dynamics with coupling to an external bath. *The Journal of Chemical Physics* **81**:3684-3690.

Berson EL (1996) Retinitis pigmentosa: unfolding its mystery. *Proceedings of the National Academy of Sciences of the United States of America* **93**:4526-4528.

Berson EL, Rosner B, Sandberg MA, Weigel-DiFranco C, Moser A, Brockhurst RJ, Hayes KC, Johnson CA, Anderson EJ, Gaudio AR, Willett WC, Schaefer EJ (2004a) Clinical trial of docosahexaenoic acid in patients with retinitis pigmentosa receiving vitamin A treatment. *Archives of ophthalmology* **122**:1297-1305.

Berson EL, Rosner B, Sandberg MA, Weigel-DiFranco C, Moser A, Brockhurst RJ, Hayes KC, Johnson CA, Anderson EJ, Gaudio AR, Willett WC, Schaefer EJ (2004b) Further evaluation of docosahexaenoic acid in patients with retinitis pigmentosa receiving vitamin A treatment: subgroup analyses. *Archives of ophthalmology* **122**:1306-1314.

Bibi E, Kaback HR (1990) In vivo expression of the lacY gene in two segments leads to functional lac permease. *Proceedings of the National Academy of Sciences of the United States of America* **87**:4325-4329.

Booth DR, Sunde M, Bellotti V, Robinson CV, Hutchinson WL, Fraser PE, Hawkins PN, Dobson CM, Radford SE, Blake CC, Pepys MB (1997) Instability, unfolding and aggregation of human lysozyme variants underlying amyloid fibrillogenesis. *Nature* **385**:787-793.

Booth PJ, Curnow P (2006) Membrane proteins shape up: understanding in vitro folding. *Current opinion in structural biology* **16**:480-488.

Booth PJ, Curnow P (2009) Folding scene investigation: membrane proteins. *Current opinion in structural biology* **19**:8-13.

Booth PJ, Farooq A (1997) Intermediates in the assembly of bacteriorhodopsin investigated by time-resolved absorption spectroscopy. *European journal of biochemistry* **246**:674-680.

Booth PJ, Farooq A, Flitsch SL (1996) Retinal binding during folding and assembly of the membrane protein bacteriorhodopsin. *Biochemistry* **35**:5902-5909.

Booth PJ, Flitsch SL, Stern LJ, Greenhalgh DA, Kim PS, Khorana HG (1995) Intermediates in the folding of the membrane protein bacteriorhodopsin. *Nature structural biology* **2**:139-143.

Borhan B, Souto ML, Imai H, Shichida Y, Nakanishi K (2000) Movement of retinal along the visual transduction path. *Science* **288**:2209-2212.

Bourne HR, Meng EC (2000) Rhodopsin Sees the Light. *Science* **289**:733-734.

Bowie JU (2005) Solving the membrane protein folding problem. *Nature* **438**:581-589.

Bownds D (1967) Site of Attachment of Retinal in Rhodopsin. *Nature* **216**:1178-1181.

Briganti G, Puvvada S, Blankscbtein D (1991) Effect of Urea on Micellar Properties of Aqueous Solutions of Nonionic Surfactants. *Journal of Physical Chemistry* **95**:8989-8995.

Brooks CL, Karplus M, Pettitt BM. 1988. Proteins: A Theoretical Perspective of Dynamics, Structure and Thermodynamics, John Wiley & Sons, New York.

Bryngelson JD, Onuchic JN, Socci ND, Wolynes PG (1995) Funnels, pathways, and the energy landscape of protein folding: a synthesis. *Proteins* **21**:167-195.

Bubis J (1998) Effect of detergents and lipids on transducin photoactivation by rhodopsin. *Biological research* **31**:59-71.

Bucci S, Fagotti C (1991) Small-Angle Neutron-Scattering Study of Ionic-Nonionic Mixed Micelles. *Langmuir* **7**:824-826.

Cai K, Klein-Seetharaman J, Altenbach C, Hubbell WL, Khorana HG (2001) Probing the dark state tertiary structure in the cytoplasmic domain of rhodopsin: proximities between amino acids deduced from spontaneous disulfide bond formation between cysteine pairs engineered in cytoplasmic loops 1, 3, and 4. *Biochemistry* **40**:12479-12485.

Cai K, Klein-Seetharaman J, Farrens D, Zhang C, Altenbach C, Hubbell WL, Khorana HG (1999a) Single-cysteine substitution mutants at amino acid positions 306-321 in rhodopsin, the sequence between the cytoplasmic end of helix VII and the palmitoylation sites: sulfhydryl reactivity and transducin activation reveal a tertiary structure. *Biochemistry* **38**:7925-7930.

Cai K, Klein-Seetharaman J, Hwa J, Hubbell WL, Khorana HG (1999b) Structure and function in rhodopsin: effects of disulfide cross-links in the cytoplasmic face of rhodopsin on transducin activation and phosphorylation by rhodopsin kinase. *Biochemistry* **38**:12893-12898.

Canet D, Sunde M, Last AM, Miranker A, Spencer A, Robinson CV, Dobson CM (1999) Mechanistic studies of the folding of human lysozyme and the origin of amyloidogenic behavior in its disease-related variants. *Biochemistry* **38**:6419-6427.

Carr HY, Purcell EM (1954) Effects of diffusion on free precession in uclear magnetic resonance experiments. *Physical review* **94**:630-638.

Chen C, Okayama H (1987) *Molecular and Cellular Biology* **7**:2745-2752.

Chen YS, Hubbell WL (1978) Reactions of the sulfhydryl groups of membrane-bound bovine rhodopsin. *Membrane biochemistry* **1**:107-130.

Chiti F, Dobson CM (2009) Amyloid formation by globular proteins under native conditions. *Nature chemical biology* **5**:15-22.

Cho JH, Sato S, Horng JC, Anil B, Raleigh DP (2008) Electrostatic interactions in the denatured state ensemble: their effect upon protein folding and protein stability. *Archives of biochemistry and biophysics* **469**:20-28.

Croonen Y, Gelade E, Van der Zegel M, Van der Auweraer M, Vandendriessche H, De Schryver FC, Almgren M (1983) Influence of salt, detergent concentration, and temperature on the fluorescence quenching of 1-methylpyrene in sodium dodecyl sulfate with m-dicyanobenzene *Journal of Physical Chemistry* **87**:1426 - 1431.

Crowell KJ, Franzin CM, Koltay A, Lee S, Lucchese AM, Snyder BC, Marassi FM (2003) Expression and characterization of the FXYD ion transport regulators for NMR structural studies in lipid micelles and lipid bilayers. *Biochimica et biophysica acta* **1645**:15-21.

Crowley KS, Liao S, Worrell VE, Reinhart GD, Johnson AE (1994) Secretory proteins move through the endoplasmic reticulum membrane via an aqueous, gated pore. *Cell* **78**:461-471.

Curnow P, Booth PJ (2007) Combined kinetic and thermodynamic analysis of alpha-helical membrane protein unfolding. *Proceedings of the National Academy of Sciences of the United States of America* **104**:18970-18975.

Curnow P, Booth PJ (2009) The transition state for integral membrane protein folding. *Proceedings of the National Academy of Sciences of the United States of America* **106**:773-778.

Daggett V, Fersht AR (2003) Is there a unifying mechanism for protein folding? *Trends Biochem Sci* **28**:18-25.

Darden T, York D, Pedersen L (1993) Particle mesh Ewald: An N-log(N) method for Ewald sums in large systems. *The Journal of Chemical Physics* **98**:10089-10092.

Dill KA (1985) Theory for the folding and stability of globular proteins. *Biochemistry* **24**:1501-1509.

Dobson CM (2001) The structural basis of protein folding and its links with human disease. *Philosophical Transactions of the Royal Society of London B Biological Sciences* **356**:133-145.

Dockter C, Volkov A, Bauer C, Polyhach Y, Joly-Lopez Z, Jeschke G, Paulsen H (2009) Refolding of the integral membrane protein light-harvesting complex II monitored by pulse EPR. *Proceedings of the National Academy of Sciences of the United States of America* **106**:18485-18490.

Doi T, Molday RS, Khorana HG (1990) Role of the intradiscal domain in rhodopsin assembly and function. *Proceedings of the National Academy of Sciences of the United States of America* **87**:4991-4995.

Dornmair K, Kiefer H, Jahnig F (1990) Refolding of an integral membrane protein. OmpA of Escherichia coli. *The Journal of biological chemistry* **265**:18907-18911.

Dutta A, Kim TY, Moeller M, Wu J, Alexiev U, Klein-Seetharaman J (2010) Characterization of membrane protein non-native states. 2. The SDS-unfolded states of rhodopsin. *Biochemistry* **49**:6329-6340.

Eilers M, Reeves PJ, Ying W, Khorana HG, Smith SO (1999) Magic angle spinning NMR of the protonated retinylidene Schiff base nitrogen in rhodopsin: expression of 15N-lysine- and 13C-glycine-labeled opsin in a stable cell line. *Proceedings of the National Academy of Sciences of the United States of America* **96**:487-492.

Engelman DM, Chen Y, Chin CN, Curran AR, Dixon AM, Dupuy AD, Lee AS, Lehnert U, Matthews EE, Reshetnyak YK, Senes A, Popot JL (2003) Membrane protein folding: beyond the two stage model. *FEBS letters* **555**:122-125.

Essmann U, Perera L, Berkowitz ML, Darden T, Lee H, Pedersen LG (1995) A smooth particle mesh Ewald method. *The Journal of Chemical Physics* **103**:8577-8593.

Farahbakhsh ZT, Hideg K, Hubbell WL (1993) Photoactivated conformational changes in rhodopsin: a time-resolved spin label study. *Science* **262**:1416-1419.

Farahbakhsh ZT, Ridge KD, Khorana HG, Hubbell WL (1995) Mapping light-dependent structural changes in the cytoplasmic loop connecting helices C and D in rhodopsin: a site-directed spin labeling study. *Biochemistry* **34**:8812-8819.

Farrens DL, Altenbach C, Yang K, Hubbell WL, Khorana HG (1996) Requirement of rigid-body motion of transmembrane helices for light activation of rhodopsin. *Science* **274**:768-770.

Farrens DL, Khorana HG (1995) Structure and function in rhodopsin. Measurement of the rate of metarhodopsin II decay by fluorescence spectroscopy. *The Journal of biological chemistry* **270**:5073-5076.

Fenimore PW, Frauenfelder H, McMahon BH, Parak FG (2002) Slaving: solvent fluctuations dominate protein dynamics and functions. *Proceedings of the National Academy of Sciences of the United States of America* **99**:16047-16051.

Fersht AR, Matouschek A, Serrano L (1992) The folding of an enzyme. I. Theory of protein engineering analysis of stability and pathway of protein folding. *Journal of molecular biology* **224**:771-782.

Franzin CM, Gong XM, Thai K, Yu J, Marassi FM (2007) NMR of membrane proteins in micelles and bilayers: the FXYD family proteins. *Methods* **41**:398-408.

Freeman R, Hill HDW (1971) Fourier Transform Study of NMR Spin-Lattic Relaxation by "Progressive Saturation". *Journal of Chemical Physics* **54**:3367-3377.

Freitas MS, Gaspar LP, Lorenzoni M, Almeida FC, Tinoco LW, Almeida MS, Maia LF, Degreve L, Valente AP, Silva JL (2007) Structure of the Ebola fusion peptide in a membrane-mimetic environment and the interaction with lipid rafts. *The Journal of biological chemistry* **282**:27306-27314.

Garriga P, Liu X, Khorana HG (1996) Structure and function in rhodopsin: correct folding and misfolding in point mutants at and in proximity to the site of the retinitis pigmentosa mutation Leu-125-->Arg in the transmembrane helix C. *Proceedings of the National Academy of Sciences of the United States of America* **93**:4560-4564.

Getmanova E, Patel AB, Klein-Seetharaman J, Loewen MC, Reeves PJ, Friedman N, Sheves M, Smith SO, Khorana HG (2004) NMR spectroscopy of phosphorylated wild-type

rhodopsin: mobility of the phosphorylated C-terminus of rhodopsin in the dark and upon light activation. *Biochemistry* **43**:1126-1133.

Goldman M (1984) Interference Effects in the Relaxation of a Pair of Unlike Spin-1/2 Nuclei. *Journal of Magnetic Resonance* **60**:437-452.

Gossen M, Bujard H (1992) Tight control of gene expression in mammalian cells by tetracycline-responsive promoters. *Proceedings of the National Academy of Sciences of the United States of America* **89**:5547-5551.

Grassetti DR, Murray JF, Jr. (1967) Determination of sulfhydryl groups with 2,2'- or 4,4'-dithiodipyridine. *Archives of biochemistry and biophysics* **119**:41-49.

Harper JD, Lansbury PT, Jr. (1997) Models of amyloid seeding in Alzheimer's disease and scrapie: mechanistic truths and physiological consequences of the time-dependent solubility of amyloid proteins. *Annual review of biochemistry* **66**:385-407.

Hartong DT, Berson EL, Dryja TP (2006) Retinitis pigmentosa. *Lancet* **368**:1795-1809.

Hayward S, Go N (1995) Collective variable description of native protein dynamics. *Annual Review of Physical Chemistry* **46**:223-250.

Hendrickson TL, de Crecy-Lagard V, Schimmel P (2004) Incorporation of nonnatural amino acids into proteins. *Annual review of biochemistry* **73**:147-176.

Heuberger EH, Veenhoff LM, Duurkens RH, Friesen RH, Poolman B (2002) Oligomeric state of membrane transport proteins analyzed with blue native electrophoresis and analytical ultracentrifugation. *Journal of molecular biology* **317**:591-600.

Hirst JD, Brooks CL, 3rd (1994) Helicity, circular dichroism and molecular dynamics of proteins. *Journal of molecular biology* **243**:173-178.

Hsu ST, Cabrita LD, Fucini P, Christodoulou J, Dobson CM (2009) Probing side-chain dynamics of a ribosome-bound nascent chain using methyl NMR spectroscopy. *Journal of the American Chemical Society* **131**:8366-8367.

Hsu ST, Fucini P, Cabrita LD, Launay H, Dobson CM, Christodoulou J (2007) Structure and dynamics of a ribosome-bound nascent chain by NMR spectroscopy. *Proceedings of the National Academy of Sciences of the United States of America* **104**:16516-16521.

Huang KS, Bayley H, Liao MJ, London E, Khorana HG (1981) Refolding of an integral membrane protein. Denaturation, renaturation, and reconstitution of intact bacteriorhodopsin and two proteolytic fragments. *The Journal of biological chemistry* **256**:3802-3809.

Hubbard R (1969) Absorption spectrum of rhodopsin: 500 nm absorption band. *Nature* **221**:432-435.

Hubbell WL, Altenbach C, Hubbell CM, Khorana HG (2003) Rhodopsin structure, dynamics, and activation: a perspective from crystallography, site-directed spin labeling, sulfhydryl reactivity, and disulfide cross-linking. *Advances in protein chemistry* **63**:243-290.

Hubbell WL, Cafiso DS, Altenbach C (2000) Identifying conformational changes with site-directed spin labeling. *Nature structural biology* **7**:735-739.

Hunt JF, Earnest TN, Bousche O, Kalghatgi K, Reilly K, Horvath C, Rothschild KJ, Engelman DM (1997) A biophysical study of integral membrane protein folding. *Biochemistry* **36**:15156-15176.

Hwa J, Garriga P, Liu X, Khorana HG (1997) Structure and function in rhodopsin: packing of the helices in the transmembrane domain and folding to a tertiary structure in the

intradiscal domain are coupled. *Proceedings of the National Academy of Sciences of the United States of America* **94**:10571-10576.

Hwang TL, Shaka AJ (1995) Water Suppression That Works. Excitation Sculpting Using Arbitrary Wave-Forms and Pulsed-Field Gradients. *Journal of Magnetic Resonance, Series A* **112**:275-279.

Iannaccone A, Man D, Waseem N, Jennings BJ, Ganapathiraju M, Gallaher K, Reese E, Bhattacharya SS, Klein-Seetharaman J (2006) Retinitis pigmentosa associated with rhodopsin mutations: Correlation between phenotypic variability and molecular effects. *Vision research* **46**:4556-4567.

Ibel K, May RP, Kirschner K, Szadkowski H, Mascher E, Lundahl P (1990) Protein-decorated micelle structure of sodium-dodecyl-sulfate--protein complexes as determined by neutron scattering. *European journal of biochemistry* **190**:311-318.

Isin B, Rader AJ, Dhiman HK, Klein-Seetharaman J, Bahar I (2006) Predisposition of the dark state of rhodopsin to functional changes in structure. *Proteins* **65**:970-983.

Ismail N, Crawshaw SG, Cross BC, Haagsma AC, High S (2008) Specific transmembrane segments are selectively delayed at the ER translocon during opsin biogenesis. *The Biochemical journal* **411**:495-506.

Jaaskelainen S, Verma CS, Hubbard RE, Linko P, Caves LS (1998) Conformational change in the activation of lipase: an analysis in terms of low-frequency normal modes. *Protein Science* **7**:1359-1367.

Jackson SE (1998) How do small single-domain proteins fold? *Fold Des* **3**:R81-91.

Jacobs DJ, Rader AJ, Kuhn LA, Thorpe MF (2001) Protein flexibility predictions using graph theory. *Proteins* **44**:150-165.

Jirgensons B (1967) Effects of n-propyl alcohol and detergents on the optical rotatory dispersion of alpha-chymotrypsinogen, beta-casein, histone fraction F1, and soybean trypsin inhibitor. *The Journal of biological chemistry* **242**:912-918.

Joh NH, Min A, Faham S, Whitelegge JP, Yang D, Woods VL, Bowie JU (2008) Modest stabilization by most hydrogen-bonded side-chain interactions in membrane proteins. *Nature* **453**:1266-1270.

Johnson SM, Wiseman RL, Sekijima Y, Green NS, Adamski-Werner SL, Kelly JW (2005) Native state kinetic stabilization as a strategy to ameliorate protein misfolding diseases: a focus on the transthyretin amyloidoses. *Accounts of chemical research* **38**:911-921.

Karnik SS, Khorana HG (1990) Assembly of functional rhodopsin requires a disulfide bond between cysteine residues 110 and 187. *The Journal of biological chemistry* **265**:17520-17524.

Kaushal S, Khorana HG (1994) Structure and function in rhodopsin. 7. Point mutations associated with autosomal dominant retinitis pigmentosa. *Biochemistry* **33**:6121-6128.

Kieltsch I, Eisenberger P, Togni A (2007) Mild electrophilic trifluoromethylation of carbon- and sulfur-centered nucleophiles by a hypervalent iodine(III)-CF3 reagent. *Angewandte Chemie International Edition* **46**:754-757.

Kim PS, Baldwin RL (1982) Specific intermediates in the folding reactions of small proteins and the mechanism of protein folding. *Annual review of biochemistry* **51**:459-489.

Klein-Seetharaman J (2005) Dual role of interactions between membranous and soluble portions of helical membrane receptors for folding and signaling. *Trends in pharmacological sciences* **26**:183-189.

Klein-Seetharaman J, Getmanova EV, Loewen MC, Reeves PJ, Khorana HG (1999a) NMR

spectroscopy in studies of light-induced structural changes in mammalian rhodopsin:

applicability of solution (19)F NMR. *Proceedings of the National Academy of Sciences of*

the United States of America **96**:13744-13749.

Klein-Seetharaman J, Hwa J, Cai K, Altenbach C, Hubbell WL, Khorana HG (1999b) Single-

cysteine substitution mutants at amino acid positions 55-75, the sequence connecting the

cytoplasmic ends of helices I and II in rhodopsin: reactivity of the sulfhydryl groups and

their derivatives identifies a tertiary structure that changes upon light-activation.

Biochemistry **38**:7938-7944.

Klein-Seetharaman J, Hwa J, Cai K, Altenbach C, Hubbell WL, Khorana HG (2001) Probing the

dark state tertiary structure in the cytoplasmic domain of rhodopsin: proximities between

amino acids deduced from spontaneous disulfide bond formation between Cys316 and

engineered cysteines in cytoplasmic loop 1. *Biochemistry* **40**:12472-12478.

Klein-Seetharaman J, Oikawa M, Grimshaw SB, Wirmer J, Duchardt E, Ueda T, Imoto T, Smith

LJ, Dobson CM, Schwalbe H (2002a) Long-range interactions within a nonnative protein.

Science (New York, NY **295**:1719-1722.

Klein-Seetharaman J, Reeves PJ, Loewen MC, Getmanova EV, Chung J, Schwalbe H, Wright

PE, Khorana HG (2002b) Solution NMR spectroscopy of [alpha -15N]lysine-labeled

rhodopsin: The single peak observed in both conventional and TROSY-type HSQC

spectra is ascribed to Lys-339 in the carboxyl-terminal peptide sequence. *Proceedings of*

the National Academy of Sciences of the United States of America **99**:3452-3457.

Klein-Seetharaman J, Yanamala NV, Javeed F, Reeves PJ, Getmanova EV, Loewen MC,

Schwalbe H, Khorana HG (2004) Differential dynamics in the G protein-coupled receptor

rhodopsin revealed by solution NMR. *Proceedings of the National Academy of Sciences of the United States of America* **101**:3409-3413.

Knab J, Chen JY, Markelz A (2006) Hydration dependence of conformational dielectric relaxation of lysozyme. *Biophysical journal* **90**:2576-2581.

Knudsen P, Hubbell WL (1978) Stability of rhodopsin in detergent solutions. *Membrane biochemistry* **1**:297-322.

Kobilka BK, Kobilka TS, Daniel K, Regan JW, Caron MG, Lefkowitz RJ (1988) Chimeric alpha 2-,beta 2-adrenergic receptors: delineation of domains involved in effector coupling and ligand binding specificity. *Science* **240**:1310-1316.

Kohn J, Wilchek M (1978) A Calorimetric Method for Monitoring Activation of Sepharose by Cyanogen Bromide. *Biochemical and biophysical research communications* **84**:7-14.

Krebs MP, Holden DC, Joshi P, Clark CL, 3rd, Lee AH, Kaushal S (2010) Molecular mechanisms of rhodopsin retinitis pigmentosa and the efficacy of pharmacological rescue. *Journal of molecular biology* **395**:1063-1078.

Kuemel G, Daus H, Mauch H (1979) Improved Method for the Cyanogen Bromide Activation of Agarose Beads. *Journal of chromatography* **172**:221-226.

Kumar S, Sharma D, Ghosh G, Kabir ud D (2005) Structural modifications of aqueous ionic micelles in the presence of denaturants as studied by DLS and viscometry. *Langmuir* **21**:9446-9450.

Kusnetzow AK, Altenbach C, Hubbell WL (2006) Conformational states and dynamics of rhodopsin in micelles and bilayers. *Biochemistry* **45**:5538-5550.

Laemmli UK (1970) *Nature* **227**:680-685.

Lau FW, Bowie JU (1997) A method for assessing the stability of a membrane protein. *Biochemistry* **36**:5884-5892.

Levinthal C (1968) Are there pathways for protein folding? *Extrait du Journal de Chimie Physique* **65**:44-45.

Li C, Deber CM (1992) Influence of glycine residues on peptide conformation in membrane environments. *International journal of peptide and protein research* **40**:243-248.

Li J, Edwards PC, Burghammer M, Villa C, Schertler GF (2004) Structure of bovine rhodopsin in a trigonal crystal form. *Journal of molecular biology* **343**:1409-1438.

Li T, Sandberg MA, Pawlyk BS, Rosner B, Hayes KC, Dryja TP, Berson EL (1998) Effect of vitamin A supplementation on rhodopsin mutants threonine-17 --> methionine and proline-347 --> serine in transgenic mice and in cell cultures. *Proceedings of the National Academy of Sciences of the United States of America* **95**:11933-11938.

Lindahl E, Hess B, Spoel Dvd (2001) GROMACS 3.0: A package for molecular simulation and trajectory analysis. *Journal of Molecular Modeling* **7**:306-317.

Link AJ, Mock ML, Tirrell DA (2003) Non-canonical amino acids in protein engineering. *Current opinion in biotechnology* **14**:603-609.

Loewen MC, Klein-Seetharaman J, Getmanova EV, Reeves PJ, Schwalbe H, Khorana HG (2001) Solution 19F nuclear Overhauser effects in structural studies of the cytoplasmic domain of mammalian rhodopsin. *Proceedings of the National Academy of Sciences of the United States of America* **98**:4888-4892.

Lomize MA, Lomize AL, Pogozheva ID, Mosberg HI (2006) OPM: orientations of proteins in membranes database. *Bioinformatics (Oxford, England)* **22**:623-625.

London E, Khorana HG (1982) Denaturation and renaturation of bacteriorhodopsin in detergents and lipid-detergent mixtures. *The Journal of biological chemistry* **257**:7003-7011.

Lu H, Booth PJ (2000) The final stages of folding of the membrane protein bacteriorhodopsin occur by kinetically indistinguishable parallel folding paths that are mediated by pH. *Journal of molecular biology* **299**:233-243.

Maggio R, Vogel Z, Wess J (1993) Reconstitution of functional muscarinic receptors by co-expression of amino- and carboxyl-terminal receptor fragments. *FEBS letters* **319**:195-200.

Manavalan P, Johnson WC, Jr. (1987) Variable selection method improves the prediction of protein secondary structure from circular dichroism spectra. *Analytical biochemistry* **167**:76-85.

Marti T (1998) Refolding of bacteriorhodopsin from expressed polypeptide fragments. *Journal of biological chemistry* **273**:9312-9322.

Martin NP, Leavitt LM, Sommers CM, Dumont ME (1999) Assembly of G protein-coupled receptors from fragments: identification of functional receptors with discontinuities in each of the loops connecting transmembrane segments. *Biochemistry* **38**:682-695.

Mascher E, Lundahl P (1989) Sodium dodecyl sulphate-protein complexes. Changes in size or shape below the critical micelle concentration, as monitored by high-performance agarose gel chromatography. *Journal of chromatography* **476**:147-158.

Mattice WL, Riser JM, Clark DS (1976) Conformational properties of the complexes formed by proteins and sodium dodecyl sulfate. *Biochemistry* **15**:4264-4272.

McDonnell PA, Opella SJ (1993) Effect of Detergent Concentration on Multidimensional Solution NMR Spectra of Membrane Proteins in Micelles. *Journal of Magnetic Resonance, Series B* **102**:120-125.

McDonnell PA, Shon K, Kim Y, Opella SJ (1993) fd coat protein structure in membrane environments. *Journal of molecular biology* **233**:447-463.

McHaourab HS, Lietzow MA, Hideg K, Hubbell WL (1996) Motion of spin-labeled side chains in T4 lysozyme. Correlation with protein structure and dynamics. *Biochemistry* **35**:7692-7704.

McKibbin C, Farmer NA, Edwards PC, Villa C, Booth PJ (2009) Urea unfolding of opsin in phospholipid bicelles. *Photochemistry and photobiology* **85**:494-500.

Meacock SL, Lecomte FJ, Crawshaw SG, High S (2002) Different transmembrane domains associate with distinct endoplasmic reticulum components during membrane integration of a polytopic protein. *Molecular biology of the cell* **13**:4114-4129.

Mehring M. 1983. Principles of High Resolution NMR in Solids, Springer-Verlag, Berlin Heidelberg NewYork.

Meiboom S, Gill D (1958) Modified Spin-Echo Method for Measuring Nuclear Relaxation Times. *Review of Scientific Instruments* **29**:688-691.

Mendes HF, van der Spuy J, Chapple JP, Cheetham ME (2005) Mechanisms of cell death in rhodopsin retinitis pigmentosa: implications for therapy. *Trends in molecular medicine* **11**:177-185.

Mielke T, Alexiev U, Glasel M, Otto H, Heyn MP (2002) Light-induced changes in the structure and accessibility of the cytoplasmic loops of rhodopsin in the activated MII state. *Biochemistry* **41**:7875-7884.

Miller D, Charalambous K, Rotem D, Schuldiner S, Curnow P, Booth PJ (2009) In vitro unfolding and refolding of the small multidrug transporter EmrE. *Journal of molecular biology* **393**:815-832.

Molday RS (1998) Photoreceptor Membrane Proteins, Phototransduction, and Retinal Degenerative Diseases. The Friedenwald Lecture. *Investigative Ophthalmology and Visual Science* **39**:2493-2513.

Molday RS, Mackenzie D (1983) Monoclonal antibodies to rhodopsin: characterization, cross-reactivity, and application as structural probes. *Biochemistry* **22**:653-660.

Morris GA (1980) Sensitivity enhancement in nitrogen-15 NMR: polarization transfer using the INEPT pulse sequence. *Journal of American Chemical Society* **102**:428-429.

Nagarajan R, Shah KM, Hammond S (1982) Viscometric Detection of Sphere to Cylinder Transition and Polydispersity in Aqueous Micellar Solutions. *Colloids and Surfaces* **4**:147-162.

Nagy JK, Lonzer WL, Sanders CR (2001) Kinetic study of folding and misfolding of diacylglycerol kinase in model membranes. *Biochemistry* **40**:8971-8980.

Nielsen SM, Elling CE, Schwartz TW (1998) Split-receptors in the tachykinin neurokinin-1 system--mutational analysis of intracellular loop 3. *European journal of biochemistry* **251**:217-226.

Noorwez SM, Kuksa V, Imanishi Y, Zhu L, Filipek S, Palczewski K, Kaushal S (2003) Pharmacological chaperone-mediated in vivo folding and stabilization of the P23H-opsin mutant associated with autosomal dominant retinitis pigmentosa. *The Journal of biological chemistry* **278**:14442-14450.

Noorwez SM, Malhotra R, McDowell JH, Smith KA, Krebs MP, Kaushal S (2004) Retinoids assist the cellular folding of the autosomal dominant retinitis pigmentosa opsin mutant P23H. *Journal of biological chemistry* **279**:16278-16284.

O'Mahoney JV, Adams TE (1994) *DNA Cell Biol* **13**:1227-1232.

Ohgane K, Dodo K, Hashimoto Y (2010) Retinobenzaldehydes as proper-trafficking inducers of folding-defective P23H rhodopsin mutant responsible for retinitis pigmentosa. *Bioorganic & medicinal chemistry* **18**:7022-7028.

Okada T, Sugihara M, Bondar AN, Elstner M, Entel P, Buss V (2004) The retinal conformation and its environment in rhodopsin in light of a new 2.2 A crystal structure. *Journal of molecular biology* **342**:571-583.

Oprian DD, Molday RS, Kaufman RJ, Khorana HG (1987) Expression of a synthetic bovine rhodopsin gene in monkey kidney cells. *Proc Natl Acad Sci U S A* **84**:8874-8878.

Otzen DE (2002) Protein unfolding in detergents: effect of micelle structure, ionic strength, pH, and temperature. *Biophys J* **83**:2219-2230.

Otzen DE (2003) Folding of DsbB in mixed micelles: a kinetic analysis of the stability of a bacterial membrane protein. *Journal of molecular biology* **330**:641-649.

Otzen DE, Oliveberg M (2002) Burst-phase expansion of native protein prior to global unfolding in SDS. *Journal of molecular biology* **315**:1231-1240.

Ovchinnikov Yu A, Abdulaev NG, Bogachuk AS (1988) Two adjacent cysteine residues in the C-terminal cytoplasmic fragment of bovine rhodopsin are palmitylated. *FEBS letters* **230**:1-5.

Oxenoid K, Chou JJ (2005) The structure of phospholamban pentamer reveals a channel-like architecture in membranes. *Proceedings of the National Academy of Sciences of the United States of America* **102**:10870-10875.

Palczewski K, Kumasaka T, Hori T, Behnke CA, Motoshima H, Fox BA, Le Trong I, Teller DC, Okada T, Stenkamp RE, Yamamoto M, Miyano M (2000) Crystal structure of rhodopsin: A G protein-coupled receptor. *Science (New York, NY* **289**:739-745.

Palmer AG, 3rd (2004) NMR characterization of the dynamics of biomacromolecules. *Chem Rev* **104**:3623-3640.

Papac DI, Thornburg KR, Bullesbach EE, Crouch RK, Knapp DR (1992) Palmitylation of a G-protein coupled receptor. Direct analysis by tandem mass spectrometry. *The Journal of biological chemistry* **267**:16889-16894.

Park JH, Scheerer P, Hofmann KP, Choe HW, Ernst OP (2008) Crystal structure of the ligand-free G-protein-coupled receptor opsin. *Nature* **454**:183-187.

Piotto M, Saudek V, Sklenar V (1992) Gradient-tailored excitation for single-quantum NMR spectroscopy of aqueous solutions. *Journal of biomolecular NMR* **2**:661-665.

Pitt GA, Collins FD, Morton RA, Stok P (1955) Studies on rhodopsin. VIII. Retinylidenemethylamine, an indicator yellow analogue. *The Biochemical journal* **59**:122-128.

Plumley FG, Schmidt GW (1987) Reconstitution of chlorophyll a/b light-harvesting complexes: Xanthophyll-dependent assembly and energy transfer. *Proceedings of the National Academy of Sciences of the United States of America* **84**:146-150.

Popot JL, Engelman DM (1990) Membrane protein folding and oligomerization: the two-stage model. *Biochemistry* **29**:4031-4037.

Provencher SW, Glockner J (1981) Estimation of globular protein secondary structure from circular dichroism. *Biochemistry* **20**:33-37.

Rackovsky S, Scheraga HA (1977) Hydrophobicity, hydrophilicity, and the radial and orientational distributions of residues in native proteins. *Proceedings of the National Academy of Sciences of the United States of America* **74**:5248-5251.

Rader AJ, Anderson G, Isin B, Khorana HG, Bahar I, Klein-Seetharaman J (2004) Identification of core amino acids stabilizing rhodopsin. *Proceedings of the National Academy of Sciences of the United States of America* **101**:7246-7251.

Ramon E, Marron J, del Valle L, Bosch L, Andres A, Manyosa J, Garriga P (2003) Effect of dodecyl maltoside detergent on rhodopsin stability and function. *Vision research* **43**:3055-3061.

Rao JK, Argos P (1981) Structural stability of halophilic proteins. *Biochemistry* **20**:6536-6543.

Rapoport TA, Goder V, Heinrich SU, Matlack KE (2004) Membrane protein integration and the role of the translocon channel. *Trends in Cell Biology* **14**:568-575.

Ray SS, Nowak RJ, Brown RH, Jr., Lansbury PT, Jr. (2005) Small-molecule-mediated stabilization of familial amyotrophic lateral sclerosis-linked superoxide dismutase mutants against unfolding and aggregation. *Proceedings of the National Academy of Sciences of the United States of America* **102**:3639-3644.

Reeves PJ, Callewaert N, Contreras R, Khorana HG (2002a) Structure and function in rhodopsin: high-level expression of rhodopsin with restricted and homogeneous N-glycosylation by a tetracycline-inducible N-acetylglucosaminyltransferase I-negative HEK293S stable mammalian cell line. *Proceedings of the National Academy of Sciences of the United States of America* **99**:13419-13424.

Reeves PJ, Kim JM, Khorana HG (2002b) Structure and function in rhodopsin: a tetracycline-inducible system in stable mammalian cell lines for high-level expression of opsin mutants. *Proceedings of the National Academy of Sciences of the United States of America* **99**:13413-13418.

Reeves PJ, Thurmond RL, Khorana HG (1996) Structure and function in rhodopsin: high level expression of a synthetic bovine opsin gene and its mutants in stable mammalian cell lines. *Proceedings of the National Academy of Sciences of the United States of America* **93**:11487-11492.

Resek JF, Farahbakhsh ZT, Hubbell WL, Khorana HG (1993) Formation of the meta II photointermediate is accompanied by conformational changes in the cytoplasmic surface of rhodopsin. *Biochemistry* **32**:12025-12032.

Ridge KD, Lee SS, Yao LL (1995a) In vivo assembly of rhodopsin from expressed polypeptide fragments. *Proceedings of the National Academy of Sciences of the United States of America* **92**:3204-3208.

Ridge KD, Lu Z, Liu X, Khorana HG (1995b) Structure and function in rhodopsin. Separation and characterization of the correctly folded and misfolded opsins produced on expression of an opsin mutant gene containing only the native intradiscal cysteine codons. *Biochemistry* **34**:3261-3267.

Ridge KD, Zhang C, Khorana HG (1995c) Mapping of the amino acids in the cytoplasmic loop connecting helices C and D in rhodopsin. Chemical reactivity in the dark state following single cysteine replacements. *Biochemistry* **34**:8804-8811.

Riley ML, Wallace BA, Flitsch SL, Booth PJ (1997) Slow alpha helix formation during folding of a membrane protein. *Biochemistry* **36**:192-196.

Rizo J, Blanco FJ, Kobe B, Bruch MD, Gierasch LM (1993) Conformational behavior of Escherichia coli OmpA signal peptides in membrane mimetic environments. *Biochemistry* **32**:4881-4894.

Roman EA, Arguello JM, Gonzalez Flecha FL (2010) Reversible unfolding of a thermophilic membrane protein in phospholipid/detergent mixed micelles. *Journal of molecular biology* **397**:550-559.

Ruddon RW, Bedows E (1997) Assisted protein folding. *The Journal of biological chemistry* **272**:3125-3128.

Saliba RS, Munro PM, Luthert PJ, Cheetham ME (2002) The cellular fate of mutant rhodopsin: quality control, degradation and aggresome formation. *Journal of cell science* **115**:2907-2918.

Sanders CR, Myers JK (2004) Disease-related misassembly of membrane proteins. *Annual review of biophysics and biomolecular structure* **33**:25-51.

Sapra KT, Park PS, Filipek S, Engel A, Muller DJ, Palczewski K (2006) Detecting molecular interactions that stabilize native bovine rhodopsin. *Journal of molecular biology* **358**:255-269.

Sapra KT, Park PS, Palczewski K, Muller DJ (2008) Mechanical properties of bovine rhodopsin and bacteriorhodopsin: possible roles in folding and function. *Langmuir* **24**:1330-1337.

Schagger H, Cramer WA, von Jagow G (1994) Analysis of molecular masses and oligomeric states of protein complexes by blue native electrophoresis and isolation of membrane protein complexes by two-dimensional native electrophoresis. *Analytical biochemistry* **217**:220-230.

Schagger H, von Jagow G (1991) Blue native electrophoresis for isolation of membrane protein complexes in enzymatically active form. *Analytical biochemistry* **199**:223-231.

Scheerer P, Park JH, Hildebrand PW, Kim YJ, Krauss N, Choe HW, Hofmann KP, Ernst OP (2008) Crystal structure of opsin in its G-protein-interacting conformation. *Nature* **455**:497-502.

Schibli DJ, Hwang PM, Vogel HJ (1999) Structure of the antimicrobial peptide tritrpticin bound to micelles: a distinct membrane-bound peptide fold. *Biochemistry* **38**:16749-16755.

Schnell JR, Chou JJ (2008) Structure and mechanism of the M2 proton channel of influenza A virus. *Nature* **451**:591-595.

Sekijima Y, Wiseman RL, Matteson J, Hammarstrom P, Miller SR, Sawkar AR, Balch WE, Kelly JW (2005) The biological and chemical basis for tissue-selective amyloid disease. *Cell* **121**:73-85.

Shaka AJ, Barker PB, Freeman R (1985) Computer-optimized decoupling scheme for wideband applications and low-level operation. *Journal of Magnetic Resonance* **64**:547-552.

Shaka AJ, Keeler J, Frenkiel T, Freeman R (1983) Evaluation of a new broadband decoupling sequence: WALTZ-16 *Journal of Magnetic Resonance* **52**:335-338.

Shichi H (1973) Conformational aspects of phodopsin associated with disc membranes. *Experimental eye research* **17**:533-543.

Shortle D (1996) The denatured state (the other half of the folding equation) and its role in protein stability. *The Faseb Journal* **10**:27-34.

Shortle D, Ackerman MS (2001) Persistence of native-like topology in a denatured protein in 8 M urea. *Science* **293**:487-489.

Soldi G, Plakoutsi G, Taddei N, Chiti F (2006) Stabilization of a native protein mediated by ligand binding inhibits amyloid formation independently of the aggregation pathway. *Journal of medicinal chemistry* **49**:6057-6064.

Soto C, Sigurdsson EM, Morelli L, Kumar RA, Castano EM, Frangione B (1998) Beta-sheet breaker peptides inhibit fibrillogenesis in a rat brain model of amyloidosis: implications for Alzheimer's therapy. *Nature medicine* **4**:822-826.

Sreerama N, Woody RW (1993) A self-consistent method for the analysis of protein secondary structure from circular dichroism. *Analytical biochemistry* **209**:32-44.

Sreerama N, Woody RW (2000) Estimation of protein secondary structure from circular dichroism spectra: comparison of CONTIN, SELCON, and CDSSTR methods with an expanded reference set. *Analytical biochemistry* **287**:252-260.

Stott K, Stonehouse, Jonathan, Keeler, James, Hwang, Tsang-Lin, and Shaka, A. J. (1995) Excitation Sculpting in High-Resolution Nuclear Magnetic Resonance Spectroscopy: Application to Selective NOE Experiments *Journal of American Chemical Society* **117**:4199 - 4200.

Suda K, Filipek S, Palczewski K, Engel A, Fotiadis D (2004) The supramolecular structure of the GPCR rhodopsin in solution and native disc membranes. *Molecular membrane biology* **21**:435-446.

Sung CH, Davenport CM, Hennessey JC, Maumenee IH, Jacobson SG, Heckenlively JR, Nowakowski R, Fishman G, Gouras P, Nathans J (1991) Rhodopsin mutations in autosomal dominant retinitis pigmentosa. *Proceedings of the National Academy of Sciences of the United States of America* **88**:6481-6485.

Sung CH, Davenport CM, Nathans J (1993) Rhodopsin mutations responsible for autosomal dominant retinitis pigmentosa. Clustering of functional classes along the polypeptide chain. *Journal of Biological Chemistry* **268**:26645-26649.

Takeda S, Kadowaki S, Haga T, Takaesu H, Mitaku S (2002) Identification of G protein-coupled receptor genes from the human genome sequence. *FEBS letters* **520**:97-101.

Tama F, Gadea FX, Marques O, Sanejouand YH (2000) Building-block approach for determining low-frequency normal modes of macromolecules. *Proteins* **41**:1-7.

Tama F, Sanejouand YH (2001) Conformational change of proteins arising from normal mode calculations. *Protein engineering* **14**:1-6.

Tastan O, Yu E, Ganapathiraju M, Aref A, Rader AJ, Klein-Seetharaman J (2007) Comparison of stability predictions and simulated unfolding of rhodopsin structures. *Photochemistry and photobiology* **83**:351-363.

Teller DC, Okada T, Behnke CA, Palczewski K, Stenkamp RE (2001) Advances in determination of a high-resolution three-dimensional structure of rhodopsin, a model of G-protein-coupled receptors (GPCRs). *Biochemistry* **40**:7761-7772.

Tomita A, Sato T, Ichiyanagi K, Nozawa S, Ichikawa H, Chollet M, Kawai F, Park SY, Tsuduki T, Yamato T, Koshihara SY, Adachi S (2009) Visualizing breathing motion of internal cavities in concert with ligand migration in myoglobin. *Proceedings of the National Academy of Sciences of the United States of America* **106**:2612-2616.

Tummino PJ, Gafni A (1993) Determination of the aggregation number of detergent micelles using steady-state fluorescence quenching. *Biophysical journal* **64**:1580-1587.

Turro NJ, Yekta A (1978) Luminescent probes for detergent solutions. A simple procedure for determination of the mean aggregation number of micelles. *Journal of the American Chemical Society* **100**:5951-5952.

Van Horn WD, Kim HJ, Ellis CD, Hadziselimovic A, Sulistijo ES, Karra MD, Tian C, Sonnichsen FD, Sanders CR (2009) Solution nuclear magnetic resonance structure of membrane-integral diacylglycerol kinase. *Science* **324**:1726-1729.

von Heijne G (2006) Membrane-protein topology. *Nature reviews* **7**:909-918.

Wald G, Brown PK (1950) The Synthesis of Rhodopsin from Retinene(1). *Proceedings of the National Academy of Sciences of the United States of America* **36**:84-92.

Wald G, Brown PK (1953a) The molar extinction of rhodopsin. *J Gen Physiol* **37**:189-200.

Wald G, Brown PK (1953b) The molar extinction of rhodopsin. *The Journal of general physiology* **37**:189-200.

Wallace BA, Lees JG, Orry AJ, Lobley A, Janes RW (2003) Analyses of circular dichroism spectra of membrane proteins. *Protein Science* **12**:875-884.

Wand AJ (2001) Dynamic activation of protein function: a view emerging from NMR spectroscopy. *Nature structural biology* **8**:926-931.

Wang G, Pierens GK, Treleaven WD, Sparrow JT, Cushley RJ (1996) Conformations of human apolipoprotein E(263-286) and E(267-289) in aqueous solutions of sodium dodecyl sulfate by CD and 1H NMR. *Biochemistry* **35**:10358-10366.

Werbelow LG, Marshall AG (1973) Internal Rotation and Nonexponential Methyl Nuclear Relaxation for Marcromolecules. *Journal of Magnetic Resonance* **11**:299-313.

Werner K, Lehner I, Dhiman HK, Richter C, Glaubitz C, Schwalbe H, Klein-Seetharaman J, Khorana HG (2007) Combined solid state and solution NMR studies of alpha,epsilon-15N labeled bovine rhodopsin. *Journal of biomolecular NMR* **37**:303-312.

Werner K, Richter C, Klein-Seetharaman J, Schwalbe H (2008) Isotope labeling of mammalian GPCRs in HEK293 cells and characterization of the C-terminus of bovine rhodopsin by high resolution liquid NMR spectroscopy. *Journal of biomolecular NMR* **40**:49-53.

White SH (2005) How hydrogen bonds shape membrane protein structure. *Advances in protein chemistry* **72**:157-172.

Wittig I, Braun HP, Schagger H (2006) Blue native PAGE. *Nature protocols* **1**:418-428.

Woods KN (2010) Solvent-induced backbone fluctuations and the collective librational dynamics of lysozyme studied by terahertz spectroscopy. *Physical review* **81**:031915.

Wrubel W, Stochaj U, Ehring R (1994) Construction and in vivo analysis of new split lactose permeases. *FEBS letters* **349**:433-438.

Wrubel W, Stochaj U, Sonnewald U, Theres C, Ehring R (1990) Reconstitution of an active lactose carrier in vivo by simultaneous synthesis of two complementary protein fragments. *Journal of bacteriology* **172**:5374-5381.

Yanamala N, Dutta A, Beck B, van Fleet B, Hay K, Yazbak A, Ishima R, Doemling A, Klein-Seetharaman J (2010) NMR-based screening of membrane protein ligands. *Chemical biology & drug design* **75**:237-256.

Yang K, Farrens DL, Altenbach C, Farahbakhsh ZT, Hubbell WL, Khorana HG (1996) Structure and function in rhodopsin. Cysteines 65 and 316 are in proximity in a rhodopsin mutant as indicated by disulfide formation and interactions between attached spin labels. *Biochemistry* **35**:14040-14046.

Yao F, Svensjo T, Winkler T, Lu M, Eriksson C, Eriksson E (1998) Tetracycline repressor, tetR, rather than the tetR-mammalian cell transcription factor fusion derivatives, regulates inducible gene expression in mammalian cells. *Human gene therapy* **9**:1939-1950.

Ye S, Huber T, Vogel R, Sakmar TP (2009) FTIR analysis of GPCR activation using azido probes. *Nature chemical biology* **5**:397-399.

Ye S, Kohrer C, Huber T, Kazmi M, Sachdev P, Yan EC, Bhagat A, RajBhandary UL, Sakmar TP (2008) Site-specific incorporation of keto amino acids into functional G protein-coupled receptors using unnatural amino acid mutagenesis. *The Journal of biological chemistry* **283**:1525-1533.

Ye S, Zaitseva E, Caltabiano G, Schertler GF, Sakmar TP, Deupi X, Vogel R (2010) Tracking G-protein-coupled receptor activation using genetically encoded infrared probes. *Nature* **464**:1386-1389.

Yu H, Kono M, McKee TD, Oprian DD (1995) A general method for mapping tertiary contacts between amino acid residues in membrane-embedded proteins. *Biochemistry* **34**:14963-14969.

Zen KH, McKenna E, Bibi E, Hardy D, Kaback HR (1994) Expression of lactose permease in contiguous fragments as a probe for membrane-spanning domains. *Biochemistry* **33**:8198-8206.

Zhou Y, Cierpicki T, Jimenez RH, Lukasik SM, Ellena JF, Cafiso DS, Kadokura H, Beckwith J, Bushweller JH (2008) NMR solution structure of the integral membrane enzyme DsbB: functional insights into DsbB-catalyzed disulfide bond formation. *Molecular cell* **31**:896-908.